1-1-2008

The importance of membrane mechanics in vesicle adhesion.

Jin Nam
University of Massachusetts Amherst

THE IMPORTANCE OF MEMBRANE MECHANICS IN VESICLE ADHESION

A Dissertation Presented

by

JIN NAM

Submitted to the Graduate School of the
University of Massachusetts Amherst in partial fulfillment
of the requirements for the degree of

DOCTOR OF PHILOSOPHY

February 2008

Polymer Science and Engineering

THE IMPORTANCE OF MEMBRANE MECHANICS IN VESICLE ADHESION

A Dissertation Presented

by

JIN NAM

Approved as to style and content by:

Maria M. Santore, Chair

Alfred J. Crosby, Member

Anthony D. Dinsmore, Member

Shaw Ling Hsu, Department Head
Polymer Science and Engineering

THE IMPORTANCE OF MEMBRANE MECHANICS IN VESICLE ADHESION

A Dissertation Presented

by

JIN NAM

Approved as to style and content by:

Maria M. Santore, Chair

Alfred J. Crosby, Member

Anthony D. Dinsmore, Member

Shaw Ling Hsu, Department Head
Polymer Science and Engineering

DEDICATION

This thesis is dedicated to my family, for providing me with endless love and support

ACKNOWLEDGMENTS

The deepest gratitude goes to my advisor, Professor Maria Santore. I would like to appreciate my advisor for her kind guidance to my project. She has been always positive about my endeavors and believing in me with amazing ideas. I could have graduate experience with both challenging and rewarding from her encouragements.

I am also grateful to Professor Al Crosby and Professor Anthony Dinsmore for good advice and very helpful discussions that led me out of the vesicle project which seemed to be endless works.

I especially thank my group members who have been my best friends for so many years. Thanks guys, Alicia Toscano, Jessica McCoy, Bing Mei, Natalia Kozlova, Bogdan Zdyrko, Pazit, Surachate Kalasin, and Jun Zhang.

Finally, I really thanks to my family for their endless support and understanding. My lovely son, Sangwoo and daughter, Jiwoo gave me lots of fun and hope during my thesis. Especially I am deeply indebted to my wife, Kyungsun for her underlying love and the sacrifices she endured.

ABSTRACT

THE IMPORTANCE OF MEMBRANE MECHANICS IN VESICLES ADHESION

FEBUARY 2008

JIN NAM, B.A., SEOUL NATIONAL UNIVERSITY

M.A., SEOUL NATIONAL UNIVERSITY

M.A., UNIVERSITY OF MASSACHUSETTS AMHERST

Ph.D., UNIVERSITY OF MASSACHUSETTS AMHERST

Directed by: Professor Maria M. Santore

This thesis explores the effects of bilayer mechanics on the adhesion of biomimetic membranes and vesicles, establishing copolymer lamellae as versatile model membranes that more widely vary membrane mechanics and chemical functionalization than can be achieved using phospholipids. This new biomimetic system provides fundamental insight into cell adhesion, and motivates new design strategies for vesicles in applications such as targeted delivery.

This study focused on the dynamic adhesion kinetics and spreading of vesicle pairs held in micropipettes at moderate tensions. The program employed two copolymers of different membrane stiffnesses, a graft copolymer of poly(dimethyl siloxane)-poly(ethylene oxide) [PDMS-PEO] and a diblock copolymer of poly(butadiene)-PEO [PBD-PEO]. The depletion-driven adhesion between pairs of these vesicles was studied, as was the avidin-biotin-driven adhesion between functionalized vesicles. This experimental grid therefore varied the membrane stiffness, adhesion strength, and point-wise versus laterally uniform application of adhesive forces.

This study systematically demonstrated, for the first time, the activated nature of vesicle adhesion and spreading, with the bending cost of kink formation at the spreading

front comprising a line tension that destabilizes adhesion nuclei. Despite modest differences between the bending moduli of phospholipid and stiffer copolymer vesicles, the effect was often sufficiently strong to prevent spreading, or at least produce a lag time prior to the onset of spreading. For instance, flexible membranes subject to depletion forces as small as 0.008 erg /cm^2 responded instantaneous to changes in membrane tension, achieving the equilibrium contact angle in less than a second. Stiff vesicles, however, never spread over a substrate vesicle or displayed an equilibrium contact angle, even when depletion forces were increased to 0.35 erg/cm^2. Avidin-biotin functionalized flexible vesicles displayed a lag time prior to spreading while fully functionalized stiff vesicles never spread over substrate vesicles. Of note, in cases where spreading did not, or had not yet occurred, there was evidence for adhesion in a contact nucleus. For instance, avidin-biotin functionalized vesicles could not be separated, and unfunctionalized vesicles subject to depletion forces deformed momentarily upon separation.

Estimates of the activation energy associated with spreading for depletion-driven adhesion were consistent with experimental observations, while a semi-quantitative treatment of avidin-biotin binding kinetics predicted the form of the concentration-dependence of the pre-spreading lag time. Once initiated, spreading kinetics were rapid and independent of membrane tension.

These results find significance in the areas of fundamental membrane physics and in biology. As micropipette manipulation is becoming an increasingly popular tool for membrane characterization, the current thesis demonstrates that the approach to equilibrium, as measured through the contact angle, may be impeded by bending mechanics, rendering the Young's analysis of adhesion strength meaningless. The findings also suggest that in cell adhesion and processes involving sharp membrane curvature, such as endocytosis, membrane mechanics likely plays an important role in the dynamic mechanism.

TABLE OF CONTENTS

LIST OF TABLES

Table Page

LIST OF FIGURES

CHAPTER 1

INTRODUCTION

1.1 Overview

For the last several decades liposomes, bilayer structures composed of phospholipids, have been an important research topic for biophysicists, physical chemists, and biotechnologists. Because phospholipid bilayers comprise a major component of cell membranes, insights into biology follow from the study of phospholipid vesicles. Besides the biological significance, phospholipid bilayers are a quintessential example of self-assembly, presenting fundamentally interesting phase behavior and providing seminal examples of how continuum properties (from surface tension to phases of matter such as solids, gels, disordered and partially ordered liquids) are controlled at the molecular level.[1-10] Phospholipid bilayers also allow testing of ideas concerning the impact of confinement on physical behaviors. Finally, phospholipid vesicles are technologically important in their roles as drug delivery agents.[5, 11, 12]

Important questions, which can be probed in quantitative detail using phospholipid vesicles, center on membrane adhesion. This particular subfield finds broad impact: Of interest to the physical chemist, vesicles are subject to the same interfacial forces (van der Waals, electrostatic, hydrogen bonding, hydrophobic interactions) that govern the behavior of colloids and films, thereby providing insight

into the impact of these interactions at fluid interfaces. Phospholipid vesicles may also be made to mimic cell membranes through the incorporation of specific ligands and receptors, invoking the more complicated biophysics of pairwise binding as a driving force for adhesion. Recently, this type of physics has been invoked in interpretation of T-cell junctions, [13, 14] leukocyte binding,[15-17] viral uptake,[18-21] and embryonic development.[22] Such pairwise binding, of course, is key to the success of targeted delivery strategies. The dynamic aspects of either continuum force-driven or ligand-receptor-driven adhesion have been considered only rarely, despite their importance: Though membranes comprise a nano-scale interphase, membrane binding is potentially subject to history dependence, hysteresis, viscous dissipation, and irreversibilities of larger scale systems, making the field quite rich.

Building on the fundamental importance of phospholipids vesicles, vesicles comprised of block copolymers were discovered less than a decade ago and have immediately become the subject of scientific scrutiny at both fundamental and applied levels.[23, 24] This interest is a result of their technological potential: While polymer vesicles exhibit many similarities to those made of phospholipids, one outstanding difference is the much greater stability and lifetime of polymer vesicles. This stability, coupled with the chemical and physical versatility of polymer vesicles makes them especially attractive in delivery applications. This doctoral program therefore undertook the study of the adhesion of polymeric vesicles, with an eye towards targeted delivery. Indeed, at the time of the inception of this research there were no published reports of fundamental adhesion of polymer vesicles.

This dissertation examines adhesion dynamics between polymer vesicles. The significance of the work derives less from the molecular distinction between polymer and phospholipid vesicles, and more from the physics accessible with polymer vesicles, which cannot be probed with phospholipid analogs. This program has, first, developed polymer vesicles as a versatile platform for adhesion studies where, in addition to surface chemistry, membrane mechanics are of importance and can be tuned. Indeed, while the program has focused on the simplest possible cases, it has demonstrated a rich variety in adhesive membrane behaviors as a result of the interplay of adhesive forces with membrane mechanics. The conclusions are important both to biology and to the development of targeted drug delivery agents.

Of the new concepts to follow from this work, the most important ideas developed here pertain to the quantitative identification of conditions where membrane mechanics, specifically bending, dominate the chemistry-controlled aspects of vesicle adhesion: With two types of amphiphilic polymers and two different adhesion mechanisms, the impact of membrane bending on adhesion kinetics and kinetic trapping was demonstrated. In these studies, the growth of the adhesion plaque, or contact between two adhesive vesicles was studied and analyzed, using a micropipette manipulation technique. Most striking was the finding that the stiffer membranes (which were not conspicuously rigid) were resistant to spreading and appeared non-adhesive until they were pulled from a substrate. The work also demonstrated the utility of the micropipette pipette manipulation in this class of studies: While other methods such a

reflectance interference contrast microscopy (RICM)[25, 26] and the surface forces apparatus (SFA) are becoming popular for measurements of adhesion,[6, 27, 28] the micropipette approach allows one to control and measure the membrane tension, an important feature in these studies.

To put the significance of this work into better perspective, the remainder of this chapter provides general background on the properties of polymer vesicles relative to their phospholipid analogs, discusses techniques for force measurement, and reviews the literature on phospholipid adhesion especially the works most closely approaching the systems in this thesis: simple avidin biotin binding and uniform attractions such as van der Waals and depletion forces.

1.2 Biomimetic Membranes

Cell and other biological membranes are complex multi-structural and multi-functional constructs whose 3-nm thick phospholipid bilayers are perforated with proteins and glycolipids, and supported from beneath by a stabilizing cytoskeleton.[29] The glycocalyx or brushy layer of glycolipids provides steric stability and likely contributes to bending resistance beyond that of a simple phospholipid bilayer.[30] Cholesterol also alters the membrane's mechanical properties, as does, in some cases, attachment to the actin cortex.[31] Despite the complexity of cell membranes, simple liposomes, liposomes containing tethered polyethylene glycol (PEG) chains,[32] and phospholipid vesicles further functionalized with adhesion molecules have been

developed as mimics of cell membranes, and used in studies targeting an understanding of the biophysics of the cell surface.[33] This approach is a reasonable start towards the development of biomimetic membranes, but is sometimes limited by stability and the ability to densely functionalize the membrane.

Block copolymers have, in recent years, provided an alternative to phospholipids, as mimics of the cell membrane, despite real chemical differences between polymer-based and phospholipid-based membranes.[23, 24, 34-41] While it can be challenging to precisely anticipate polymer architectures (the amount of hydrophilic versus hydrophobic block size) that produce lamellar structures and vesicles,[42] once this is known for a particular choice of chemistry, vesicles can be made with reproducible batch-batch properties, despite potential discrepancies resulting from polydispersity. Indeed, advances in anionic living polymerization techniques have made moderate batches sizes of di- and tri-block copolymers accessible for research and within economic reach for drug delivery and bio-scavenging applications.[5, 43-45]

1.3 Properties of Amphiphilic Copolymer Bilayer Membranes

When amphiphilic diblock copolymers self assemble into membrane structures, they offer a variety of tunable properties including stability, fluidity, and permeability, which are influenced by the polymer characteristics, in addition to the potential for substantial chemical modification by biomolecules. A number of important features were highlighted in the original *Science* paper which introduced polymer vesicles[24]: (1)

Polymer vesicles have superior mechanical properties compared with their phospholipid analogs. In particular, the critical strain to rupture the polymer vesicles proved to be an order of magnitude (20% strain) greater than for phospholipids such as SOPC (1-Stearoyl-2-Oleoyl-*sn*-Glycero-3-Phosphocholine) (2-3% strain). With lysis tensions on the order of 10 mN /m, this makes polymer vesicles particularly tough relative to liposomes. That is, much energy is required to rupture polymer vesicles. (2) Bilayer polymer membranes have relatively thick hydrophobic cores, increasing robustness and reducing permeability, thus aqueous contents are more effectively encapsulated in polymer vesicles than in liposomes. (3) Polymer vesicles are inherently stable in quiescent conditions: The steric stabilization provided by a polymer brush corona such as poly(ethylene glycol) on polymer vesicles is much more effective than that the hydration of polar head groups that stabilize liposomes, as the former can extend many nanometers (10 or more) from the PEG-hydrophobe interface. This, combined with the slower dynamics of the hydrophobic membrane core, increases the shelf life of polymer vesicles to months and years, relative to hours and days for liposomes.[46] (In a later paper it was demonstrated that the chain mobility in polymer vesicles is substantially slower than the diffusivity in liposomes, a result of the higher molecular weights in the polymer membranes.) Of relevance to the current thesis, the mechanical properties (area expansion modulus, bending modulus) of relatively low molecular weight copolymer vesicles (order 4000) were reported, in the original *Science* paper, to be similar to those of phospholipids, and only in a later paper was it demonstrated that for increases in the diblock molecular weight the bending modulus increased by the stretching modulus was relatively unaffected by chain length.[23] The oversight

concerning the distinction between the bending moduli of modest molecular weight polymer vesicles and those of phospholipids is somewhat ironic, as this thesis will demonstrate how even this slight mechanical difference profoundly alters adhesion behavior.

Beyond these simple membrane properties, copolymer systems are interesting because although some architectures form vesicles, slight architectural alterations can produce other morphologies, for instance, cylindrical micelles.[40, 45, 47, 48] There is the potential, therefore, with polymer vesicles, to trigger interesting phase transitions starting with a membrane.

Polymer vesicles can also tolerate substantial chemical modification, as a result of their robust natures. While polymer vesicles can support one or more PEG chains on every hydrophobic chain, stealth phospholipid vesicles have been reported to accommodate only 15 mol % of PEG-conjugated lipids, due to curvature effects that favor micellization over bilayer formation.[46] The greater density of PEG chains on the polymer vesicles therefore can support a potentially greater density of biomolecular groups, compared with phospholipid vesicles, even those containing some PEG chains.

1.4 Giant Unilamellar Vesicles

While pharmaceutical formulations typically employ small (order 10nm) or large (order 100nm) vesicles, scientific studies often employ giant (order 10 μm) vesicles, preferably unilamellar in nature. Giant unilamellar vesicles (GUVs) allow precise

quantitative study of individual vesicles and the application of micropipettes. GUVs are produced by hydration of a dried polymer film in aqueous solution, which swells the amphiphilic molecules and aids in their locally planar organization: The surface of the swollen dried film is comprised of the hydrophilic portions of the molecules and this sets up the directionality of the lamellar ordering. When simply hydrated from a film, vesicles pinch off as a result of instabilities and thermal fluctuations that cause the film to bend. Often these vesicles are multilamellar but some are unilamellar. Giant unilamellar vesicles are favored by an electroformation method where an AC electrical field helps to separate bilayers and helps undulations that cause each lamellae to pinch off into its own vesicle.[49-51] The resulting vesicles also seem to have fewer tethers and lower polydispersity.

Giant vesicles can undergo dramatic shape changes from flattened discoid (like biological cells, approaching the red blood cell) to perfect spheres, or strings of pearls (a series of budded structures). These shape changes occur in response to temperature changes, which cause the bilayer to expand to a different extent than the fluid within the vesicle, creating or consuming excess area. Likewise, changes in the osmotic pressure of the external solution drive shape changes as water slowly diffuses across the membrane to balance the osmotic pressure. Relevant to the work in this thesis, the average excess area of a vesicle sample can be manipulated through the relative osmotic pressures of the solutions originally on the interior and exterior of the vesicles.[34] In this thesis, vesicles were studied in open chambers (to accommodate the micropipettes), which allowed for slow evaporation. Despite the low water permeability of the polymer

membranes, water does diffuse into and out of the vesicles over tens of minutes,[52] increasing the excess area as the chamber dries. This tends to increase the projection of a vesicle further into its micropipette, but also, at some point, makes micromanipulation unmanageable, as very flaccid vesicles tend to bud or "bleb" into the pipettes when suction is applied.

The osmotic pressure difference defined by the sucrose solution in which the vesicles are electroformed and the glucose solution to which vesicles are transferred allows control over the excess area of the vesicles, or their flaccidness. The difference in solutions also renders the vesicles heavy so the settle to the bottom of the chamber making them easy to find. Finally, the two sugar solutions create a refractive index mismatch that allows the vesicles to be easily visualized in a phase contrast optical microscopy.

1.5 Mechanical Characterization of Vesicle Membranes

The micropipette manipulation technique adopted from biology into the materials arena by Evans and Needham works well to quantitatively assess fundamental mechanical membrane properties.[53-55] The method, employed extensively in this thesis, utilizes glass micropipettes, 5-10 μm in inner diameter to which suction is applied. When a vesicle is aspirated into a pipette, the suction produces a uniform tension, τ, across the membrane, in accordance with the Laplace equation:[76-79]

$$\tau = \frac{\Delta P R_p}{2\left(1 - \frac{R_p}{R_V}\right)} \tag{1.1}$$

Here, ΔP is the applied suction, R_p is the pipette radius, and R_v is the vesicle radius outside the pipette. From analysis of video images, the area and volume of the vesicles are also determined. For isotropic membranes such as those in this thesis, τ is simple; however, it is rigorously defined, for anisotropic membranes, as the average of the two principle membrane tensions, $\tau = (\tau_1 + \tau_2)/2$. The relationship between the membrane tension and areal strain, $\alpha = (A - A_o) / A_o$, defines the area expansion modulus, K_a:

$$\tau = K_a \alpha \tag{1.2}$$

This equation is one of three first-order conservative relations for surface-isotropic materials.[56] That is, membrane stretching (pure areal strain, without shear or change in curvature) is one of three independent modes of membrane deformation. The second type of deformation is bending (at constant membrane area and zero shear). A change in membrane curvature is defined $\Delta C = \Delta(1/R_c)$, with R_c the radius of curvature. In reality, there can be two principle radii of curvature. The bending moment, M, (the force applied along the membrane contour) then defines the bending modulus, κ_b:

$$M = \kappa_b \Delta(1/R_{c1} + 1/R_{c2}) \tag{1.3}$$

These first two membrane properties, the area expansion and bending moduli have formed the basis for mechanical characterization and ranking of phospholipid and copolymer vesicle membranes. Of note, typical values of K_a for liquid-phase

phospholipid vesicles fall near 160-180 mN /m while bending moduli are order 10kT. [24, 55, 57-59] For phospholipid layers, the sentiment is that this level of bending resistance is negligible as a result of the extreme 2-3 nm bilayer thinness. The original *Science* paper on polymer vesicles reported 120 mN /m and 30kT, for K_a and κ_b, respectively, for 3800 molecular weight copolymer membranes, deemed not to be significant differences from the phospholipid analogs.[24]

The third conservative relation relates shear stress applied to a membrane to shear deformation (at constant area and curvature), and applies only for solid membranes, as fluid membranes cannot sustain a shear load. For fluid membranes, the more relevant property would be a two dimensional shear viscosity, which is impractical to measure because of dissipative coupling between the membrane and the surrounding fluid. However, it is worth noting that there are potentially three rate-dependent properties relating to rates of deformation:[53]

$$\bar{\tau} = \kappa \frac{\partial \ln(1+\alpha)}{\partial t} \tag{1.4}$$

$$\tau = 2\eta \frac{\partial \ln(\bar{\lambda})}{\partial t} \tag{1.5}$$

$$M = \upsilon \frac{\partial(\Delta C)}{\partial t} \tag{1.6}$$

None of these three properties have been evaluated for phospholipid (let alone the newer polymer-based) bilayers, though their potential relevance to the spreading process lies at the heart of this thesis. Indeed, as lateral membrane diffusion is related to the viscosity of the membrane, probe diffusion studies suggest that even low molecular

polymer bilayers are 100 or more times more dissipative in shear compared with fluid phospholipid analogs.[41] The same might be expected to be true for stretching and bending dissipative processes. Tank treading or the rolling forward of a kink in a membrane is an example of bending dissipation.

From the practical perspective, measuring a vesicle's K_a is straightforward using micropipettes.[53] Giant unilamellar vesicles with diameters on the order of 20-30 microns, (so they are about 3 times or more great than the pipette size) are made flaccid before the membrane mechanics measurement, by adjustment of solution osmolarity. Individual vesicles are aspirated into a micropipette and the excess surface area forms a projection inside the pipette, even at very low tensions. Subsequent increases in pipette suction stretch the membrane, causing the projection length to increase measurably, while the main bulb of the vesicle outside the pipette decreases systematically, but to a much smaller extent than the projection increase the result from each increase in suction. The area change is calculated according to

$$\alpha = \frac{2\pi R_p \Delta L}{A_o}\left(1 - \frac{R_p}{R_V}\right) \tag{1.7}$$

This simplification results from the assumption of constant volume over the course of the experiment. This is reasonable as membrane mechanics studies take only about a minute for each vesicle. From Equation 1.7, and the known membrane tension from the LaPlace Equation 1.1, Equation 1.2 provides the area expansion modulus.

Bending moduli are measured in the same fashion as the experiments for the area expansion modulus, except that here the low tension behavior of the force transducers must be carefully calibrated and the zero suction point identified precisely, based on the lack of motion of a micron-scale dust particle near the pipette tip. A flaccid vesicle is then aspirated into the micropipette, and the growth of the projection measured for very small increases in suction pressure. In this regime, the process of vesicle aspiration is one in which the thermal undulations in the main part of the vesicle are removed and translated into the projection, at the cost of bending energy.[60] An assessment of κ_b follows from

$$\kappa_b \approx \frac{k_B T \ln \tau}{8\pi\alpha} \tag{1.8}$$

1.6 From Cell Adhesion to Simpler Systems

The specific binding processes of cell adhesion molecules (integrins, cadherins, ICAM's), and the related ligand-receptor interactions that comprise intercellular communication, take place in the background field of other molecules on the cell surface: a glycocalyx provides electrosteric repulsions while the bending fluctuations of some cells compound this background repulsive field.[30, 61-65] Even without specific receptors, however, cells experience global attractions as a result of van der Waals forces. It is therefore important to think about both the uniform non-specific interactions that drive cells together or provide stabilization, and the complex binding interactions of ligands and receptors.[27, 66]

One important feature concerning any uniform (laterally homogenous) interactions between cells is that they are generally long range, with electrostatic interactions on the order of a nanometer and steric repulsions much longer. These features, combined with van der Waals interactions may place the equilibrium cell separation on the order of several nanometers, which is much greater than the close contact involved with ligand receptor interactions. Hence when combined in biological environments these different types of forces produce complex energy landscapes that govern adhesive interactions. Indeed, simulations of membrane adhesion subject to double well potentials,[67] and treatments of T-cell junctions that involve different receptors with different ranges in their interactions,[68] predict phase separation of the adhesive region between two cells into weakly and strongly binding mains. The general idea that phase separation may be promoted in an adhesion plaque was observed for the first time in an artificial system developed by the Sackmann group.[4, 26, 69-71] There is also reason to expect that adhesive domains may form when adherent membranes are subject to normal forces that attempt to separate vesicles and cells. This separation or domain formation is thought to strengthen the adhesive region.

The level of complexity of interactions that produce phase separated adhesion plaques is an experimental area ripe for study. To move in this direction with a well defined system first requires that the components of such systems be well understood on their own. Indeed, this thesis reveals rich behavior for simple systems with single types of ligands and receptors[72-74] and simple long range-potentials such as the depletion

forces produced by dissolved polymer.[46] The next section of this introduction therefore reviews the basic studies of membranes and interfaces subject to simple long-range attractive forces. This is followed by a discussion of a well-studied ligand-receptor model: avidin-biotin.

1.7 Non-Site Specific Adhesion

Though they are typically classified as weak and usually operate at longer range than ligand-receptor interactions, nonspecific forces contribute in an important way in biology and have been carefully studied with model membranes. For instance, freeze-fracture replicas of adherent egg phosphatidylcholine vesicles in different states of membrane tension (tuned by osmolarity differences between the insides and outsides of vesicles) reveal significant adhesion between flaccid vesicles. This was determined to be the sum of attractive van der Waals and hydrophobic forces, balanced by repulsive hydration, undulation, and electrostatic forces.[75] While these interactions have been measured between a variety of surfaces with many different techniques, that most relevant to this thesis is the use of micropipettes to measure these interactions between phospholipid bilayer vesicles.

Use of micropipette manipulation to measure adhesive forces between two vesicles or between a vesicle and another surface (or between red blood cells) was introduced by Evans several decades ago.[54, 76-78] In these experiments, an adhesive vesicle is aspirated into a micropipette, with its excess area taken up by the projection inside the pipette. The vesicle is then positioned in contact with a target object, which

could be a cell, a solid bead, or another vesicle, and the tension is reduced stepwise to permit adhesion. As adhesion proceeds, the contact zone between a vesicle and the target object increases as does the contact angle. This alteration of the vesicle shape consumes excess area so that the projection inside the pipette is reduced. Increases in tension may cause the vesicle to de-adhere from its substrate (partially or completely), and the projection inside the pipette increases in this case. Though it is not immediately obvious, for reversible vesicle adhesion that has reached mechanical equilibrium, a Young's equation relates the macroscopic contact angle, θ, to the reversible work of adhesion ω_A, per unit area.

$$\omega_A = \tau (1-\cos \theta) \qquad (1.9)$$

Equation 1.9, though simple, is not an obvious result for vesicle adhesion. The proof of its validity was therefore the subject of several publications, focusing on a detailed analysis of vesicle shape and mechanical quantification. Clearly, equation 1.9 holds only when adhesion is truly reversible, in the thermodynamic sense. Then θ corresponds to a free energy reduction (per unit area) for contact formation, essentially a chemical affinity. Of note, in some versions of the application of 1.9, instead of reporting a contact angle, θ, the diameter of the contact zone was instead analyzed.[76-79] This, however, is related to the contact angle through a sine proportionality.[80]

It is worth emphasizing that the type of information provided by the micropipette technique, when the Young's equation is applied, is simply the net binding interaction, resulting for instance, from van der Waals forces or other sources of attraction.[76, 77, 79]

The work of adhesion, in such situations is the energy difference between complete separation of the surfaces and the configuration of the surfaces at their minimum energy, for instance in an attractive well:

$$\omega_a = -\int_{\infty}^{z_0} \sigma_z dz \qquad (1.10)$$

Here z_0 is the separation distance at the attractive minimum. σ_z is the normal force between the membrane and its target, treated as flat plate potential (an approximation which works well due to the large radii of the vesicle / cell curvature compared with the separation distances where attractive forces are significant.)

The micropipette adhesion technique does not measure the local force-distance relationship that can be obtained, for instance using the SFA (surface forces apparatus)[2, 28, 81-85] or AFM (atomic force microscope)[77, 86]. Still the micropipette method is quantitatively rigorous and extremely sensitive (measuring adhesion strengths as low as 0.0001 erg / cm^2). Further, the micropipette method's advantages include its direct potential application to living cells and membranes. With micropipettes, membrane tension can be adjusted and the fluid nature of the membrane preserved, which is not possible in the AFM or SFA, which require rigid supports for membranes.

With micropipettes, Evans could measure surface affinity for a large phospholipid bilayer vesicle with a sensitivity on order of $10^{-4} - 10^{-3}$ erg/cm^2 and for red cell membrane in the range of 10^{-2} – 10 erg / cm.[2,76] Evans and Metcalfe quantified the van der Waals interactions between neutral lecithin bilayers, and reported this adhesion to be completely reversible. A total free energy reduction of 1.5 x 10^{-2} erg / cm^2 was

attributed to combined van der Waals and hydrophobic attractions.[78] While hydrophobic attractions between phospholipid membranes are typically well-shielded by the hydration layer and polar head groups, Evans points out that swelling stresses or the tensions imposed by the micropipettes may stretch the membrane slightly, somewhat exposing the hydrocarbon tails and making the vesicles sticky. Opposing these attractions are hydration forces, electrostatic repulsions, and undulation forces. The latter two are negligible for the neutral vesicles held at moderate tensions in pipettes to reduce the thermal undulations. Though suppressed in micropipette studies, the form for the undulation forces is worth reproducing here as it is related to bending energy[2]:

$$E_{Helfrich}(z) = \frac{(k_B T)^2}{1.6\pi^2 \kappa_b} \frac{1}{z^2} \tag{1.11}$$

Where, κ_b is the bilayer rigidity modulus of curvature. These two contributions depend on the separation distance z between the vesicles

Evans also measured depletion forces between vesicle pairs, induced by dissolved polymer, and showed that the experimental data were in excellent agreement with mean-field estimates of the depletion attractions.[54, 87] In the mean field treatment, Equation 1.10 was integrated to determine the attractive strength. It was proven that σ_r was the osmotic pressure at the center of the gap between two vesicles, minus that in bulk solution.

1.8 Site- Specific Adhesion

Relevant to cell signaling and adhesion, a number of different ligands and receptors act on cell surfaces (integrins, selectins, cadherins, and ICAMs).[26, 88-92] One of the most-studied and experimentally accessible ligand-receptor pairs, however, is avidin-biotin. While typical interactions between conjugated ligands and receptors fall in the range of 5-20 kT (with some much weaker, to produce reversible interactions), the avidin-biotin interaction is extreme, often called the strongest physical bond in nature: 35 kT in free solution, with a free solution de-bonding rate constant, k_d, of 10^{-15} M. Of note, avidin contains separate binding pockets for four biotins, which interact through strong hydrogen bonding.[82, 93]

To quantitatively access this strong physical binding with avidin and biotin, one must avoid the non-specific interactions which make avidin more generally adhesive: Avidin, a 66,000 molecular weight tetrameric glycoprotein of 256 amino acids, is substantially cationic with an isoelectric point near 10.5. Both the positively charged residues and the oligosaccharide component (heterogeneous structures comprised largely of mannose and n-acetylglucosamine) can interact nonspecifically with negatively charged cells and nucleic acids.[94]

A popular, but expensive alternative is streptavidin, a nonglycosylated 52800 molecular weight protein of lower isoelectric point. Streptavidin, however, contains a peptide sequence RYD (Arg-Tyr-Asp) that apparently mimics RGD (Arg-Gly-Asp), a

highly adhesive binding sequence found in fibronectin, a component of the extracellular matrix that promotes cell adhesion.[94, 95]

Another alternative, NeutrAvidin, a patented compound from Pierce Biotechnology, is a non-glycosylated form of avidin with a pI near 6.3, imparting a slight net negative charge at physiological pH. NeutrAvidin lacks the RYD binding sequence eliminating this particular type of cell adhesion in future studies.[96]

Different forms of avidin, streptavidin, and NeutrAvidin have been extensively studied for their capacity to bind targets while immobilized on surfaces. Indeed, these molecules find application in chemical modifications of surfaces, for instance to immobilize enzymes and immunotargets.

Table 1.1 Avidin, Streptavidin, and NeutrAvidin (www.piercenet.com/products/)

	Avidin	Streptavidin	NeutrAvidin
Molecular Weight	67 K	53 K	60 K
Biotin-binding Sites	4	4	4
Isoelectric Point (pI)	10	6.8-7.5	6.3
Specificity	Low	High	Highest
Affinity for Biotin (K_d)	10^{-15} M	10^{-15} M	10^{-15} M
Nonspecific Binding	High	Low	Lowest

Avidin-biotin-driven binding between phospholipid membranes has naturally been a subject of study, given the general interest in avidin-biotin binding. An important work is this area was the investigation, using the surface-forces apparatus (SFA) of binding between avidin and biotins on the distal ends of polyethylene glycol

(PEG) tethers, extending from a surface-immobilized phospholipid bilayer. Without these PEG tethers, the interactions between surface-immobilized avidin and biotins was extremely short range, on the order of 5 Å. With placement of the receptors and ligands on PEG tethers, however, attractions were measurable at very large separations, 160 Å, corresponding to full extension of the modest molecular weight PEG tethers. Of course the exact range of the attraction, along with some kinetic features of the binding was shown to depend on the molecular weight of the PEG tethers.[32, 97]

An interesting point, however, was borne out in a control study: The onset of repulsions between PEG layers not avidin- or biotin-functionalized was shorter ranged than the onset of attractions between the same PEG layers with the ligands and receptors on their distal ends. This suggests that chains stretch across the gap to achieve binding. Said differently, the forming of avidin-biotin bonds exploits fluctuations in PEG chain extension normal to the interface.[85]

In the SFA, the difference between the ranges of the binding attractions and the steric repulsions was further borne out by compressing the bound layers more tightly than the equilibrium separation.[6, 27, 28] This caused a repulsion to be registered, with a form corresponding to steric interactions. In cells and free vesicles, additional repulsions would result from thermal undulations. In either the case of the SFA or free cells and vesicles, the potential experienced between the two surfaces is the sum of attractive and repulsive contributions. With the additional repulsive contribution

between adhesive cells, the equilibrium separation measured in the surface forces is expected to be smaller than that between adherent cells and vesicles.

In the surface forces apparatus, the irreversible nature of the avidin-biotin binding was clear. Upon separation of the adherent surfaces, PEG chains reached their full extensions and separation forces suggested chain pull-out rather than avidin-biotin bond breakage. The observed separation forces were consistent with those of membrane lysis or PEG-lipid pull-out 23 pN, as opposed to breakage of biotin-streptavidin bonds, > 130 pN.

1.9 Ligand-Receptor–Driven Vesicle Adhesion

There have been some important studies of avidin-biotin binding at fluid interfaces. The most relevant of these to the current thesis is the work by Noppl-Simson employing dual micropipette aspiration to study the binding kinetics of vesicles containing 5 mol% or less avidin-biotin functionality.[97] In this study, the avidin and biotin moieties were placed on PEG arms (of 750 molecular weight) to facilitate adhesion. The study included basic characterization of lipid mobility and calibrations for the density of avidin functionality, providing a benchmark for one of our studies, in Chapter 3, where some explicit comparisons are made. The Noppl-Simson study is one of the few to document the adhesion and spreading kinetics between avidin- and biotin-functionalized vesicles. In some cases, with the denser (5 mol%) functionality, spreading was rapid; however, in all cases, it was irreversible: Vesicles could not be separated without rupture. This study demonstrated that the spreading rates were

limited by diffusion of functionalized groups to the adhesion plaque and explicitly demonstrated, by fluorescent labeling, the concentration of receptors in the bonded region, relative to the rest of the vesicle. This observation motivated analysis based on the spreading pressure as a chemical driving force for spreading.

In separate but related work, DSPC vesicles were studied, with PEG functionalization to make a bimodal brush.[32] Avidin-biotin functionality placed on long PEG arms; however, vesicles also contained and unfunctionalized shorter PEG arms for stability, and to prevent protein adsorption. Vesicle detachment forces on the order of 100 nN were reported, compared with the avidin-biotin attraction of 80 pN. The greater detachment force suggests substantial dissipative membrane contributions prior to interfacial failure, still most likely through pull-out rather than avidin-biotin bond breakage.

Besides vesicle adhesion driven by avidin-biotin binding, a number of other ligand-receptor pairs have been studied with dual micropipettes. Notably, the Pincet lab compared the adhesion energies obtained via micropipettes to those from the SFA, for biotin-streptavidin binding and for antibody binding to the CD10 receptor of B-cells.[98] Comparison of SFA and micropipette adhesion data for glycolipids demonstrated that even though these molecules were relatively low in molecular weight, their treatment via polymer theory adequately explained the combined observations.[99] The dual micropipette method was also employed to characterize the carbohydrate recognition by LewisX determinants (relative to the Ca^{2+} homotypic interaction) for glycosides with

different head group flexibilities and size (500-1500 molecular weight).[100] Adhesion between vesicles carrying nucleosides was also studied: the non-specific adhesion of adenosine and thymidine was differentiated from their specific binding interactions.[101] The dual micropipette method has also been extended to characterize attractions from metal coordination bonding such as that between nitrilotriacetate groups sharing a nickel ion.[102]

In these studies in which vesicles membranes were held in micropipettes, the excess area of the membrane was taken up in the projection in the pipette, smoothing out thermal undulations. While this reduces the Helfrich repulsion, it also affects the spreading mechanism, as the rate at which vesicles spread by a crack closing mechanism depends on the probability of binding ahead of the closed region of the gap.[103] Hence these micropipette studies of adhesion are quite different in mechanism from those in which flaccid vesicles settle on a surface of adhesive complimentarity.

In a series of model systems of increasing complexity developed in the Sackmann lab,[26, 62, 95, 104-106] the adhesion of heavy flaccid vesicles to planar surfaces comprising the floor of the sample chamber was studied with reflectance interference contrast microscopy. This technique employs the interference pattern set up by a vesicle and the substrate, especially that in the "crack tip" where the vesicle starts to curve up from the substrate, to describe the evolving contour of the spreading vesicle. In this regard, the technique is similar to contact angle measurements with micropipettes, except that RICM is much higher in resolution and provides information about the

shape of the membrane in the regime where the macroscopic contact angle is established. Sackmann et al used the method to quantify the sizes and growth rates of tightly adherent contact nuclei in membranes near zero tension, providing impetus for much theoretic modeling. Most notably, Boulbitch *et al.*[103] measured spreading rates of vesicles functionalized with cell adhesion molecules, and identified diffusion-limited and surface kinetic limited regimes for that particular system. Cuvelier and Nassoy,[80] in a study more relevant to the current thesis, employed the method to study avidin-biotin driven adhesion kinetics of flaccid vesicles on avidin-functionalized solid substrates. Their results turned out to be greatly dependent on how the avidin was immobilized on the solid support, raising the more general issue that the chemical handling of biomolecules can have a huge impact on their binding strengths and kinetics. This truth makes comparison of data between different laboratories challenging, or at least a process which, though absolutely necessary, should be undertaken with some care.

1.10 Adhesion of Polymer Vesicles

At the time this thesis program was initiated, there were no reports in the literature of adhesion involving polymer vesicles. Since that time, the Hammer lab at the University of Pennsylvania is the only group to publish on polymer vesicle adhesion.[37, 107] Their inaugural studies employed micropipettes to measure the adhesion strengths between a biotinylated polybutadiene vesicle and an avidin-coated solid bead. They found, first of all, that the avidin-driven binding was fairly reversible, in the sense that the biotinylated vesicle could be peeled from the avidin-bead, and adhesion

experiments reproduced. Therefore, critical peeling forces were measured, the strongest of which was 0.45 mN/m. This binding strength is on the order of that reported for strong depletion forces,[54, 87] making the value somewhat small compared with expectations based on avidin-biotin being the strongest physical bond in nature. This small peeling forces observed in the Hammer lab are also surprising in light of the many other labs that report avidin-biotin binding of vesicle membranes to be nearly irreversible. (Of note, the vesicle-bead adhesion study in the Hammer lab involved densely functionalized surfaces such that many bonds were expected to form in the contact zone. Therefore, the issue of biotin-avidin binding reversibility is not the same as raised by Evans: In dynamic force spectroscopy studies of single-ligand receptor bonds,[17, 108] slow application of force can allow even the strongest of bonds to be disrupted, with binding forces quantified. In the case where many bonds are formed, pulling slowly will not substantially increase the chances of disbonding.) Given Cuvelier's observation of the sensitivity of avidin binding strength to the surface preparation method, a reasonable explanation for the data published by Hammer, is that the avidin on the solid support was somehow compromised by its method of surface immobilization. It is worth pointing out however, that even with adhesion forces of 0.45 mN/m, Evans' observations with van der Waals,[78] and particularly with depletion forces,[54, 109] suggest that more spreading and larger contact angles would be expected between biotin vesicles and avidin beads than those appearing in the publications from the Hammer lab. This apparent discrepancy between reported adhesion strength and the appearance of the vesicles themselves is explained by the work in this thesis:

membrane mechanics, particularly those of polymer membranes, alter the adhesion and spreading behavior of vesicles.

With polymer vesicles, the Hammer group studied the impact of functionalization on bimodal brushes.[37, 38, 107, 110] An important conclusion was that the best binding behavior was observed for a truly bimodal interface: Functionalization of brushes that were either all short, or nearly all long set up competition between the steric entropy of the chains, and the adhesion of the "sticky" end groups. Bimodal brush architecture placing functionality out beyond the steric layer best facilitated adhesion. This principle was established firmly using the avidin-biotin model, and later extended to antibody-target binding. In all cases, however, 0.45 mN /m was the strongest adhesion reported, and a substantial contact angle or spreading was never reported. (Notably, avidin was employed as a means to further modify the bead surface in the antibody studies.)

1.11 This Thesis: The Role of Membrane Mechanics in Vesicle Adhesion and Spreading

The current work on polymer vesicle adhesion distinguishes itself from the prior literature in several regards: First, this program has focused not only on quantifying the adhesion strengths obtainable in vesicles adhesion, it has, through the study of adhesion dynamics, scrutinized the mechanism for vesicles spreading, engulfment, and establishing of a thermodynamically meaningful contact angle. This work describes the

adhesion between two fluid vesicles in the tensed regime, where thermal undulations are suppressed by holding vesicles in micropipettes. This level of qualification alone narrows the focus of the work considerably, such that the most relevant prior papers are those of Noppl-Simson and Needham[97], Cuvelier and Nassoy[80], and Boulbitch *et al*[103]., with the last two papers focusing on flaccid rather than tensed vesicles. The current work simplifies the situation studies by Noppl-Simson and Needham by focusing on the densely functionalized regime of avidin-biotin binding: In our case, spreading kinetics cannot be limited by diffusion of functionalized molecules within the membrane. Rather this thesis focuses on membrane binding physics and not transport properties.

As we did not wish to define our physical membrane model so narrowly that the results might be looked upon as applicable to only a few cases, this program also benchmarks the binding dynamics of densely functionalized membranes against depletion forces, which act uniformly, rather than point wise, at an interface.

Most importantly, however, this work has exploited polymer vesicles as a means of probing the influence of membrane mechanics on adhesion and spreading kinetics. While this work comprises the first study of adhesion between polymer vesicle pairs (as opposed to a polymer vesicle and a bead) making it fairly unique and significant to the field of polymer vesicles, it was the versatility of polymer vesicles that enabled the coupling between adhesion and membrane mechanics to be deeply probed. This thesis reveals a rich parameter space in which vesicle adhesion may be strong (indeed completely irreversible) or weak, and spreading delayed or altogether prevented by the

bending cost associated with vesicle shapes during spreading. Of particular note, some of the most dramatic behaviors observed in this work involved polymer vesicles of modest (3800) molecular weight whose bending moduli were elevated, but not conspicuously so, relative to phospholipid vesicles. This makes the point that the mechanical properties of "polymersomes", though only slightly different from those of phospholipids, can have dramatic impact on processes where the bending energy appears in an exponential term of, for instance, a rate law.

The impact of these findings is first relevant to the interpretation of contact angles a means of assessing adhesion energies in the micropipette technique. One must first be confident that the contact angle observed is that corresponding to equilibrium and not a metastable value influenced by bending energy. Beyond this technicality, however, bending is potentially important in biology: Uptake of viral and drug delivery particles via endocytosis requires very sharp bending of a cell membrane which may not be overcome by binding energy. This may be especially important for cells whose effective surface bending moduli can be much higher than that of phospholipid bilayers, as a result of coupling to the actin cortex.

The remainder of this thesis is organized as follows:

Chapter 2 provides a detailed description of the copolymers employed in our study, the vesicle formation technique, and chemistry employed to modify attach avidin and biotin to the polymer vesicles for the particular studies of ligand-receptor adhesion. Two vesicle-forming copolymers are introduced: A PDMS-PEO [poly(dimethyl

siloxane) – poly(ethylene oxide)] graft copolymer possessing phospholipid-like bending flexibility and a PBD-PEO [poly(butadiene)-PEO] diblock copolymer that is considerably stiffer.

Chapter 3 provides a broad but thorough perspective on the qualitative and quantitative features of irreversible ligand-receptor-driven adhesion plaque formation between flexible vesicle pairs densely functionalized with avidin and biotin, and held at moderate membrane tensions in micropipettes. The work focuses on the regime where, due to a large number of adhesive groups per area, there is no need for lateral diffusion in the development of an adhesion plaque. The chapter introduces the observation of 3-stage spreading kinetics, including a latent or pre-spreading stage, a sudden and rapid spreading stage, and a subsequent slower growth of the contact zone. Also introduced is the observation that chemical modification of the polymer with avidin and biotin alter the mechanical properties, a topic developed throughout the thesis as a secondary theme. The geometrical aspects of the adhesion and spreading process are analyzed, and bounds placed on the adhesion strength, demonstrating that, based on the observed contact angles, our adhesion strengths are stronger than previously reported in vesicle adhesion studies. The impact of membrane tension was closely examined and none was found for vesicles held reasonably taut, 0.1 – 1 mN /m.

Chapter 4 more closely examines the physics of flexible membrane adhesion and spreading, driven by avidin-biotin binding in the densely functionalized (non-diffusive) regime. In particular, the impact of the density of avidin and biotin functionality is

considered, with variations in receptor density sufficient to show important kinetic behaviors, still staying in the regime where membrane diffusion is unimportant to the development of the adhesion plaque. The duration of the pre-spreading period is scrutinized and interpreted in the context of nucleation theory for a critical amount of adhesion needed to overcome the bending energy associated with vesicle shapes during spreading.

Chapter 5 more broadly develops the concept that membrane bending energy can be an important detractor from adhesion plaque growth and spreading. Here a quantitative interpretation is aggressively pursued through the study of vesicle membranes of different bending stiffnesses and through the extension from ligand-receptor attractions to depletion attractions which are carefully quantified and compared with mean field treatments. The adhesion nucleation model is further developed and used to predict conditions where spreading is prevented by membrane bending energy. The duration of the pre-spreading period is further analyzed and shown consistent with that of an activated process.

Chapter 6 discusses potential extension of the work presented here and makes suggestions for future work.

REFERENCE

1. Korlach, J.; Schwille, P.; Webb, W. W.; Feigenson, G. W., Characterization of lipid bilayer phases by confocal microscopy and fluorescence correlation spectroscopy. *Proceedings of the National Academy of Sciences of the United States of America* **1999,** 96, (15), 8461-8466.

2. Cevc, G.; Marsh, D., Phospholipid Bilayers (Wiley, New York). **1987.**

3. McIntyre, J. C.; Sleight, R. G., Fluorescence assay for phospholipid membrane asymmetry. *Biochemistry* **1991,** 30, (51), 11819-11827.

4. Sackmann, E.; Feder, T., Budding, fission and domain formation in mixed lipid vesicles induced by lateral phase-separation and macromolecular condensation. *Molecular Membrane Biology* **1995,** 12, (1), 21-28.

5. Gregoriadis, G.; Florence, A. T., Liposomes in drug delivery - clinical, diagnostic and ophthalmic potential. *Drugs* **1993,** 45, (1), 15-28.

6. Israelachvili, J. N.; Wennerstrom, H., Entropic forces between amphiphilic surfaces in liquids. *Journal of Physical Chemistry* **1992,** 96, (2), 520-531.

7. Jahnig, F., Molecular theory of lipid-membrane order. *Journal of Chemical Physics* **1979,** 70, (7), 3279-3290.

8. Helfrich, W., Steric interaction of fluid membranes in multilayer systems. *Zeitschrift Fur Naturforschung Section a-a Journal of Physical Sciences* **1978,** 33, (3), 305-315.

9. Helfrich, W., Elastic properties of lipid bilayers - theory and possible experiments. *Zeitschrift Fur Naturforschung C-a Journal of Biosciences* **1973,** C 28, (11-1), 693-703.

10. Trauble, H.; Sackmann, E., Studies of crystalline-liquid crystalline phase-transition of lipid model membranes .3. structure of a steroid-lecithin system below and above lipid-phase transition. *Journal of the American Chemical Society* **1972,** 94, (13), 4499-&.

11. Allen, T. M.; Hansen, C., Pharmacokinetics of stealth versus conventional liposomes - effect of dose. *Biochimica Et Biophysica Acta* **1991,** 1068, (2), 133-141.

12. Lasic, D. D., Novel applications of liposomes. *Trends in Biotechnology* **1998,** 16, (7), 307-321.

13. Lane, P. J. L.; McConnell, F. M.; Clark, E. A.; Mellins, E., Rapid signaling to b-cells by antigen-specific t-cells requires cd18 cd54 interaction. *Journal of Immunology* **1991,** 147, (12), 4103-4108.

14. D'Souza-Schorey, C.; Boettner, B.; Van Aelst, L., Rac regulates integrin-mediated spreading and increased adhesion of T lymphocytes. *Molecular and Cellular Biology* **1998,** 18, (7), 3936-3946.

15. Evans, E.; Heinrich, V.; Leung, A.; Kinoshita, K., Nano- to microscale dynamics of P-selectin detachment from leukocyte interfaces. I. Membrane separation from the cytoskeleton. *Biophysical Journal* **2005,** 88, (3), 2288-2298.

16. Evans, E.; Leung, A.; Heinrich, V.; Zhu, C., Mechanical switching and coupling between two dissociation pathways in a P-selectin adhesion bond. *Proceedings of the National Academy of Sciences of the United States of America* **2004,** 101, (31), 11281-11286.

17. Evans, E.; Heinrich, V.; Ludwig, F.; Rawicz, W., Dynamic tension spectroscopy and strength of biomembranes. *Biophysical Journal* **2003,** 85, (4), 2342-2350.

18. Zamir, E.; Geiger, B., Molecular complexity and dynamics of cell-matrix adhesions. *Journal of Cell Science* **2001,** 114, (20), 3583-3590.

19. Kumar, S.; Hoh, J. H., Direct visualization of vesicle-bilayer complexes by atomic force microscopy. *Langmuir* **2000,** 16, (25), 9936-9940.

20. Duzgunes, N.; Delima, M. C. P.; Stamatatos, L.; Flasher, D.; Alford, D.; Friend, D. S.; Nir, S., Fusion activity and inactivation of influenza-virus - kinetics of low ph-induced fusion with cultured-cells. *Journal of General Virology* **1992,** 73, 27-37.

21. Cathcart, M. K.; Culp, L. A., Phospholipid-composition of substrate adhesion sites of normal, virus-transformed, and revertant murine cells. *Biochemistry* **1979,** 18, (7), 1167-1176.

22. Vittet, D.; Prandini, M. H.; Berthier, R.; Schweitzer, A.; MartinSisteron, H.; Uzan, G.; Dejana, E., Embryonic stem cells differentiate in vitro to endothelial cells through successive maturation steps. *Blood* **1996,** 88, (9), 3424-3431.

23. Discher, D. E.; Eisenberg, A., Polymer vesicles. *Science* **2002,** 297, (5583), 967-973.

24. Discher, B. M.; Won, Y. Y.; Ege, D. S.; Lee, J. C. M.; Bates, F. S.; Discher, D. E.; Hammer, D. A., Polymersomes: Tough vesicles made from diblock copolymers. *Science* **1999,** 284, (5417), 1143-1146.

25. Radler, J.; Sackmann, E., Imaging optical thicknesses and separation distances of phospholipid-vesicles at solid-surfaces. *Journal De Physique Ii* **1993,** 3, (5), 727-748.

26. Albersdorfer, A.; Feder, T.; Sackmann, E., Adhesion-induced domain formation by interplay of long-range repulsion and short-range attraction force: A model membrane study. *Biophysical Journal* **1997,** 73, (1), 245-257.

27. Helm, C. A.; Knoll, W.; Israelachvili, J. N., Measurement of ligand receptor interactions. *Proceedings of the National Academy of Sciences of the United States of America* **1991,** 88, (18), 8169-8173.

28. Wong, J. Y.; Kuhl, T. L.; Israelachvili, J. N.; Mullah, N.; Zalipsky, S., Direct measurement of a tethered ligand-receptor interaction potential. *Science* **1997,** 275, (5301), 820-822.

29. Bloom, M.; Evans, E.; Mouritsen, O. G., Physical-properties of the fluid lipid-bilayer component of cell-membranes - a perspective. *Quarterly Reviews of Biophysics* **1991,** 24, (3), 293-397.

30. Hammer, D. A.; Tirrell, M., Biological adhesion at interfaces. *Annual Review of Materials Science* **1996,** 26, 651-691.

31. Limozin, L.; Barmann, M.; Sackmann, E., On the organization of self-assembled actin networks in giant vesicles. *European Physical Journal E* **2003,** 10, (4), 319-330.

32. Kim, D. H.; Klibanov, A. L.; Needham, D., The influence of tiered layers of surface-grafted poly(ethylene glycol) on receptor-ligand-mediated adhesion between phospholipid monolayer-stabilized microbubbles and coated class beads. *Langmuir* **2000,** 16, (6), 2808-2817.

33. Maier, C. W.; Behrisch, A.; Kloboucek, A.; Simson, D. A.; Merkel, R., Specific biomembrane adhesion - Indirect lateral interactions between bound receptor molecules. *European Physical Journal E* **2001,** 6, (4), 273-276.

34. Fendler, J. H., Polymerized Surfactant Vesicles - Novel Membrane Mimetic Systems. *Science* **1984,** 223, (4639), 888-894.

35. Hill, R. M.; He, M. T.; Lin, Z.; Davis, H. T.; Scriven, L. E., Lyotropic liquid-crystal phase-behavior of polymeric siloxane surfactants. *Langmuir* **1993,** 9, (11), 2789-2798.

36. Bermudez, H.; Brannan, A. K.; Hammer, D. A.; Bates, F. S.; Discher, D. E., Molecular weight dependence of polymersome membrane structure, elasticity, and stability. *Macromolecules* **2002,** 35, (21), 8203-8208.

37. Lin, J. J.; Ghoroghchian, P.; Zhang, Y.; Hammer, D. A., Adhesion of antibody-functionalized polymersomes. *Langmuir* **2006,** 22, (9), 3975-3979.

38. Silas, J. A.; Lin, J.; Bates, F. S.; Hammer, D. A., Mechanics of adhesion at the surface of polymer vesicles. *Abstracts of Papers of the American Chemical Society* **2006,** 231.

39. Nam, J.; Santore, M. M., Adhesion plaque formation dynamics between polymer vesicles in the limit of highly concentrated binding sites. *Langmuir* **2007,** 23, (13), 7216-7224.

40. Won, Y. Y.; Paso, K.; Davis, H. T.; Bates, F. S., Comparison of original and cross-linked wormlike micelles of poly(ethylene oxide-b-butadiene) in water: Rheological properties and effects of poly(ethylene oxide) addition. *Journal of Physical Chemistry B* **2001,** 105, (35), 8302-8311.

41. Lee, J. C. M.; Bermudez, H.; Discher, B. M.; Sheehan, M. A.; Won, Y. Y.; Bates, F. S.; Discher, D. E., Preparation, stability, and in vitro performance of vesicles made with diblock copolymers. *Biotechnology and Bioengineering* **2001,** 73, (2), 135-145.

42. Hillmyer, M. A.; Bates, F. S., Synthesis and characterization of model polyalkane-poly(ethylene oxide) block copolymers. *Macromolecules* **1996,** 29, (22), 6994-7002.

43. Webster, O. W., Living polymerization methods. *Science* **1991,** 251, (4996), 887-893.

44. Choucair, A.; Soo, P. L.; Eisenberg, A., Active loading and tunable release of doxorubicin from block copolymer vesicles. *Langmuir* **2005,** 21, (20), 9308-9313.

45. McCormick, C. L.; Kirkland, S. E.; York, A. W., Synthetic routes to stimuli-responsive micelles, vesicles, and surfaces via controlled/living radical polymerization. *Polymer Reviews* **2006,** 46, (4), 421-443.

46. Evans, E.; Klingenberg, D. J.; Rawicz, W.; Szoka, F., Interactions between polymer-grafted membranes in concentrated solutions of free polymer. *Langmuir* **1996,** 12, (12), 3031-3037.

47. Cornelissen, J.; Fischer, M.; Sommerdijk, N.; Nolte, R. J. M., Helical superstructures from charged poly(styrene)-poly(isocyanodipeptide) block copolymers. *Science* **1998,** 280, (5368), 1427-1430.

48. Lin, Z.; Hill, R. M.; Davis, H. T.; Scriven, L. E.; Talmon, Y., Cryo-Transmission Electron-Microscopy Study of Vesicles and Micelles in Siloxane Surfactant Aqueous-Solutions. *Langmuir* **1994,** 10, (4), 1008-1011.

49. Rodriguez, N.; Pincet, F.; Cribier, S., Giant vesicles formed by gentle hydration and electroformation: A comparison by fluorescence microscopy. *Colloids and Surfaces B-Biointerfaces* **2005,** 42, (2), 125-130.

50. Angelova, M. I.; Dimitrov, D. S., Swelling of Charged Lipids and Formation of Liposomes on Electrode Surfaces. *Molecular Crystals and Liquid Crystals* **1987,** 152, 89-104.

51. Dimitrov, D. S.; Angelova, M. I., Lipid swelling and liposome formation mediated by electric-fields. *Bioelectrochemistry and Bioenergetics* **1988,** 19, (2), 323-336.

52. Santore, M. M.; Discher, D. E.; Won, Y. Y.; Bates, F. S.; Hammer, D. A., Effect of surfactant on unilamellar polymeric vesicles: Altered membrane properties and stability in the limit of weak surfactant partitioning. *Langmuir* **2002,** 18, (20), 7299-7308.

53. Evans, E.; Needham, D., Physical-Properties of Surfactant Bilayer-Membranes - Thermal Transitions, Elasticity, Rigidity, Cohesion, and Colloidal Interactions. *Journal of Physical Chemistry* **1987,** 91, (16), 4219-4228.

54. Evans, E.; Needham, D., Attraction between lipid bilayer-membranes in concentrated-solutions of nonadsorbing polymers - comparison of mean-field theory with measurements of adhesion energy. *Macromolecules* **1988,** 21, (6), 1822-1831.

55. Rawicz, W.; Olbrich, K. C.; McIntosh, T.; Needham, D.; Evans, E., Effect of chain length and unsaturation on elasticity of lipid bilayers. *Biophysical Journal* **2000,** 79, (1), 328-339.

56. Evans, E., Adhesion of Surfactant Membrane Covered Droplets - Special Features and Curvature Elasticity Effects. *Colloids and Surfaces* **1990,** 43, (2-4), 327-347.

57. Evans, E.; Rawicz, W., Entropy-Driven Tension and Bending Elasticity in Condensed-Fluid Membranes. *Physical Review Letters* **1990,** 64, (17), 2094-2097.

58. Heinrich, V.; Rawicz, W., Automated, high-resolution micropipet aspiration reveals new insight into the physical properties of fluid membranes. *Langmuir* **2005,** 21, (5), 1962-1971.

59. Claessens, M.; van Oort, B. F.; Leermakers, F. A. M.; Hoekstra, F. A.; Stuart, M. A. C., Charged lipid vesicles: Effects of salts on bending rigidity, stability, and size. *Biophysical Journal* **2004,** 87, (6), 3882-3893.

60. McIntosh, T. J.; Advani, S.; Burton, R. E.; Zhelev, D. V.; Needham, D.; Simon, S. A., Experimental Tests for Protrusion and Undulation Pressures in Phospholipid-Bilayers. *Biochemistry* **1995,** 34, (27), 8520-8532.

61. Haluska, C. K.; Riske, K. A.; Marchi-Artzner, V.; Lehn, J. M.; Lipowsky, R.; Dimova, R., Time scales of membrane fusion revealed by direct imaging of vesicle fusion with high temporal resolution. *Proceedings of the National Academy of Sciences of the United States of America* **2006,** 103, (43), 15841-15846.

62. Sackmann, E., Thermo-elasticity and adhesion as regulators of cell membrane architecture and function. *Journal of Physics-Condensed Matter* **2006,** 18, (45), R785-R825.

63. Coombs, D.; Dembo, M.; Wofsy, C.; Goldstein, B., Equilibrium thermodynamics of cell-cell adhesion mediated by multiple ligand-receptor pairs. *Biophysical Journal* **2004,** 86, (3), 1408-1423.

64. Bell, G. I., Models for Specific Adhesion of Cells to Cells. *Science* **1978,** 200, (4342), 618-627.

65. Bell, G. I.; Dembo, M.; Bongrand, P., Cell-adhesion - competition between nonspecific repulsion and specific bonding. *Biophysical Journal* **1984,** 45, (6), 1051-1064.

66. Leckband, D., Novel recognition mechanisms in biological adhesion. *Current Opinion in Colloid & Interface Science* **2001,** 6, (5-6), 498-505.

67. Hategan, A.; Law, R.; Kahn, S.; Discher, D. E., Adhesively-tensed cell membranes: Lysis kinetics and atomic force microscopy probing. *Biophysical Journal* **2003,** 85, (4), 2746-2759.

68. Hori, Y.; Raychaudhuri, S.; Chakraborty, A. K., Analysis of pattern formation and phase separation in the immunological synapse. *Journal of Chemical Physics* **2002,** 117, (20), 9491-9501.

69. Sackmann, E.; Kas, J.; Radler, J., On shape transformations and shape fluctuations of cellular compartments and vesicles. *Physica Scripta* **1993,** T49A, 111-118.

70. Sackmann, E., Membrane bending energy concept of vesicle-shape and cell-shape and shape-transitions. *Febs Letters* **1994,** 346, (1), 3-16.

71. Simon, J.; Kuhner, M.; Ringsdorf, H.; Sackmann, E., Polymer-induced shape changes and capping in giant liposomes. *Chemistry and Physics of Lipids* **1995,** 76, (2), 241-258.

72. Smith, A. S.; Seifert, U., Effective adhesion strength of specifically bound vesicles. *Physical Review E* **2005,** 71, (6).

73. Pincet, F.; Husson, J., The solution to the streptavidin-biotin paradox: The influence of history on the strength of single molecular bonds. *Biophysical Journal* **2005,** 89, (6), 4374-4381.

74. Pincet, F.; Le Bouar, T.; Zhang, Y. M.; Esnault, J.; Mallet, J. M.; Perez, E.; Sinay, P., Ultraweak sugar-sugar interactions for transient cell adhesion. *Biophysical Journal* **2001,** 80, (3), 1354-1358.

75. Bailey, S. M.; Chiruvolu, S.; Israelachvili, J. N.; Zasadzinski, J. A. N., Measurements of Forces Involved in Vesicle Adhesion Using Freeze-Fracture Electron-Microscopy. *Langmuir* **1990,** 6, (7), 1326-1329.

76. Evans, E. A., Analysis of adhesion of large vesicles to surfaces. *Biophysical Journal* **1980,** 31, (3), 425-431.

77. Evans, E. A., Minimum energy analysis of membrane deformation applied to pipet aspiration and surface-adhesion of red-blood-cells. *Biophysical Journal* **1980,** 30, (2), 265-284.

78. Evans, E.; Metcalfe, M., Free-Energy Potential for Aggregation of Giant, Neutral Lipid Bilayer Vesicles by Vanderwaals Attraction. *Biophysical Journal* **1984,** 46, (3), 423-426.

79. Evans, E. A., Analysis of Adhesion of Large Vesicles to Surfaces. *Biophysical Journal* **1980,** 31, 425-432.

80. Cuvelier, D.; Nassoy, P., Hidden dynamics of vesicle adhesion induced by specific stickers. *Physical Review Letters* **2004,** 93, (22).

81. Moy, V. T.; Florin, E. L.; Gaub, H. E., Intermolecular Forces and Energies between Ligands and Receptors. *Science* **1994,** 266, (5183), 257-259.

82. Green, N. M., Avidin and Streptavidin. *Methods in Enzymology* **1990,** 184, 51-67.

83. Kuhl, T. L.; Berman, A. D.; Hui, S. W.; Israelachvili, J. N., Part 1. Direct measurement of depletion attraction and thin film viscosity between lipid bilayers in aqueous polyethylene glycol solutions. *Macromolecules* **1998,** 31, (23), 8250-8257.

84. Kuhl, T. L.; Berman, A. D.; Hui, S. W.; Israelachvili, J. N., Part 2. Crossover from depletion attraction to adsorption: Polyethylene glycol induced electrostatic repulsion between lipid bilayers. *Macromolecules* **1998,** 31, (23), 8258-8263.

85. Jeppesen, C.; Wong, J. Y.; Kuhl, T. L.; Israelachvili, J. N.; Mullah, N.; Zalipsky, S.; Marques, C. M., Impact of polymer tether length on multiple ligand-receptor bond formation. *Science* **2001,** 293, (5529), 465-468.

86. Pignataro, B.; Steinem, C.; Galla, H. J.; Fuchs, H.; Janshoff, A., Specific adhesion of vesicles monitored by scanning force microscopy and quartz crystal microbalance. *Biophysical Journal* **2000,** 78, (1), 487-498.

87. Evans, E. A., Force between surfaces that confine a polymer-solution - derivation from self-consistent field-theories. *Macromolecules* **1989,** 22, (5), 2277-2286.

88. Lasky, L. A., Selectins - interpreters of cell-specific carbohydrate information during inflammation. *Science* **1992,** 258, (5084), 964-969.

89. Chu, Y. S.; Thomas, W. A.; Eder, O.; Pincet, F.; Perez, E.; Thiery, J. P.; Dufour, S., Force measurements in E-cadherin-mediated cell doublets reveal rapid adhesion strengthened by actin cytoskeleton remodeling through Rac and Cdc42. *Journal of Cell Biology* **2004,** 167, (6), 1183-1194.

90. Martinez-Rico, C.; Pincet, F.; Perez, E.; Thiery, J. P.; Shimizu, K.; Takai, Y.; Dufour, S., Separation force measurements reveal different types of modulation of E-cadherin-based adhesion by nectin-1 and-3. *Journal of Biological Chemistry* **2005,** 280, (6), 4753-4760.

91. Lawrence, M. B.; Springer, T. A., Leukocytes roll on a selectin at physiological flow-rates - distinction from and prerequisite for adhesion through integrins. *Cell* **1991,** 65, (5), 859-873.

92. Bevilacqua, M. P., Endothelial-leukocyte adhesion molecules. *Annual Review of Immunology* **1993,** 11, 767-804.

93. Livnah, O.; Bayer, E. A.; Wilchek, M.; Sussman, J. L., 3-Dimensional Structures of Avidin and the Avidin-Biotin Complex. *Proceedings of the National Academy of Sciences of the United States of America* **1993,** 90, (11), 5076-5080.

94. Hiller, Y.; Gershoni, J. M.; Bayer, E. A.; Wilchek, M., Biotin binding to avidin - oligosaccharide side-chain not required for ligand association. *Biochemical Journal* **1987,** 248, (1), 167-171.

95. Marchi-Artzner, V.; Lorz, B.; Gosse, C.; Jullien, L.; Merkel, R.; Kessler, H.; Sackmann, E., Adhesion of Arg-Gly-Asp (RGD) peptide vesicles onto an integrin surface: Visualization of the segregation of RGD ligands into the adhesion plaques by fluorescence. *Langmuir* **2003,** 19, (3), 835-841.

96. Woolley, D. W.; Longsworth, L. G., Isolation of an antibiotin factor from egg white. *J. Biol. Chem.* **1942,** 142, 285-90.

97. Noppl, D. A.; Needham, D., Avidin-biotin interactions at vesicle surfaces: Adsorption and binding, cross bridge formation, and lateral interactions. *Biophysical Journal* **1996,** 70, (2), SU359-SU359.

98. Sarda, S.; Pointu, D.; Pincet, F.; Henry, N., Specific recognition of macroscopic objects by the cell surface: Evidence for a receptor density threshold revealed by micrometric particle binding characteristics. *Biophysical Journal* **2004,** 86, (5), 3291-3303.

99. Gourier, C.; Pincet, F.; Le Bouar, T.; Zhang, Y.; Esnault, J.; Mallet, J. M.; Sinay, P.; Perez, E., Can small complex chains be treated as polymers? *Macromolecules* **2004,** 37, (23), 8778-8784.

100. Gourier, C.; Pincet, F.; Perez, E.; Zhang, Y. M.; Zhu, Z. Y.; Mallet, J. M.; Sinay, P., The natural Lewis(X)-bearing lipids promote membrane adhesion: Influence of ceramide on carbohydrate-carbohydrate recognition. *Angewandte Chemie-International Edition* **2005,** 44, (11), 1683-1687.

101. Pincet, F.; Perez, E.; Loudet, J. C.; Lebeau, L., From macroscopic adhesion energy to molecular bonds: A test of the theory. *Physical Review Letters* **2001,** 8717, (17).

102. Tareste, D.; Pincet, F. R.; Brellier, M.; Mioskowski, C.; Perez, E., The binding energy of two nitrilotriacetate groups sharing a nickel ion. *Journal of the American Chemical Society* **2005,** 127, (11), 3879-3884.

103. Boulbitch, A.; Guttenberg, Z.; Sackmann, E., Kinetics of membrane adhesion mediated by ligand-receptor interaction studied with a biomimetic system. *Biophysical Journal* **2001,** 81, (5), 2743-2751.

104. Bruinsma, R.; Behrisch, A.; Sackmann, E., Adhesive switching of membranes: Experiment and theory. *Physical Review E* **2000,** 61, (4), 4253-4267.

105. Ratanabanangkoon, P.; Gropper, M.; Merkel, R.; Sackmann, E.; Gast, A. P., Mechanics of streptavidin-coated giant lipid bilayer vesicles: A micropipet study. *Langmuir* **2003,** 19, (4), 1054-1062.

106. Sackmann, E.; Goennenwein, S., Cell adhesion as dynamic interplay of lock-and-key, generic and elastic forces. *Progress of Theoretical Physics Supplement* **2006**, (165), 78-99.

107. Lin, J. J.; Silas, J. A.; Bermudez, H.; Milam, V. T.; Bates, F. S.; Hammer, D. A., The effect of polymer chain length and surface density on the adhesiveness of functionalized polymersomes. *Langmuir* **2004,** 20, (13), 5493-5500.

108. Evans, E. A.; Calderwood, D. A., Forces and bond dynamics in cell adhesion. *Science* **2007,** 316, (5828), 1148-1153.

109. Evans, E.; Klingenberg, D., Adhesion of polymer-grafted membrane-vesicles in concentrated-solutions of nonadsorbing free polymer. *Abstracts of Papers of the American Chemical Society* **1995,** 210, 50-COLL.

110. Lin, J. J.; Bates, F. S.; Hammer, D. A.; Silas, J. A., Adhesion of polymer vesicles. *Physical Review Letters* **2005,** 95, (2).

CHAPTER 2

MODIFICATION OF POLYMERS AND FUNCTIONALIZED VESICLES

This chapter describes the materials employed to form vesicles in the studies in the following chapters. A number of different types of polymeric and phospholipid components were employed to form vesicles. While some of these were store bought, others were custom synthesized, and then modified in-house. Examples of the latter include fluorescent labeling and biotinylation. The different copolymers were soluble, to different extents, in the solvents for labeling, and this seemed to affect the efficiency of the labeling in a dramatic way. Therefore, it was necessary to develop slightly different labeling protocols for the different samples. The details of the materials themselves and the labeling procedures are the focus of this chapter.

2.1 Copolymers for Vesicle Formation

Over the course of this thesis, studies were done with three copolymer samples: DC5329, PBD-PEO [poly(butadiene)-poly(ethylene oxide)] diblock copolymer, and a PEO-polydimethyl siloxane-PEO ABA tri-block copolymer. These structures are shown in Figure 2.1. Additionally, phospholipids were purchased for particular studies, either to compare copolymer vesicle properties with those of pure phospholipids vesicles, or to form mixed phospholipids/copolymer vesicles, as a means of imparting functionality to the copolymer vesicles.

DC5329 is a commercially available graft-architecture siloxane copolymer wetting agent from Dow Corning. Polysiloxane-based block copolymers couple substantial hydrophobicity, flexibility, optical transparency, and biocompatibility with the low cohesive energy of polydimethyl siloxane. Nonionic polysiloxane and comb-like block copolymers tend to aggregate in aqueous solutions.[1-3]

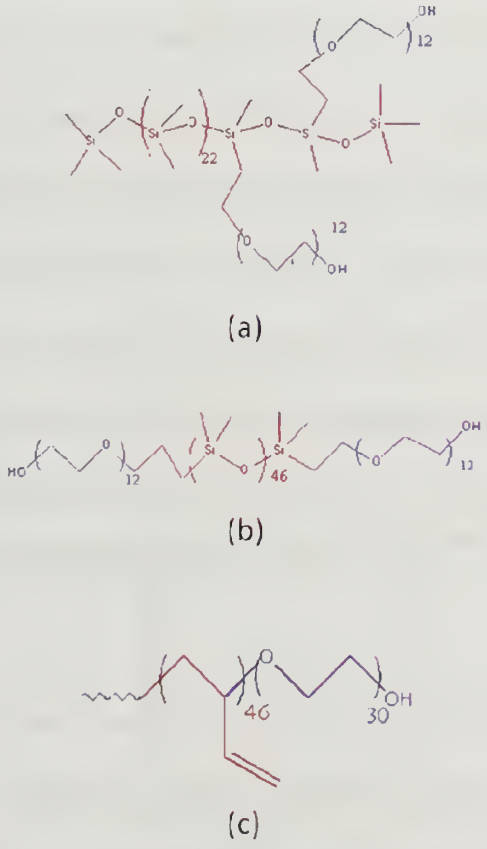

Figure 2.1 Structure of two different types of amphiphilic diblock copolymers; (a) Graft(DC5329), (b) ABA type PDMS-PEO, poly(dimethylsiloxane)-(polyethylene glycol) and (c) PBD-PEO, poly(butadiene)-poly(ethylene oxide) were used to make giant polymeric vesicles

The overall average molecular weight of DC5329 is 3250, as reported by Dow Corning. The main backbone is PDMS (polydimethyl siloxane); the PEG (polyethylene glycol) side arms contain approximately 12 EO units each, and there is roughly 1 PEG side arm per every 1500 molecular weight of polymer. DC5329 has been previously reported to spontaneously form vesicles in aqueous solution in its product literature,[2 3] and in a separate publication, the membrane thickness of a similar copolymer, has been reported to be about 5 nm.[2, 4] According to its MSDS, DC5329 also contains a small amount (7~12 wt%) of PEO-PPO (polyethylene oxide- polypropylene oxide) copolymer. This additive is not expected to incorporate into the vesicle wall in a way critical to vesicle formation. Indeed, the PEO-PPO copolymer seems to wash free of the vesicles after they are formed, as their mechanical properties are highly reproducible.[5] This reproducibility would not be expected if the additive inserted into the membrane, because of the different concentrations of vesicles employed in the studies. Recently, an in-house analysis (at Becton Dickinson) of DC5329 sample revealed that the PEO-PPO copolymer content was actually far lower than 7~12%, indeed too low to be quantified.

PBD-PEO diblock copolymer was purchased from Polymer Source Inc., as a custom-synthesized material. Its overall molecular weight was reported, by Polymer Source, to be 3800, with 46 BD units and 30 EO units. The polydispersity was reported to be 1.04. ^{1}H-NMR (Nuclear Magnetic Resonance Spectroscopy) data taken as part of this thesis (Figure 2.2), confirm the manufacturer's report. The NMR spectrum in Figure 2.2 also confirms that the PBD chain is primarily a product of 1-2 addition, per the peak at ~4.9ppm (-CH=CH_2). These features make this PBD-PEO sample nearly identical to

the much publicized OB3 sample from the Discher and Bates labs,[6, 7] providing a useful benchmarking point for the studies in this thesis

A third copolymer, a siloxane ABA tri-block copolymer, was a gift from Dow Corning. It contained PEO outer arms of 12 units, and a middle PDMS block of 46 units. Because of the limited supply of this polymer and some restrictions on publication, it was employed only in a small number of studies.

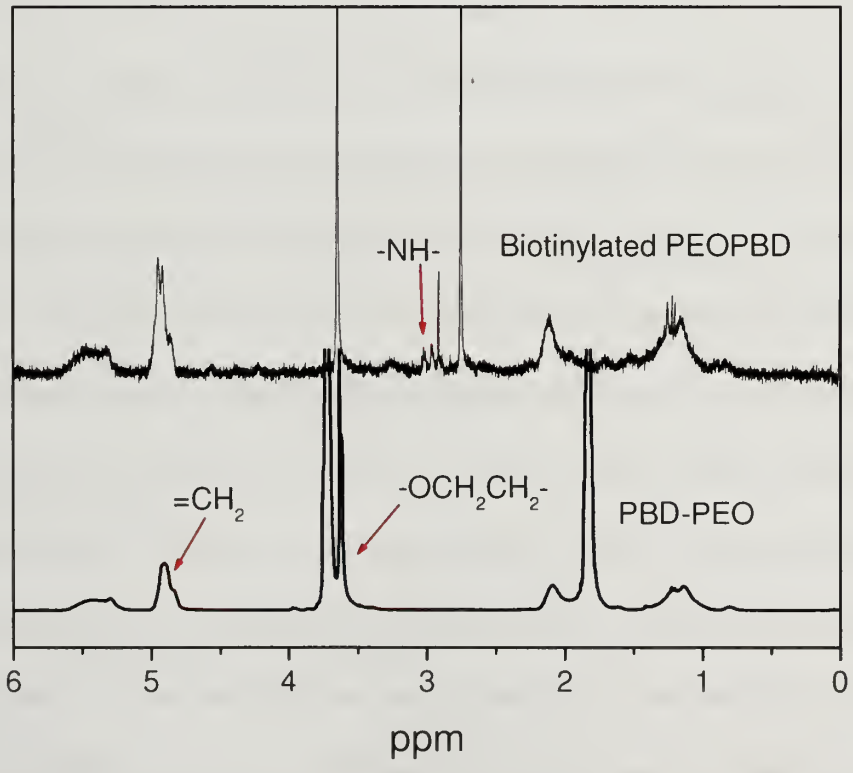

Figure 2.2 300MHz ^{1}H NMR of PBD-PEO and Biotinyl PEO-PBD in $CDCl_3$

2.2 Biotinylation of Copolymers

In studies employing biotinylated vesicles, the copolymers were biotinylated prior to vesicle formation. Because of the involved nature of the vesicle studies themselves, the vesicles were often formed well in advance of adhesion and mechanical studies. Thus, in addition to the need to modify the hydroxyl termini of the PEG components of the copolymers, the biotinylation chemistry needed to be robust. Only a few biotinylated batches of each polymer were made over the course of the thesis, and these were used repeatedly throughout.

The general strategy for the biotinylation reaction employed a modified version of a p-toluenesulfonyl chloride protocol published twenty-five years ago by Nilsson and Mosbach for the incorporation of enzymes and ligands into hydroxymethacrylate and agarose gels.[8, 9] This approach, as presented in the original publication, began with a tosylation step using tresyl chloride or tosyl chloride in dry acetone at room temperature. The product was then washed, with the details of the washing procedure dependent on the particular polymer. The tosylated product was then coupled, in the original publications, to a number of different proteins including trypsin, trypsin inhibitor, and albumin in cold sodium biocarbonate or sodium phosphate buffer. The coupling procedure links to primary amines on the proteins to the gels, with the tosyl functionality acting as a large leaving group. The general utility of this chemistry is that it is appropriate for attachment of proteins. Though we did not pursue protein labeling in this thesis, we expect that future work may move in this direction. The biotin

employed in this thesis, in Figure 2.3 was 5-(biotinoamido) pentylamine (MWt. 328) from Pierce Biotechnology (Rockford, IL). It contains a 5-carbon spacer (18.9Å) which may facilitate better interactions with NeutrAvidin.

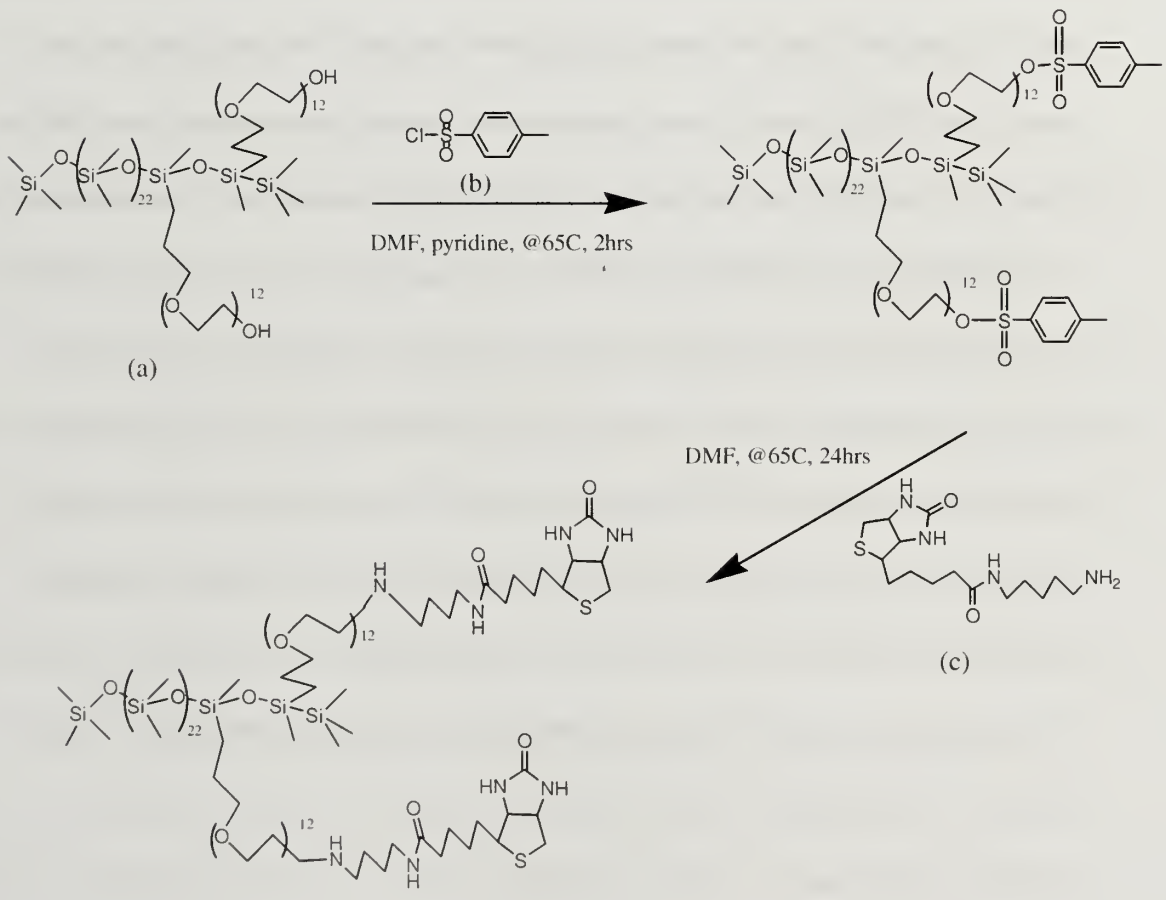

Figure 2.3 Scheme of biotinylation route for (a) DC5329 via (b) *p*-toluenesulfonyl chloride with (c) 5-(biotinoamido) pentytlamine

The protocol for biotinylating DC5329, in Figure 2.3, first dried the copolymer under vacuum to ensure dryness and remove any residual solvents. These turned out to be small, with only 0.5 wt% loss. The DC5329 was then dissolved in DMF (dimethyl formamide, Aldrich) at a concentration of 5 wt%. Excess p-toluenesulfonyl chloride was dissolved in DMF at 50°C and then added to the DC5329 solution. The equivalent molar amount of DMAP (dimethylamino pyridine, Aldrich) as a base, matching the amount of p-toluenesulfonyl chloride, was also dissolved in DMF at 50°C and dropped into the reaction vessel over the course of a few minutes. The reaction mixture was stirred at 60°C for 2 hours. After completion of the tosylation reaction, the DMF was removed by vacuum, and then pentane (Aldrich, a non-solvent for unreacted p-toluene sulfonyl chloride and DMAP) was added and the precipitate removed by filtration with 0.2 μm PTFE filters. The filtered solution was then vacuum-dried to remove the solvent, producing a clear viscous liquid, not too different from the DC5329 liquid. The product was weighed and transferred to a reaction vessel. Excess 5-(biotinoamido) pentytlamine was dissolved in DMF at 50°C and added to the reaction vessel. The reaction proceeded at 60°C for 24 hours. The final product was dried under vacuum and then transferred to chloroform, the solvent of choice for vesicle formation. Of note, unreacted 5-(biotinoamido) pentylamine is substantially insoluble in chloroform, so the precipitate (which settled to the bottom of the vial) was avoided when drawing solution for vesicle formation. Only trace amounts of unreacted biotin are expected to be transformed to the electroforming chamber during vesicle production. In our hands, 5-(biotinoamido) pentylamine is insoluble in buffer at room temperature, and therefore may stay on the electroforming wires. We expect the incorporation of the free biotin in

to the membrane to be minimal, as the mechanical properties (below) were highly reproducible, not reflecting any batch-batch variations that would be expected if biotin did incorporate.

The protocol used above for the modification of DC5329 was found also to work well with the tri-block siloxane copolymer (ABA type); however, it failed to satisfactorily modify the PBD-PEO copolymer. A useful protocol, developed here, was similar to that for the DC5329 but instead of p-toluenesulfonyl chloride, *N,N'*-Disuccinimidyl carbonate (Figure 2.4) was employed. The coupling of the *N,N'*-Disuccinimidyl carbonate to the PBD-PEO was conducted in DMF at 70°C for 8 hours. The intermediate mixture was used in the biotinylation step without purification. Biotinylation was conducted with excess 5-(biotinoamido) pentylamine as before, but now at 70°C for 24 hours. The solvent was removed under vacuum and the subsequent residue washed repeatedly with diethyl ether or pentane to remove unreacted products. Finally, the biotinylated PBD-PEO was transferred to chloroform, to constitute the vesicle-forming stock solution. The protocol described above is fairly aggressive and is reported to go nearly to completion in other systems.[10-13]

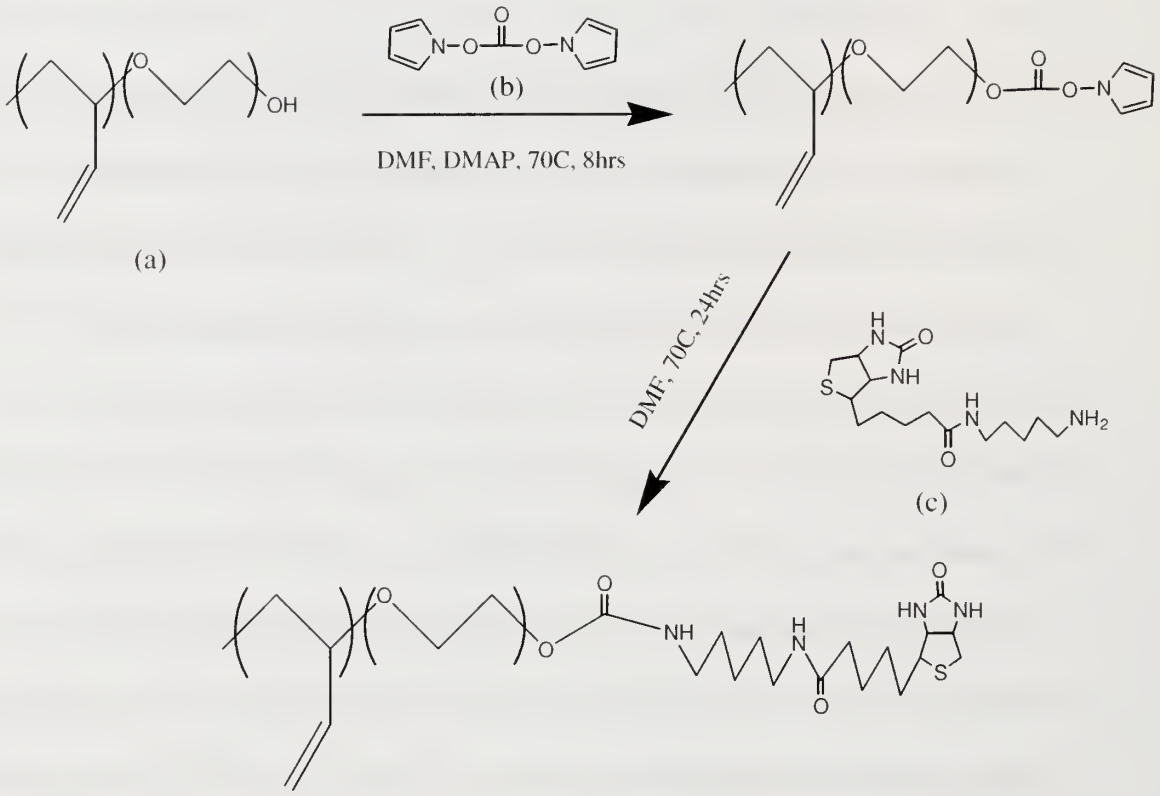

Figure 2.4 Scheme of biotinylation route of (a) PBD_{46}-PEO_{30} via (b) *N,N'*-Disuccinimidyl carbonate with (c) 5-(biotinoamido) pentylamine.

Attempts were made to quantify the efficiency of hydroxyl biotinylation for the vesicle-forming copolymers. For instance, ^{1}H-NMR measurements were made on $CDCl_3$ solutions of PBD-PEO and DC5329. For the case of DC5329, there are 3 kinds of proton peaks. One is the CH_3 (~0ppm), a second is -CH_2 (~1.6ppm), and the third is -

CH_2CH_2O- (~3.8ppm). The terminal OH is difficult to detect because the peak position changes widely depending on factors such as configuration, water content, hydrogen bonding and solvent. It is worth mentioning that while the exact position of the terminal PEG OH end group in DC5329 cannot be identified with NMR, its existence was confirmed with IR.

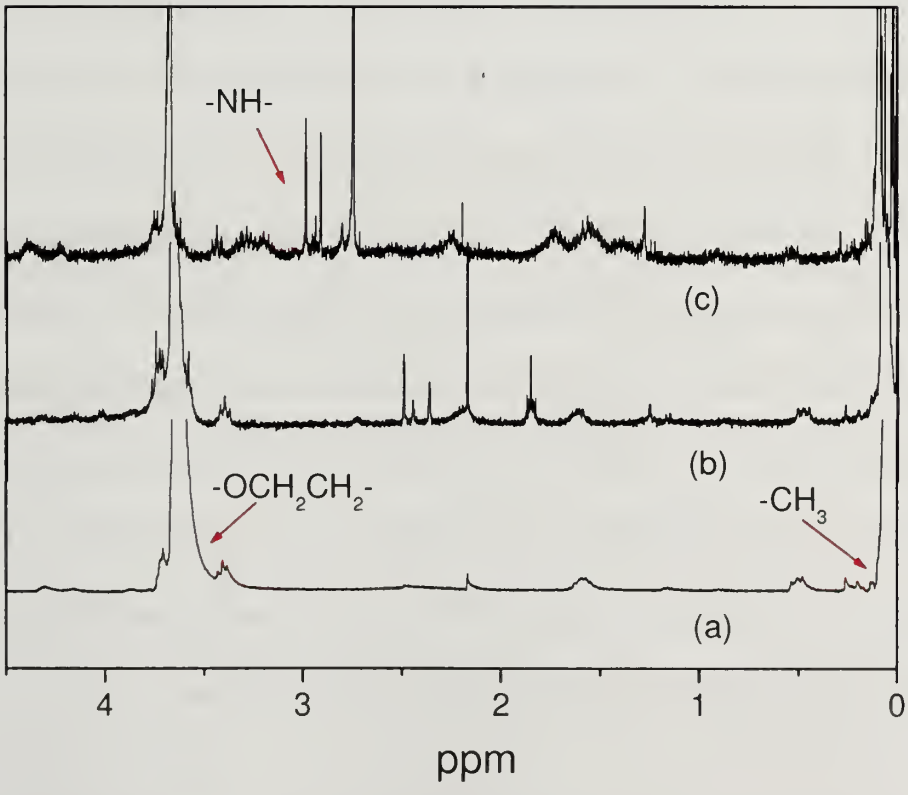

Figure 2.5 300MHz ^{1}H-NMR spectra of biotinylation of DC5329 (PEO-PDMS); (a) DC5329, (b) Tosylated DC5329, and (c) Biotinyl DC5329 in $CDCl_3$

It is difficult to determine whether the tosylation region was successful based on the spectra of the intermediate product because there is no distinctive difference between the spectrum from a mixture of polymer and p-toluene sulfonyl chloride and the tosylated intermediate. The NMR spectra showed all peaks from 5329 and *p*-tosylsulfonyl chloride and peaks from small remaining base and solvent. In the case of the biotinylated DC5329, we attempted to examine the ratio of the -CH_2-proton peak from the PEO backbone relative to the secondary amine proton peak of the reacted biotin in Figure 2.5. The secondary amine peak seemed to shift substantially, depending on the concentration, solvent, and temperature, but was usually observed near 2.9 ppm in Figure 2.5. The peaks at 2.8~3.2 ppm in Figure 2.2(PBD-PEO) or 2.5(DC5329) were identified to be those corresponding to the secondary amine of the reacted biotin. The peak of -NH-(from biotin) at 2.8 ppm increased with increasing biotinyl PEO-PBD relative to non-biotinyl PEO-PBD. This result was in good agreement with the increase of fluorescent intensity of the mixture (shown ahead in Figure 3.1). Taking the ratio of the -NH- peak to the -OCH_2CH_2O- proton peak (at 3.6 ppm) gives 65% biotinylation efficiency, relative to biotinylation of all hydroxyls, as a worst case estimate. This quantitative analysis of the biotinylation efficiency for either DC5329 or PBD-PEO was, however, confounded by a high signal to noise ratio, and the small peak area of amine peak compared to the large ones from the polymer backbone.

IR measurements were also performed to make a qualitative assessment of biotinylation efficiency, but turned out to be quantitatively inconclusive. An example in Figure 2.6, compares native DC5329, unreacted 5-(biotinoamido) pentylamine, and a

biotinylated DC5329 samples. The hydroxyl peak in the DC5329 sample, originally at 3200~3600 cm^{-1}, is substantially diminished in the biotinylated version of the same polymer, consistent with biotinylation and loss of the terminal hydroxyl. However, it is nearly impossible to rule out the possibility of slight differences in the dryness of the two specimens. The biotinylated PBD-PEO also contains an amide peak at 1710 cm^{-1}, Figure 2.7 which is absent from the native PBD-PEO. 5-(biotinoamido) pentylamine, in unreacted form, contains an amide link, and its attachment to DC5329 produces a second amide link. Hence, the amide peak in the biotinylated DC5329 spectrum is encouraging; however, a quantitative determination of the relative numbers of these bonds is not possible.

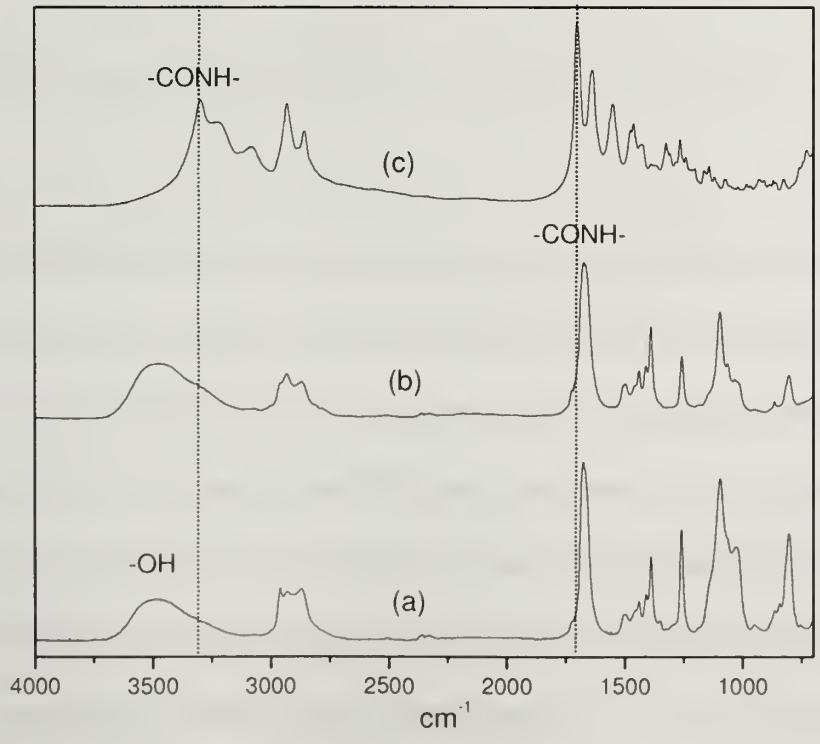

Figure 2.6 IR spectrum of Biotinylation of DC5329(PEO-PDMS) ; (a)DC5329, (b) Biotinyl DC5329, and (c) 5-(biotinoamido)pentylamine

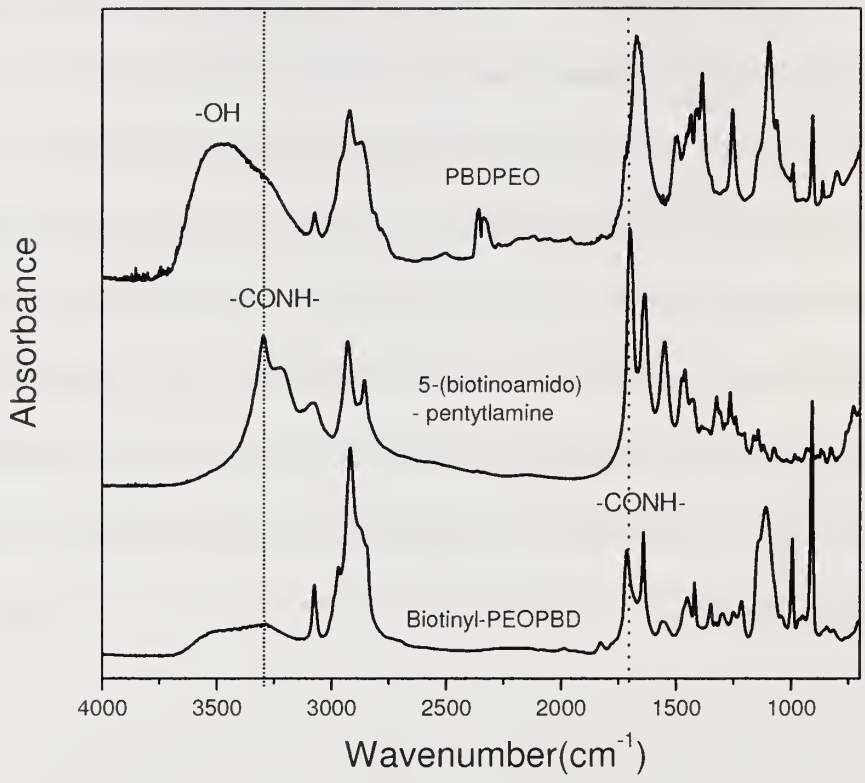

Figure 2.7 IR spectra of PBDPEO, 5-(biotinoamido) pentytlamine, and Biotinyl-PEOPBD

Because of the difficulty in quantitatively interpreting the IR and NMR spectra, avidin binding was used as proof of successful biotinylation. In this control, biotinylated vesicles were formed, and incubated in fluorescent NeutrAvidin solutions and imaged via fluorescence microscopy. The details are provided in Chapters 3, 4, and 5, however the important points are enumerated here. First, there was no difficulty forming vesicles using completely biotinylated polymer specimens. (Figure 2.8) When the biotinylated vesicles were incubated with FITC-labeled NeutrAvidin solutions, the fluorescence images were quite bright. For the case of DC5329, but not for the case of

PBD-PEO, adhesion studies required vesicles containing less than full functionalization. In this case vesicles were formed from mixtures of native and biotinylated DC5329. The fluorescence from the FITC-NeutrAvidin-conjugated forms of the binary mixture vesicles is discussed in Chapters 3 and 4 and is consistent with densely biotinylated vesicles.

2.3 Vesicle Formation

While there exist a number of different procedures for producing vesicles, electroformation, a process which is not well-understood, works well to make giant unilamellar vesicles for both phospholipids and polymers. This procedure employs an electroforming chamber consisting of 2 platinum wires of 1 mm diameter, threaded across and liquid chamber and held in place with a Teflon spacer. The front and back walls of the chamber are comprised of cover slips to facilitate viewing the process on a microscope. Small (order 1μL or less) drops of polymer solution (5~20 mg/mL), with approximately 20 μL total, are placed on the platinum wires and the chloroform is driven off in a nitrogen stream. The open chamber is then placed in a dessicator under vacuum for at least 5 hours. The chamber is then filled with sucrose solution (250~275 mOsm) and sealed. The platinum leads are then connected to a function generator, which imposes a 3V sine wave at 11 Hz. The chamber is kept in a warm lab at 28°C and the electroforming proceeds over the next several hours. Vesicles in sucrose solution are harvested by syringe and stored under refrigeration.

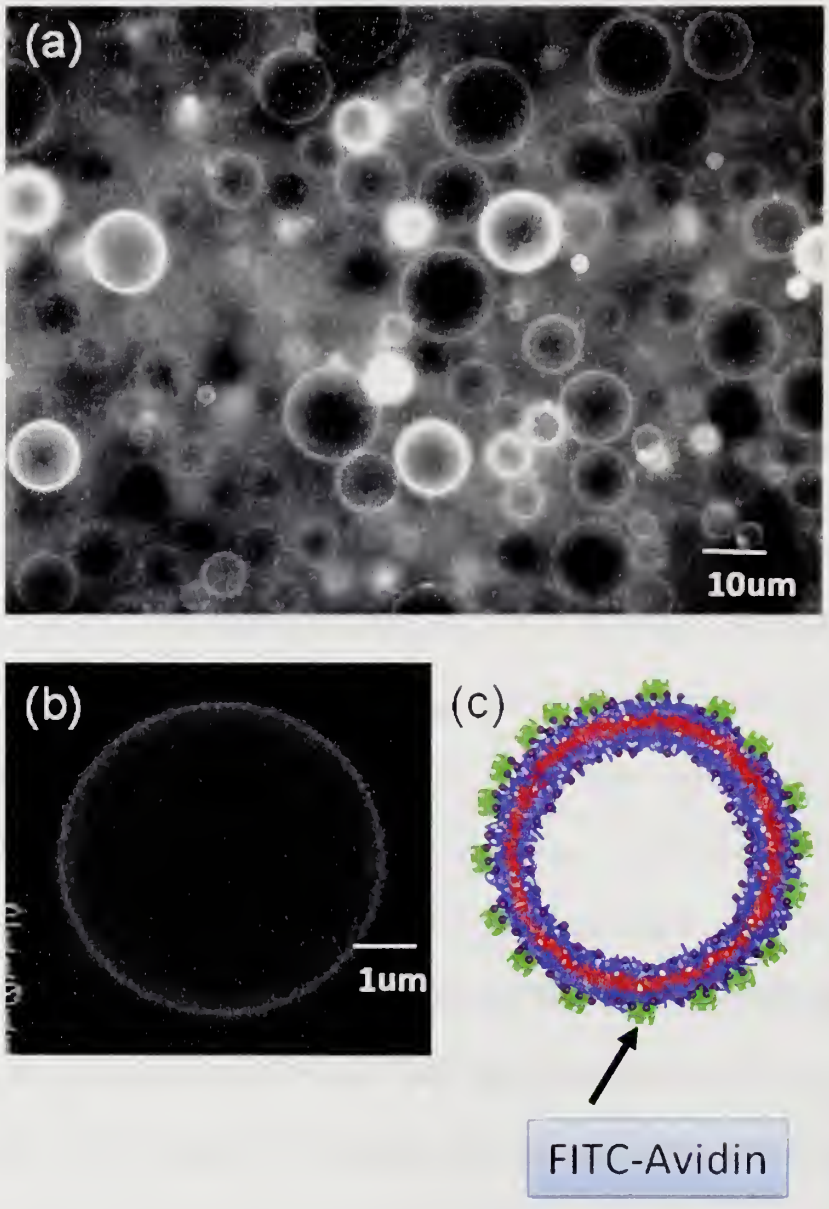

Figure 2.8 Fluorescent micrograph images (a), (b) and schematic image (c) of FITC-NeutrAvidin conjugated biotinyl-DC5329 vesicle.

REFERENCE

1. Kickelbick, G.; Bauer, J.; Husing, N.; Andersson, M.; Palmqvist, A., Spontaneous vesicle formation of short-chain amphiphilic polysiloxane-b-poly(ethylene oxide) block copolymers. *Langmuir* **2003,** 19, (8), 3198-3201.

2. Lin, Z.; Hill, R. M.; Davis, H. T.; Scriven, L. E.; Talmon, Y., Cryo-Transmission Electron-Microscopy Study of Vesicles and Micelles in Siloxane Surfactant Aqueous-Solutions. *Langmuir* **1994,** 10, (4), 1008-1011.

3. Hill, R. M.; He, M. T.; Lin, Z.; Davis, H. T.; Scriven, L. E., Lyotropic Liquid-Crystal Phase-Behavior of Polymeric Siloxane Surfactants. *Langmuir* **1993,** 9, (11), 2789-2798.

4. Snow, S. A.; Hill, R. M.; He, M. T.; Lin, Z. C.; Davis, H. T.; Scriven, L. E., Liquid-Crystal Phase-Behavior of Siloxane Surfactants. *Abstracts of Papers of the American Chemical Society* **1993,** 205, 244-COLL.

5. Santore, M. M.; Discher, D. E.; Won, Y. Y.; Bates, F. S.; Hammer, D. A., Effect of surfactant on unilamellar polymeric vesicles: Altered membrane properties and stability in the limit of weak surfactant partitioning. *Langmuir* **2002,** 18, (20), 7299-7308.

6. Hillmyer, M. A.; Bates, F. S., Synthesis and characterization of model polyalkane-poly(ethylene oxide) block copolymers. *Macromolecules* **1996,** 29, (22), 6994-7002.

7. Discher, B. M.; Won, Y. Y.; Ege, D. S.; Lee, J. C. M.; Bates, F. S.; Discher, D. E.; Hammer, D. A., Polymersomes: Tough vesicles made from diblock copolymers. *Science* **1999,** 284, (5417), 1143-1146.

8. Nilsson, K.; Norrlow, O.; Mosbach, K., Para-Toluenesulfonyl Chloride as an Activating Agent of Agarose for the Preparation of Immobilized Affinity Ligands and Proteins - Optimization of Conditions for Activation and Coupling. *Acta Chemica Scandinavica Series B-Organic Chemistry and Biochemistry* **1981,** 35, (1), 19-27.

9. Nilsson, K.; Mosbach, K., Para-Toluenesulfonyl Chloride as an Activating Agent of Agarose for the Preparation of Immobilized Affinity Ligands and Proteins. *European Journal of Biochemistry* **1980,** 112, (2), 397-402.

10. Lin, J. J.; Silas, J. A.; Bermudez, H.; Milam, V. T.; Bates, F. S.; Hammer, D. A., The effect of polymer chain length and surface density on the adhesiveness of functionalized polymersomes. *Langmuir* **2004,** 20, (13), 5493-5500.

11. Kidd, D.; Liu, Y. S.; Cravatt, B. F., Profiling serine hydrolase activities in complex proteomes. *Biochemistry* **2001,** 40, (13), 4005-4015.

12. Minard-Basquin, C.; Weil, T.; Hohner, A.; Radler, J. O.; Mullen, K., A polyphenylene dendrimer-detergent complex as a highly fluorescent probe for bioassays. *Journal of the American Chemical Society* **2003,** 125, (19), 5832-5838.

13. Anderson, E.; Brown, T.; Picken, D., Novel photocleavable universal support for oligonueleotide synthesis. *Nucleosides Nucleotides & Nucleic Acids* **2003,** 22, (5-8), 1403-1406.

CHAPTER 3

ADHESION PLAQUE FORMATION DYNAMICS BETWEEN POLYMER VESICLES IN THE LIMIT OF HIGHLY CONCENTRATED BINDING SITES

This chapter was reproduced, with permission, in part from Nam and Santore, *Langmuir* **23**, 7216-24 (2007).

3.1 Introduction

Developing an understanding of membrane adhesion and a means to control it in biomimetic systems is important for a number of reasons: At the fundamental level, well-defined model membranes can provide quantitative predictive insight into key aspects of cellular behavior, including cell adhesion, signaling, and other functions relying on cell membrane tension. Membrane adhesion fundamentals also must form the basis for design rules for applications such as targeted delivery systems (liposomes and polymeric vesicles), artificial white blood cells, and membrane-based micro-scavengers for environmental clean-up.

Our understanding of membrane adhesion at the super-molecular or micron scale has evolved substantially in the past several decades, especially with the advent of sensitive force-based methods (for instance AFM, colloidal probe, and micropipette aspiration). Most textbooks on the subject of membrane adhesion address its physical chemical (van derWaals, electrostatic, donor-acceptor), and mechanical physical origins

(bending fluctuations), while much of the recent theory also focuses on equilibrium aspects of adhesion such as vesicle shape.[1, 2] As many model adhesive membranes employ avidin / biotin molecules,[3-8] additional considerations must take into account the incorporation of strongly-binding ligand-receptor pairs, including the discrete nature of the stickers[9] along with non-equilibrium and kinetic aspects of adhesion, for instance energy dissipation and spreading dynamics.

One of the most important ways to characterize an interface is through the adhesion strength, often determined by studies in which the interface is separated, for instance by peeling. Applied to weakly-binding membrane systems, as with a dual micropipette technique, the contact angle allows determination of the reversible work of adhesion through a modified Young's equation.[10] For more strongly adherent situations, peeling studies access interfacial strength;[11] however, the values reported exceed the reversible work of adhesion by the effort expended to deform the membrane,[12] and are likely dependent on the rate of applied peeling force.[13] When adhesion is completely irreversible (meaning that the strength of the contact area is greater than that of the membranes themselves), then the membrane lysis tension sets the lower bound for the adhesion strength. (That is, the actual adhesion strength cannot be quantified experimentally.) Relevant to the current work, the lysis tensions of most giant unilamellar copolymer membranes exceed those of liposomes, increasing the range of adhesion strengths that can be measured experimentally.[14] However, in the case of avidin-biotin binding, one still expects multiple ligand-receptor interactions within an adhesive plaque to exceed the lysis strength of copolymer membranes.

Separate from the issue of adhesion strength is the process by which adhesive bonds form at the molecular level and by which macroscopic adhesive contact grows. With strongly- or irreversibly-binding membrane systems, especially where discrete binding sites produce adhesion, one envisions certain physical or mechanical processes contributing to the adhesion mechanism and rate:[15, 16] upon close approach of 2 membrane surfaces, complimentary species on opposing sides of a fluid-filled gap must register via diffusion in-plane within each membrane, and via local reorientations which include the chemical groups that anchor them to each side of the interface. Once the binding sites reach sufficient proximity and orientation, binding occurs. For many such binding events to produce an adhesion plaque (as opposed to just a few bonds), the membrane itself must deform to produce a growing contact area, hence the spreading process.[17-20] Separate from spreading, additional bonds may form across the gap to strengthen an established adhesion plaque. Thus, establishing adhesive contact involves translational[16] and configurational[5] diffusive processes and membrane deformation, in addition to the binding kinetics of complimentary groups across a gap. In addition to these molecular processes, membrane bending in flaccid systems gives rise to repulsions (through fluctuations),[21] and the development of adhesion through the initiation of adhesive islands.[22]

The current work examines adhesive plaque formation dynamics of unilamellar copolymer membranes, driven by avidin-biotin binding. Here, a dual-pipette method maintains relatively high membrane tensions (order 0.1 or 1 mN/m) relative to studies in which flaccid vesicles settle on rigid surfaces and develop patch-wise adhesion. This

current work advances previously published results[6, 8, 11, 17, 19, 23] in that here (1) membrane tension is controlled (2) irreversible membrane-membrane contact is studied, and (3) the limit of very dense binding sites is studied. The latter constraint reduces the potential contribution of translational diffusion to the plaque formation kinetics, since the biotins on one interface need not diffuse (in plane) far to align with an avidin on the opposing membrane. Hence, adhesion and spreading kinetics will be dominated by configurational motions of the ligands and receptors, membrane deformation processes, and the underling ligand-receptor binding kinetics. The findings include relatively fast and sudden growth of contact area and angle compared with the literature. It turns out that the interfaces could not be peeled apart; however, the paper presents discussion of adhesion strength in the context of driving forces for and resisting forces against spreading of the contact zone. The limit of membrane cohesion strength, which sets a lower bound for the interfacial strength of the adhesion plaque, exceeds values in other reports.

3.2 Materials

3.2.1 PEO-PDMS (DC5329 Performance modifier)

Vesicles were made from the commercial copolymer surfactant Dow Corning 5329, obtained from Dow Corning. Dow Corning product literature reports DC 5329 to be vesicle-forming, with its chemical structure containing polyethylene glycol arms averaging 12 monomers in length on a polydimethyl siloxane (PDMS) polymer. We estimate DC5329 to be roughly 3000 molecular weight, with one 12-unit oligomeric PEG arm for each 1500 molecular weight or polymer, based on manufacturer's reports and the literature: Comb type copolymers of PEG-12 on PDMS, despite their polydispersity in the EO length and distribution of PEG arms on the PDMS backbone, are known to form giant multilamellar vesicles, when there is one PEG-12 for every 1450 molecular weight of polymer.[24, 25] Indeed this proportion of EO to hydrophobic backbone (30 wt% EO, 70wt% hydrophobe) is similar to that reported for nonionic vesicle-forming diblock copolymers with different hydrophobic chemistry.[14, 26, 27] The molecular weight of 3000 was estimated from the bulk melt viscosity of DC5329, reported from its product literature, along with viscosity and molecular weight values of similar compounds of known molecular weight from other companies, for instance Geltech.[28]

3.2.2 Vesicle Formation (Electroformation)

Classical electroformation on platinum wires[29] produces large numbers of giant unilamellar vesicles of DC5329, appropriate for quantitative micropipette studies. Electroforming was done in sucrose solutions near 250 mOsm. The electroforming condition was 5 hours at 3V and 11Hz at 28°C. Adhesion studies and other vesicle manipulations were conducted in phosphate-buffered (pH 7.4) glucose solutions having a total osmolarity near 270 mOsm.

3.2.3 Biotinylation of PEO-PDMS

Biotinylated vesicles were made by chemical modification of the DC5329 prior to vesicle electroformation, following an established tosylation protocol.[30, 31] Here, any possible residual solvents were removed from the DC5329, by drying under vacuum overnight, resulting in 0.5 wt% loss. The DC5329 was then dissolved in DMF (dimethyl formamide, Aldrich) and excess toluene sulfonyl chloride (Aldrich) was added, along with the equilivalent molar amount of DMAP (4-dimethylaminopyridine). The mixture was stirred at 60°C for 2 hours and then the DMF removed under vacuum. Pentane, a non-solvent for unreacted tosyl chloride and DMAP was then used to remove these species by precipitation. The tosylated 5329 was recovered as a filtration supernatant and then reacted with excess 5-(biotinamido) pentylamine (Pierce Biotechnology Inc., Rockford IL) in DMF at 60°C for 24 hours. Excess biotin, a result of insolubility in aqueous solution, was thought to remain on the electroforming wires. There was no evidence of its incorporation into vesicles, as there was great vesicle-vesicle and batch-batch reproducibility in mechanical and adhesive properties of the

vesicles such that only the conjugated biotin species, Biotinyl DC-5329, contributed to adhesion.

3.2.4 Fluorescent Images of NA-Biotinyl-DC5329 vesicles

Though NMR and IR spectra in Chapter 2 showed evidence of biotinylation, the peak positions and intensities were inconclusive, due to the long polymer chains and relatively small numbers of end groups. To confirm the biotinylation reaction, fluorescence microscopy was used with fluorescein-tagged NeutrAvidin (FITC-NA) from Pierce Biotechnology Inc. (Rockford, IL). Neutravidin was chosen because of its reported lower non-specific interactions compared with avidin[32, 33] and its economy compared with streptavidin. Fluorescein conjugated Neutravidin lacks glycosylated groups which could interact non- specifically. It has an iso-electronic point near neutral pH. NeutrAvidin therefore exhibits significantly less nonspecific binding than pure avidin. According to Pierce, the fluorescently labeled Neutravidin has, on average, 6.3 fluorophores per molecule. F-Neutravidin-coated vesicles were made by incubating biotinylated vesicles in phosphate-buffered glucose solutions of F-Neutravidin (0.05 mg/ml), and then recovering the vesicles by centrifugation (or settling under gravity). Conjugation of FITC-NA to the Biotinyl-DC5329 vesicles produced strong fluorescent intensity that could be observed at the edge of vesicle membranes. (Figure 3.1(A))

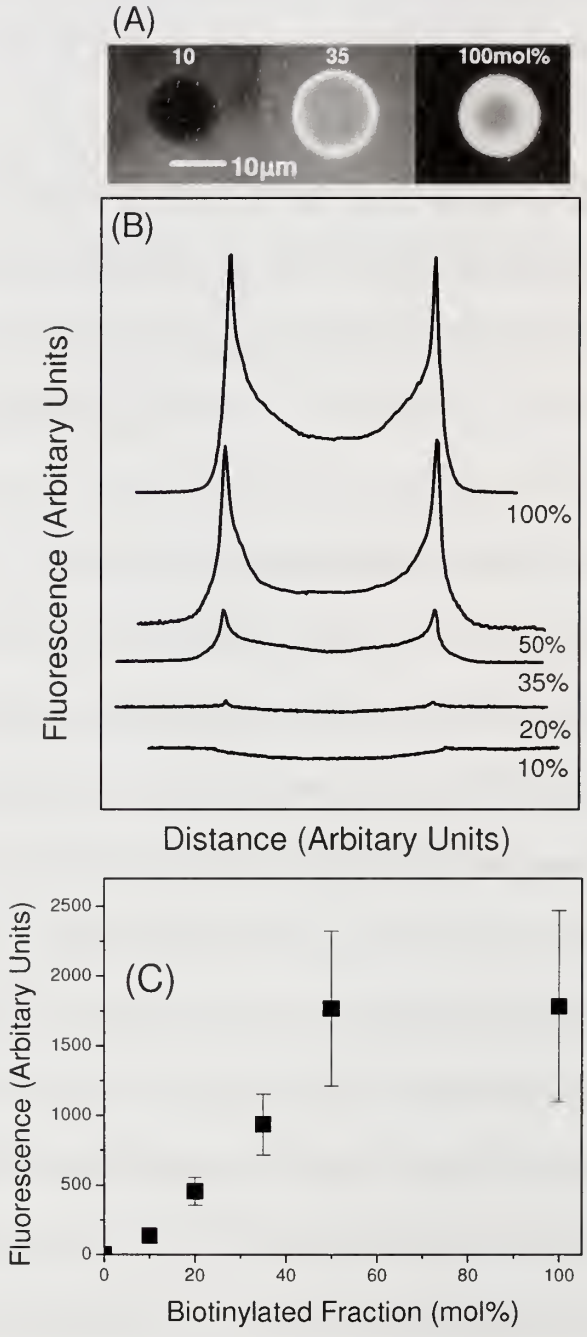

Figure 3.1 (A) Fluorescent micrographs of biotinyl DC5329 vesicles with 10,35, and 100% biotinyl modification, and surface saturation by FITC-NeutrAvidin. (B) Line profiles corresponding to vesicles of different labeling densities. (C) Fluorescence as a function of biotinyl functionality.

3.3 Experimental Methods

3.3.1 Dual Micropipette Manipulation

A micropipette aspiration apparatus, following previously published designs,[11, 34, 35] employed Narishige micromanipulators mounted on a Nikon Eclipse TE300 optical / fluorescence microscope, with primary use of a 40x Hoffman contrast objective, in addition to several others. Suction to the micropipettes was controlled with siphon manometers and measured with Validyne (Northridge, CA) transducers. The measurement range of the manometer system went up to 100 cm H_2O.

The micropipettes themselves were drawn on a Kopf Model 730 micropipette puller (Tujunga, CA) and finished on a Technical Products International (St. Louis, MO) micro-forge to give straight tips with inner diameters in the range of 5~10 μm. To prevent vesicles from sticking to the inner walls of the micropipettes, they were immersed in 0.2wt% aqueous solutions of bovine serum albumin (BSA, fatty acid free, Sigma) and refrigerated overnight before use. Prior to adhesion experiments, the BSA solution was replaced with phosphate-buffered glucose. Before doing experiments, the micropipettes were filled with buffered glucose, identical to that in the sample chamber.

Membrane mechanics and adhesion studies were carried out in home-built glass-walled aspiration chambers,[11] into which one or two micropipettes were inserted. Cover slips used for top and bottom walls were spaced a few millimeters apart so that the vesicle solution was held in place by surface tension. To prevent vesicle adhesion to the

glass chamber walls, the chambers were pre-treated with BSA solution prior to filling with the test fluid, typically phosphate buffered glucose solution. Then a small amount of sucrose-based vesicle suspension (10~20 μL) was added. The resulting situation, in which the vesicle interiors were filled with sucrose solution while the exterior was phosphate buffered glucose was useful for several reasons: First with the low membrane permeability to water and sugar, the vesicle volumes were kept essentially constant on the timescales of study. The refractive index difference between the interior sucrose and exterior glucose solutions facilitated imaging of the vesicles in phase contrast and Hoffman imaging. Finally, the density difference between the interior and exterior sugar solutions caused the vesicles to settle under gravity or centrifugation, aiding in their manipulation.

Adhesion experiments were recorded using a video camera along with a fluorescence camera (Roper Scientific HQ_2). Video signals were routed through a date/time stamping unit (Model 403, VISTA Electronic Co.) which writes the elapsed time and pipette suction pressure on each frame of the recorded images. To minimize vibrations the whole experiment was constructed on a Newport Vibration Isolated Workstation kept by nitrogen gas flow. Recording were later analyzed with Scion Image software.

3.3.2 Membrane Modulus

In studies of membrane mechanics, each vesicle was aspirated into a micropipette and the suction was first increased relatively quickly to draw out any wrinkles and tethers in the membrane. The suction was then decreased to nearly zero, to initiate the experiment: The suction was then increased again, this time step wise and relatively slowly (0.1 mN/m/s between pulling steps, holding tension for several seconds for each datum before slowly increasing again) to obtain approximately 10 data points at increasing membrane tensions. This process continued until the vesicle broke. Vesicle images, recorded on video, were analyzed to obtain the membrane area at each suction level, and the LaPlace equation was applied to translate the suction values to the isotropic membrane tension, τ:

$$\tau = \frac{\Delta P \times R_p}{2\left(1 - \frac{R_p}{R_o}\right)} \tag{3.1}$$

Here P_s is the suction pressure, R_p the pipette radius and R_v the radius of the spherical part of the vesicle outside the pipette. The plot of membrane tension as a function of areal strain gives the area expansion modulus, K_a, as the slope. The lysis conditions are also apparent.

3.3.3 Two Vesicles Adhesion System

The membrane adhesion studies reported here were essentially spreading experiments, in which an attempt was made to parallel previously published strategies.[6, 10] One vesicle, held at low tension, was allowed to spread over a second vesicle, held at higher tension. In such a situation, the high tension vesicle usually maintains a spherical

bulb outside the pipette, allowing for consistent geometrical design of the contact region, and interpretation of results in terms of a contact angle-Young's equation analysis or peeling work. While copolymer vesicles are typically more robust than liposomes in their lysis stresses and strains, this work reports weakening of the membrane by dense functionalization, especially for the avidin coated vesicles. Therefore, the NeutrAvidin-coated vesicle (of the avidin-biotin pair) was set to the low tension while the biotinylated vesicle was maintained at the higher of the two tensions.

Execution of the adhesion protocol involved insertion of two pipettes into a chamber filled with buffered glucose solution, which contained biotinylated vesicles (in one region of the chamber) and biotin vesicles that had been conjugated with F-NeutrAvidin (in another region of the chamber.) The two could be distinguished due to the fluorescence of the latter. A biotinylated vesicle was aspirated into one micropipette while a NeutrAvidin-conjugated vesicle was aspirated into the second pipette. Vesicles were then subject to a K_a measurement to ensure that each was unilamellar. (A multilamellar vesicle will have a substantially larger K_a value than that for a unilamellar vesicle.) The biotinylated vesicle was then held at a relatively high suction, while the avidin vesicle was held at lower suction. The two vesicles were brought into contact and the progress of their adhesion and spreading at constant tension and fixed pipette separation was recorded on video. Often, the adhesion run terminated in the escape of one of the two vesicles from its pipette. Subsequently attempts were made to re-aspirate the vesicle and to pull the pair apart, a separate peeling study.

3.4 Results and Discussion

3.4.1 Receptor Surface Density

The average spacing between biotins on biotinylated vesicles is estimated from basic arguments: To the extent that the biotinylation chemistry successfully labeled all terminal hydroxyls on the PEG side arms, and estimating a non-biotinylated membrane mass of 5 mg/m^2 (from a hydrophobic membrane core thickness of about 5 nm,[24]) the nominal 12-EO-arm graft density of 1 / 1500 molecular weight units of polymer leads to a biotinylation surface concentration of 1.5 / nm^2, an extremely dense arrangement of ligands. This figure represents an upper limit on the biotin surface density of the "100%" biotinylated vesicles.

The relative densities of avidin receptors on F-NeutrAvidin-saturated vesicles were assessed from the analysis of fluorescence images of the F-NeutrAvidin-conjugated b-vesicles, in Figure 3.1 Here, the biotinylation density was varied by mixing biotinyl-DC5329 and native DC5329 in different proportions prior to electroformation. The resulting vesicles, with their different biotinyl surface densities were then incubated in a solution of F-NeutrAvidin, sufficient to saturate the biotinyl surface groups, and recovered by centrifugation. A series of F-NeutrAvidin-coated vesicles, with underlying biotinylated fractions ranging from 0-100% is presented in Figures 3.1A and 3.1B (which show the vesicle images, and the typical edge-bright cross-sectional profiles) and quantified in Figure 3.1C. In Figure 3.1C, the fluorescence from F-NeutrAvidin is linear in biotinyl functionality at low concentrations up to about

50% nominal biotinylation functionality. At greater biotin surface densities, the fluorescence from the bound F-NeutrAvidin does not further increase, suggesting no further binding of F-NeutrAvidin.

The fluorescence data in Figure 3.1C follow expectations: in the dilute limit, all exterior surface biotins bind F-NeutrAvidin conjugates, giving linearity between the biotin (and F-NeutrAvidin) surface density and the fluorescence signal. At saturation, however, F-NeutrAvidin binding becomes limited by vesicle capacity. If 100% biotin corresponds to a receptor density of 1.5/nm^2, the avidin saturation at 50% biotin corresponds to 0.75 avidins/nm^2, or 1.3 nm^2 per F-NeutrAvidin, (if each avidin binds one biotin). The F-NeutrAvidin spacing at saturation (50-100% biotin vesicle make-up) may be as much as 4 times greater (5.2 nm^2 /avidin) since avidins have 4 biotin binding sites. The estimated F-NeutrAvidin saturation level is therefore consistent with the avidin size (4.1 x 5.5 x 1.5 nm),[6] although if all the avidin pockets were occupied with biotin, the vesicles would be non-adhesive.

The current adhesion study focuses on the limit of highly concentrated receptor density. Therefore, fully biotinylated vesicles were paired with F-NeutrAvidin-saturated versions of the same. From the calculations and fluorescence data, it is estimated that biotinylated vesicle surfaces with an approximate density of 1.5 biotins / nm^2 were paired with vesicles presenting approximately 0.19-0.75 avidins / nm^2, the upper limit for each species.

3.4.2 Membrane Mechanics

Given the large ligand and receptor densities on the vesicles in this study, we considered the possibility that membrane functionalization might alter membrane mechanics. Figure 3.2 compares the stretching behavior of native DC5329 and fully biotinylated vesicles with F-NeutrAvidin-saturated vesicles. The data are typical of the 10 vesicles tested at each level of functionality. The unfunctionalized membrane follows a linear stress-strain relationship with an average lysis strain near 8% and a K_a of 92 mN/m, slightly less than values reported for PBD-PEO and PEE-PEO membranes.[27] The fully biotinylated membrane is more easily stretched, with a lower K_a value, a greater lysis strain but a lower lysis tension. Conjugation with a saturated layer of FITC-NeutrAvidin increases the stretching modulus somewhat, relative to that of the biotinylated vesicles, but further compromises membrane integrity, giving more fragile lysis conditions. These observations suggest that some of the functional groups may, to some extent, be buried beneath the outer corona of the vesicle, an important consideration for adhesion studies.

The greater impact of functionalization on mechanical properties in this study compared with others in the literature[11, 36] may be a result of the large number of functionalizable groups on the DC5329, facilitated by the graft architecture. With 12-PEG units (hydroxyl terminated) for roughly every 1500 molecular weight of polymer, full functionalization means 2 or more times the biotin density compared with systems of higher molecular weight and chain end functionality.

The lysis conditions in Figure 3.2 place limits on the conditions that can be applied during the micropipette-based adhesion studies. Because the biotinylated vesicles were more robust than those having F-NeutrAvidin conjugation, the biotinylated vesicles were chosen for the higher-tension component of each vesicle pair, held at tensions below 2 mN /m (well below the 4 mN/m lysis tension, to avoid statistical breakage.) The more fragile F-NeutrAvidin conjugated vesicles were held at lower tension and allowed to spread over the biotinylated vesicles.

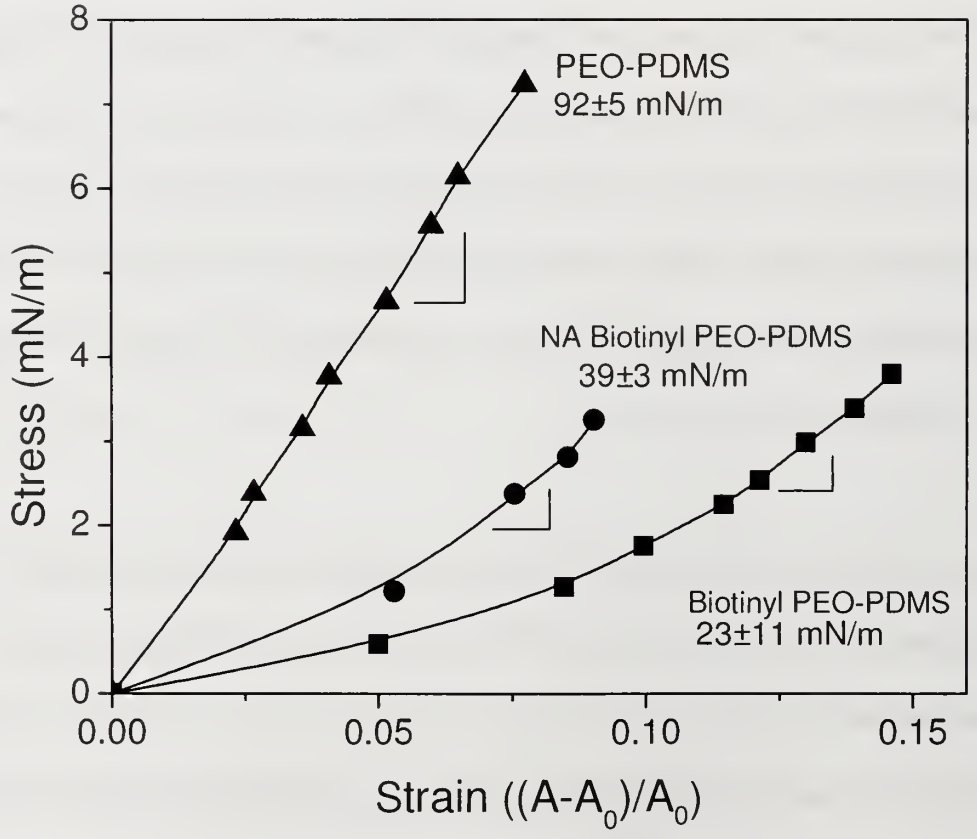

Figure 3.2 Fluorescent micrographs of biotinyl DC5329 vesicles with 10,35, and 100% biotinyl modification, and surface saturation by FITC-NeutrAvidin. (B) Line profiles corresponding to vesicles of different labeling densities. (C) Fluorescence as a function of biotinyl functionality

3.4.3 Adhesion Studies

Without biotinylation and avidin conjugation, the DC5329 polymeric vesicles did not exhibit significant adhesion, as shown in Figure 3.3. While the vesicles could experience a range of potential van der Waals, hydrophobic, hydration, or electrostatic forces, none were observed. This is significant as these weak adhesive interactions have been studied between phospholipid vesicles with a variety of elaborate techniques (such as AFM(scanning force microscopy)[37], Surface force apparatus [38], Micropipette manipulation [39], and Quartz crystal microbalance). The micrographs in Figure 3.3 show how the vesicles simply slip over each other when brought closed together. Even long contacting times did not produce adhesion. Therefore, we conclude that in the studies to follow, the adhesive interactions were a result of F-NeutrAvidin-biotin interactions.

Figure 3.3 Video micrographs of DC5329 vesicle pairs at 40X: (A) DC5329 vesicles did not show any adhesion when they were forced into contact. (B) Instead they simply slipped over each other with further approach of the micropipettes.

3.4.4 Analysis of Vesicle Adhesion

Different geometrical parameters, in Figure 3.4 were considered in the analysis of adherent vesicles pairs, with video analysis conducted frame by frame as a function of elapsing time. While contact angle and projection lengths of the two vesicles in the pipettes were the obvious variables to measure, others were also considered. The first of these is the contact height. Because the substrate vesicle is held at high tension which maintains its near-spherical geometry, the adhesion plaque is curved. The contact height is therefore defined as shown, not quite equal to the radius of the adhesion plaque because of its curvature. Also measured were the "heights" of the vesicles themselves, which allowed an assessment of the vesicle area and volume. Additionally, the apparent vesicle "widths" were measured as an assessment of any left- right movement of the vesicle pair.

3.4.5 Spreading at Constant Tension

Figure 3.5 shows images from an adhesion experiment in which both vesicles are held at constant tension: the left biotinylated vesicle at 1.45 mN/m and the right avidin-coated vesicle at 0.55 mN/m. The projections of the two vesicles inside the pipettes are indicated by arrows. In this run, the first 62 seconds following initial contact show barely-discernable increases in the contact area and angle. Then, beyond 62 seconds, adhesion and spreading advance suddenly, along with rapid and dramatic increases in both contact area and angle. Adhesion is sufficiently strong that, in addition to one vesicle spreading over the second, both vesicles deform, manifest by a decrease

in vesicle dimension (height) in the direction perpendicular to the pipettes. At times longer than this rapid contact (beyond 69 seconds), adhesion continues to evolve

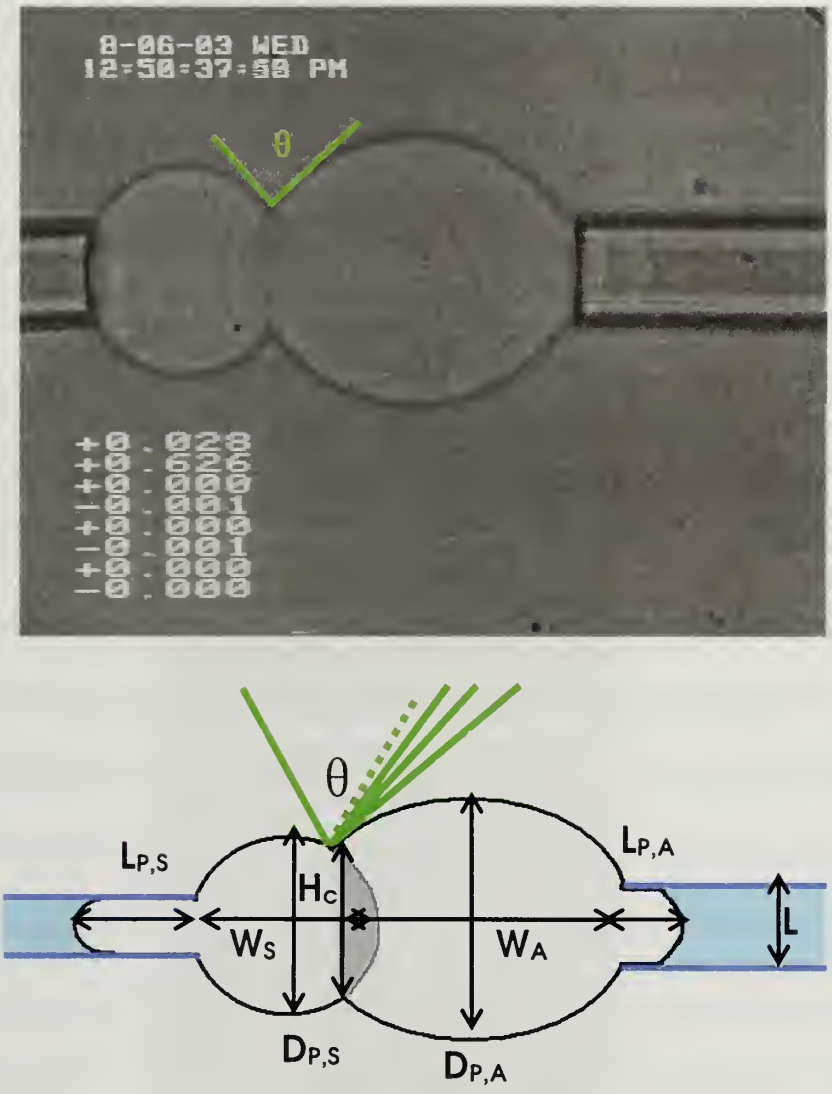

Figure 3.4 Schematic analysis of adhering vesicles pair; Projection length ($L_{P,S}$), Width (W_S), Diameter ($D_{P,S}$)of substrate vesicle and Projection length ($L_{P,A}$), Width (W_A), Diameter ($D_{P,A}$) of adherent vesicle and Micropipette inner diameter (L_D),Contacting height (H_c), Contacting angle (θ_c).

further, as evidenced by slower changes in the contact angle and projection lengths. Ultimately, the right (low tension) vesicle continues to spread over the higher tension vesicle on the left, until the right vesicle escapes its pipette.

The example in Figure 3.5 typifies the constant tension runs in our study, involving 18 vesicles, with the high-tension biotin-side held from 0.1 ~ 2.5 mN/m, and the lower-tension avidin side held at 0.05~1.3 mN/m. The ratio of high tension to low tension varied from 1.5~10, with the statistics of the tensions and tension ratios shown in Figure 3.6 B (G). In describing these results, we identified 3 general phases of the spreading process: Phase 1, pre-spreading, begins with the initial macroscopic contact and persists up to the period of rapid growth. It involves very minor but real changes in vesicle shape, as intimate contact is established. For the 18 vesicles examined, Phase 1 lasted no longer than 90 seconds and, for 15 of these vesicles, it lasted less than 20 seconds. These statistics are also summarized in Figure 3.6 A and B. In many cases, that is, for 11 vesicles, Phase 1 was quite short, lasting 5 seconds or less. Indeed while Figure 3.5 exhibits a long Phase 1 pre-spreading phase, the subsequent adhesive behavior was average relative to other vesicles in the study. The time variations of Phase 1 may result from variations in the cleanliness of the vesicle surface at the nanometer scale. Even a few nanoscale particulates near the point of initial contact will impede the close membrane approach needed for avidin-biotin engagement across the gap. Of note, we observed no significant correlation between the imposed membrane tension and the duration of Phase 1.

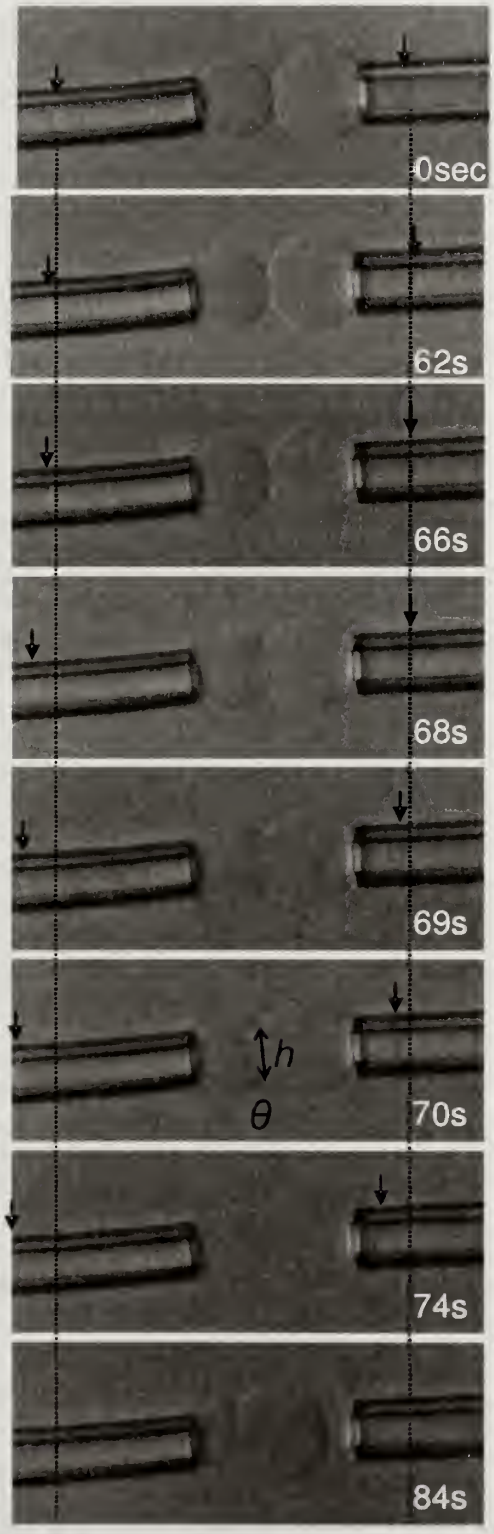

Figure 3.5 A series of video images illustrating typical vesicle adhesion dynamics at constant suction. The left (biotinyl-DC5329) vesicle is held at high suction pressure, while that on the right side is at lower suction. Dashed lines indicate the initial projections in the two pipettes. The left projection becomes progressively longer and eventually leaves the video frame. θ and h are defined here.

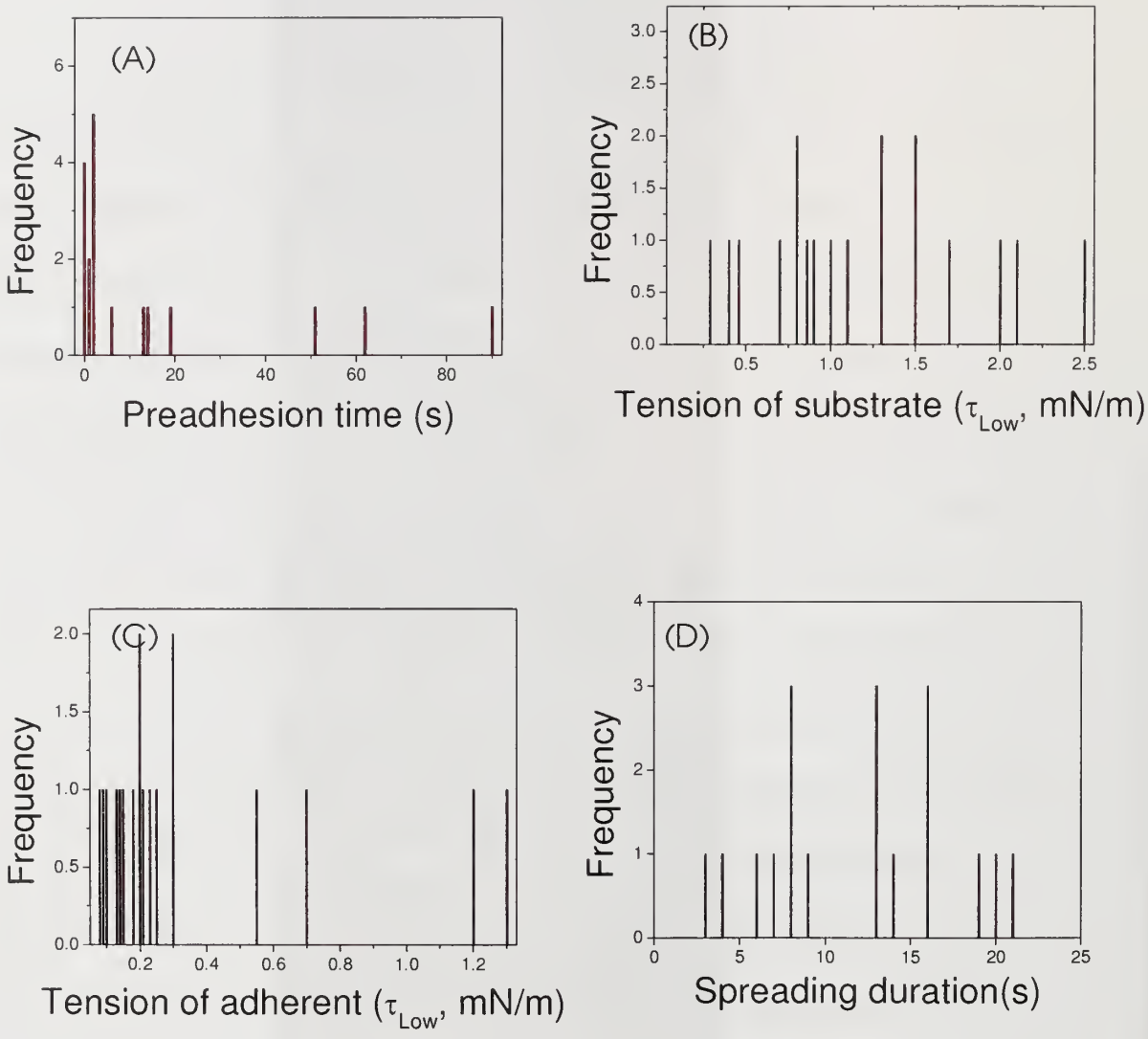

Figure 3.6A Histograms showing the statistical distribution of parameters that were considered in understanding adhesion of functionalized DC5329. (A) Frequency *vs.* Pre-adhesion time (B) Frequency *vs.* Initial Stress (C) Frequency *vs.* Initial tension (D) Frequency *vs.* Spreading duration (Figure continues on next page)

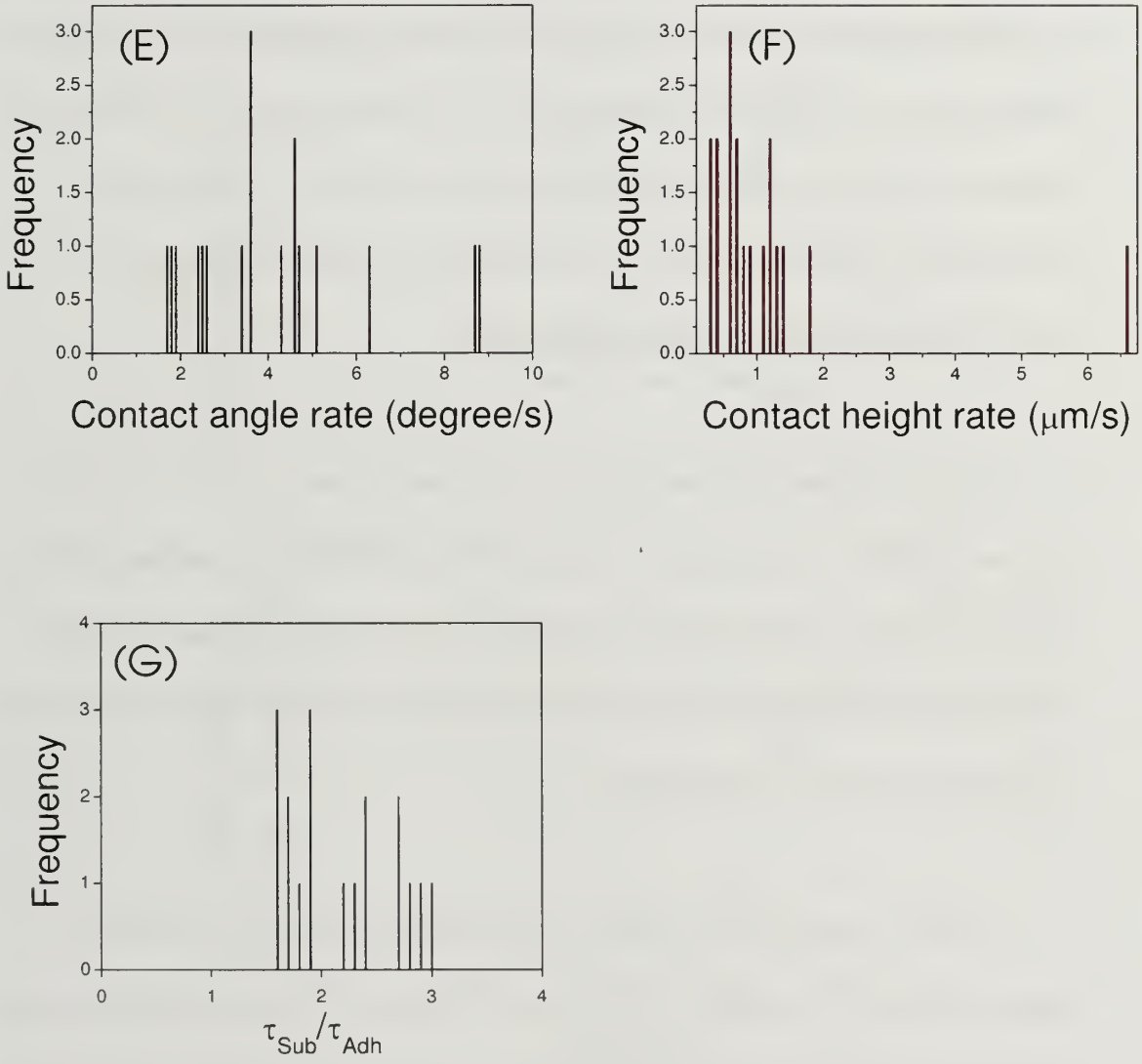

Figure 3.6B (E) Frequency *vs.* Contact angle increasing rate (F) Frequency *vs.* Contact height increasing rate time (G) Frequency *vs.* membrane tension ratio of substrate vesicle to adherent one.

Unlike the Pre-spreading Phase 1 which is typified by subtle changes, Phase 2-Rapid Adhesion is marked by rapid and dramatic alterations in vesicle shape. In a matter of seconds, the contact zone grows, the contact angle increases, the main parts of the vesicles abandon their spherical shapes to become somewhat flattened or ellipsoidal, and the projection lengths in the pipettes evolve. Watching the video tape, Phase 2 has the appearance of the vesicles snapping into contact, perhaps in response to some instability that developed previously. Video replay and quantitative analysis do, however, reveal measurable kinetics in this regime.

Phase 3 involves continued adhesion, manifest by slow growth in the contact angle and evolution of the projection lengths.Often the experiment ended during Phase 3 when the low tension vesicle escaped its pipette, as was the case in Figure 3.5. Upon escape from the pipette, the contact angle decreased back to a relaxed, if not equilibrium value (from the mechanics perspective).

Figure 3.7 quantifies the adhesion and spreading processes for the vesicles imaged in Figure 3.5. In part A of Figure 3.7, the projection length evolution is shown for the left and right vesicles, respectively. It is the case for the vesicles in Figure 3.5 (and also generally true), that the projection on the high-tension side increased and that on the low-tension side decreased during spreading. This behavior was not generally seen in other labs (or in different studies in our lab) where the high tension projection was static. Also, it is worth noting that during Phase 1 Pre-Spreading, with nearly

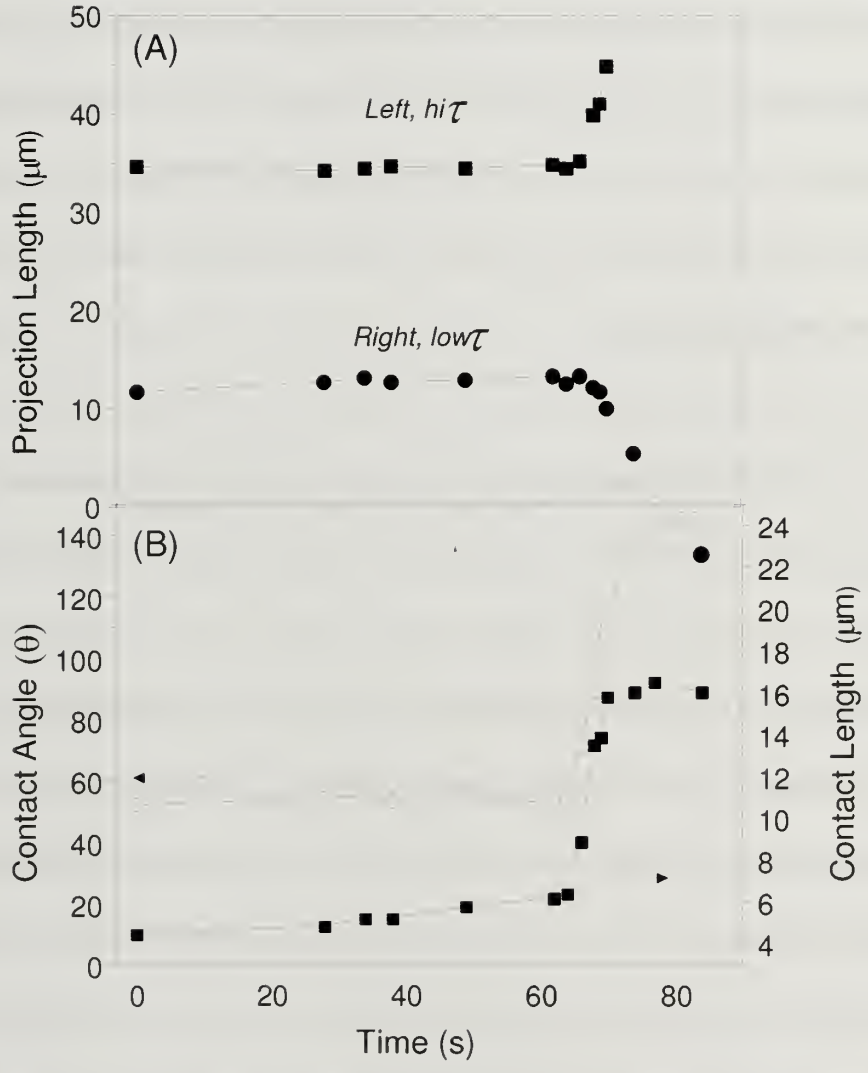

Figure 3.7 Quantitative adhesion dynamics with the vesicle pair from Figure 5 (A) left and right projection lengths and (B) contact angle and contact height, h, as a function of time. In (B), the contact angle relaxes downward after the vesicle escapes the right pipette, shown by the solid circle.

spherical vesicles, the LaPlace equation adequately describes the membrane tension. However, once the vesicles deviate substantially from spheres, it becomes necessary to calculate the membrane tension by measuring the total skin area of each vesicle, and back-calculating τ from the mechanical property data of Figure 3.2. We found in these studies that despite the dramatic Phase 2 changes in vesicle shape and projection length, membrane area and tension were constant to within a few percent, the error in measuring non-spherical vesicle areas. This is consistent with the constant suction experimental protocol.

Part B of Figure 3.7 focuses on features related to adhesion and spreading: the contact angle and the height of the contact region (defined in Figure 3.5). In Phase 2, these evolve rapidly and the abrupt onset of their growth, which defines the beginning of Phase 2, is suggestive of instability. It was generally observed that the growth in contact height was more abrupt and shorter lived than that of the contact angle, with the fastest evolution of the contact height in Phase 2 typically finished within 1~3 seconds. The break between phases 2 and 3 was therefore a matter of judgment, identifiable by eye within a margin of a few seconds. For the vesicle pair in Figure 3.7, phase 2 lasted just under 10 seconds, which was typical of all the data: For the 18 vesicles studied, Phase 2 lasted 20 seconds or less, and for 8 vesicles it lasted 10 seconds or less, showing no dependence on the tension in either pipette. Also, during Phase 2 for the vesicle in Figures 3.5 and 3.7, the contact angle and contact length growth rates were 13 degrees /s and 2 microns / second, typical of other vesicles in this study (2-14 degrees / s and 0.8 to 7 um/s). These statistics are summarized in Figure 3.6 A and B.

The particular run in Figures 3.5 and 3.7 terminated with the escape of the low-tension vesicle from its pipette during Phase 3, which was common. It is worth noting, however, that in Figures 3.5 and 3.7, and in general that, at the time of vesicle escape, the contact angle was continuing to grow, not yet having reached its maximum value. Were the initial projection length of the low tension side longer, escape from the pipette would have been delayed, so that a greater contact angle would have been achieved. Indeed, for vesicles with short initial projections, vesicle escape occurred in Phase 2. These prematurely terminated runs were not counted among the 18 we report here. (The initial flaccidity or initial projection length is a random trait that depends not only on the osmolarity difference between the solutions inside and outside the vesicle but also on the intrinsic area / volume ratio of the vesicle during electroforming.)

In a few cases, vesicles with very long initial projections elucidated the terminal adhesion behavior. Here, Phase 3 was protracted, and we observed compromise of the vesicle membrane: either sudden rupture or evidence for leakiness, with the vesicle volume decreasing more rapidly than would occur due to slow evaporation from the chamber and slow water transport across the vesicle membrane. It may be that large numbers of avidin-biotin bonds formed in the junction between the two vesicles compromise the bilayer structure. We never did observe membrane fusion, however, or transfer of F-NeutrAvidin from one vesicle to the other. When vesicle rupture occurred, a small cap, consisting of the remains of the broken vesicle which resealed on itself, remained adhered to the partner vesicle, in Figure 3.8.

Fluorescence microscopy images like Figure 3.8 demonstrate that the F-NeutrAvidin molecules stay on their original vesicle. Not only is there no transfer of the receptor to the other vesicle, there is also no evidence for diffusion of the F-NeutrAvidin towards the adhesion plaque or its depletion from the main part of the vesicle.

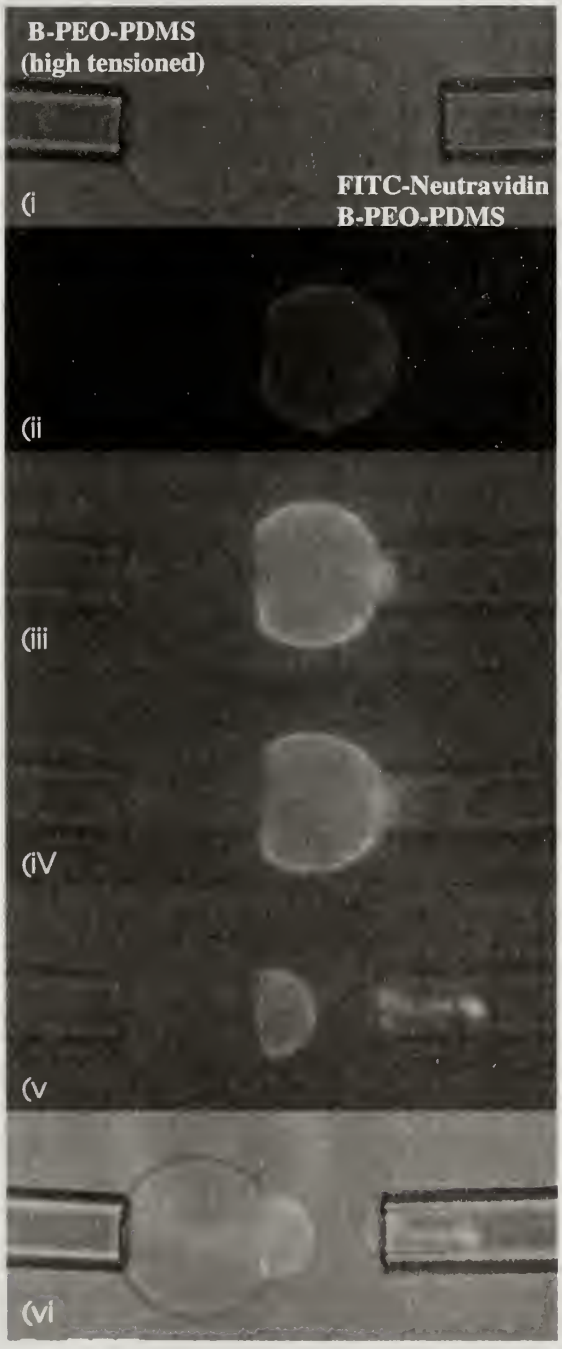

Figure 3.8 Adherent vesicle pair after the right vesicle escapes the pipet. The right vesicle is subsequently re-aspirated into the right pipet and suction increased until it breaks. The bottom images, with fluorescent illumination, show that the adhesion plaque is not altered by this attempt at peeling, that no F-NeutrAvidin is transferred from the right to the left vesicle, and that part of the right vesicle reseals on itself after the rupture. (the membrane tension of adherent vesicle(right) increased up to ~4mN/m. (ii)~(v) fluorescent image and (vi) epi-fluorescent image.

3.4.6 Analysis of Adhesion: Surface and Volume Change

Because the adhesion in these studies was so strong and because the tensions that could be applied to the substrate vesicle were limited by lysis conditions, we sometimes observed deformation of the substrate vesicle as part of the adhesion process. To ensure that our adhesion physics were simply those of membrane adhesion and spreading with minimal stretching or volume change, we closely examined the vesicle shapes over the course of the second phase of adhesion. This is shown in Figure 3.9, where the clock is started at the beginning of phase 2, as this particular vesicle pair begins to spread in earnest. Figure 3.9 contains a schematic indicating the general change of the contour of the low tension vesicle during spreading, in addition to 4 sets of countour data during Phase 2 fast spreading. It is clear from these data that the strong adhesion process causes the substrate vesicle to flatten or somewhat decrease in height. Hence the curvature of both vesicles changes slightly.

The vesicle areas and volumes, both from the main parts of the vesicles outside the pipettes and the projections themselves were calculated, summarized in Figure 3.10. Figure 3.10A, which shows the evolution of the measured variables, indicates that as spreading proceeds, the right projection decreases dramatically as expected. The area and volume lost from the right projection appear, as an increase in the size of the main part of the right vesicle, as its height increases during spreading. At the same time, the projection on the left vesicle increases, thought not as much as the projection on the right vesicle decreased. This increasing left projection is compensated by a decreasing

in the size of the left vesicle. The volume changes that correspond to the area changes in Part A

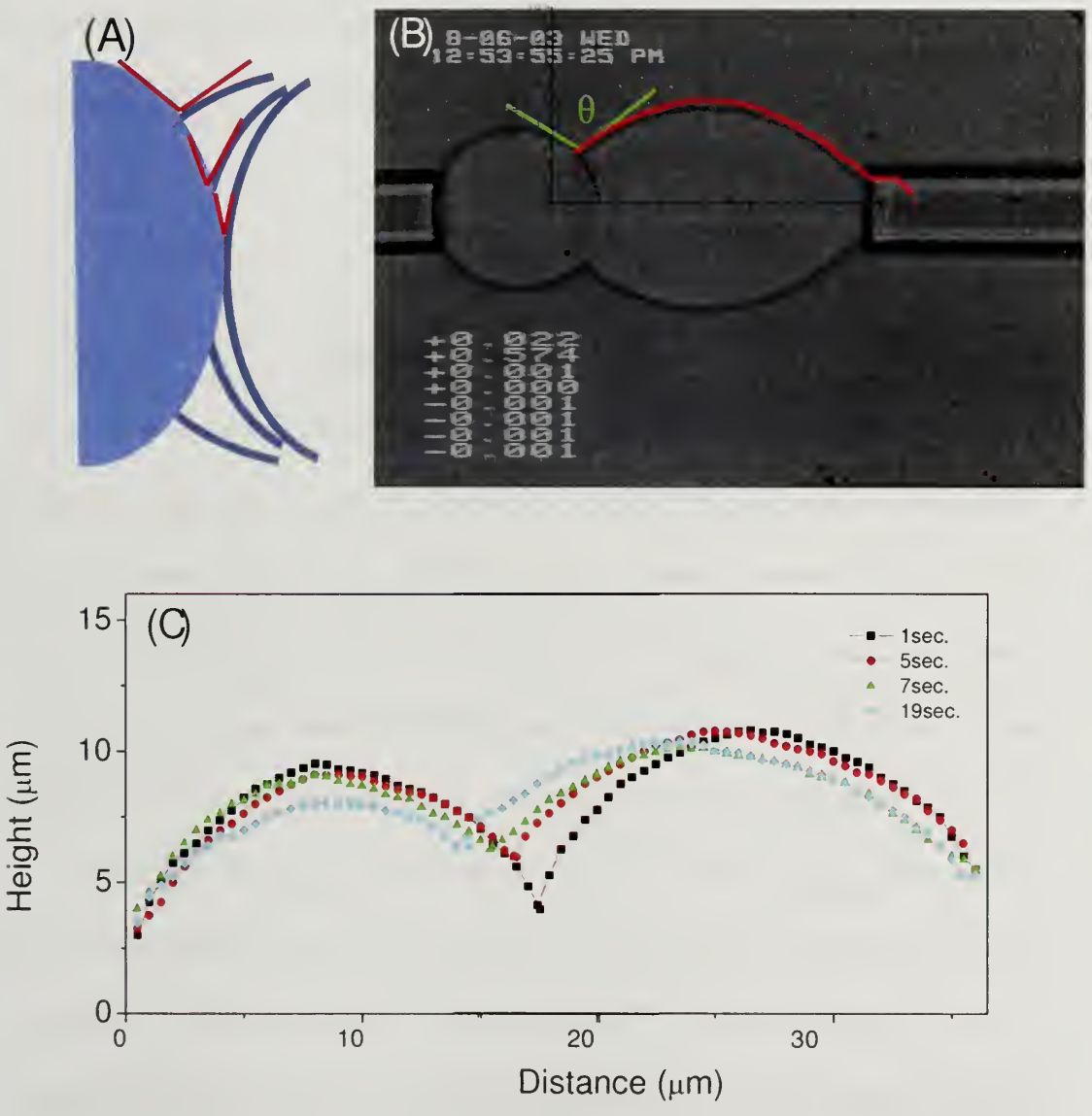

Figure 3.9 Typical example of contour profiles as a function of time. (A) Schematic of advancing spreading contact, (B) NA-conjugated Biotinyl-DC5329 vesicles pair overlapped with contour tracing, and (C) Contour changes of substrate and adherent vesicles as a function of time.

are summarized in part C of this figure. Figure 3.10(B) shows that the overall area changes (the sum of the projection and main vesicle body) are neglible for both the left and right vesicles while Figure 3.10(D) shows that the same is essentially true for the volume. Hence we conclude that the despite the complexities that arise from slight deformation of the substrate vesicle, there is no leakage or water uptake during adhesion which could produce volume changes and, likewise there is no loss or exchange of membrane area between the two vesicles.

3.4.7 Adhesion Strength

In this work, measuring the adhesion strength was a challenge because the contact zone was irreversibly bound in the practical sense: All attempts at peeling the vesicles apart, either by increasing tension or pulling back on the pipette resulted in membrane rupture (or release of a vesicle from its pipette), with no reduction in contact area. Such peeling experiments were attempted by re-aspirating the low tension vesicle which had escaped its pipette during Phase 3. Slow peeling forces (0.02~ 0.04 mN/m/s) were applied, which would tend to increase the chances for avidin-biotin bond disruption, relative to faster peeling. The contact time prior to peeling did not affect the results: Once adhesion began, the contact region could not be divided. Membrane rupture occurred between 1.5 and 4 mN/m, setting a lower bound on the adhesion strength.

Adhesion strength values in the range 1.5~ 4 mN/m are not particularly large. A point of comparison, the reversible depletion attraction (typically considered weak) induced by free polymer can be as large as 0.5 mN/m depending on polymer molecular

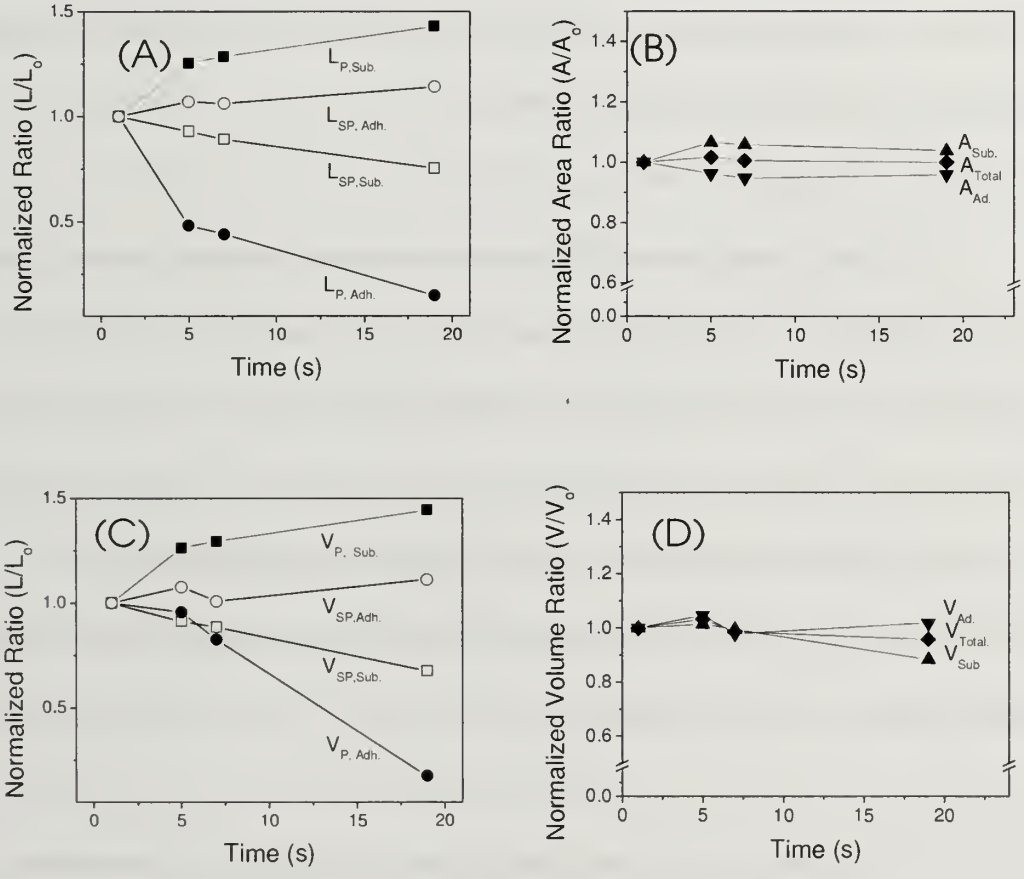

Figure 3.10 Surface area and volume changes of two adhering vesicles (shown in Figure 3.4); (A) surface area changes of sphere part(L_{SP}) and projection part(L_P) of substrate vesicle(L_{Sub}) and adherent one (L_{Adh}), (B) Total surface area changes of substrate(L_{Sub}), adherent(L_{Sub}), and both (L_{Total}), (C) volume changes of sphere part(V_{SP}) and projection part(V_P) of substrate vesicle(V_{Sub}) and adherent one (V_{Adh}), (D) total volume changes of substrate(V_{Sub}), adherent(V_{Adh}), and both (V_{Total})

weight and concentration, in agreement with mean field calculations.[10] Our lysis values of 1.5~4.0 mN/m, which represent a lower limit for the adhesion of the avidin biotin system, exceed depletion attractions by no more than by an order of magnitude, arguing that the lysis energies are also weak, especially compared with the avidin-biotin adhesion. Therefore, the irreversible nature of the observed avidin-biotin membrane adhesion suggests that the actual adhesion strength in our case is much much greater than this observed lower limit of 4 mN/m.

It is worth noting that the literature on membrane adhesion driven by avidin-biotin binding is varied. Some labs employing two contacting phosophophlipid membranes find essentially permanent binding like us;[6] but other labs investigating biotinylated copolymer vesicle adhesion to avidin-coated beads report weak peeling tensions, with a maximum of 0.45 mN/m, depending on biotin density.[11, 23, 25, 36] Hence for the scenario of modified copolymers, our adhesion measurements indicate greater binding forces than these other labs.

3.4.8 Interpreting Constant Tension Data in Terms of Spreading

The data measured at constant tension represent fascinating wetting behavior, where the timescales of the most dramatic and rapid features exceed those of membrane diffusion. Even in the limit of irreversible avidin-biotin binding exceeding the membrane strength, one might imagine various scenarios (densities of avidin-biotin crossbridges, different tethering schemes) giving rise to different levels of strong adhesion (relative to the membrane cohesion). Such differences, not accessible via

peeling, might be apparent in the wetting and spreading behavior. Hence the work to pull two vesicles apart should not be the only means to gauge adhesion.

Following the theory of Bell *et al.*,[40] Noppl-Simson[6] identified spreading pressure as being related to the chemical driving force for liposome adhesion and used it to quantify the density of avidin-biotin crossbridges in the contact zone. The excess spreading pressure of avidin (bound to biotins across the adhesive plaque), $\Delta\Pi_{Av}$, which increases as spreading proceeds, is the summation of the surface pressures, Π_i for the various avidin components within and outside the contact zone:

$$\Delta\Pi_{Av} = \Pi_{Av}(c_x^p) - \Pi_{Av}(c_u^p) + \Pi_{Av}(c_u^r) \qquad (3.2)$$

Here $\Pi_{Av}(c_x^p)$ is the spreading pressure of cross-bridged avidin in the adhesion plaque, while $\Pi_{Av}(c_u^p)$ and $\Pi_{Av}(c_u^r)$ are the spreading pressures of uncrossbridged avidin in the plaque and in the rest of the vesicle, respectively. Each of these surface pressures, in the limit of 2-d ideal solution membrane behavior, is exclusively a function of the concentration of each species. In the Noppl-Simson study, the concentration of biotins and avidins on the membrane was 5 mol-% or less: With the assumption that the strong binding of avidin and biotin caused all the avidin in the contact zone to be bound to biotin and, with diffusion of avidins and biotins from the rest of the vesicle into the contact zone to strengthen the adhesive plaque, the situation in this dilute study was one where the receptor concentration in the contact zone eventually exceeded that in the rest of the vesicle, producing the excess spreading pressure. (And indeed, the movement of

these receptors into the adhesive plaque was thought to be diffusion limited.) In the current work, this perspective on spreading pressure breaks down for 2 reasons: The first is the densely functionalized nature of the vesicle surfaces: At the start our experiments, the portions of the vesicles that ultimately join to form the adhesion plaque already contain their maximum densities (or nearly so) of avidin and biotin. (Given this jammed interface and the need for molecular mating across the interface, it is quite likely that in the plaque, not all the avidins and biotins are mated, but rather some remain unjoined as a result of kinetic jamming.) The second reason is that, with 4 binding sites per avidin, and an average of 2 biotins per copolymer chain, the avidinated vesicle is very likely crosslinked, preventing diffusion between the contact zone and the rest of the vesicle. Therefore, in our studies, were spreading pressure approximated by concentration, per Noppl-Simson, it would vanish identically at all instants during an adhesion run.

Despite the breakdown of the spreading pressure argument, it remains useful to consider a chemical driving force for adhesion which, at equilibrium, is balanced by a mechanical opposing force: the membrane tension and geometrical factors. The relevant mechanical counter-force is $\tau_L(1-\cos\theta)$, where τ_L corresponds to the lower of the two membrane tensions (because the lower tension vesicle does more of the spreading than the high tension side), and θ is the evolving contact angle. In works where the vesicle adhesion is reversible, $\tau_L(1-\cos\theta)$ has been equated with the reversible work of adhesion.[10] In the adhesion studies of Noppl-Simson, this quantity was set equal to the spreading pressure, with the assumption of mechanical equilibrium at each instant of the

relatively slow spreading study. In the current work, with the rapid spreading at the onset of Phase 2, it would seem that the chemical driving force for spreading exceeds this mechanical counter-force.

Figure 3.11 shows the evolution of τ_L (1- cos θ) with time for 3 representative vesicle pairs (all constant tension) involving different suctions on the low tension vesicle. Here, time zero corresponds to the beginning of Phase 2, and in all cases, a rounding off in Phase 3 is apparent before the lower tension side of each vesicle pair escapes its pipette. In general, experiments with greater values of the low vesicle tension were able to access greater values of τ_L (1- cos θ). It is worth noting that for a particular value of τ_L, τ_L (1- cos θ) is bounded with a maximum value of $2\tau_L$ when θ approaches perfect spreading of 180 degrees. Thus the spreading curves, at constant tension, must ultimately plateau, though these runs ended in escape from the pipette.

Besides the general shapes of the curves in Figure 11, another important point is the magnitude of τ_L (1- cos θ) accessed in these experiments: Values near 2 mN/m were consistently obtained with low-side membrane tensions exceeding 1 mN/m, far exceeding the maximum spreading pressures reported by Noppl-Simson for more sparsely functionalized liposomes (order 0.1 mN/m = 0.1 dyn / cm) , and also exceeding the critical peeling work of densely functionalized polymer vesicles reported by Lin *et al*, (0.45 mN/m)[11, 23] which includes a dissipative component.

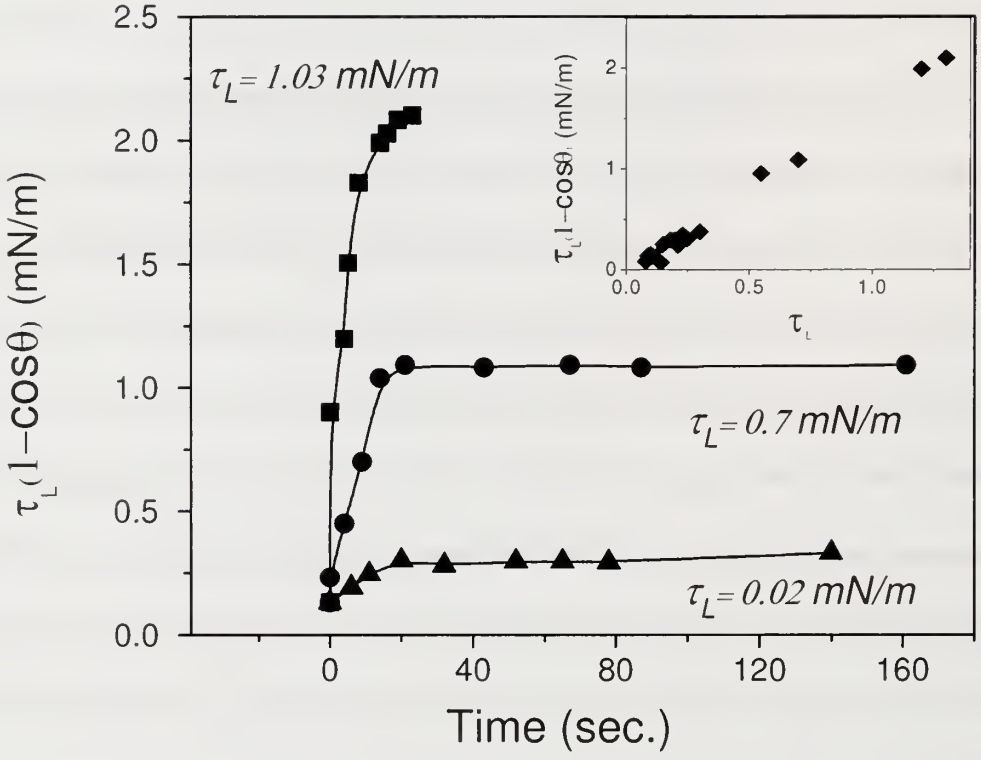

Figure 3.11 Representative plots of the evolution of the mechanical force as a function of time, for 3 different vesicles, at different tensions on the right side. The inset shows the ultimate values as a function of the tension in the right vesicle for all vesicles studied. The right membrane stress is designated τ_L because it is the lower of the two vesicles and the high stress on the left merely holds the left (substrate) vesicle in place.

A second important point about Figure 3.11 is that the 3 curves, at different τ_L values, do not collapse. Instead, the ultimate values of τ_L (1- cos θ) for each for the 18 runs are proportional to τ_L, as shown in the inset of Figure 11. That is, the range of timescales and ultimate contact angle values accessed in the all the runs is very nearly similar, though τ_L (1- cos θ) is should be more relevant to adhesion than contact angle alone. This is a quantitative indication that the chemical driving force for adhesion in our experiments far outweighs any opposing mechanical forces, consistent with the rapid Phase 2 spreading observed. The 3 data sets in Figure 3.11 employed vesicles with the same receptor density and presumably the same chemical driving force for adhesion. Were this chemical driving force balanced by the mechanical counter force, τ_L (1- cos θ), then this counter force would be identical for all 3 experiments and, for higher values of the imposed τ_L, θ would compensate so that the curves would collapse. Indeed, Noppl-Simson *et al.* never explicitly report their τ_L values, but rather present only spreading pressure or τ_L (1- cos θ) data, implying that their data did indeed collapse (i.e. that the exact value of τ_L was unimportant.) Because the mechanical force in the current constant tension studies has little influence in how spreading proceeds, it implies that the chemical adhesive strength is much larger than the O(1 mN/m) mechanical counter-force, which represents a lower bound to the adhesive strength of our system.

3.4.9 Ramping the Low-Tension Membrane

Since the constant-tension studies imply the chemical driving force for adhesion far exceeds the mechanical counter-force against spreading, always giving rapid Phase 2 spreading independent of fixed τ_L, we were motivated to consider a second experimental protocol: We made the high-tension vesicle as tight as possible and began with the low tension vesicle at small or moderate suction before putting the two vesicles in contact. Then, once Phase 2 spreading was underway, we increased the low tension suction in an attempt to provide a force which would at least temporarily arrest the spreading process.

This approach was of interest for two reasons: First for practicality, it allowed us to access higher membrane tensions than the constant tension protocol. In the constant tension approach, when relatively high tensions were applied to the two vesicles prior to contact, many vesicles broke before adhesion began. In the ramp protocol, if the low tension vesicle broke as we ramped its suction, the experiment would terminate, but we would still have data on the initial spreading kinetics. Scientifically important, the ramp protocol focuses on adhesion at short times, with limited numbers of avidin-biotin contacts (before additional bonds can form through interfacial reconfigurations). One might imagine that on timescales of seconds or shorter, the driving force for adhesion would involve the avidins and biotins that were oriented for immediate engagement. At the longer timescales a greater adhesive driving force might result from the rotational diffusion of avidins and biotins on the PEG chain ends, or the diffusion of buried biotins and avidins from beneath the outer surface of the

corona (or the diffusion of longer PEG strands out of the way of avidin-biotin approach).

Figure 3.12 shows a particularly interesting example of a ramp experiment: Initially, two vesicles were put into contact with the low tension vesicle near $\tau_L = 0.9$ mN/m. At the onset of Phase 2, we increased the low side tension (on the right axis), and found that we were unable to stop the growing vesicle contact and contact angle. While in this particular example, the rate of increase in τ_L is modest extending into Phase 3, the contact angle continued to grow until the vesicle was pulled out of the pipette. We were unable to hold onto the vesicle, even with a tension of 4 mN/m. We have other example of ramp procedures in which the increase in τ_L was sharper (up to 0.2 mN/m/s); however, we were never able to arrest spreading or prevent vesicles escaping the pipette (though we did break the vesicles in a number of cases). Of note for the particular run in Figure 3.12, the value of $\tau_L(1-\cos\theta)$, exceeds 7 mN/m before the vesicle escapes the pipette. This is the largest mechanical resisting force we were able to measure, indicating an even larger driving force for adhesion than was measured at constant tension.

From this we conclude that the spreading process, driven by the formation of avidin-biotin bonds at the contact line has a much greater forward rate constant than any elastic or mechanical resistance by the membrane. This does not seem so remarkable at first given the dense membrane functionalization in the current work; however, of the avidins and biotins at the moving contact line, one expects only a fraction to be

available for immediate bonding as others may be oriented incorrectly or buried within the bilayer brush, as is suggested by the effect of functionalization on membrane mechanics in Figure 3.2.

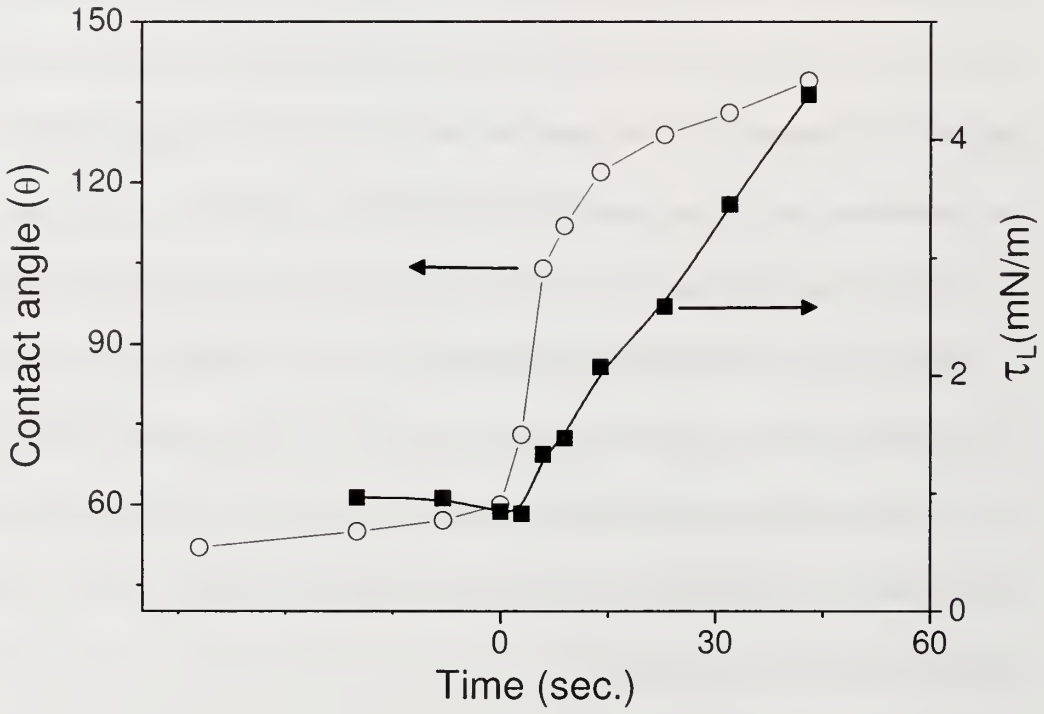

Figure 3.12 Example of vesicle adhesion when the right vesicle tension is ramped up during Phase 2 of spreading

3.5 SUMMARY

The adhesion of NeutrAvidin- and Biotin-functionalized membranes, in the limit of dense receptor functionality, follows kinetics best described in 3 phases. Early adhesion involves minimal deformation of the vesicle membrane; however at some point marking the start of Phase 2, the vesicles snap into contact abruptly in a manner that deforms both vesicles. Beyond this time, in Phase 3, the contact angle continues to grow as the adhesion strength evolves. Runs terminate with the escape of vesicles from the micropipette or the compromise of the membranes themselves. The rapid snapping into contact, not mentioned previously in the vesicle adhesion literature, is reminiscent of instability, for instance that seen during the approach of an AFM tip to a surface or in the Surface Forces apparatus. During the onset of rapid adhesion, the adhesion rates were as high as 7 um /s, or 14 degrees/s, greater than other reports we find in the literature, and likely a direct result of the irrelevance of lateral receptor diffusion to the adhesion mechanism. Indeed, for the timescales involved (no more than a few seconds, and often much less), the adhesion plaque growth is likely controlled by the rate of membrane bending and the energy dissipation involved in progressive bending.

Consistent with expectations for strong NeutrAvidin-biotin interactions, NeutrAvidin-biotin-driven membrane adhesion is irreversible, preventing peeling apart of the adhesion plaque at experimentally accessible rates. Membrane cohesion strengths as large as 4 mN/m (4 mJ/m^2) set the lower bound on the membrane adhesion strength.

This value, when used to calculate the minimal mechanical force of adhesion, $\tau_L(1-\cos\theta)$ exceeds, by over an order of magnitude, that reported previously for biotinylated liposomes in the more dilute membrane functionalization limit, though those latter results also were sufficiently strong to prevent peeling. The adhesion values reported here also exceed those reported for biotinylated copolymer vesicle interactions with avidin-coated beads, over the full range of receptor surface densities.

For runs at fixed surface receptor density, but in which the low-side tension, τ_L, is varied by over an order of magnitude, the spreading rate curves fail to collapse when $\tau_L(1-\cos\theta)$ is plotted as a function of time, unlike the implications from other labs. This suggests that the mechanical resisting force is much smaller than the chemical driving force for adhesion. Hence the system in this work may be one of the strongest membrane adhesive systems reported thus far.

REFERENCES

1. Capovilla, R.; Guven, J., Geometry of lipid vesicle adhesion. *Physical Review E* **2002,** 66, (4).

2. Tordeux, C.; Fournier, J. B.; Galatola, P., Analytical characterization of adhering vesicles. *Physical Review E* **2002,** 65, (4).

3. Helm, C. A.; Knoll, W.; Israelachvili, J. N., Measurement of Ligand Receptor Interactions. *Proceedings of the National Academy of Sciences of the United States of America* **1991,** 88, (18), 8169-8173.

4. Pignataro, B.; Steinem, C.; Galla, H. J.; Fuchs, H.; Janshoff, A., Specific adhesion of vesicles monitored by scanning force microscopy and quartz crystal microbalance. *Biophysical Journal* **2000,** 78, (1), 487-498.

5. Jeppesen, C.; Wong, J. Y.; Kuhl, T. L.; Israelachvili, J. N.; Mullah, N.; Zalipsky, S.; Marques, C. M., Impact of polymer tether length on multiple ligand-receptor bond formation. *Science* **2001,** 293, (5529), 465-468.

6. NopplSimson, D. A.; Needham, D., Avidin-biotin interactions at vesicle surfaces: Adsorption and binding, cross-bridge formation, and lateral interactions. *Biophysical Journal* **1996,** 70, (3), 1391-1401.

7. Kim, D. H.; Klibanov, A. L.; Needham, D., The influence of tiered layers of surface-grafted poly(ethylene glycol) on receptor-ligand-mediated adhesion between phospholipid monolayer-stabilized microbubbles and coated class beads. *Langmuir* **2000,** 16, (6), 2808-2817.

8. Cuvelier, D.; Nassoy, P., Hidden dynamics of vesicle adhesion induced by specific stickers. *Physical Review Letters* **2004,** 93, (22).

9. Zuckerman, D. M.; Bruinsma, R. F., Vesicle-vesicle adhesion by mobile lock-and-key molecules: Debye-Huckel theory and Monte Carlo simulation. *Physical Review E* **1998,** 57, (1), 964-977.

10. Evans, E.; Needham, D., Attraction between Lipid Bilayer-Membranes in Concentrated-Solutions of Nonadsorbing Polymers - Comparison of Mean-Field Theory with Measurements of Adhesion Energy. *Macromolecules* **1988,** 21, (6), 1822-1831.

11. Lin, J. J.; Silas, J. A.; Bermudez, H.; Milam, V. T.; Bates, F. S.; Hammer, D. A., The effect of polymer chain length and surface density on the adhesiveness of functionalized polymersomes. *Langmuir* **2004,** 20, (13), 5493-5500.

12. Chaudhury, M. K., Rate-dependent fracture at adhesive interface. *Journal of Physical Chemistry B* **1999,** 103, (31), 6562-6566.

13. Ghatak, A.; Vorvolakos, K.; She, H. Q.; Malotky, D. L.; Chaudhury, M. K., Interfacial rate processes in adhesion and friction. *Journal of Physical Chemistry B* **2000,** 104, (17), 4018-4030.

14. Bermudez, H.; Brannan, A. K.; Hammer, D. A.; Bates, F. S.; Discher, D. E., Molecular weight dependence of polymersome membrane structure, elasticity, and stability. *Macromolecules* **2002,** 35, (21), 8203-8208.

15. de Gennes, P. G.; Puech, P. H.; Brochard-Wyart, F., Adhesion induced by mobile stickers: A list of scenarios. *Langmuir* **2003,** 19, (17), 7112-7119.

16. Brochard-Wyart, F.; de Gennes, P. G., Adhesion induced by mobile binders: Dynamics. *Proceedings of the National Academy of Sciences of the United States of America* **2002,** 99, (12), 7854-7859.

17. Boulbitch, A.; Guttenberg, Z.; Sackmann, E., Kinetics of membrane adhesion mediated by ligand-receptor interaction studied with a biomimetic system. *Biophysical Journal* **2001,** 81, (5), 2743-2751.

18. Guttenberg, Z.; Lorz, B.; Sackmann, E.; Boulbitch, A., First-order transition between adhesion states in a system mimicking cell-tissue interaction. *Europhysics Letters* **2001,** 54, (6), 826-832.

19. Kloboucek, A.; Behrisch, A.; Faix, J.; Sackmann, E., Adhesion-induced receptor segregation and adhesion plaque formation: A model membrane study. *Biophysical Journal* **1999,** 77, (4), 2311-2328.

20. Bernard, A. L.; Guedeau-Boudeville, M. A.; Jullien, L.; di Meglio, J. M., Strong adhesion of giant vesicles on surfaces: Dynamics and permeability. *Langmuir* **2000,** 16, (17), 6809-6820.

21. Israelachvili, J. N.; Wennerstrom, H., Entropic Forces between Amphiphilic Surfaces in Liquids. *Journal of Physical Chemistry* **1992,** 96, (2), 520-531.

22. Albersdorfer, A.; Feder, T.; Sackmann, E., Adhesion-induced domain formation by interplay of long-range repulsion and short-range attraction force: A model membrane study. *Biophysical Journal* **1997,** 73, (1), 245-257.

23. Lin, J. J.; Bates, F. S.; Hammer, D. A.; Silas, J. A., Adhesion of polymer vesicles. *Physical Review Letters* **2005,** 95, (2).

24. Hill, R. M.; He, M. T.; Lin, Z.; Davis, H. T.; Scriven, L. E., Lyotropic Liquid-Crystal Phase-Behavior of Polymeric Siloxane Surfactants. *Langmuir* **1993,** 9, (11), 2789-2798.

25. Lin, Z.; Hill, R. M.; Davis, H. T.; Scriven, L. E.; Talmon, Y., Cryo-Transmission Electron-Microscopy Study of Vesicles and Micelles in Siloxane Surfactant Aqueous-Solutions. *Langmuir* **1994,** 10, (4), 1008-1011.

26. Bermudez, H.; Hammer, D. A.; Discher, D. E., Effect of bilayer thickness on membrane bending rigidity. *Langmuir* **2004,** 20, (3), 540-543.

27. Discher, B. M.; Won, Y. Y.; Ege, D. S.; Lee, J. C. M.; Bates, F. S.; Discher, D. E.; Hammer, D. A., Polymersomes: Tough vesicles made from diblock copolymers. *Science* **1999,** 284, (5417), 1143-1146.

28. *With comb type polymers, melts were likely unentangled, with viscosity proportional to molecular weight, allowing us to estimate the DC5329 molecular weight.*

29. Dimitrov, D. S.; Angelova, M. I., Lipid Swelling and Liposome Formation Mediated by Electric-Fields. *Bioelectrochemistry and Bioenergetics* **1988,** 19, (2), 323-336.

30. Nilsson, K.; Norrlow, O.; Mosbach, K., Para-Toluenesulfonyl Chloride as an Activating Agent of Agarose for the Preparation of Immobilized Affinity Ligands and Proteins - Optimization of Conditions for Activation and Coupling. *Acta Chemica Scandinavica Series B-Organic Chemistry and Biochemistry* **1981,** 35, (1), 19-27.

31. Nilsson, K.; Mosbach, K., Para-Toluenesulfonyl Chloride as an Activating Agent of Agarose for the Preparation of Immobilized Affinity Ligands and Proteins. *European Journal of Biochemistry* **1980,** 112, (2), 397-402.

32. Vanroy, N.; Mangelschots, K.; Speleman, F., Improved Immunocytochemical Detection of Biotinylated Probes with Neutralite Avidin. *Trends in Genetics* **1993,** 9, (3), 71-72.

33. Hiller, Y.; Gershoni, J. M.; Bayer, E. A.; Wilchek, M., Biotin Binding to Avidin - Oligosaccharide Side-Chain Not Required for Ligand Association. *Biochemical Journal* **1987,** 248, (1), 167-171.

34. Longo, M. L.; Waring, A. J.; Hammer, D. A., Interaction of the influenza hemagglutinin fusion peptide with lipid bilayers: Area expansion and permeation. *Biophysical Journal* **1997,** 73, (3), 1430-1439.

35. Santore, M. M.; Discher, D. E.; Won, Y. Y.; Bates, F. S.; Hammer, D. A., Effect of surfactant on unilamellar polymeric vesicles: Altered membrane properties and stability in the limit of weak surfactant partitioning. *Langmuir* **2002,** 18, (20), 7299-7308.

36. Lin, J. J.; Ghoroghchian, P.; Zhang, Y.; Hammer, D. A., Adhesion of antibody-functionalized polymersomes. *Langmuir* **2006,** 22, (9), 3975-3979.

37. Pignataro, B.; Steinem, C.; Galla, H. J.; Fuchs, H.; Janshoff, A.

38. Wong, J. Y.; Kuhl, T. L.; Israelachvili, J. N.; Mullah, N.; Zalipsky, S., Direct measurement of a tethered ligand-receptor interaction potential. *Science* **1997,** 275, (5301), 820-822.

39. Evans, E. A., Analysis of Adhesion of Large Vesicles to Surfaces. *Biophysical Journal* **1980,** 31, 425-432.

40. Bell, G. I.; Dembo, M.; Bongrand, P., Cell-Adhesion - Competition between Nonspecific Repulsion and Specific Bonding. *Biophysical Journal* **1984,** 45, (6), 1051-1064.

CHAPTER 4

THE ADHESION KINETICS OF STICKY VESICLES IN TENSION: THE DISTINCTION BETWEEN SPREADING AND RECEPTOR BINDING

This chapter is reproduced, in large part, with permission, from Nam and Santore, Langmuir 23, 10650-10660 (2007).

4.1 Introduction

In the 80's, Evans introduced a dual micropipette aspiration technique to assess the adhesion between two biomimetic membranes, for instance liposomes.[1-4] The adhesion strength was calculated from the contact angle and membrane tension according to a modified Young's equation, and this value was meaningful for reversible membrane interactions, especially those of a non-specific origin. To validate the contact angle analysis, depletion forces induced by dissolved polymer were measured by dual pipettes and the resulting reversible work of adhesion was shown to be in quantitative agreement with mean field calculations.[5, 6]

Variants of the method have since been embraced by the biophysics and biomedical engineering communities as a means to assess binding interactions, sometimes between two membranes, other times between a membrane and a functionalized rigid bead, bubble, or planar surface.[7-13] Micropipettes have also been used to elucidate bioadhesive mechanisms and cellular adhesive behavior.[14-21] The

community generally accepts that the contact angle analysis cannot be applied rigorously when adhesion is irreversible. In such cases, the contact angle typically sets a lower bound on the interfacial energy. Nonetheless, there have been numerous reports of contact angle-based estimates of membrane bioadhesion mimics.

Some labs interested in the binding energies of bio-functionalized membranes and cells have resorted to micropipette-based peel tests as a means to assess adhesion involving vesicles, cells, bubbles, and beads[7, 9, 10, 14, 15, 22] Peeling forces overestimate the thermodynamic work of adhesion because of the unavoidable dissipation in the "bulk" phase, even when the latter is a biomimetic membrane only a few nanometers in thickness. (Peeling can also produce artifacts if one does not take care to avoid, or at least notice, when the interface is destroyed, for instance via lipid pull-out.) In this manner, the interfacial energy of adhesion is bounded on the low side by the contact angle estimate and on the high side by peeling forces.

We noticed, when reading some of the articles on vesicle peeling,[7, 10] that the images of the adherent vesicles, for instance those with ligands and receptors such as avidin and biotin, exhibited contact angles smaller than those published for adhesion driven by depletion forces (which are considered to be extremely weak).[5, 6] While the contact angle alone is not an indicator of adhesion strength (as the membrane tension is an equally important part of the equation), we began to suspect that, all other things being equal, some of the strongly binding systems in the literature showed surprisingly low contact angles relative to systems that were more weakly binding. Indeed, in our

lab we were able to confirm instances where biotinylated polymer vesicles appeared more weakly bound to avidin counterparts (based on contact angle) than did analogous native vesicles subject to depletion forces. We thus came to realize that there exist situations where an equilibrium contact angle is not achieved in practice, when energy barriers retard the approach to (restricted) equilibrium.

This work therefore examines the process by which two vesicles adhere in a dual micropipette experiment, with attention to situations that produce meaningful contact angles (but ones which may still under-predict the adhesion strength for strong ligand-receptor interactions). This paper documents, for avidin-conjugated and biotinylated vesicles, the role of receptor density in the kinetics of adhesion plaque formation. We previously reported on the role of membrane tension with this system, and demonstrated that our system may be more strongly binding than other irreversible NeutrAvidin-biotin systems previously described.[23] While other labs have studied adhesion plaque formation and binding strength of vesicles presenting avidin and biotin,[8-10, 24] this study differs in (1) the high density of avidin and biotin in the current work which eliminates the contributions of translational in-membrane ligand and receptor diffusion to binding and (2) attention to kinetic behavior, and (3) attention to a possible instability that affects the contact angle. The work is somewhat related to a body of literature studying the adhesion of heavy flaccid vesicles on functionalized planar substrates,[24-28] but in those studies, without micropipettes to maintain a constant membrane tension, the membrane tension is estimated to be 100-1000 times less than the tensions in the current

program. Thus, the bending fluctuations that were key to the spreading behavior of flaccid vesicles are damped in the current situation.

In elucidating the mechanism of adhesion plaque formation between membranes relatively dense with ligands and receptors, this paper makes the distinction between membrane binding and spreading or engulfment (even partial). We observe that membrane binding occurs relatively quickly at the point of contact; however, the process of spreading under tension requires the system overcome a bending energy associated with the contact line. As a result, binding proceeds from time zero and roughly follows a first order rate law, but spreading occurs only after a latent period, and subsequently proceeds after an abrupt change in vesicle shape which produces a macroscopically-meaningful contact angle.

The finding that irreversibly strong binding of densely distributed ligands does not always lead to spreading is important, first scientifically, because it is counter-intuitive. The literature has argued that densely distributed "stickers" on membranes should produce behavior like that of simple liquid spreading.[29] The current findings argue otherwise, and demonstrate a regime where membrane mechanics overwhelm classical spreading behavior. The potential for membrane properties to mask the contact angle and prevent adhesive spreading, even when the membrane is nanoscopic in thickness, is an increasingly important consideration, given the rapidly-evolved interest in polymer-derived vesicle structures.[30-33] Our results suggest that there exist large regions of parameter space where adhesive polymer vesicles will behave very differently

from their phospholipid analogs. These substantial qualitative differences in behavior will carry over to the design of polymer vesicles for drug delivery and scavenging applications.

4.2 Experimental Description

4.2.1 Materials

Vesicles were made from Dow Corning silicone surfactant, DC5329, a graft copolymer with a polydimethyl siloxane (PDMS) backbone with polyethylene glycol (PEG) side arms, known to produce giant vesicles.[34] Based on product literature from Dow Corning and from other sources of silicone surfactants, we estimate DC5329 to be approximately 3000 in molecular weight, containing roughly 2 side-arms of 12 PEG's each,[23] though the material is clearly polydisperse. Functionalized vesicles required biotinylation of the DC5329, which was accomplished via a tosylation protocol[35, 36] employing 5-(biotinamido) pentylamine (Pierce Biotechnology, Rockford IL), as previously described in detail.[23] The reaction is estimated to attach biotins to nearly all the terminal hydroxyls of the PEG side chains on the DC5329.[35, 36]

Giant unilamellar vesicles were electroformed[37] on platinum wires in a sucrose solution of approximately 260 mOsm. The density of biotin functionality was varied at this stage of the vesicle production by employing mixed solutions of biotinyl-DC5329 and DC5329 in different proportions on the electroforming wires. Adhesion and other vesicle studies were conducted in phosphate-buffered (pH 7.4) glucose solutions having a total osmolarity near 270 mOsm. The difference in sugar solutions on the vesicle

interior and exterior provided optical contrast so that the vesicles could be imaged, set up an osmotic pressure that defined the vesicle volume (since the vesicles are impermeable to the sugar over long periods of time, and impermeable to water on the timescale of adhesion experiments), and made the vesicles "heavy" so that they settled under gravity or could be centrifuged.

Fluorescein-tagged NeutrAvidin (Pierce biotechnology, Rockford, IL) was chosen as the avidin molecule because it facilitates location of avidins in fluorescence, and because the NeutrAvidin is reported to have lower non-specific interactions compared with avidin.[38, 39] FITC-NeutrAvidin-coated vesicles were produced by incubating biotinylated vesicles in FITC-NeutrAvidin solutions in phosphate-buffered glucose and recovering the vesicles by centrifugation or settling under gravity.

4.2.2 Methods

A micropipette apparatus, previously described in detail,[40] employed siphon manometers to control the aspiration suction of the vesicles, measured with Validyne (Northridge, CA) CD 223 transducers. The micropipettes themselves were drawn on a Kopf (Tujunga, CA) puller and finished on a Technical Products International (St. Louis, MO) microforge to give straight tips with inner diameters from 5-10 um. Adhesion and membrane mechanics studies were conducted in home-built glass-walled aspiration chambers into which one or two micropipettes were inserted.[23] Studies employed a Nikon Eclipse TE300 inverted fluorescence microscope, with 10x phase contrast, 20 x bright field, and 40x fluorescence and Hoffman contrast objectives.

In studies of the area expansion, K_a, and bending moduli, κ_b, each vesicle was aspirated into a micropipette and the suction first increased relatively rapidly to draw out any wrinkles and tethers in the membrane. The suction, P_s, was then decreased to nearly zero to initiate the experiments. Indeed, in studies of the bending modulus, care was taken to define the zero suction pressure, based on the stagnant position of a spec of dust near the micropipette tip (without a vesicle in place.) The suction on the test vesicle was increased in small steps, relatively slowly. In bending measurements, there were approximately 0.05 mN/m between data points and in measurements of K_a, stretching was done at approximately 0.1 mN/m/s holding tension for several seconds at each datum before slowing increasing it again. The stretching process continued until the vesicle broke, enabling a determination of the lysis conditions. Video images of the vesicles allowed a determination of the membrane area while the membrane tension, τ, was calculated from the LaPlace equation:

$$\tau = P_s R_p / (2 - 2R_p / R_v) \qquad (4.1)$$

Here R_p and R_v are the pipette and vesicle (the main bulb part) radii, respectively. A plot of the membrane tension as a function of the area strain gives $K_a = d\tau/d(\Delta A/A_o)$ at sufficiently large strains, while a semi-log plot of the low-suction regime gives the bending modulus, κ_b:[41]

$$\kappa_b = \frac{kT}{8\pi} \frac{\partial \ln \tau}{\partial(\Delta A / A_0)} \qquad (4.2)$$

In spreading and adhesion experiments, one vesicle, held at tensions on the order of 0.1 ~1 mN/m was allowed to spread over a vesicle held at higher tension. In such situations the latter typically maintained a spherical bulb outside its pipette, giving consistent contact geometry and facilitating the Young's analysis of the contact angle if adhesion was reversible. While copolymer vesicles are typically more robust than liposomes in their lysis stresses and strains, we found weakening of the DC5329 membranes by dense biofunctionalization, especially for the NeutrAvidin-coated vesicles. Therefore the NeutrAvidin-coated vesicle (of the avidin-biotin pair) was set to the low tension while the biotinylated vesicle was maintained at the higher of the two tensions.

4.3 Results and Discussion

4.3.1 Physical properties

While we have generally assumed that the level of biotin functionality on electroformed vesicles is proportional to that in the DC5329 and Biotinyl-DC5329 mixture placed on the electroforming wires, this was confirmed, in a relative sense, by measuring the fluorescence from vesicles conjugated with FITC-NeutrAvidin.[23] Here, vesicles with different fractions of biotin functionality were saturated with FITC-NeutrAvidin by incubation in FITC-NeutrAvidin solutions, and then purified by repeated washing in phosphate-buffered glucose and centrifugation or settling under gravity. (To be clear, "30% biotinylation" for example, refers to vesicles that were electroformed using a mixture of 70 wt% native and 30 wt% biotinyl DC5329. The

"avidinated" form of 30% functionality is simply 30% biotinylated vesicles that have been saturated with FITC-NeutrAvidin.) The relative fluorescence levels are shown in Figure 4.1 which indicates proportionality between vesicle fluorescence and the biotinylated fraction, below 50% biotinylation, and an independence of fluorescence on the biotin composition above 50% biotinylation. These results confirm that below 50% biotin functionality, the biotin incorporation in the vesicles proceeded as intended, with the amount of biotinyl-DC5329 taken into the vesicles proportional to that in the mixture on the electroforming wires. At higher biotin densities, the fluorescence becomes independent of the biotin composition. This behavior most likely results from avidin crowding, rather than a problem with the biotin composition of the vesicles. Indeed with 100% biotinylation of the DC5329, the material on the electroforming wires is purely from the functionalized sample, not a mixture, so there is no chance that an unfunctionalized fraction is selectively taken up into the vesicles. It is worth noting, as previously estimated,[23] that with 100% biotinylation, the spacing between biotins is roughly 0.8 nm, smaller than the size of avidin molecules (4.1 x 5.5 x 1.5 nm).[8]

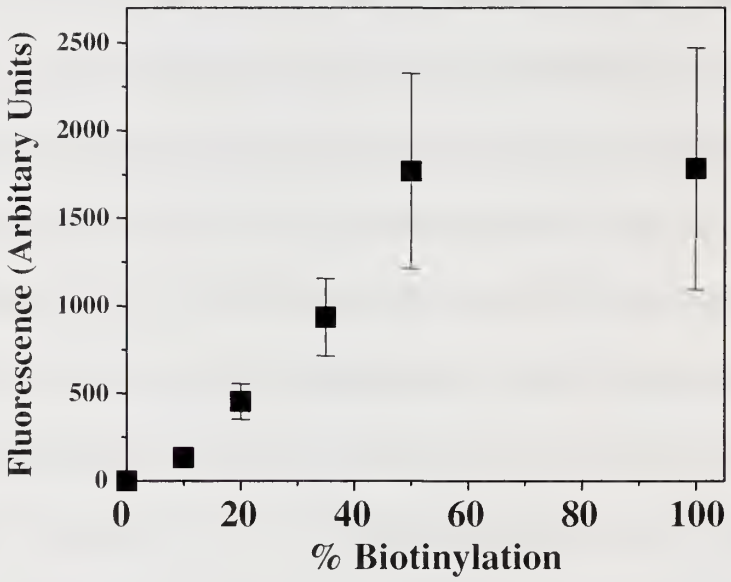

Figure 4.1 Relative fluorescence from FITC-NeutrAvidin-conjugated vesicles containing different biotin densities.

Therefore, the turnover in Figure 4.1 must result, at least in part, from the crowding of the surface by avidin. (The turnover cannot be caused by incomplete labeling of the stock solution, which would merely shift the concentration-axis. It is also unlikely to result from an inner filter effect because the fluorophores are located roughly in a single, albeit curved, plane at the vesicle surface. Reabsorption of fluorescent emissions by excess fluorophores, the inner filter effect, occurs better when the sample pathlength is large, with the fluorophores distributed in large numbers through many millimeters of sample.) At 50% functionalization, there is an estimated 1.15 nm between biotins, more in line with smallest avidin dimension. Also, at these compositions, there is a

likelihood that several of the 4 avidin binding pockets are occupied by biotin, which increases the effective molecular weight of the 5329 through crosslinking. The extremely dense functionalization in this study reduces the need for in-plane diffusion of functionalized species to gather in an adhesion plaque, while the crosslinking of biotins on neighboring chains by multiple binding to avidin slows the diffusive process considerably.

Besides the chemical aspect of membrane functionalization, membrane mechanics are an important consideration in establishing a model system for studies of adhesion plaque formation. Figure 4.2 summarizes the area expansion moduli for different biotinylation compositions as well as vesicles that were completely biotinylated and then conjugated with avidin. Biotinylation softens the vesicles, reducing the area expansion modulus, while the FITC-NeutrAvidin coating increases K_a

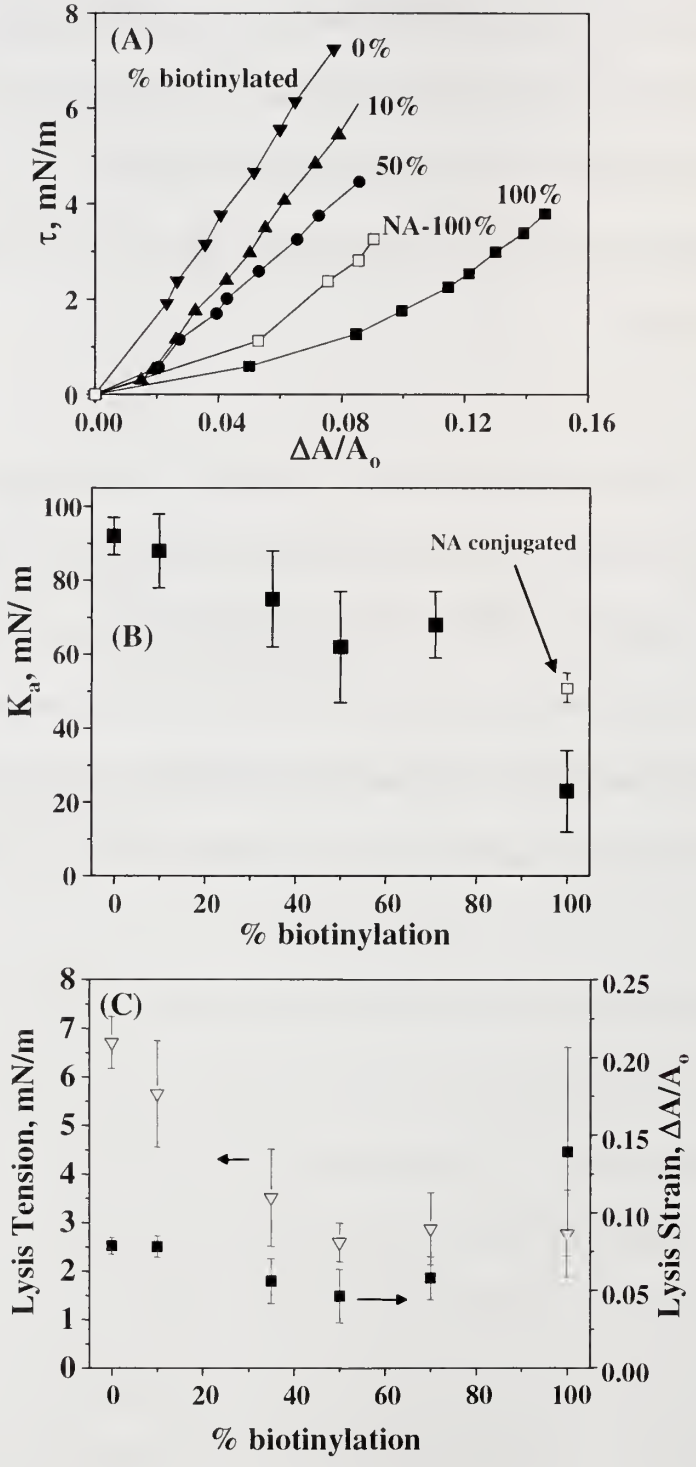

Figure 4.2 (A) Representative stress/strain plots with indications of slopes used to determine K_a, and (B) area expansion modulus for DC5329 vesicles having different amount of biotinyl DC5329. Data for 100% biotinylated vesicles with avidin conjugation are also shown. (C) Lysis conditions for biotinylated DC5329 vesicles.

somewhat, but not back up to the level of native DC5329. The lysis conditions are also influenced by functionalization, with the avidin-conjugated vesicles being more fragile than their biotinylated counterparts. Figure 4.2 suggests that the dense biotinylation forces some of the biotins into the membrane, away from the surface of the corona. This may be more favorable than the stretching of the PEG corona chains because they are relatively short (on the order of 12 PEG units) and because the biotin anchoring chemistry includes a short hydrocarbon spacer which imparts hydrophobicity. Since FITC-NeutrAvidin conjugation primarily coats the outer membrane surface, the slight increase in area expansion modulus is expected: The membrane becomes less stretchy. These area expansion and lysis results affected our experimental design. We chose to use the more fragile avidin-conjugated vesicles as the lower tensioned membranes in our experiments, subjecting the biotinylated vesicles to greater micropipette suction to maintain their shape more nearly spherical.

Besides the influence of functionalization on stretching and lysis, the bending modulus is also affected, in Figure 4.3 Here, the bending modulus of native DC5329 vesicles is about 10kT, slightly softer than that of Poly(ethylethylene)-PEO and poly(butadiene)-PEO vesicles, perhaps a result of the more liquid like nature of PDMS compared with PBD at these molecular weights.[10] Biotinylation of the membrane further reduces this bending modulus, while conjugation with FITC-NeutrAvidin increases the bending stiffness of the membrane compared to the same membrane without FITC-NeutrAvidin. The functionalized membranes, both the biotinylated

DC5329 and that conjugated with FITC-NeutrAvidin, are softer than the native DC5329. The results in Figure 4.3 for bending run parallel to those in Figure 4.2 for stretching and suggests that functionalization may cause the membrane to become thinner.

Such thinning, though speculation, could result from the hydrophobicity of the biotinylated chain ends (recall that the particular biotins employed are attached to the PEG termini by way of a short 5-carbon spacer). This hydrophobicity, though small, might cause the chain ends to "adsorb" at the interface at the base of the membrane corona where the PEG chains meet the siloxanes. This would reduce the surface tension at this buried interface. Since this surface tension is what drives brush formation in the first place,[42] there would be less driving force for PEG chain stretching normal to the interface, explicitly resulting in membrane thinning.

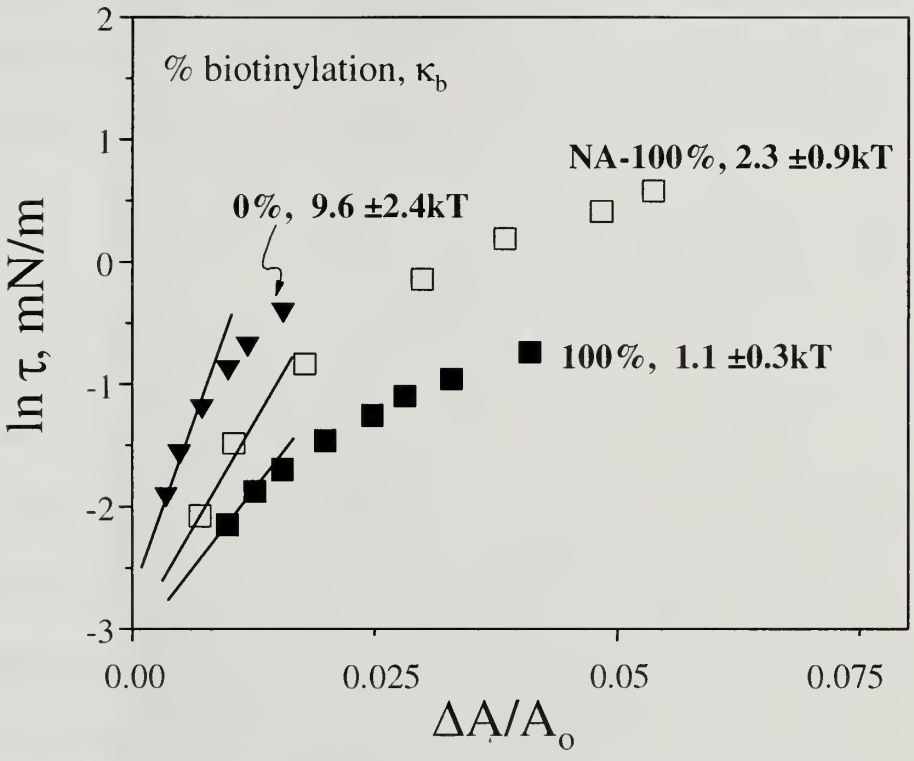

Figure 4.3 Sample bending moduli data for native, 100% biotinylated, and f-neutravidin conjugated 100% biotinylated DC5329 vesicles. The lines indicate how the slope was taken to determine κ_b. The bending moduli reported next to each data set represent the average values for each kind of vesicle.

4.3.2 The Appearance of Adhesion and Spreading

Figure 4.4A presents a series of video images for the adhesion of two vesicles containing 30% FITC-NeutrAvidin (on the right) and biotin (on the left) functionality. Initially the vesicles are held at suctions producing 2.1mN/m and 0.6mN/m tensions in the left and right membranes. After the vesicles are put into contact at time zero, subtle changes in the developing contact region suggest that avidin-biotin binding proceeds slowly without significant growth of the contact zone or contact angle. During this time

there is no significant change in vesicle shape or in the lengths of the projections of the vesicles in the pipettes, indicated by arrows. This latency period persists for several minutes, after which time, spreading initiates abruptly, in this case between 413 and 414 seconds.

During spreading, the contact height (defined as the diameter of the contact region, measured flat in plane) and the contact angle increase rapidly at first and then almost level off in less than a minute. Even after the changes in the adhesion plaque region have slowed considerably, adhesion continues at a substantial rate as indicated by continued changes in the projection lengths of the vesicles in the two pipettes. Eventually the lower tensioned FITC-NeutrAvidin vesicle, on the right, escapes its pipette, terminating the experiment. (As this occurs, the membrane temporarily catches on the end of the right pipette, altering the kinetics. In the final escaped state, the contact angle is lower than that when the right vesicle was in the pipette.)

An interesting point worth noting about Figure 4.4A, and in general, is that during the latent period, the apparent contact angle is poorly defined and mostly dependent on how the user brings the two vesicles together. (A true tangent point is clearly impossible to achieve in practice.) Once spreading initiates in earnest, the contact angle is easily measured. This small distinction is an important for interpreting the dynamic mechanism, below.

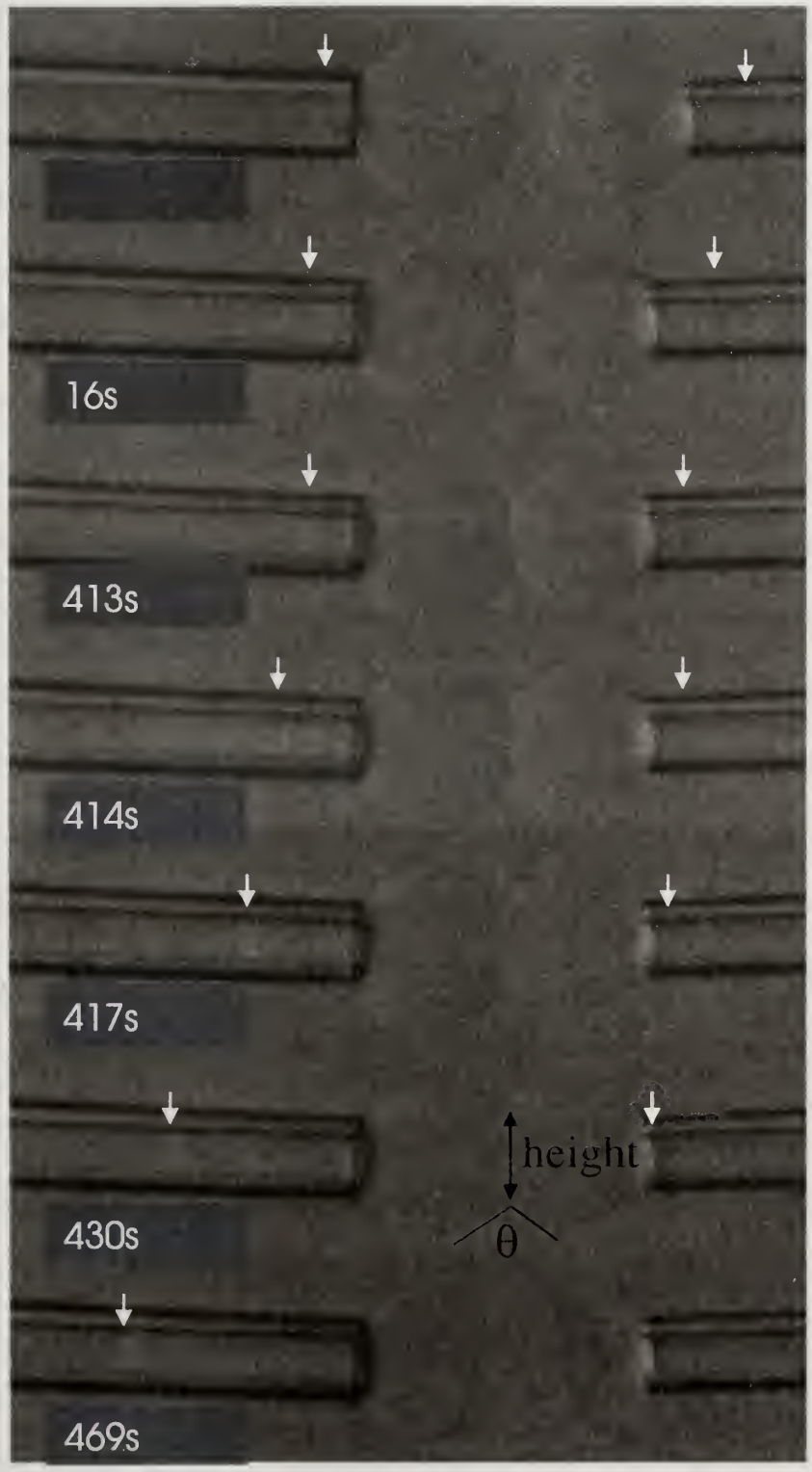

Figure 4.4A Video still images of dynamic adhesion between a vesicle containing 30mol% b-5329 (left: 2.1mN/m) and one presenting FITC-NeutrAvidin-conjugated 30%-b-5329 right (0.6mN/m). Contact angle and contact height are defined here.

Adhesion and spreading kinetics for the vesicles in Figures 4.4A are summarized quantitatively in Figure 4.4B and 4.4C, where the former shows the entire experiment and the latter focuses on the rapid spreading process. The projection length evolution is summarized in Figure 4.4D. As we demonstrated previously for vesicles with 100% avidin and biotin functionality,[23] the dynamic process for 30% avidin and biotin functionalization appears tri-phasic, with latent, rapid spreading, and slower spreading phases. (While the turnover from rapid spreading to slow spreading was always a small matter of judgment for the 100% functionalized vesicles of the previous study, the distinction is more subtle at lower membrane functionalities. Therefore we do not wish to make a strong argument for a distinction between the 2nd and 3rd phase of the kinetics.) In the current work, we observe the tri-phasic character for all vesicle pairs with 30% or greater functionality, and more generally when adhesion is sufficiently strong to produce spreading. To emphasize, it is spreading that is being documented in Figures 4.4B-D, a somewhat distinct and more complicated physics than that of avidin-biotin binding alone. At membrane functionalities of 25% and lower, spreading (and therefore tri-phasic kinetics) was not observed, even though there was concrete evidence for avidin-biotin binding. Put differently, the latent period was indefinite from a practical experimental perspective. We waited between 20 and 30 minutes in most cases and up to 40 minutes in others and never observed spreading, with the upper limit

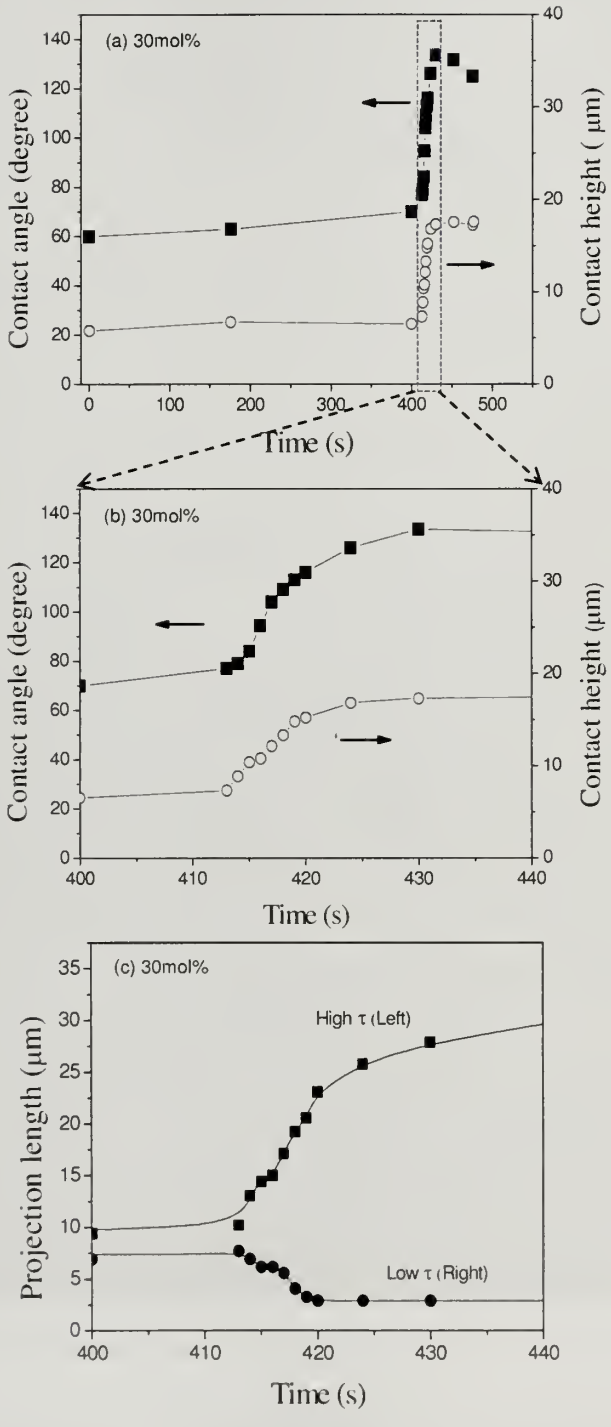

Figure 4.4B Contact angle and contact height evolution for the data in 4.4A.; 4(b) close-up of (a). (c) shows evolution of projection lengths in the pipettes. The right vesicle becomes stuck on the pipette tip around 420 seconds, and later escapes.

on the waiting period capped by the evaporation from the vesicle chamber. There was, however, evidence for adhesion at times shorter than this practical limit, as illustrated in Figure 4.5 A and 4.5 B. Here, after 20 minutes of contact but without spreading, attempts were made to separate the vesicles, by increasing membrane tension on the left side from 2.9 to 6.6 mN/m. This caused the left vesicle to rupture, but in a way that an adhesion plaque remained. Indeed, the left vesicle tore partway between the plaque and the pipette, so that the part of the membrane adhering to the surviving vesicle closed back on itself to form a small adherent vesicle (which is difficult to see because of the loss of the refractive index contrast fluid, ie. escape of interior sucrose solution). In Figure 4.5A and in at least 3 other cases where we broke vesicle pairs with 25% functionality that had been in contact for 10 minutes or more, we never observed peeling of the contact zone, an indication of irreversible adhesion that never produced spreading. Also of note, if we put two 25% vesicles into contact for shorter times, we would not always observe breaking but instead would find evidence for pull-out, for instance a slight transfer of fluorescent material across the interface, or a patch on one vesicle near the contact region that appeared darker in Hoffman contrast, and the inability of the vesicle pair to adhere when contacted a second time. We therefore believe that, in general at these lower levels of functionality, avidin-binding proceeded within the contact zone with the number of cross-bridges increasing with time, but of insufficient strength to produce spreading.

For membranes with 30% biotin functionality or greater, sufficient to produce spreading, the biotin concentration influenced the kinetics of adhesion and spreading. This is most apparent in Figure 4.6A, which demonstrates that the duration of

Figure 4.5A Video images of a "peeling attempt" of a 25 mol% functionalized vesicle pair. Time zero here denotes the start of the peeling experiment where the left tension was increased. As a result, the left projection stretches to the left side of the video frame. Note the time in milliseconds. At 31 ms, the left vesicle starts to rupture, and optical contrast is lost. The final cap is shown in the frame at 43 ms.

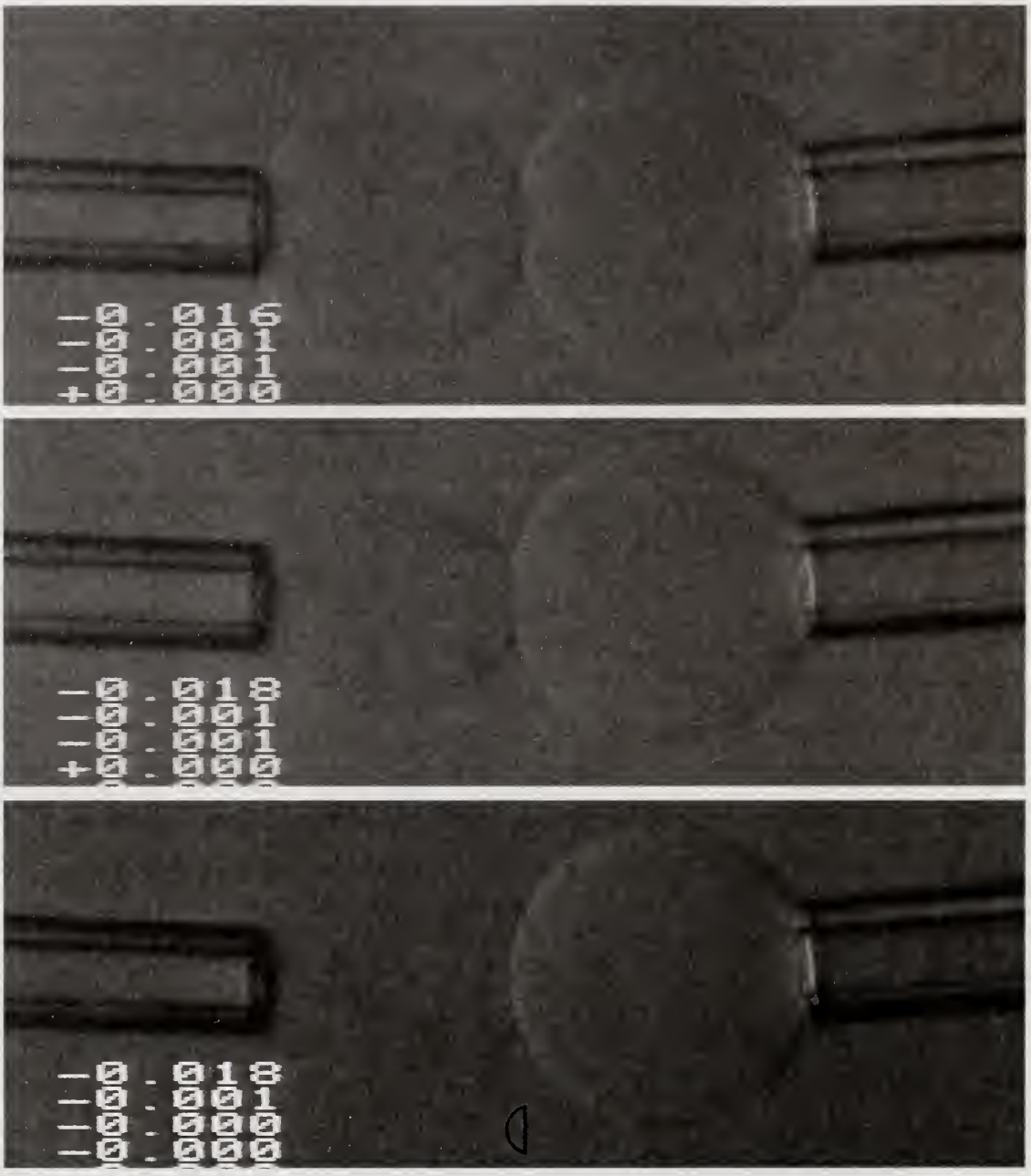

Figure 4.5B Another video images of a "peeling attempt" of a 25 mol% functionalized vesicle pair.

the latent phase, τ_{Lat}, increases as the loading of biotin and avidin is decreased. Within the nominal concentration range 50-100%, there is no significant impact of biotin and FITC-NeutrAvidin density on τ_{Lat}. This is consistent with the fluorescence data in Figure 4.1, which indicate a limit on FITC-NeutrAvidin loading above a nominal biotin functionalization of 100%. In the range 20-50% of membrane functionalization, however, the results are dramatic, and the latent time, τ_{Lat}, diverges near 20% functionalization. At lower FITC-NeutrAvidin and biotin concentrations in the membrane spreading is not accessible from the practical experimental perspective.

The impact of FITC-NeutrAvidin and biotin density on the spreading kinetics themselves is evident in Figure 4.7 and 4.8 (for contact angle and height, respectively), which show linear spreading kinetics at biotin and FITC-NeutrAvidin concentrations of 50 and 100% and a more curved kinetic character at lower membrane functionalizations. The latter is best described by an exponential form, however the fit to a $t^{1/2}$ form is worth examining, as shown in parts B and C. Relative to contact angle behavior, similar dynamics (with differences in the quantitative details) are apparent when one considers the spreading height evolution in Figure 4.8. The failure of the $t^{1/2}$ form to describe the data is consistent with our expectations that translational diffusion is not an important mechanism, due to the dense membrane functionality and the potential for membrane crosslinking by multifunctional FITC-NeutrAvidin.

The spreading rates, (or, in the case of nonlinear spreading behavior, the initial spreading rates) are quantified, as a function of biotin and FITC-NeutrAvidin membrane

functionalization, in Figure 4.9A. Here, at biotin and FITC-NeutrAvidin concentrations exceeding 50%, there is no impact of concentration on kinetics, consistent with the limit

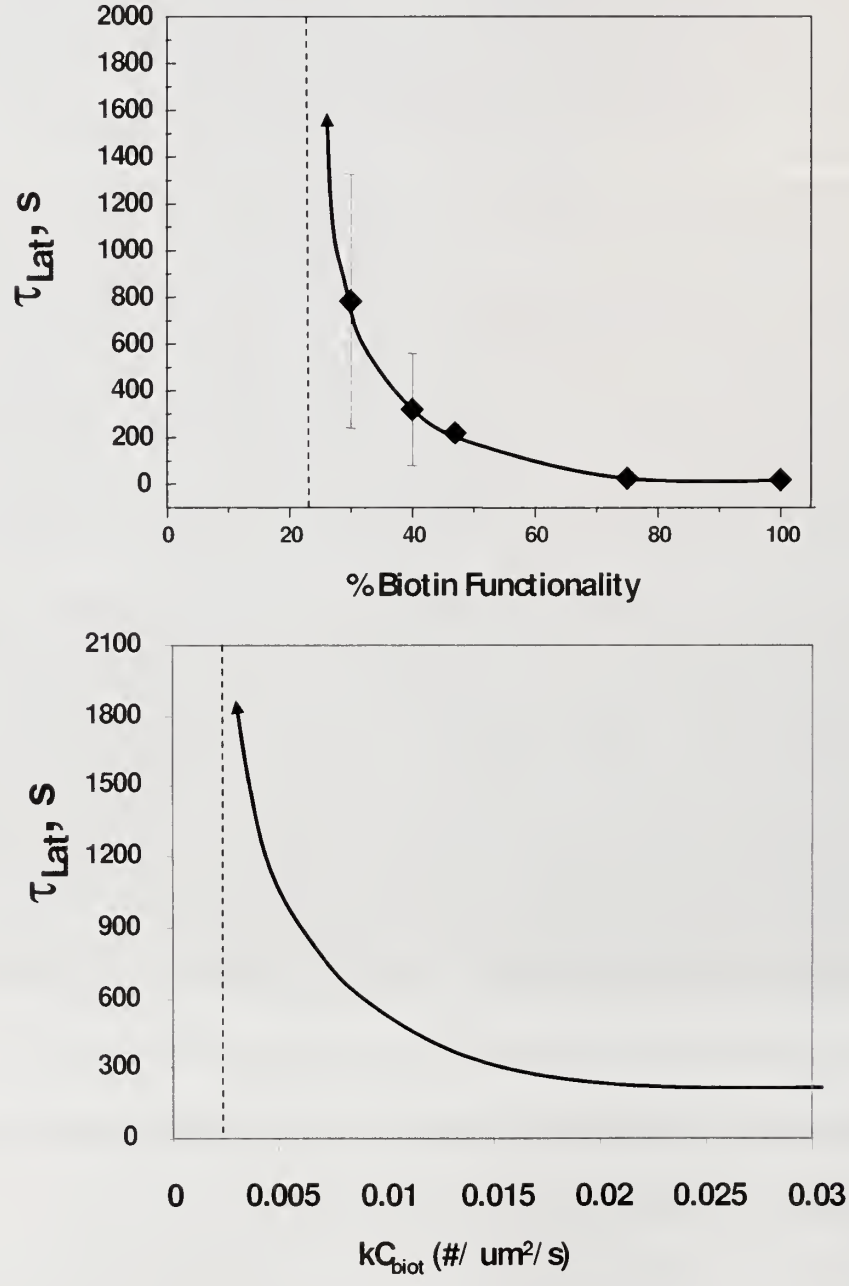

Figure 4.6 (A) Duration of experimentally-observed latent period, prior to the initiation of spreading. (Curve simply guides the eye) (B) Duration of latent period predicted by equation 4.4.

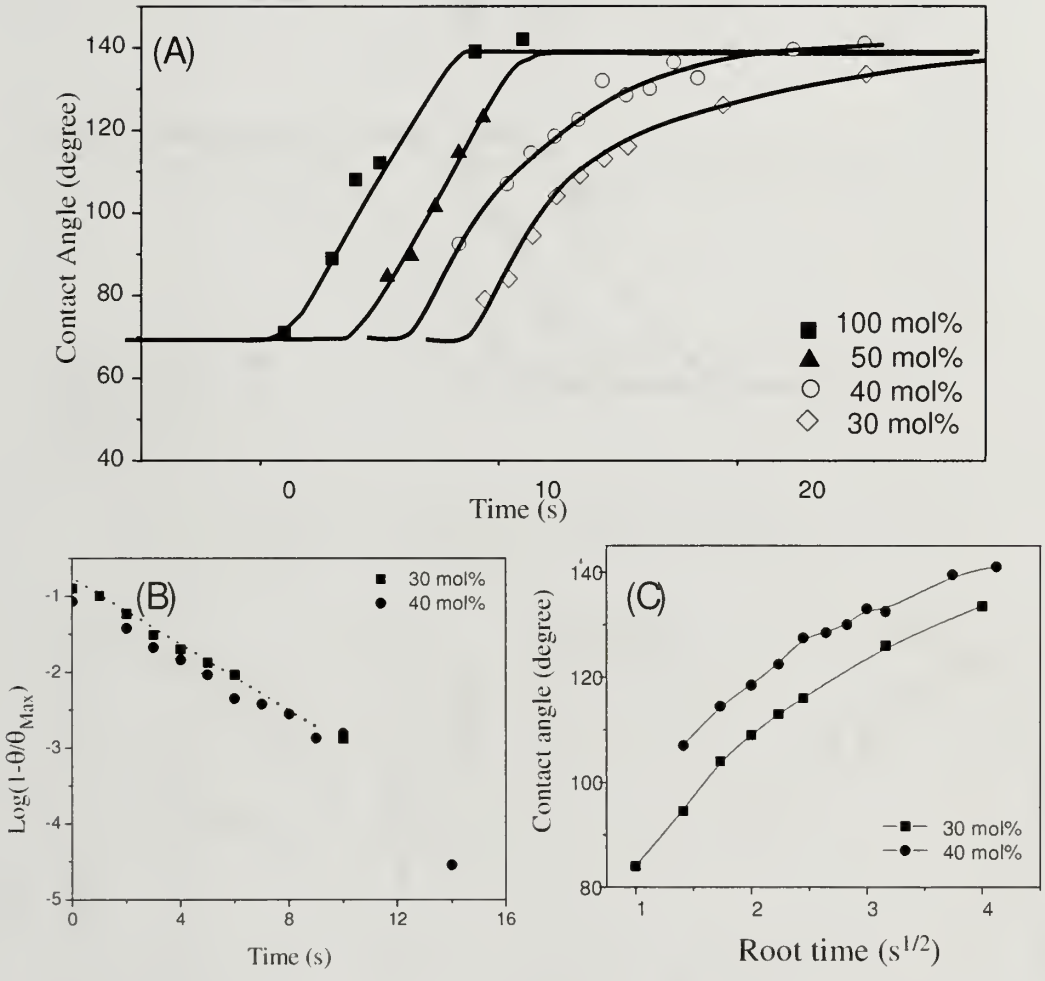

Figure 4.7 Spreading rates, as gauged by contact angle evolution for different levels of membrane functionalization, with time starting at the end of the latent period. In (A), the data are shifted, relative to each other, for ease of viewing. Curves guide the eye. (B) Semi-log plot tests exponential form for 30% and 40% functionalization. Here the time constant was 4.6 ± 2 s for all the 30% and 40% vesicles studied. (C) Testing the square root time dependence for the 30% and 40% functionalization argues against $t^{1/2}$ forms.

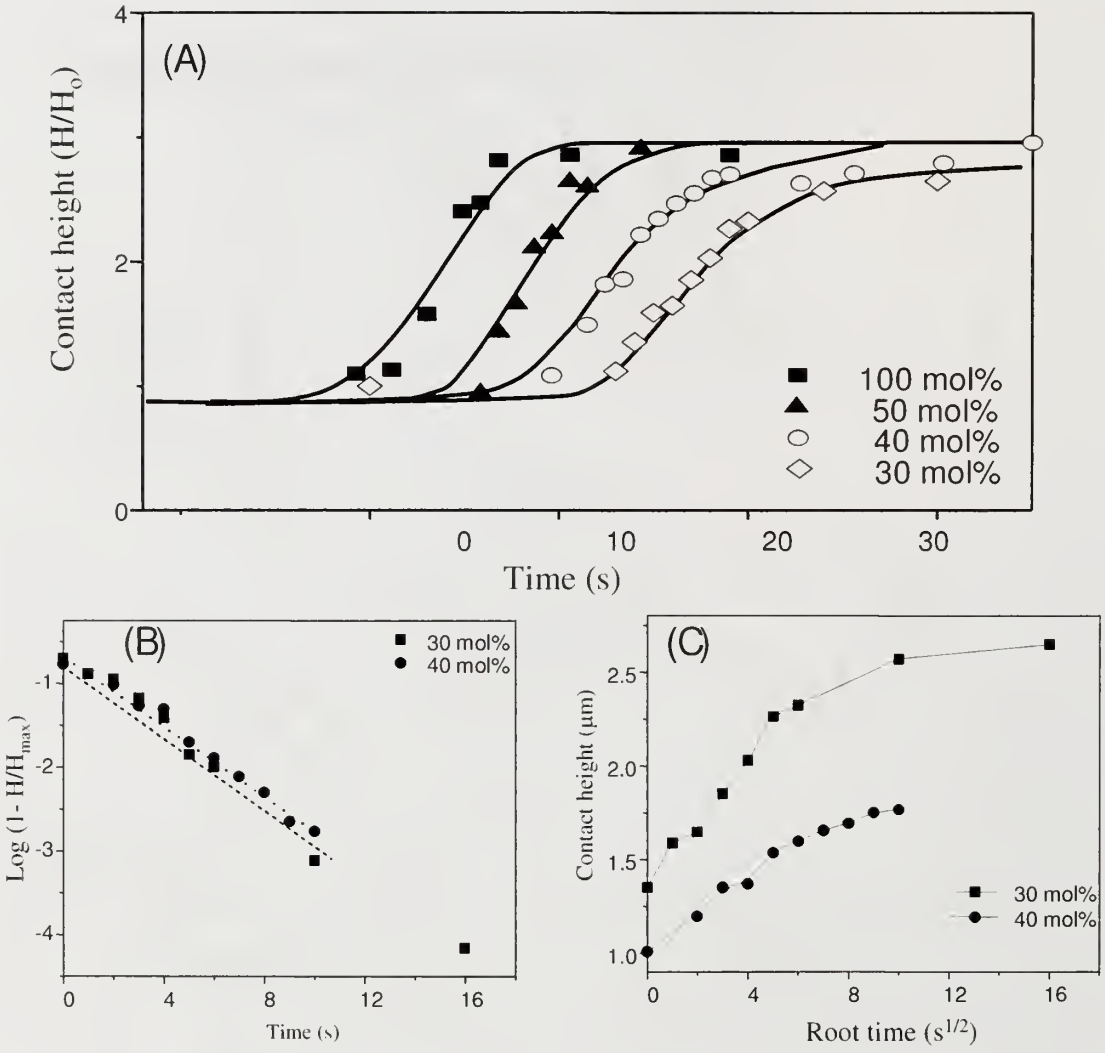

Figure 4.8 Spreading rates, as gauged by contact height, for different levels of membrane functionalization, with time starting at the end of the latent period. In (A), the data are shifted, relative to each other, for ease of viewing. Curves guide the eye. (B) Semi-log plot tests exponential form for 30% and 40% functionalization. Here the time constant was 4.6 ± 2 s for all the 30% and 40% vesicles studied. (C) Testing the square root time dependence for the 30% and 40% functionalization argues against $t^{1/2}$ forms.

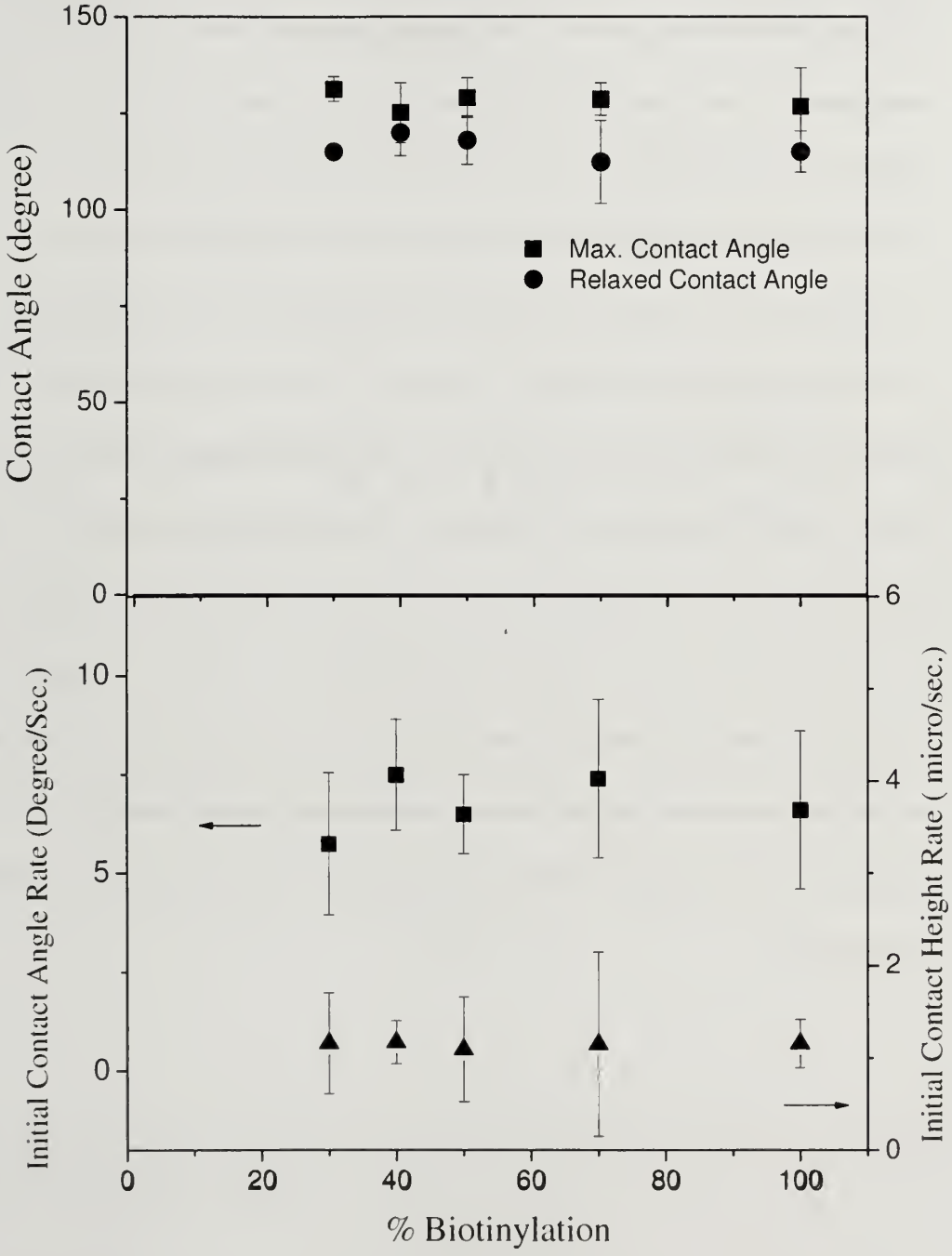

Figure 4.9 (A) The maximum contact angle achieved before escape and the relaxed contact angle after escape (B) The initial spreading rates, as measured by the rate of change of contact angle and rate of change of contact height.

of FITC-NeutrAvidin functionalization illustrated in Figure 4.1. In the range from 30-50% functionalization, however, the spreading rate continues to be relatively independent of membrane functionalization, with the same true of the ultimate contact angle in Figure 4.9B. These observations may suggest that in the limit of strong driving forces for spreading and engulfment, the processes is limited by other physics, perhaps viscous processes within the membranes or surrounding fluid. The adhesion is sufficiently strong that the ultimate contact angle cannot describe the adhesion strength. Indeed, the maximum adhesion work which can be calculated from the contact angle is 2θ(low-side), as θ approaches 180 degrees. This quantity is on the order of mN/m, which is smaller than thought to occur with NeutrAvidin and biotin. These observations are also consistent with our previous observation that, at 100% functionalization, variations in membrane tension in the range 0.1 to 2 mN/m (for the low tensioned vesicle) had no impact on the adhesion and spreading kinetics. Indeed, in the current work we also see negligible impact of tension in the range for any of the membrane compositions.

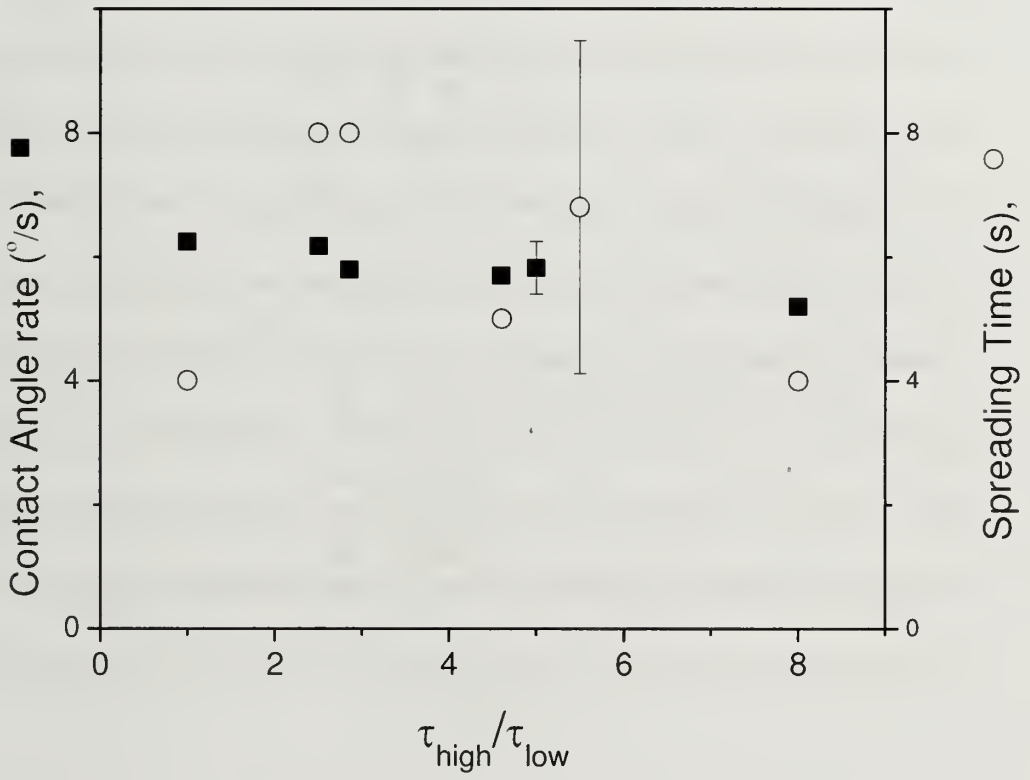

Figure 4.10 Rate of contact angle growth and and duration of phase 2, as function of the membrane tension ratio ($\tau_{Substrate}$ / $\tau_{Adherent}$) in adhesion experiments with 50mol% biotinyl DC5329/5329 vesicles.

For a number of different vesicles, it was found that neither the value of the low tension, nor its ratio relative to the level of the high-side vesicle tension had any impact on the adhesion behavior, as indicated in Figures 4.11 and 4.12. As was shown in detail for fully functionalized vesicles in our prior paper[23], we also find here for lower levels of membrane functionalization, that the membrane tension (on the low side in the range from 0.1 to 2 mN /m) influenced neither the spreading rates nor the ultimate contact angles observed. This is an indication that once spreading initiates, the driving force for adhesion far outbalances any tension-related mechanical counter-forces. Figures 4.11 and 4.12 also emphasize that the spreading rates and the ultimate contact angles are insensitive to the density of membrane functionalization. Because spreading likely results from the relaxation of a metastable state, the rate limiting spreading step is likely due to membrane dissipation. The nearly constant levels of the ultimate contact angle qualitatively indicate strong adhesion, and cannot differentiate between different levels of membrane functionalization, as the adhesion is so strong as to be irreversible.

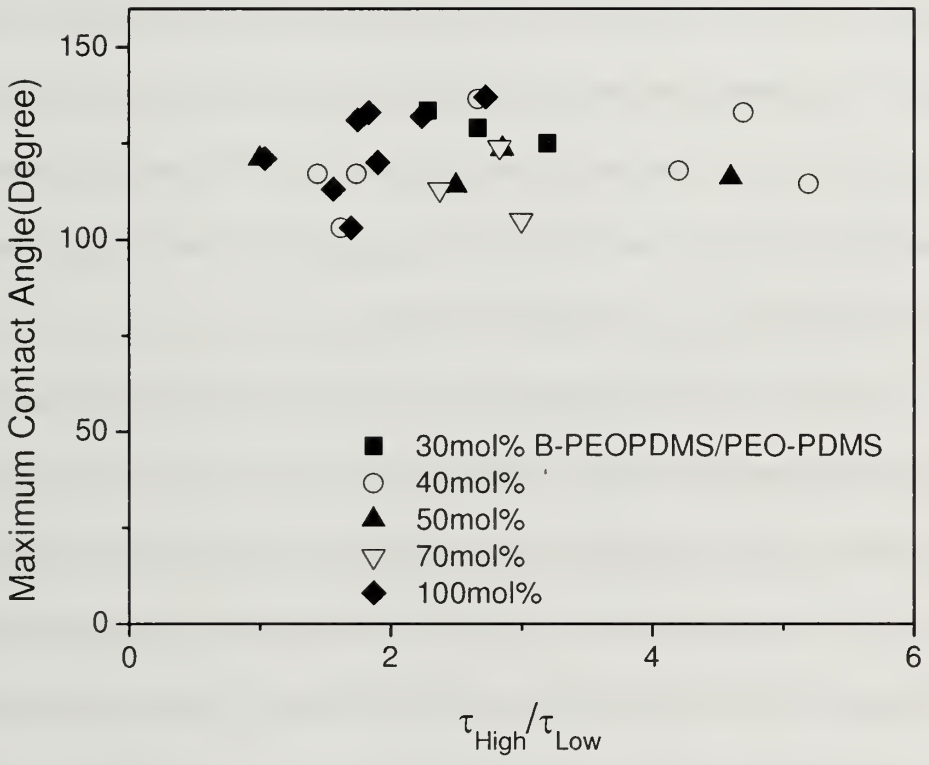

Figure 4.11 The maximum observed contact angle as a function of the tension ratio of the substrate membrane to the adherent vesicle, for different levels of membrane functionalization.

4.3.3 Mechanism: Latency and Nucleation

The latent period, whose duration diverges around 20% membrane functionality, is reminiscent of a nucleation process. Instead of requiring a nucleus of a critical size to initiate condensation of a bulk phase, one could imagine needing an adhesion-plaque nucleus with a critical adhesion energy (number of crossbonds) or size to initiate spreading. The energy of avidin-biotin binding, which drives spreading, must overcome the energy barrier posed by and the line tension around the plaque. In our system, we expect the line tension to be dominated by bending.

In Figure 4.4, the distinguishing feature which marks the beginning of spreading is a sudden and dramatic change in vesicle shape, to produce a finite macroscopic contact angle. Figure 4.12 illustrates our explanation concerning the microscopic events taking place in the adhesion plaque. During the latent period, the size of the contact zone depends on how the two vesicles are brought together, with a single point of tangency impossible to achieve in practice. With the two vesicles mildly compressed against each other, the contact angle is difficult to define macroscopically, initially approaching zero microscopically. During the latent period, bonds form in the contact zone, as evidenced in Figure 4.5. When spreading initiates at the end of the latent period, the vesicles snap into contact (with the snapping slowed and damped by viscous resistance), giving a better-defined macroscopic contact angle as a result of a sharp bend of the low-tensioned membrane near the edge of the adhesion plaque. As spreading proceeds, the contact area grows and the sharp bend or kink rolls forward. Both the

initial kinking of the membrane at the edge of the adhesion plaque and its rolling forward (like a reverse peel test, or driving on a flat tire) expend energy.

While our study does not measure the kink directly, other labs studying the adhesion of heavy flaccid vesicles on planar substrates have introduced the related concept of a transition zone, based on data from reflectance interference contrast microscopy (RICM).[25, 27] In the case of heavy flaccid vesicles with τ estimated to be 1-5 μN/m,[25] the transition zone bridging between the local contact and the macroscopic contact angle, was about 100-200 nm.[25] This value represents a radius of curvature that costs bending energy. We expect, due to the tension applied by our pipettes, that our transition region will contain a sharper kink than observed with flaccid vesicles. Indeed, scaling arguments that balance surface tension and bending energy (with constant adhesion implied) estimate that the kink radius goes as the square root of the multiplicative change in tension.[43] ($r_c = [\kappa_b/\tau]^{1/2}$) Therefore as the vesicle tension is increased 100- or 1000-fold, from the situation with flaccid vesicles (1-5 μN/m) to the tension of 0.1 – 1 mN/m in our experiments, the radius of the kink will decrease as $(100)^{1/2}$ or $(1000)^{1/2}$. We therefore estimate that the kink radius that occurs at the end of the latency period to be in the range 5-10 nm.

Attempting a semi-quantitative formulation, we weigh binding and bending energies. For the former, we assume that local chain reconformations but not lateral translation within the membrane are needed to facilitate the formation of NeutrAvidin-biotin cross bridges. The adhesion energy within the plaque nucleus goes as $\pi r_n^2 E_{Na}$-

$_bC_{xb}$, where r_n is the radius of the adhesion plaque nucleus or contact zone, which we treat as roughly constant during the latent phase of a given experiment, on the order of a micron. $E_{Na\text{-}b}$ is the interfacial binding energy of a single NeutrAvidin-biotin bond, and C_{xb} is the number of cross-bonds formed per unit area. During the latent phase, we observed qualitatively that C_{xb} increases with time, a process which we treat as irreversible and first order, with $C_{xb}(t) = k_i C_{biot} t$. ($k_i$ is an interfacial avidin biotin-binding rate constant, influenced and likely dominated by PEG local chain reconformations). In the contact zone, only a fraction of the NeutrAvidins and biotins actually seem to be available for crossbridge formation. This may be because the NeutrAvidin may be somewhat buried in the PEG corona, or because more than one of the four binding pockets on each NeutrAvidin molecule may be occupied by a biotin from the first side of the interface. We could therefore modify the first order rate law to include α, the fraction of NeutrAvidins which could, through configurational polymer chain motions on the timescale of interest, become available for binding: $C_{xb}(t) = \alpha k_i C_{biot} t$. C_{xb} is, therefore, a surface concentration considerably smaller, we estimate by more than one order of magnitude, than the actual concentration of biotins and NeutrAvidins present. (It is also worth noting that, with the adhesion plaque nucleus of constant area being formed at time zero, the concentration of crossbridges should not be spatially dependent in the contact zone. At every point in the contact zone, the contact was established at the same instant.)

Opposing the chemical attraction and preventing spontaneous spreading, a line tension-type bending term goes as $2\pi r_n \kappa_b / r_c$. Here κ_b is the bending modulus and r_c is

the radius of curvature of the kink. In our simple treatment, we estimate κ_b to be independent of the radius of the kink, an assumption which will break down as r_c approaches the membrane thickness. With the adhesion and bending terms making up the free energy to initiate a spreading process, spreading will occur when enough bonds form so that the total energy, E_a is minimized.

$$E_a = 2\pi r_n \kappa_b / r_c - \pi r_n^2 E_{Na\text{-}b} C_{xb} \tag{4.3}$$

Here, with κ_b order 10kT, r_c roughly 10 nm, r_n of the contact zone about a micron, $E_{Na\text{-}b}$ about 35 kT,[44] one estimates that 30 crossbridges per um^2 will suffice to initiate spreading. (If the NeutrAvidin-biotin bond energy is actually weaker in our system, a greater number of bond would be needed.)

While equation 4.3 is useful, it does not predict the nucleation time. For this we must consider the probability of overcoming the energy barrier posed by membrane bending. This energy barrier decreases with time as interfacial bonds form; however, the barrier need not drop to zero for nucleation to occur. To quantify this, we consider an activation process with an (unknown) attempt frequency, ω:

$$\tau_{Lat} = \omega^{-1} e^{Ea/kT} = \omega^{-1} \exp\left(2\pi r_n \kappa_b / r_c - \pi r_n^2 E_{Na\text{-}b} C_{xb}(C_{biot}, \tau_{Lat})\right)/kT \tag{4.4}$$

Note that in equation 4.4 the duration of the latent period, τ_{Lat}, appears implicitly in the exponential on the right hand side, giving an increasing number of crossbridges with time. Solution of equation 4.4 requires knowledge of the kinetics of crossbond formation, which we assume to be a first order rate process, described above. While ω is unknown, we expect it to be substantially damped with respect to kT/h, and it turns

out, even within 12 orders of magnitude, ω does not much affect the shape of how equation 4.4 diverges. Figure 4.6.B shows the solution to equation 4 with κ_b = 10kT (treated as constant for a first pass calculation), r_c = 10 nm, r_n = 1 um, and $E_{Na\text{-}b}$ = 35 kT for 2 values of ω, 2.2 and 2.2 x 10^6 s^{-1}. The x-axis, $k\alpha C_{biot}$, when compared with the experimental results in Figure 4.6A, allows a determination of $k\alpha$, the forward rate constant times the fraction of biotins or avidins which are actually available. Indeed we find that $k\alpha$ is roughly 10^{-7} s^{-1}, the product of a slow reaction rate constant and a small fraction of biotins or NeutrAvidins actually being available. While the actual value of $k\alpha$ depends on the bending energy of the kink and size of the adhesion plaque nucleus, it is clear that interfacial bond formation is a slow process for our particular system: Even with 20% nominal membrane functionalization, we never once observed in 20-40 minute contact times, enough bonds to form to initiate spreading. We conclude that α is order of 0.01 or smaller, and that the forward binding constant in our particular crowded interfacial environment is also quite slow. (We note here that taking the concentration dependence of κ_b into account will change the quantitative assessment of K_a; however, the current simplified constant-κ_b treatment suffices at the level of a first pass calculation).

Growth and Spreading. The linear or single exponential spreading kinetics in Figures 4.7 and 4.8 display two noteworthy features: First, the kinetics are virtually independent of membrane functionalization, as long as there is sufficient functionalization to produce spreading at all. Second, the timescale for spreading is generally on the order of 10 seconds, with spreading rates on the order of 1+ um/s and 6-7 degrees/s. (We note that the less densely functionalized membranes did exhibit an

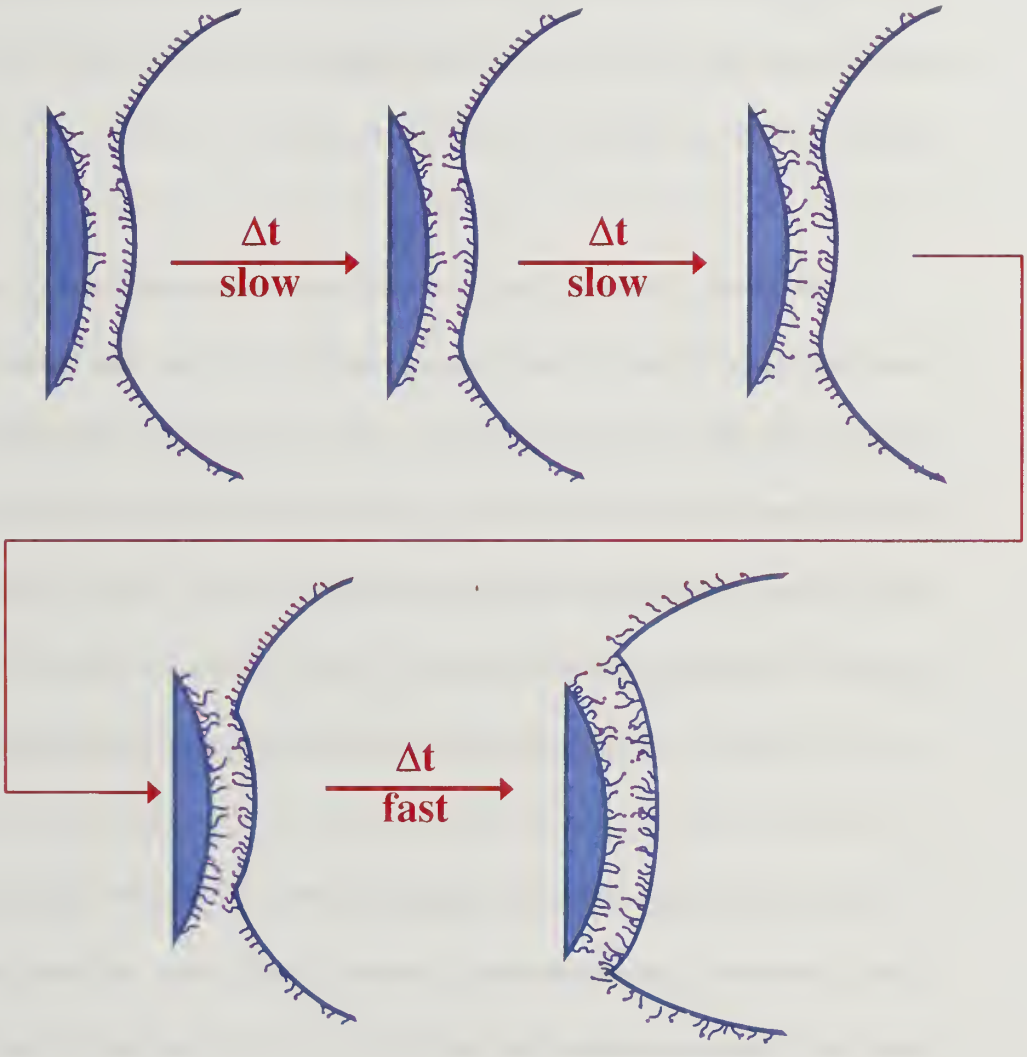

Figure 4.12 Schematic of bond formation during the latent phase (first row of 3 images) and then the establishment of the kink and spreading (2 images in second row). Note that as spreading proceeds, the kink may stay at nearly constant radius, but it wraps further away from the static vesicle.

exponential tail in the spreading dynamic, and also that the duration of the spreading process depended on the initial vesicle flaccidness, that is the initial length of the projection in the pipette. The more initially flaccid vesicles, those with longer initial projections, gave more protracted spreading processes and were able to engulf a greater area percentage of a target vesicle of a given size.)

As already discussed, the dense membrane functionality, the potential for membrane crosslinking by avidin, and the lack of a $t^{1/2}$ spreading kinetic all argue against in-membrane receptor diffusion as a rate limiting step in spreading. Spreading kinetics must therefore be limited by processes and conditions right at the spreading front, the equivalent of surface limitations in the classical situation of heterogeneous reactions. Our system fails to exhibit the expected linear concentration dependence, seen, for instance, with a model system employing integrins at much lower concentrations than the avidin concentrations here.[27] One explanation for our first order kinetics during the latent period, but apparent lack of first order kinetics during our growth phase is the small available number of receptors and the importance of corona chain reconformations in making receptors available for binding. In the latent phase, the time available for binding and interfacial reconformations is generally long, so that the first order rate law, albeit dominated by chain reconformations, becomes apparent. In the spreading process, there is only a short opportunity time during which receptors at the edge of the plaque can bind: Once the crack tip closes, any subsequent binding does not contribute to the spreading rate.

Our spreading rates, in Figures 4.9, are among the fastest reported in the literature, regardless of the nature of the receptor or its presentation on the membrane.[8, 25, 27] While we are tempted to expect even faster spreading kinetics given the appearance of a strong chemical driving force for spreading, it is worth considering that in our case viscous resistance could be more important in determining the spreading rate. One type of viscous resistance where out-flow of water dominates closing crack at the edge of the plaque is expected to follow a single exponential form with a characteristic time inversely proportional to membrane tension,[45] on the order of 0.1 to 0.01 s for our system. Thus, at our high membrane tensions, viscous resistance from effluent water is too small to limit spreading. It is, however, worth mentioning that the viscous resistance from water seems to explain spreading of heavy flaccid vesicles.[25] Indeed, for the situation of heavy flaccid vesicles settling on a densely functionalized avidin surface, the spreading rate did not depend on avidin concentration.[25]

For our system, the membrane bending energy was a critical part of the nucleation processes, and so it is worth considering the possibility that membrane bending itself might also limit spreading. While our data do not conclusively argue for or against this possibility, the scenario is worth describing: The bending dissipation opposing spreading is different than that opposing nucleation. The latter requires kink formation, directly related to the bending modulus. To oppose spreading, the bending process is essentially one of viscous dissipation where the sharp kink rolls forward at the spreading front, in a tank treading motion, like a reverse peel test. Additionally, the kink wraps a greater fraction around the bend, as shown in Figure 4.12, as the front

progresses. Further, as spreading proceeds, the perimeter of the adhesion plaque grows, costing an additional energy. Hence, one envisions 3 bending type terms work together to limit spreading: sharp tank treading, more extensive wrapping around as the contact angle grows, and the increase in plaque perimeter. The latter two contributions can be readily formulated with known bending moduli, however, the relaxation and dissipation processes involved in tank treading or kink rolling are, at this point, difficult to describe.

4.4 Summary

This work examined the formation dynamics of adhesion plaques between densely-functionalized irreversibly-binding vesicle membranes fixed at moderate tension in micropipettes. For variations in the density of receptors in the range relevant to spreading, adhesion and spreading kinetics were fundamentally controlled by chemical binding, chain relaxations, and membrane mechanics. In-membrane translational diffusion of functionalized chains towards the adhesion plaque was not part of the adhesion or spreading mechanisms.

Adhesion and spreading was observed to occur in distinct stages: During the initial latent period, avidin-biotin bonds formed progressively in the contact region, but there was no spreading or growth of the contact area. Even without spreading, the binding between the two vesicles was stronger than the membranes themselves, producing pullout or membrane rupture if separation was attempted. After some time, however, spreading initiated rapidly, and continued until the lower-tensioned vesicle escaped its pipette. For vesicles with the highest densities of ligands and receptors, the latent stage was short. At lower densities of ligands and receptors (but not so low as to enter the regime where lateral diffusion becomes important) the latent period became protracted: Around 20 % membrane functionalization, it was indefinite from the practical experimental perspective. In general, when spreading was observed, the kinetics were only weakly dependent on the density of ligands and receptors.

Membrane tension, which was on the order of 0.1 – 1 mN/m had negligible impact on the adhesion and spreading kinetics.

The observation of a multi-step adhesion process, especially the abrupt onset of spreading, was explained by a nucleation-growth model in which an energy barrier, associated with the formation of a sharp membrane kink (with curvature on the order of 10 nm) at the contact line bordering the plaque, was overcome at the start of spreading. During the latent period, the bond formation in the contact region reduced the energy barrier, so that kink formation became feasible on experimental timescales. Once the vesicles snapped into contact, spreading proceeded. Since spreading, or at least the initial phases of spreading, were the result of an instability, they were expected proceed very quickly. They were, however, observed to take place on a timescale of about 10 seconds, with little dependence on the membrane concentration. The most likely explanation is that an otherwise rapid spreading was is damped by viscous dissipation, such as the rolling forward or tank-treading of the kink, in addition to changes in the extent of the kink and the perimeter of the contact zone.

Among the details revealed by this study was the fact that, within densely functionalized avidin-biotin bearing membranes, only a small fraction of the ligands and receptors were available for binding across an interface. The quantitative assessment further revealed the likelihood that the binding rate constant was substantially smaller than that for solution phase binding. Sample calculations for the duration of the latent period were in excellent agreement with observations, arguing in favor of the

nucleation-instability model, which included first order rate kinetics for interfacial avidin-biotin binding, and particular values for the strength of avidin-biotin bonds and the system geometry. Even with variations in the parameters we employed, for instance a moderately different value of avidin-biotin binding strength as a result of interfacial conditions, we expect the main tenets of the model to hold. The observed dependence of the bending modulus on membrane composition, which was not included in the model, would also give longer latent periods for less densely functionalized membranes, and relax the assumption of first order binding kinetics. Even with this level of uncertainty, the model makes a compelling case for the role of membrane mechanics, and the concept of nucleation of a spreading process via membrane kinking.

Beyond a mechanistic explanation of adhesion plaque formation in simple membrane systems, the significance of this work lies in its emphasis of the role of membrane mechanics, particularly bending, on adhesion. It perhaps warrants reiteration that bulk contributions to adhesion can still be important, even when the "bulk phase" is only nanometers in thickness. While one might expect such "bulk" contributions to be important in peeling experiments, we show here that they are equally important in cases of crack healing. The implications are substantial when contact angle analysis is invoked to assess adhesion. Not only can the strong or effectively irreversible nature of membrane attractions confound a contact angle analysis in the usual way, but energy barriers deriving from the membrane themselves can prevent a meaningful contact angle from being obtained in the first place. The cases in point are systems with strong bending moduli: if sufficient bonds do not form on experimental timescales, the

apparent contact angles can be extremely low, and a proper contact angle not truly established. The new finding that irreversible adhesion does not necessarily produce spreading and engulfment has qualitative implications for the use of vesicles as drug-delivery vehicles and scavengers. Though polymeric vesicles have the advantage of robustness and versatility, they will behave very differently from liposomes in their interactions with cells and other objects.

REFERENCES

1. Evans, E. A., Analysis of Adhesion of Large Vesicles to Surfaces. *Biophysical Journal* **1980,** 31, (3), 425-431.

2. Evans, E. A., Minimum Energy Analysis of Membrane Deformation Applied to Pipette Aspiration and Surface-Adhesion of Red-Blood-Cells. *Biophysical Journal* **1980,** 30, (2), 265-284.

3. Evans, E.; Metcalfe, M., Free-Energy Potential for Aggregation of Giant, Neutral Lipid Bilayer Vesicles by Vanderwaals Attraction. *Biophysical Journal* **1984,** 46, (3), 423-426.

4. Evans, E.; Needham, D., Physical-Properties of Surfactant Bilayer-Membranes - Thermal Transitions, Elasticity, Rigidity, Cohesion, and Colloidal Interactions. *Journal of Physical Chemistry* **1987,** 91, (16), 4219-4228.

5. Evans, E.; Needham, D., Attraction between Lipid Bilayer-Membranes in Concentrated-Solutions of Nonadsorbing Polymers - Comparison of Mean-Field Theory with Measurements of Adhesion Energy. *Macromolecules* **1988,** 21, (6), 1822-1831.

6. Evans, E. A., Force between Surfaces That Confine a Polymer-Solution - Derivation from Self-Consistent Field-Theories. *Macromolecules* **1989,** 22, (5), 2277-2286.

7. Lin, J. J.; Ghoroghchian, P.; Zhang, Y.; Hammer, D. A., Adhesion of antibody-functionalized polymersomes. *Langmuir* **2006,** 22, (9), 3975-3979.

8. NopplSimson, D. A.; Needham, D., Avidin-biotin interactions at vesicle surfaces: Adsorption and binding, cross-bridge formation, and lateral interactions. *Biophysical Journal* **1996,** 70, (3), 1391-1401.

9. Lin, J. J.; Bates, F. S.; Hammer, D. A.; Silas, J. A., Adhesion of polymer vesicles. *Physical Review Letters* **2005,** 95, (2).

10. Lin, J. J.; Silas, J. A.; Bermudez, H.; Milam, V. T.; Bates, F. S.; Hammer, D. A., The effect of polymer chain length and surface density on the adhesiveness of functionalized polymersomes. *Langmuir* **2004,** 20, (13), 5493-5500.

11. Kim, D. H.; Klibanov, A. L.; Needham, D., The influence of tiered layers of surface-grafted poly(ethylene glycol) on receptor-ligand-mediated adhesion between phospholipid monolayer-stabilized microbubbles and coated class beads. *Langmuir* **2000,** 16, (6), 2808-2817.

12. Poteau, S.; Argillier, J. F.; Langevin, D.; Pincet, F.; Perez, E., Influence of pH on stability and dynamic properties of asphaltenes and other amphiphilic molecules at the oil-water interface. *Energy & Fuels* **2005,** 19, (4), 1337-1341.

13. Pincet, F.; Le Bouar, T.; Zhang, Y. M.; Esnault, J.; Mallet, J. M.; Perez, E.; Sinay, P., Ultraweak sugar-sugar interactions for transient cell adhesion. *Biophysical Journal* **2001,** 80, (3), 1354-1358.

14. Evans, E.; Berk, D.; Leung, A., Detachment of Agglutinin-Bonded Red-Blood-Cells .1. Forces to Rupture Molecular-Point Attachments. *Biophysical Journal* **1991,** 59, (4), 838-848.

15. Evans, E.; Berk, D.; Leung, A.; Mohandas, N., Detachment of Agglutinin-Bonded Red-Blood-Cells .2. Mechanical Energies to Separate Large Contact Areas. *Biophysical Journal* **1991,** 59, (4), 849-860.

16. Richert, L.; Lavalle, P.; Vautier, D.; Senger, B.; Stoltz, J. F.; Schaaf, P.; Voegel, J. C.; Picart, C., Cell interactions with polyelectrolyte multilayer films. *Biomacromolecules* **2002,** 3, (6), 1170-1178.

17. Merkel, R.; Simson, R.; Simson, D. A.; Hohenadl, M.; Boulbitch, A.; Wallraff, E.; Sackmann, E., A micromechanic study of cell polarity and plasma membrane cell body coupling in Dictyostelium. *Biophysical Journal* **2000,** 79, (2), 707-719.

18. Strigl, M.; Simson, D. A.; Kacher, C. M.; Merkel, R., Force-induced dissociation of single protein A-IgG bonds. *Langmuir* **1999,** 15, (21), 7316-7324.

19. You, J.; Mastro, A. M.; Dong, C., Application of the dual-micropipet technique to the measurement of tumor cell locomotion. *Experimental Cell Research* **1999,** 248, (1), 160-171.

20. Satomaeda, M.; Uchida, M.; Graner, F.; Tashiro, H., Quantitative-Evaluation of Tissue-Specific Cell-Adhesion at the Level of a Single-Cell Pair. *Developmental Biology* **1994,** 162, (1), 77-84.

21. Anderson, K. W.; Li, W. I.; Cezeaux, J.; Zimmer, S., Invitro Studies of Deformation and Adhesion Properties of Transformed-Cells. *Cell Biophysics* **1991,** 18, (2), 81-97.

22. Brochard-Wyart, F.; de Gennes, P. G., Unbinding of adhesive vesicles. *Comptes Rendus Physique* **2003,** 4, (2), 281-287.

23. Nam, J.; Santore, M. M., Adhesion Plaque Formation Dynamics between Polymer Vesicles in the Limit of Highly Concentated Binding Sites. *Langmuir* **2007,** 23, (13), 7216-7224.

24. Albersdorfer, A.; Feder, T.; Sackmann, E., Adhesion-induced domain formation by interplay of long-range repulsion and short-range attraction force: A model membrane study. *Biophysical Journal* **1997,** 73, (1), 245-257.

25. Cuvelier, D.; Nassoy, P., Hidden dynamics of vesicle adhesion induced by specific stickers. *Physical Review Letters* **2004,** 93, (22).

26. Kloboucek, A.; Behrisch, A.; Faix, J.; Sackmann, E., Adhesion-induced receptor segregation and adhesion plaque formation: A model membrane study. *Biophysical Journal* **1999,** 77, (4), 2311-2328.

27. Boulbitch, A.; Guttenberg, Z.; Sackmann, E., Kinetics of membrane adhesion mediated by ligand-receptor interaction studied with a biomimetic system. *Biophysical Journal* **2001,** 81, (5), 2743-2751.

28. Bernard, A. L.; Guedeau-Boudeville, M. A.; Jullien, L.; di Meglio, J. M., Strong adhesion of giant vesicles on surfaces: Dynamics and permeability. *Langmuir* **2000,** 16, (17), 6809-6820.

29. de Gennes, P. G.; Puech, P. H.; Brochard-Wyart, F., Adhesion induced by mobile stickers: A list of scenarios. *Langmuir* **2003,** 19, (17), 7112-7119.

30. Hales, K.; Pochan, D. J., Using polyelectrolyte block copolymers to tune nanostructure assembly. *Current Opinion in Colloid & Interface Science* **2006,** 11, (6), 330-336.

31. McCormick, C. L.; Kirkland, S. E.; York, A. W., Synthetic routes to stimuli-responsive micelles, vesicles, and surfaces via controlled/living radical polymerization. *Polymer Reviews* **2006,** 46, (4), 421-443.

32. Kita-Tokarczyk, K.; Grumelard, J.; Haefele, T.; Meier, W., Block copolymer vesicles - using concepts from polymer chemistry to mimic biomembranes. *Polymer* **2005,** 46, (11), 3540-3563.

33. Discher, D. E.; Eisenberg, A., Polymer vesicles. *Science* **2002,** 297, (5583), 967-973.

34. Hill, R. M.; He, M. T.; Lin, Z.; Davis, H. T.; Scriven, L. E., Lyotropic Liquid-Crystal Phase-Behavior of Polymeric Siloxane Surfactants. *Langmuir* **1993,** 9, (11), 2789-2798.

35. Nilsson, K.; Mosbach, K., Para-Toluenesulfonyl Chloride as an Activating Agent of Agarose for the Preparation of Immobilized Affinity Ligands and Proteins. *European Journal of Biochemistry* **1980,** 112, (2), 397-402.

36. Nilsson, K.; Norrlow, O.; Mosbach, K., Para-Toluenesulfonyl Chloride as an Activating Agent of Agarose for the Preparation of Immobilized Affinity Ligands and Proteins - Optimization of Conditions for Activation and Coupling. *Acta Chemica Scandinavica Series B-Organic Chemistry and Biochemistry* **1981,** 35, (1), 19-27.

37. Dimitrov, D. S.; Angelova, M. I., Lipid Swelling and Liposome Formation Mediated by Electric-Fields. *Bioelectrochemistry and Bioenergetics* **1988,** 19, (2), 323-336.

38. Hiller, Y.; Gershoni, J. M.; Bayer, E. A.; Wilchek, M., Biotin Binding to Avidin - Oligosaccharide Side-Chain Not Required for Ligand Association. *Biochemical Journal* **1987,** 248, (1), 167-171.

39. Vanroy, N.; Mangelschots, K.; Speleman, F., Improved Immunocytochemical Detection of Biotinylated Probes with Neutralite Avidin. *Trends in Genetics* **1993,** 9, (3), 71-72.

40. Santore, M. M.; Discher, D. E.; Won, Y. Y.; Bates, F. S.; Hammer, D. A., Effect of surfactant on unilamellar polymeric vesicles: Altered membrane properties and stability in the limit of weak surfactant partitioning. *Langmuir* **2002,** 18, (20), 7299-7308.

41. Evans, E.; Rawicz, W., Entropy-Driven Tension and Bending Elasticity in Condensed-Fluid Membranes. *Physical Review Letters* **1990,** 64, (17), 2094-2097.

42. Milner, S. T., Polymer Brushes. *Science* **1991,** 251, (4996), 905-914.

43. Bruinsma, R.; Sackmann, E., Bioadhesion and the dewetting transition. *Comptes Rendus De L Academie Des Sciences Serie Iv Physique Astrophysique* **2001,** 2, (6), 803-815.

44. Helm, C. A.; Knoll, W.; Israelachvili, J. N., Measurement of Ligand Receptor Interactions. *Proceedings of the National Academy of Sciences of the United States of America* **1991,** 88, (18), 8169-8173.

45. Brochard-Wyart, F.; de Gennes, P. G., Adhesion induced by mobile binders: Dynamics. *Proceedings of the National Academy of Sciences of the United States of America* **2002,** 99, (12), 7854-7859.

CHAPTER 5

THE EFFECT OF VARIATIONS IN MEMBRANE MECHANICS ON SPREADING

Giant unilamellar vesicles, when partially "deflated," often appear flaccid or floppy. Upon contact with an adhesive object, they are typically expected to spread spontaneously, consuming their excess area and ultimately, in the case of reversible adhesion, producing a unique contact angle related to the adhesion strength. The current study showcases counterintuitive findings by identifying regimes where membrane bending dominates adhesion. In such situations, which can occur with moderately (but not conspicuously) stiff vesicles, even strong adhesive interactions (such as those resulting from avidin-biotin binding) are insufficient to drive vesicle spreading, though binding may be sufficient to prevent vesicle separation. This work quantifies bending domination by comparing stiff and flexible polymer vesicle pairs in micropipette experiments, which fix vesicle tension. A wide range of depletion forces, arising from polymer solutions of varied concentration, cause flexible vesicles to immediately assume the contact angle associated with the reversible work of adhesion (for a particular membrane tension) while stiff vesicles in the same solutions generally do not respond when brought into contact. Parallel behavior is evident for irreversible avidin-biotin-driven adhesion, except that a lag-time precedes spreading, depending on the density of membrane functionality. An analysis, based on the adhesion energy and the bending cost of forming a sharp kink at the edge of the spreading contact zone, predicts

in which systems spreading and equilibration occur, which systems resist spreading, and which systems exhibit a lag time before the onset of spontaneous spreading.

5.1 Introduction

The topic of adhesion between vesicles and target objects has long captivated scientists because it provides perspective on inter-cellular adhesion, targeted drug delivery, and viral infection. These situations rely on the engagement of receptors and adhesion molecules on the surfaces of cells; however, the cell membrane plays an equally important role. Additionally, with targeted drug delivery, vesicular carriers comprise a second membrane whose properties must be considered. Likewise, non-vesicular drug packages rely on interactions with the cell membrane for their action.

Among the mechanisms through which the membrane influences vesicle and cell adhesion are receptor diffusion and membrane deformation. Treatments of adhesive processes involving giant liposomes are often simplified, and reasonably so, as Evans[1-3] showed that estimates of continuum adhesion energies (e.g. depletion forces, van der Waals interactions), when reversible, can be quantified through the shapes and contact angles of adherent vesicles without accounting for a bending energy. Typically in such systems, however, the bending moduli are low: 10 kT or less.[4] There are situations where bending is more important. For instance polymer vesicles, which are becoming increasingly popular platforms for scientific study and drug delivery,[5] possess bending moduli that can be as high as 465 kT, due to their greater membrane thicknesses.[6]

Densely functionalized phospholipid membranes, with thick PEG coronas or protein overlayers that contain receptors and signaling molecules, will also be stiffer than naked liposomes.[7-9] More extreme membrane influence is expected in biology: The attachment of the cell membrane to the underlying cytoskeleton alters its thermal bending fluctuations. Indeed, cells with actin cortices have large bending moduli on the order of 500kT.[10-12] Both membrane bending and tension have proved important in general to cell adhesion and to the ability of membranes and cells to engulf nano-scale objects (drug particles, viruses).[13, 14] Engulfment may be prevented if adhesion is insufficient,[15] or a lag time prior to engulfment may arise from energy barriers to the engulfment process.[16] The contributions of bending can therefore be important for systems stiffer than simple fluid liposomes and for processes involving sharp curvatures.

Sackmann's team has evolved, through a series of membrane models of increasing complexity, systems which contain an artificial glycocalyx with embedded adhesion molecules.[17-21] When these membranes lock onto their target, membrane phase separation occurs as glycocalyx molecules (and the phospholipids to which they are connected) are excluded from growing contact zones. The spreading kinetics for this system exhibits different regimes, with receptor diffusion dominating at low concentrations and membrane bending fluctuations playing a critical role to enable closing of a crack tip at the perimeter of the contact zone. To our knowledge, this series of works is the only experimental program to identify the role of membrane bending in

the spreading process. The approach, however, involved a rather complex interface, did not systematically vary bending mechanics, and was in the flaccid/fluctuating regime.

These experiments stimulated modeling efforts focusing on the concept of an adhesion nucleus,[11, 12] a small region of membrane-substrate contact which might grow, depending on the its stability.[10] Our lab recently discovered activated adhesion and spreading processes with a simpler system.[22] Flexible vesicles, densely functionalized with receptors to reduce the importance of lateral receptor diffusion and held tense in micropipettes to suppress bending fluctuations, exhibited a functionalization-dependent lag time prior to snapping into adhesive contact and subsequent spreading. Key to this behavior, the micropipette tension imposes a sharp kink at the perimeter of the contact zone, in Figure 5.1, prerequisite to the development of a meaningful contact angle. Without such a kink, the membranes may adhere in an adhesion nucleus forced by the pipette position, but spreading and further adhesive contact does not occur.

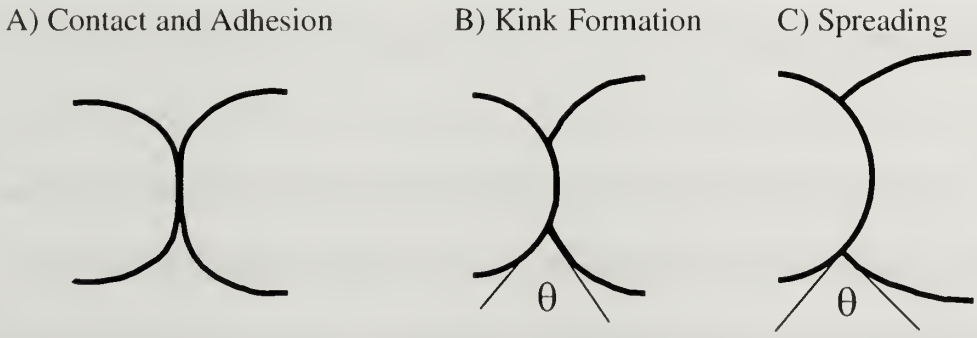

Figure 5.1 Adhesive progression for spreading membranes: (A) Initial contact and adhesion initiation, (B) Membrane kinking, and (C) Spreading

The current work explores this behavior more closely with an experimental grid of simple systems, illustrating the rich qualitative diversity of bending-influenced membrane adhesive behaviors. Here we compare vesicle pairs comprised of stiff and of flexible bilayer membranes, and employ two adhesive driving forces: avidin-biotin binding versus depletion attractions. For the former we again employ dense membrane functionality to avoid the complexities associated with receptor diffusion at this stage in our program. As for the latter, depletion forces can be tuned and measured, so that their adhesion energy is quantified. At this level of simplicity, the ligand-receptor interactions are treatable as continuum attractions,[23, 24] so that both avidin-biotin and depletion attractions should, in the absence of bending complications, produce trivial wetting behavior. The more complex results showcased here demonstrate how, even in the simplest of systems, bending produces a qualitatively different appearance to the adhesive behavior. Importantly this influence of bending occurs for conditions where the membrane stiffness, though greater than that of liquid-phase phospholipids vesicles, is rather inconspicuous.

The importance of these findings falls in several arenas: First, the growing popularity of micropipette manipulation to assess biological behaviors requires a complete understanding of all the physics contributing to the contact angle and radius of the adhesion plaque. There have been previous micropipette studies of adhesive vesicles in which the contact angles were quite small relative to the anticipated binding energies of the receptors involved, likely a result, in part, of membrane bending contributions in those systems.[25] Second, the micropipette approach maintains moderate

membrane tension, addressing cell behavior in the tensed regime,[26] where the geometrical constraints of a cell or vesicle engulfing a target may lead to regions of relatively tight local curvature, where bending energies become important. Finally, though the micropipette approach is macroscopic, it forces a sub-micron and even nanoscale curvature in the membrane that is relevant to the sharp curvatures that membranes experience during nanoparticle and viral uptake, even with more locally flaccid cell membranes.

5.2 Experimental Description

5.2.1 Vesicles

Giant unilamellar vesicles were electroformed[27] in solutions containing approximately 265 mOsm sucrose and transferred to 275mOsm glucose solutions for characterization and adhesion studies. The difference in sugar solutions produces a refractive index contrast enabling the vesicles to be imaged in a light microscope and also maintains a fixed osmotic pressure difference between the inside and outside of the vesicles on timescales of micropipette studies, during which water does not permeate the membrane. The latter defines the vesicle volume when suction is applied and the membrane is stretched in micropipettes. This combination of osmolarity was found to produce, in most cases, sufficient excess area so that the vesicles could be aspirated into micropipettes, with substantial projections at low tensions. As a result, a wide range of contact angles and tensions were sampled in adhesion studies.

"Flexible" vesicles were made from DC5329 from Dow Corning, a graft copolymer of overall molecular weight near 3000, comprised of a poly(dimethyl siloxane) (PDMS) backbone and approximately 2 poly(ethylene oxide) (PEO) side arms of roughly 12 oligomers each.[28, 29] "Stiff" vesicles were electroformed from a poly(butadiene) $(PBD)_{46}$-PEO_{30} diblock copolymer of 3800 molecular weight purchased from Polymer Labs. The bending moduli of the former were 9.6± 2.4 kT while for the latter the bending moduli were 28± 6 kT, as measured by micropipette aspiration. Proof of the unilamellar nature of the vesicles came from measurements of the stretching modulus, K_a, also in Table 5.1. These values were reproducible (within 10% error) for many different vesicles and consistent with the literature for the PBD-PEO sample.[5] Table 5.1 indicates that biotinylation and avidin conjugation alter the membrane properties. We present this here as a reproducible observation, which was discussed in more detail in Chapter 4. This complication was one of the motivating factors to conduct separate studies of depletion attraction, which avoids this complication.

Table 5.1 Binding for 100% labeled or unlabeled ones

	Ka (mN/m)	κ_b (k_BT)
SOPC	180	22
DC5329 (PDMS-PEO)	92±5	9.6±2.4
Biotinyl DC5329	23±11	1.07±0.3
NeutrAvidin conjugated B-DC5329	51±4	2.33±0.9
PBD-PEO	109±2	28±6
Biotinyl-PEO-PBD	135±15	8±1
PEE-PEO [5]	120±20	33±7

While the work to impose a sharp bend in a membrane is an important consideration in vesicle spreading, as described by the bending modulus, it is a static measure of bending energy. Spreading may also involve dynamic dissipative bending processes, such as tank-treading motions. While we have no quantitative measures of a tank-treading type viscosity, qualitative differences in relaxation dynamics of the stiff and flexible vesicle specimens are clear: First, we note that the DC5329 is a pourable viscous liquid with a viscosity of 371 cP reported by Dow Corning in product literature. By contrast the PBD-PEO copolymer is a solid at room temperature for practical purposes, albeit one that can be deformed with some force. Giant unilamellar vesicles of PBD-PEO are slow to relax, as shown in Figure 5.2A, for an adherent vesicle held and stretched in a micropipette, and then released. Here the shape of the projection and the elongated vesicle are not completely relaxed even after a minute outside the pipette. The same process for a DC5329 vesicle is so rapid that it cannot be captured on standard video. Likewise in Figure 5.2B for a PBD-PEO vesicle held in a micropipette and lysing under high tension, the vesicle is slow to respond to the suction which draws the broken membrane into the pipette. Here, the dynamic resistance of the membrane to forming tight bends is revealed by its shape. The softer DC5329 vesicles bend quickly upon lysis and aspiration into the pipette, so that no images are available.

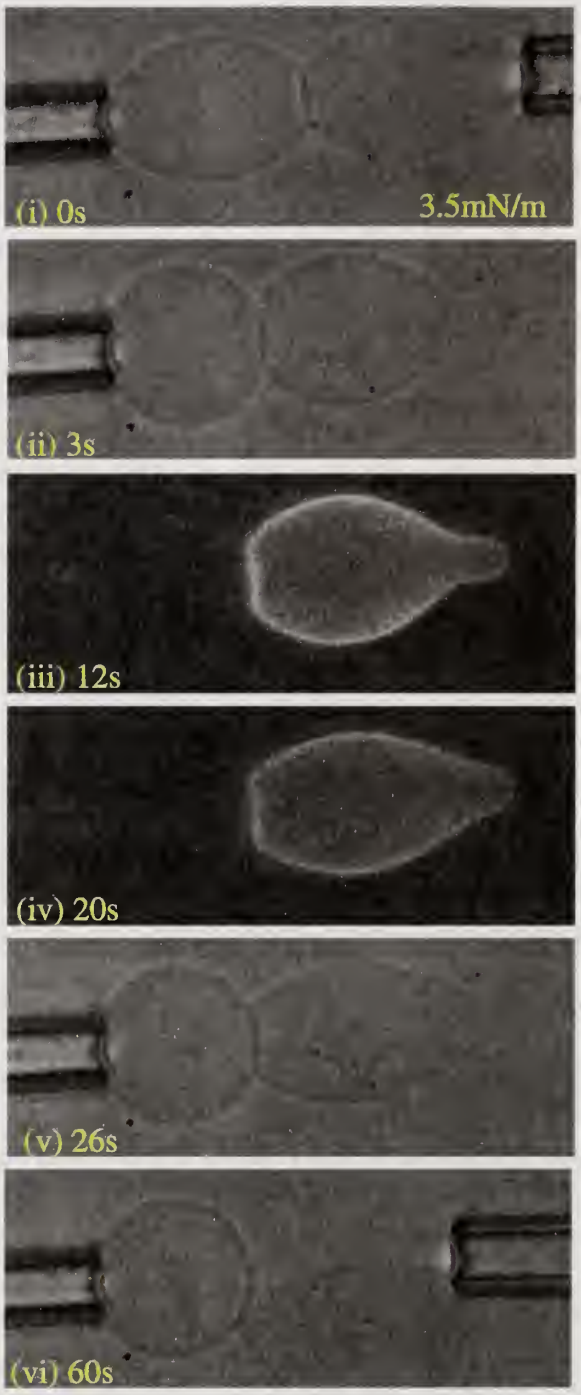

Figure 5.2A Sequence showing slow relaxation of a stiff PBD-PEO vesicle functionalized with biotin (left) and FITC-NeutrAvidin (right). After adhesive plaque develops, the right tension is increased to 3.5 mN /m to aspirate the vesicle, and the pipette is pulled backwards, until the vesicle escapes, starting the clock. The projection shape is initially retained in the right vesicle and slowly relaxes over the course of a minute, after which time the sharp bends of the projection are lost but the longer-wavelength elongated vesicle shape is not yet relaxed.

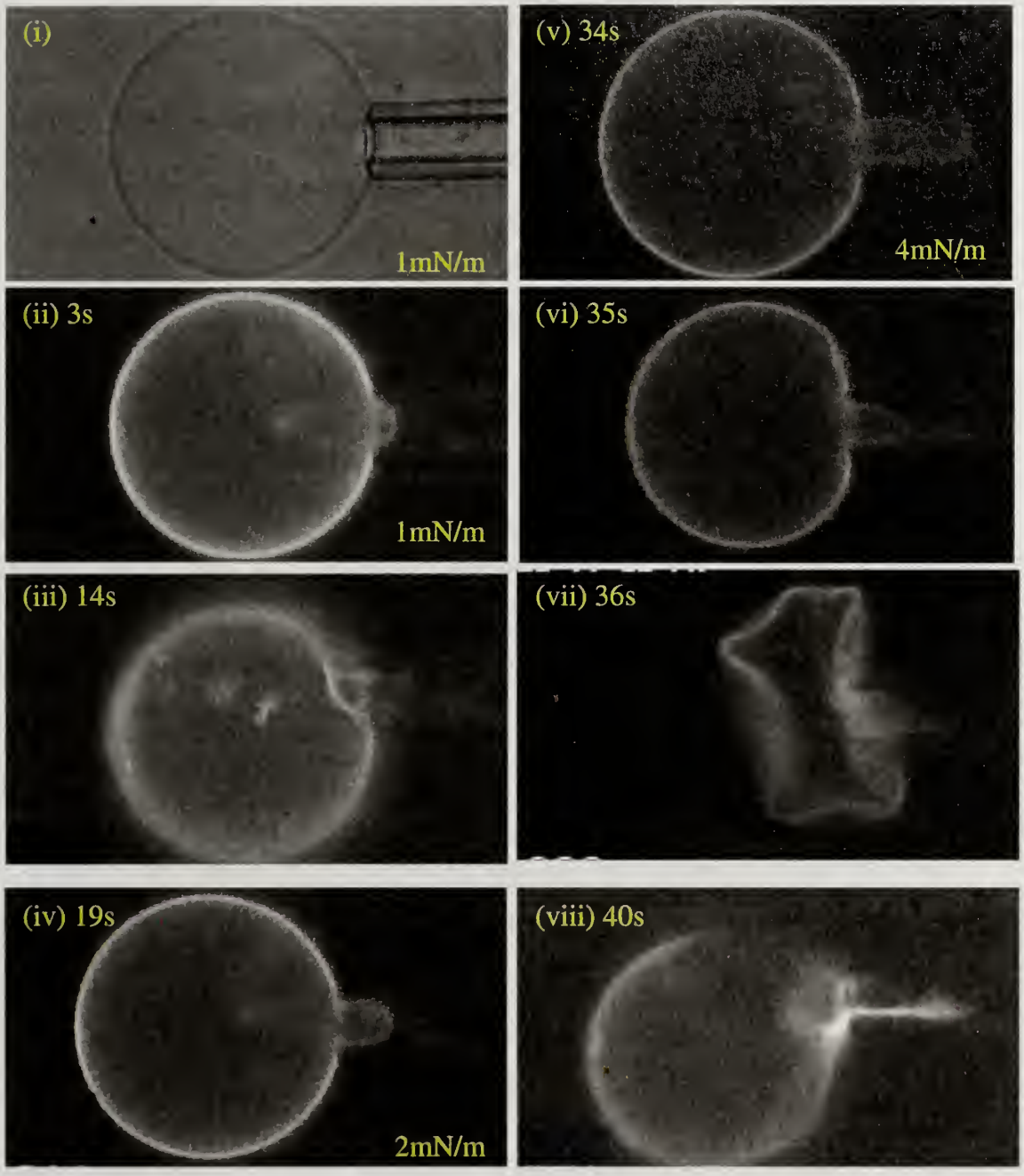

Figure 5.2B shows a single FITC-NeutrAvidin-conjugated biotinylated PEO-PBD vesicle held with a micropipette. The tension is increased, decreased, and increased again, causing the vesicle to rupture. The broken membrane in frame vii is slow to draw into the pipette revealing its shape and resistance to folding into sharp bends. Application of positive pressure in frame (viii) causes the vesicle to temporarily inflate, though its hole is visible. Such processes would not be visible with a vesicle possessing faster relaxation times

5.2.2 Attractive Forces

Avidin-biotin binding was employed in some studies as a type of adhesive driving force which, in our hands, was completely irreversible. In this case, both "flexible" and "stiff" vesicles were functionalized at the terminal OH groups of PEO chains by biotinylating the polymers prior to vesicle formation. For the DC5329, the copolymer was reacted with *p*-toluenesulfonyl chloride. The intermediate was purified, and then reacted with 5-biotinamido pentylamine (Pierce Biotechnology, Rockford IL), as previously described in detail.28 Due to slight differences in the solubilities of the DC5329 and PBD-PEO copolymers in various solvents, we found a different procedure to be more efficient for the PBD-PEO. Instead of p-toluenesufonyl chloride, N,N`-Disuccinimidyl carbonate (Aldrich) was coupled to PBD-PEO in DMF at 70°C for 8 hours. Without any purification, the intermediate was then reacted with excess 5-biotinamido pentylamine at 70°C for 24 hours. The solvent was removed under vacuum and the subsequent residue was washed repeatedly with diethyl ether or pentane to remove unreacted materials. Finally, the biotinylated PBD-PEO was transferred to chloroform.

Spectroscopic quantification, for instance by NMR, of the reaction yield is confounded by the small numbers of reactive hydroxyl groups relative to the overall polymer repeat units; however, the procedures are reported to be aggressive and expected to approach completion.[30, 31] In our work, this was supported by the high

fluorescence levels from biotinylated vesicles conjugated with fluorescein-NeutrAvidin (FITC-NeutrAvidin).[28] (Pierce Biotechnology), which was chosen as the avidin molecule because of its reduced non-specific interactions relative to that of avidin.[32, 33] FITC-NeutrAvidin conjugation resulted when biotinylated vesicles were added to an F-NeutrAvidin solution, incubated for at least 30 minutes, collected by centrifugation or settling under gravity, and rinsed repeated in phosphate-buffered glucose. Most studies involved fully functionalized vesicles, electroformed directly without dilution with non-biotinylated polymer from the biotinylated polymer batch. In adhesion studies, these vesicles were paired with F-NeutrAvidin-conjugated versions of the same biotinylated vesicles, such that both members of an adhesive pair contained the same level of underlying biotinylation. For the DC5329 flexible vesicles, we also studied less densely functionalized vesicles electroformed using a mixture of biotinylated and native DC5329. Here, the complimentary F-NeutrAvidin conjugated vesicles always contained the same underlying level of biotinylation.

Fully functionalized DC5329 vesicles contain a full overlayer of F-NeutrAvidin, limited not by the available numbers of biotins in the vesicle corona but by the NeutrAvidin size (4.1 x 5.5 x 1.5 nm^3).[34] This assessment was the result of a previous analysis in which we examined the fluorescence from a series of vesicles with variations in the density of the underlying biotin, but saturation of the F-NeutrAvidin overlayer.[28] As shown schematically in Figure 5.3(A), in the limit of dilute biotinylation, the fluorescence from the F-NeutrAvidin conjugation is linear in the underlying biotinylation, up to about 50% biotinylation. At higher densities of biotinylation,

vesicles saturated with F-NeutrAvidin show no further increase in fluorescence. Indeed, for the DC5329 with 100% biotinylation, there would be 1.5 biotins / nm^2, a footprint smaller than that of the F-NeutrAvidin. We therefore estimate that the fully functionalized flexible vesicle have 1.5 biotins and 0.19-0.75 NeutrAvidin /nm^2.

In ligand-receptor studies of stiff PBD-PEO vesicles, only 100% functionalization was employed. With its diblock rather than graft architecture, at full biotinylation, (using a previously reported membrane core thickness of 9.6 nm in our calculation),[6] we estimate 1.16 biotins / nm^2. This biotin footprint is again smaller than the NeutrAvidin protein size, so at saturation, similar levels of F-NeutrAvidins are expected on fully functionalized PBD-PEO and DC5329 vesicles. A side-by-side comparison of fluorescence from F-NeutrAvidin conjugated stiff and flexible vesicles, in Figures 5.3(B) and (C), confirms that this is the case.

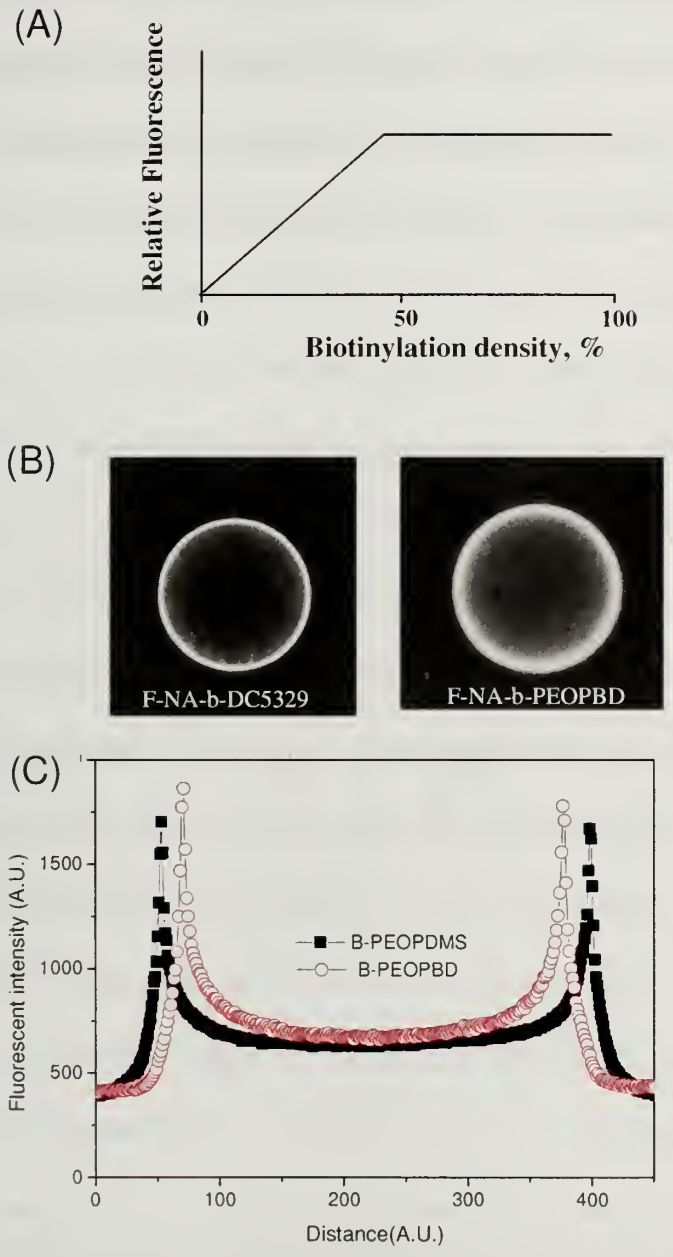

Figure 5.3 (A) Schematic of fluorescence intensity as a function of Biotinylation fraction of DC5329 vesicles. (B) Micrographs and (C) measured fluorescence intensities of similarly sized PEO-PDMS and DC5329 vesicles that are 100% biotinylated and subsequently FITC-NeutrAvidin conjugated.

Depletion forces between unfunctionalized vesicles were explored as a driving force for reversible adhesion, employing solutions of 8000 molecular weight polyethylene glycol (PEG) from Polysciences Inc., in phosphate buffered glucose. Once the PEG concentration, c, of 0.1, 0.5, 2.0 or 7.0 wt% was chosen, the phosphate-buffered glucose was titrated into the solution to give an overall osmotic pressure of 275 mOsm, to offset the sucrose osmolarity on the vesicle interior, producing excess area. Osmotic pressure was measured using an Advanced Instruments Model 3300 freezing point micro-osmometer. The depletion forces arise from the osmotic pressure of the PEG component of the solution (above the background glucose and buffer osmolarities), shown in Figure 5.4. An interesting feature of this data, well known for PEO solutions, is the flatness of the osmotic pressure /c curve at low concentrations, corresponding to a small second virial coefficient and a substantial third virial coefficient. More linear plots result from greater second virial coefficients and small third virial coefficients.2 Thus, our PEG solutions need to be somewhat concentrated to build up measurable depletion forces. Fitting the data in Figure 5.4 to the form $\pi/c = A_1 + A_2 C + A_3 C_2$ gives a $A_1 = 5.5$ atm cm^3/g, $A_2 = 64$ atm cm^6/g^2, $A_3 = 1440$ atm cm^9/g^3. This value of the "first virial coefficient" gives a molecular weight of 10,900, slightly elevated but within reasonable experimental error. Our second virial coefficient is in good agreement with that (0.00335 ml mol/g^2 = 82 atm cm^6/g^2) reported by Fraden[35] and by Kinugasa et al.[36] (0.0030 ml mol/g^2 = 74 atm cm^6/g^2) for 8,000 molecular weight PEG. Our largish third virial coefficient is also consistent with the literature.[35-39]

Using the fitted virial coefficients for our particular PEO solutions in the mean field treatment of Evans[2, 3] provides an estimate of expected depletion forces in our vesicle experiments, shown in Figure 5.5. In some cases, we performed calculations using literature values of the virial coefficients, to give an idea of the error range in the estimate. Of note, the strength of the depletion force is proportional to the contribution of the polymer to the osmotic pressure of the solution.

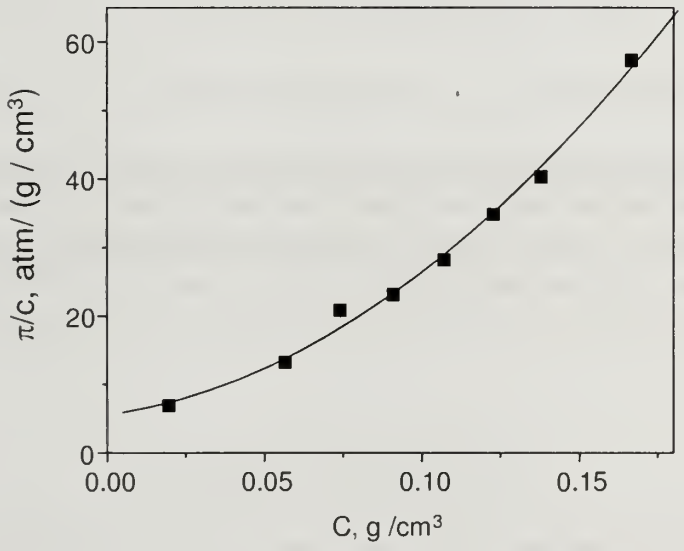

Figure 5.4 Concentration dependence of (osmotic pressure / concentration). Curve is the polynomial virial coefficient fit described in the text.

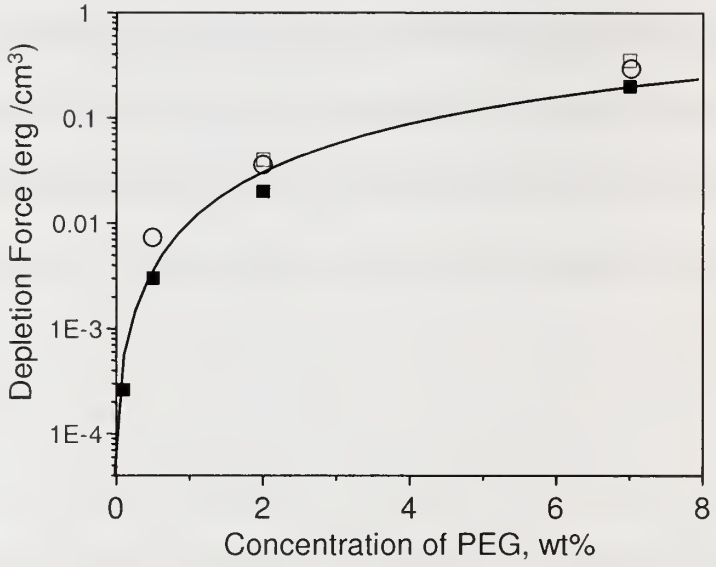

Figure 5.5 Calculated and measured values of depletion forces. Solid squares are mean field calculations using measured virial coefficients. Hollow squares are calculated using literature values of the second virial coefficient. Circles are measured with micropipettes with flexible vesicles. The curve guides the eye.

5.2.3 Micropipette Aspiration

Micropipette aspiration, using a homebuilt apparatus modeled after that in the Hammer lab,[40] was employed in dual vesicle adhesion experiments. The key features of the instrument are siphon manometer control of the pipette suction, which is manually adjusted using a syringe, and a video system for data collection, that prints the manometer pressures on each video frame. The adhesion chambers themselves were disposable, similar to that previously described, with open sides for access by the two

pipettes, and liquid held in place by surface tension between "floor" and "ceiling" slides.

In studies of ligand-receptor binding, vesicles were placed in chambers containing phosphate-buffered glucose, while in studies of depletion forces, phosphate-buffered PEG /glucose solution was employed. A first vesicle was picked up in the left pipette and its tension increased almost to the lysis value, so that it would maintain a spherical shape throughout the experiment. The complimentary vesicle was aspirated in the right pipette and the suction increased stepwise to acquire a measurement of the area expansion modulus, K_a, to ensure that the vesicle was unilamellar. The suction was then adjusted to give a tension in the range 0.1 ~ 1 mN /m and the vesicles placed in contact to initiate adhesion. Of note, while the pipettes allow control of the tension, τ, choosing an exact predetermined tension is not practical, as one actually specifies the suction pressure, P, on the pipette, and the tension follows from the LaPlace equation,

$$\tau = P R_p (2 - 2R_p / R_v) \qquad (5.1)$$

which also includes the pipette and vesicle radii, R_p and R_v. Hence, one chooses a P that will give τ close to the desired value. It is not possible, however, to conduct all experiments at a chosen value of τ.

In the case of avidin-biotin binding, once vesicles were placed in contact, the adhesion behavior (typically including spreading and evolution of the contact angle) was recorded at constant membrane tension until the experiment was over, typically when

the lower tensioned (right) vesicle escaped its pipette. As avidin-biotin binding was completely irreversible, the membranes could not be separated. Attempting separation always caused one vesicle to break. Hence, each experiment at a particular value of tension consumed a vesicle pair.

In the case of depletion forces, reversible interactions allowed more elaborate experimentation. Here the left substrate vesicle was always maintained in a spherical shape with a high suction. Initially the right vesicle was held at a medium-high tension, near 1 mN /m and initial contact was made. Changes in the vesicle shape were recorded, until none was observed. The right tension was then reduced suddenly and held constant, and while further changes in the vesicles were monitored. This process was repeated until the vesicle escaped the pipette. Then the vesicle was reaspirated, and peeled from the substrate vesicle using a series of step-wise increasing tensions. At each step, the tension was held constant until no changes in vesicles were seen, before the next step.

5.3 Results

5.3.1 Depletion Adhesion

Flexible Membranes; For flexible vesicles subject to depletion forces, we generally found that once vesicle pairs were made to touch, they jumped rapidly into adhesive contact, with the right (lower tensioned) vesicle spreading to consume some of its excess area, and quickly (in less than second) displaying the equilibrium contact angle, defined in Figure 5.1. Upon a subsequent sudden decrease in the membrane tension, the increase in contact area (spreading) was immediate, as was the increase in contact angle. This is shown in Figures 5.6A, B, and C for pairs of DC5329 vesicles in 7 wt%, 2 wt%, and 0.5 wt% PEG solutions. Many such step-decreases in the tension of the right vesicle were sampled for each vesicle pair. The graphs in Figure 5.6, each focusing on a single step change in tension, illustrate the practical time limit on our ability to quickly adjust the membrane tension. They show the extremely rapid response of the contact angle, all happening on a time of less than a second. Of note, the figures focus on step changes in tension once the vesicles are already in contact. We were unable to obtaining meaningful kinetic data for the initial contact at fixed tension because the membrane response was so rapid that the pipettes were still moving to manipulate the vesicles.

The exception to this behavior occurred for flexible vesicles in solutions of 0.1 wt% PEG, which was apparently too dilute to produce noticeable membrane spreading,

even after 20 minutes of contact (beyond which time we lost confidence in the PEG concentration in the test chamber, which would increase with time due to evaporation.) Mean field calculations estimate the depletion forces from 0.1 wt% PEG solution to be 0.0003 erg /cm^2 in Figure 5.5. Figure 5.7D shows that a vesicle pair in this dilute PEG solution does not establish adhesive contact, no matter how low the tension. When the tension on the right pipette is made positive, the right vesicle simply slides away and loses (the previously forced) contact with the left vesicle.

Figures 5.6 A, B, and C show kinetic contact angle data for a single step change in tension in each of the three PEG solutions. Figure 5.7 presents a more comprehensive perspective for the appearance of the vesicles at several different tensions in each of the three PEG solutions: 0.5, 2.0, and 7 wt%, and also in the dilute 0.1 wt% PEG solution for which no adhesion was discernable. In the three more concentrated solutions, the adhesive nature of the systems is most apparent when the contact angles approach and exceed 90 degrees. The adhesive nature of the systems at smaller contact angles is more evident in video than in still captured images.

The contact angle responses to step changes in tension, in Figures 5.6 represent travel between equilibrium states. The observation that, following a step change in tension, the contact angle evolves and then arrests, is not seen below for avidin-biotin binding. The arrest of the contact angle following spreading is one factor suggesting equilibration of the flexible vesicles subject to depletion forces. The possibility that these vesicle systems equilibrate in response to depletion forces is confirmed by a

Young's equation analysis of the contact angles,[1] in Figure 5.8. Here 1-cos θ is plotted as a function of $1/\tau$, with the limiting slope towards the origin (at higher membrane tensions) giving the reversible work of adhesion, in accord with

$$W_a = \tau (1-\cos\theta) \qquad (5.2)$$

The graph includes data for three concentrations of PEG, each with step functions of decreasing (spreading) and increasing (peeling) tension, which fall on the same curve, arguing in favor of reversibility. The limiting slopes are 0.33, 0.04, and 0.008 erg/cm^2 for the 7, 2, and 0.5 wt% PEG solutions, respectively. These values, also plotted in Figure 5.5, compare well with the mean field predictions that were based on the measured osmotic pressures of our solutions, also arguing in favor of reversible adhesion. We note here, that Evans performed the same analysis of depletion forces between phospholipids vesicles,[2, 3] demonstrating the ability to quantify depletion forces with micropipettes and demonstrating the reversibility of this type of interaction. We present our own data with the flexible copolymer vesicles to illustrate the timescales for equilibration as a point of comparison to systems exhibiting very different behavior.

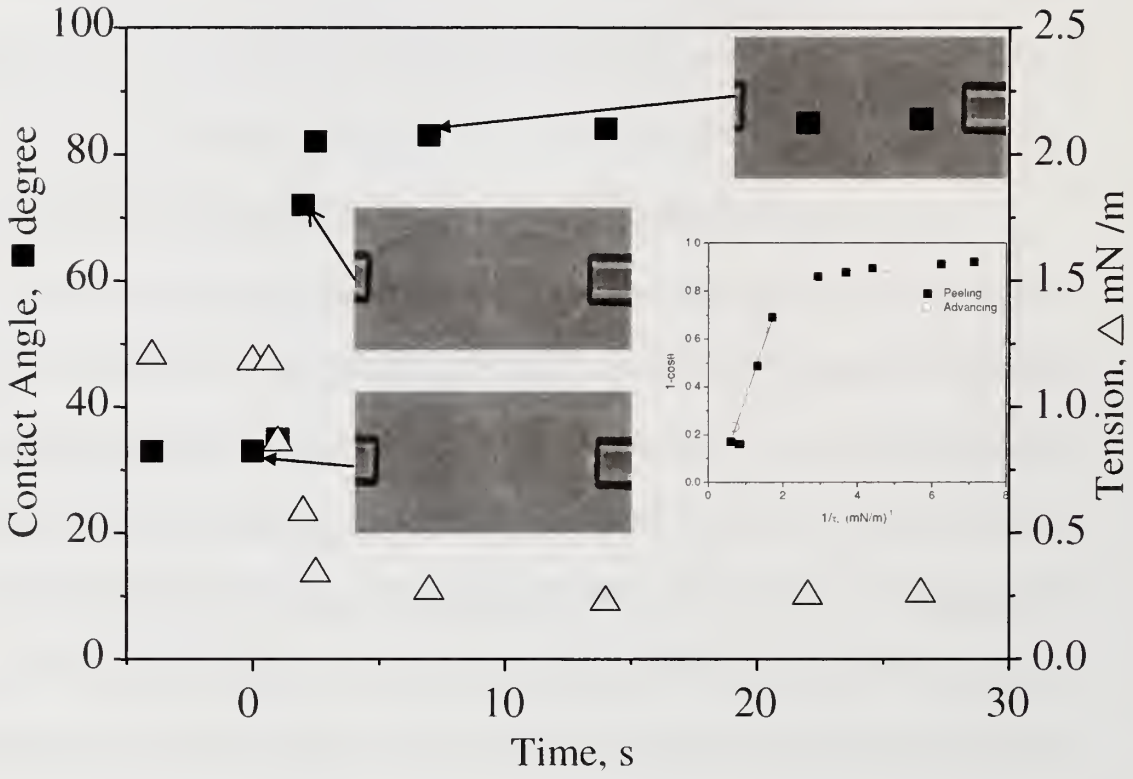

Figure 5.6A Flexible vesicle response to a step decrease in tension in 7 wt % PEG solution.

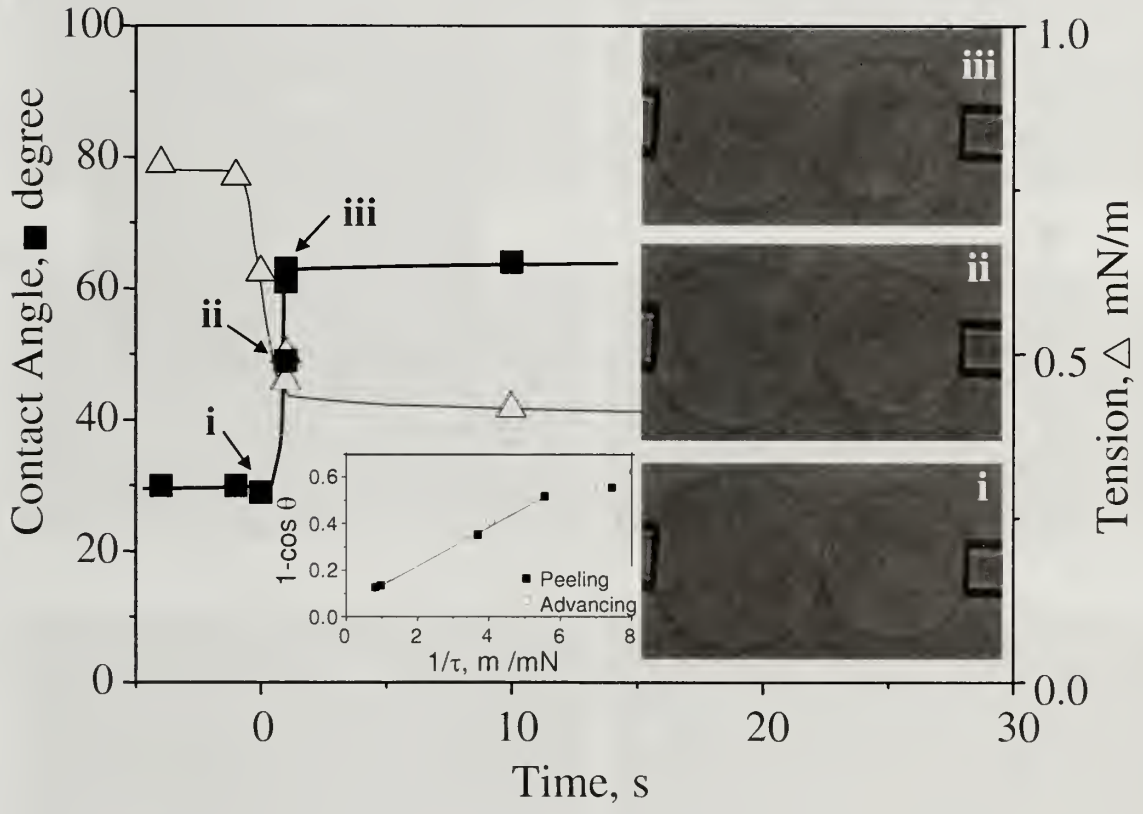

Figure 5.6B Flexible vesicle response to a step decrease in tension in 2 wt % PEG solution.

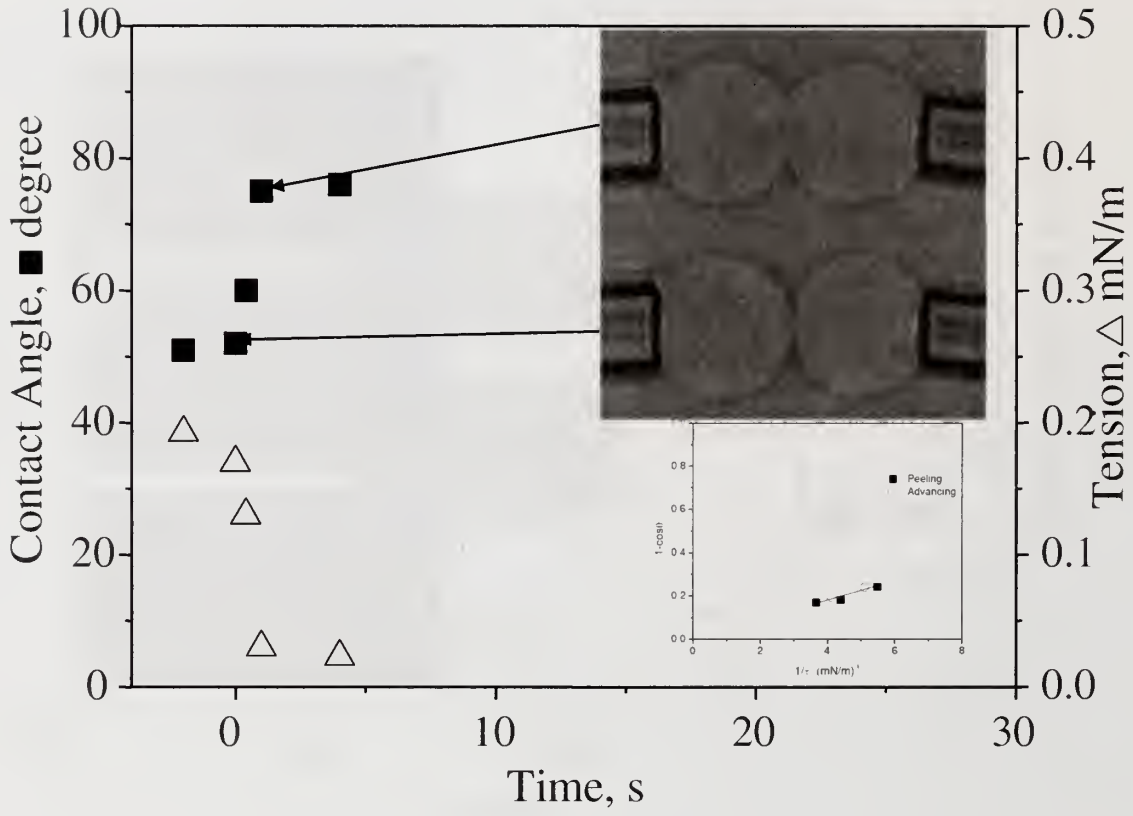

Figure 5.6C Flexible vesicle response to a step decrease in tension in 0.5 wt % PEG solution.

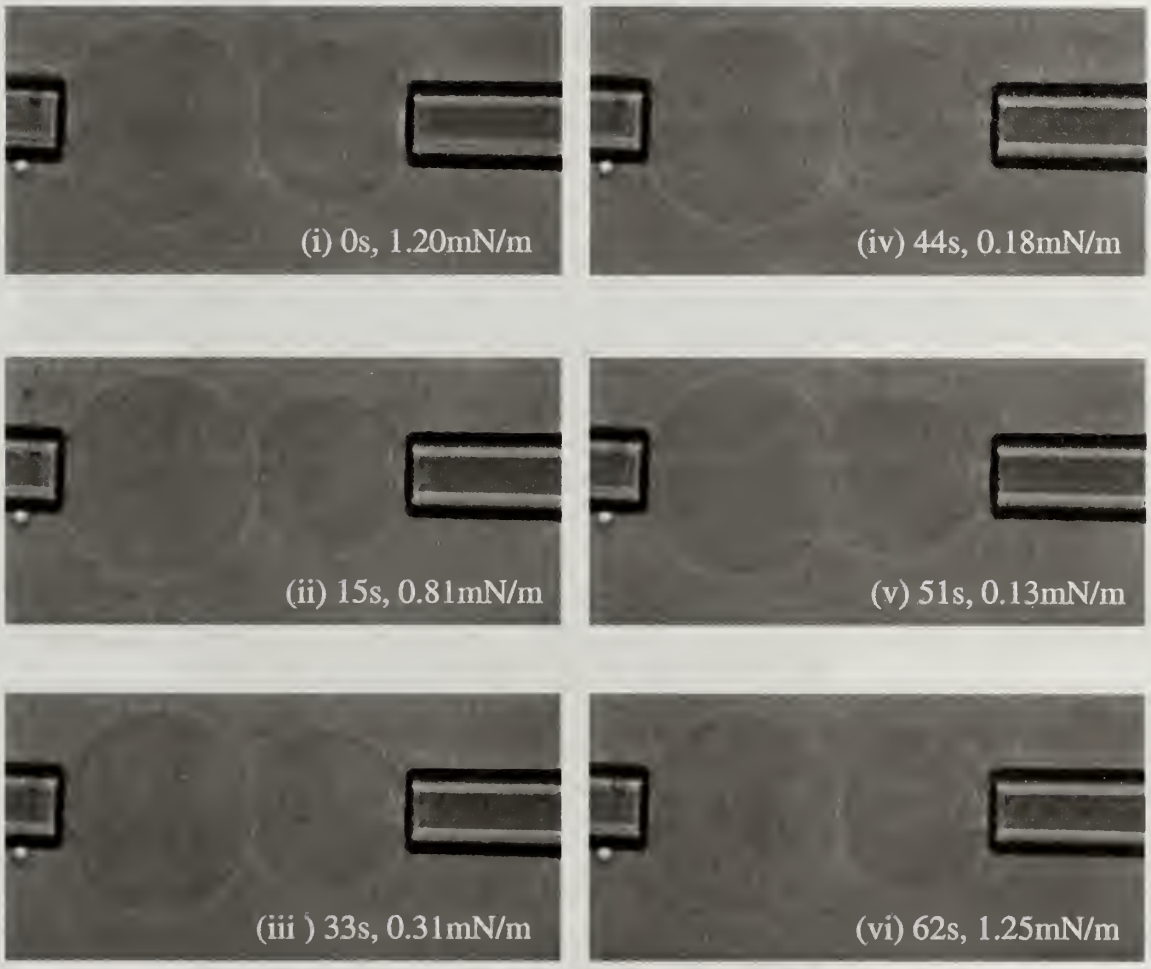

Figure 5.7A Video microscope images of flexible vesicles at different tensions in tension in 7 wt % PEG solution.

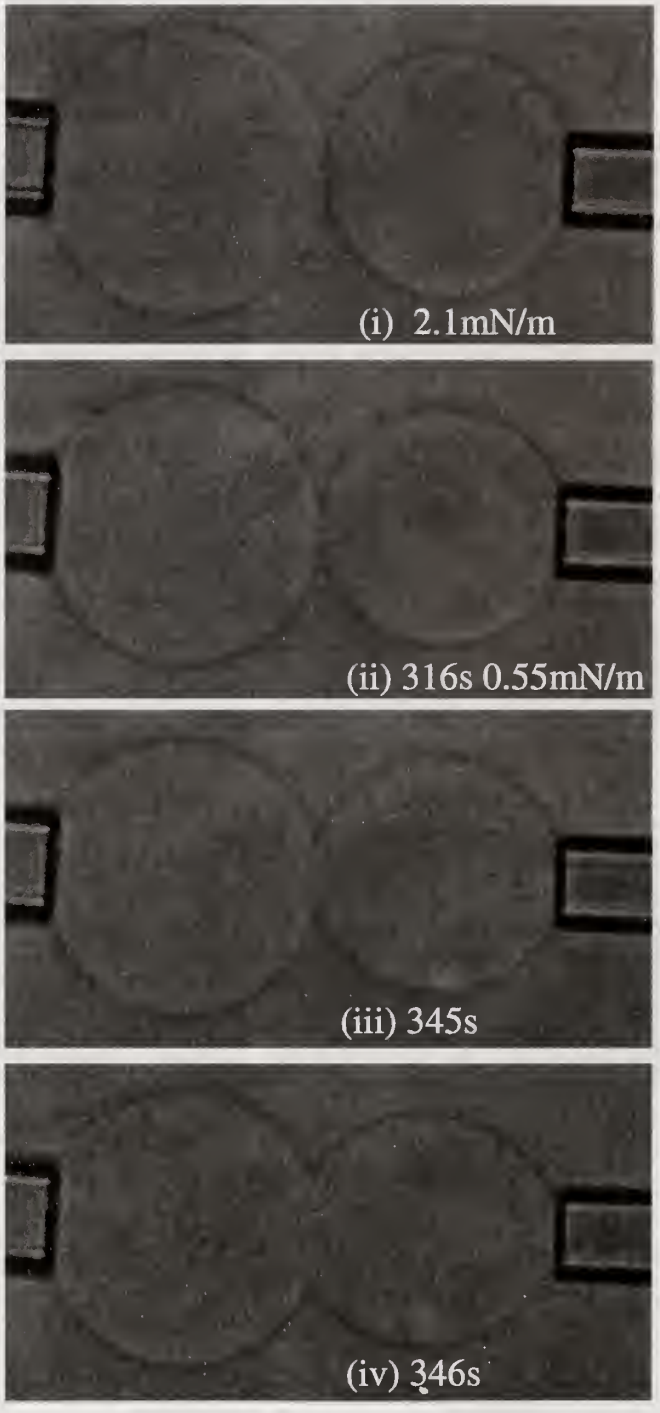

Figure 5.7B Video microscope images of flexible vesicles at different tensions in a 2 wt % PEG solution.

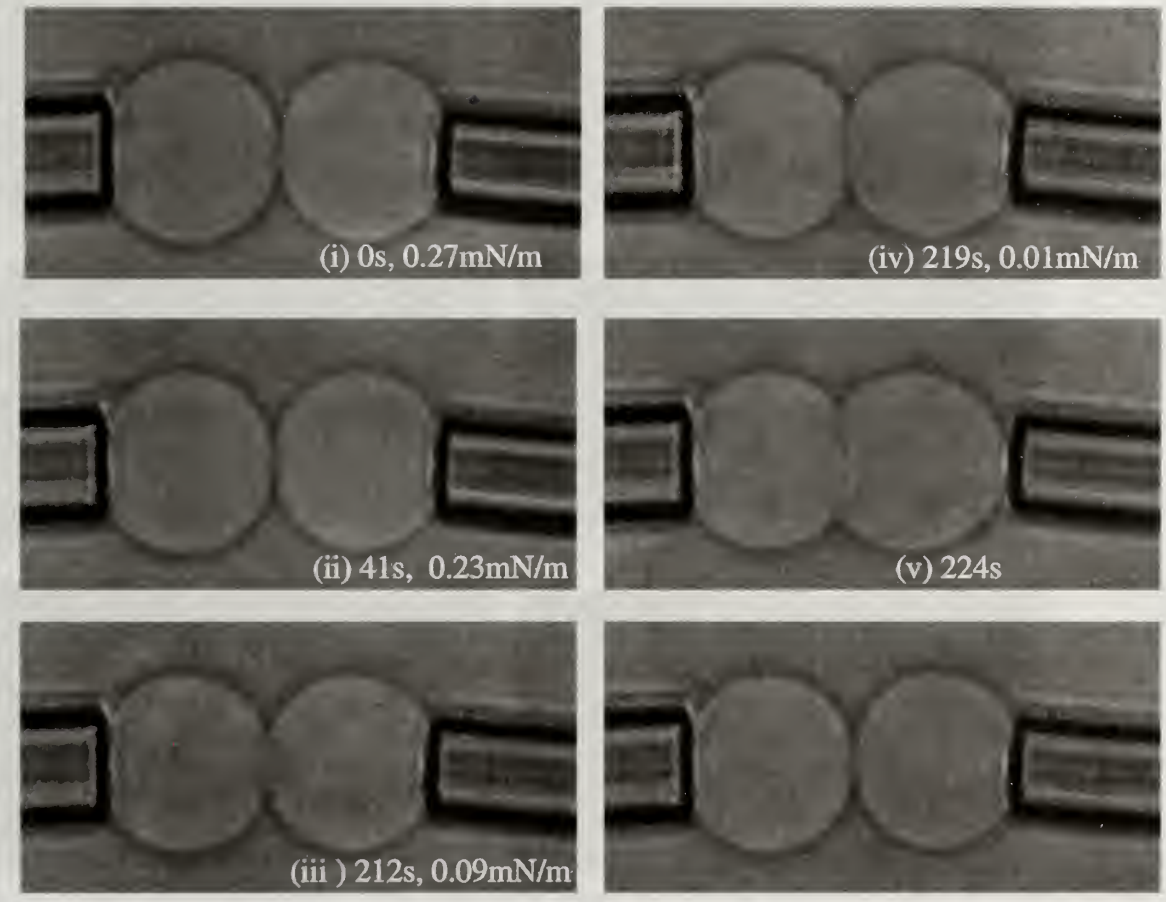

Figure 5.7C Video microscope images of flexible vesicles at different tensions in a 0.5 wt % PEG solution.

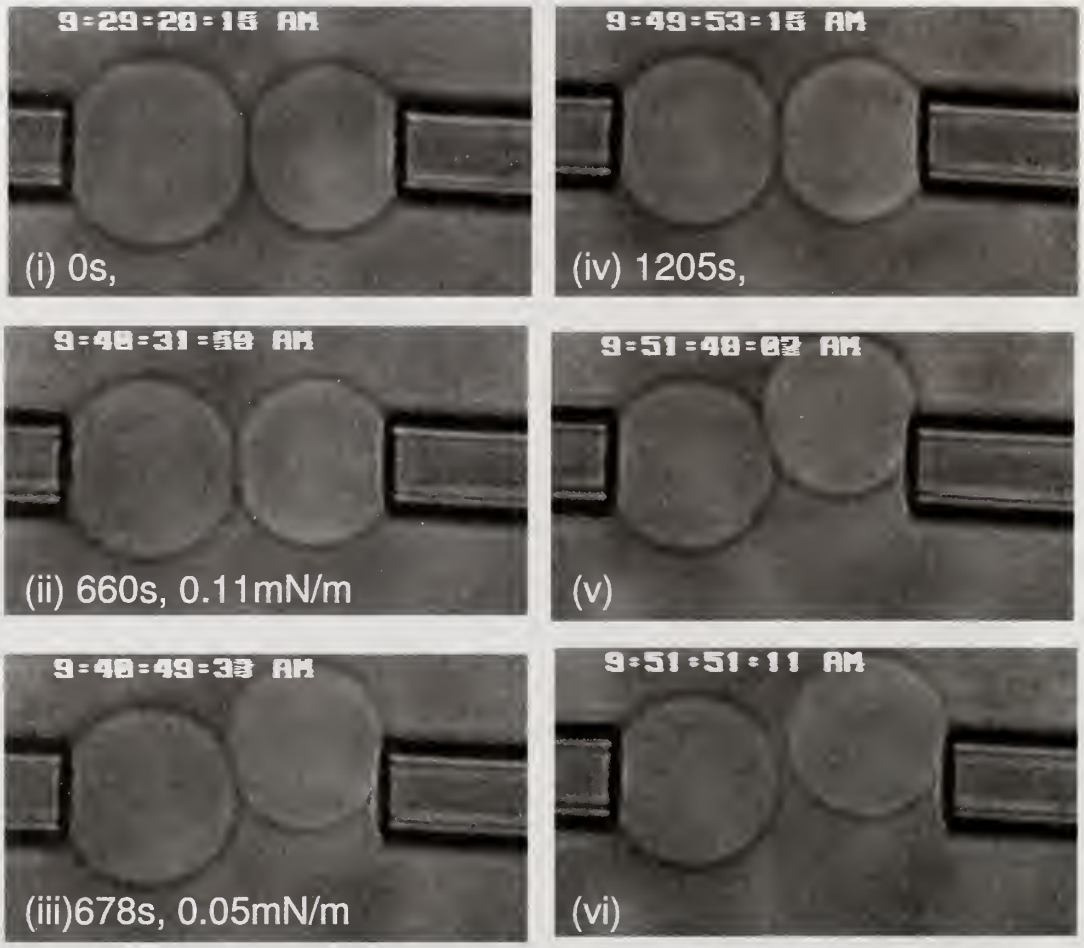

Figure 5.7D Flexible vesicle response to a step decrease in tension in 0.01 wt % PEG solution. Two DC5329 vesicles did not show adhesion but just slipped away at very low tension, ~ 0.05mN/m.

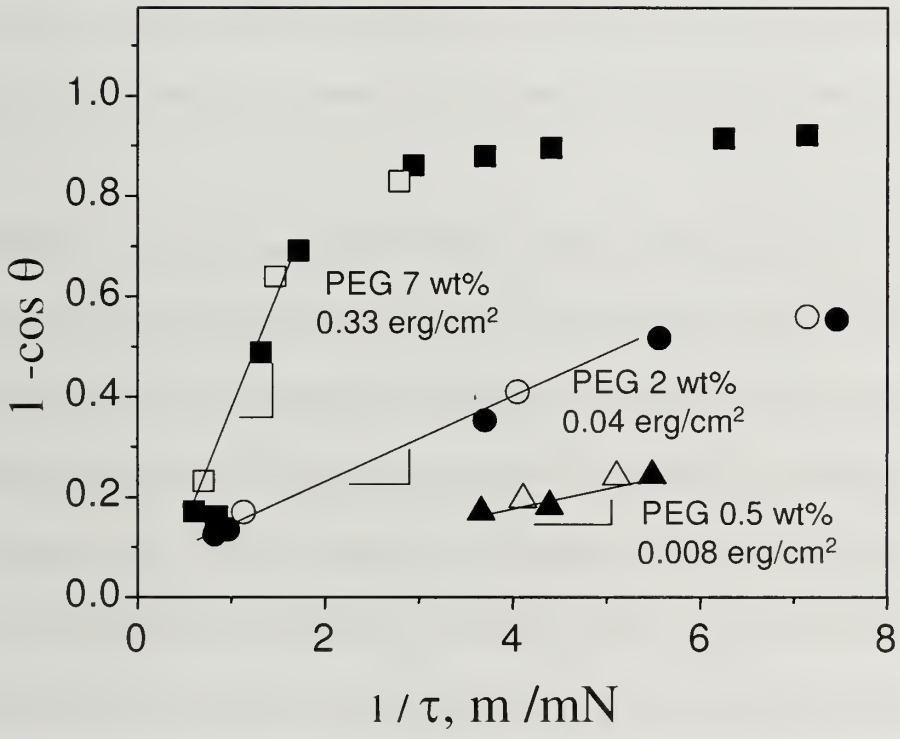

Figure 5.8 Determining the reversible work of adhesion from a Young's analysis of contact angle data for flexible DC5329 vesicles in PEG solutions. Solid symbols are advancing, while hollow symbols are peeling.

Stiff Membranes: Dramatically different behavior is observed for stiff vesicles in the same PEG solutions, subject to the same depletion forces that were applied to the flexible vesicles. Stiff vesicles were made to touch using the pipettes, and then we waited 20-30 minutes for any changes to occur, with the upper time limit set by evaporation from the chamber. With only one exception, we did not observe the development of adhesive contact or spreading. Rather, vesicles appeared to be in forced non-adhesive contact, with contact angles less than predicted by the Young's equation.

The exception to this lack of spreading was observed in 7 wt% PEG solution, which generates depletion forces of 0.33 erg/cm^2, based on measurements using flexible vesicles, and on mean field predictions. In Figure 5.9, when stiff vesicles were placed in contact, no spreading was seen when the tension was high, greater than 1 mN/m. Lowering the tension did not produce spreading. Finally, the pressure on the pipette was made slightly positive, (at time zero), so that the right adherent vesicle was slowly extruded from the pipette. This is seen in Figure 5.9A, and the projection, originally inside the right pipette, inverts and invaginates inside the right vesicle, budding at several points as it does this. This vesicle is held in place by the alignment of the pipettes and the positive pressure from the right, though its membrane tension is essentially zero throughout the process. After 80 seconds, however, spreading initiates spontaneously and abruptly. Between 80 and 80.3 seconds, the rounded region near the perimeter of the original contact region develops a sharp edge or kink, and then over the next several seconds, spreading proceeds, with kinetics shown in Figure 5.10. The notable features about this sequence are (1) that there is a lag time between the

adjustment of the membrane tension to nearly zero and the initiation of spreading and (2) that the membrane bends to form a kink at the perimeter of the contact zone at the start of spreading. Indeed, for the all the flexible vesicles that spread, exemplified in Figure 5.6, this bend or kink is always present at the spreading contact line and was formed immediately when the flexible vesicles were initially put into contact. Also of note, spreading near zero tension was seen for several different stiff vesicle pairs, and the lag time for these other experiments (starting from τ=0 mN/m) was 110s.

Similar adhesion behavior in 7 wt% PEG solutions for the stiff vesicles were observed with additional vesicle pairs, documented here in Figures 5.9B and C. In the sequence in Figure 5.9B, as the right vesicle slowly escapes the pipette due to the positive pressure, it slides upward, but still manages, around 110 s, to snap into adhesive contact. As adhesion proceeds, the right vesicle completely escapes the pipette, and any invaginations disappear. In another example in Figure 5.9C, after several minutes of contact near zero tension, separation is attempted and a tether is seen. Placing the vesicle back into contact after tether formation quickly produces spreading. This last example is included, but is an odd case because of the invaginations which persist even once the right vesicle is free of its pipette. This may be a result of different numbers of polymers on the inner and outer vesicle leaflet producing residual membrane tension, and propensity towards tether formation. The general observation of a lag time and kink formation prior to spreading only at near zero tensions is upheld by these additional cases.

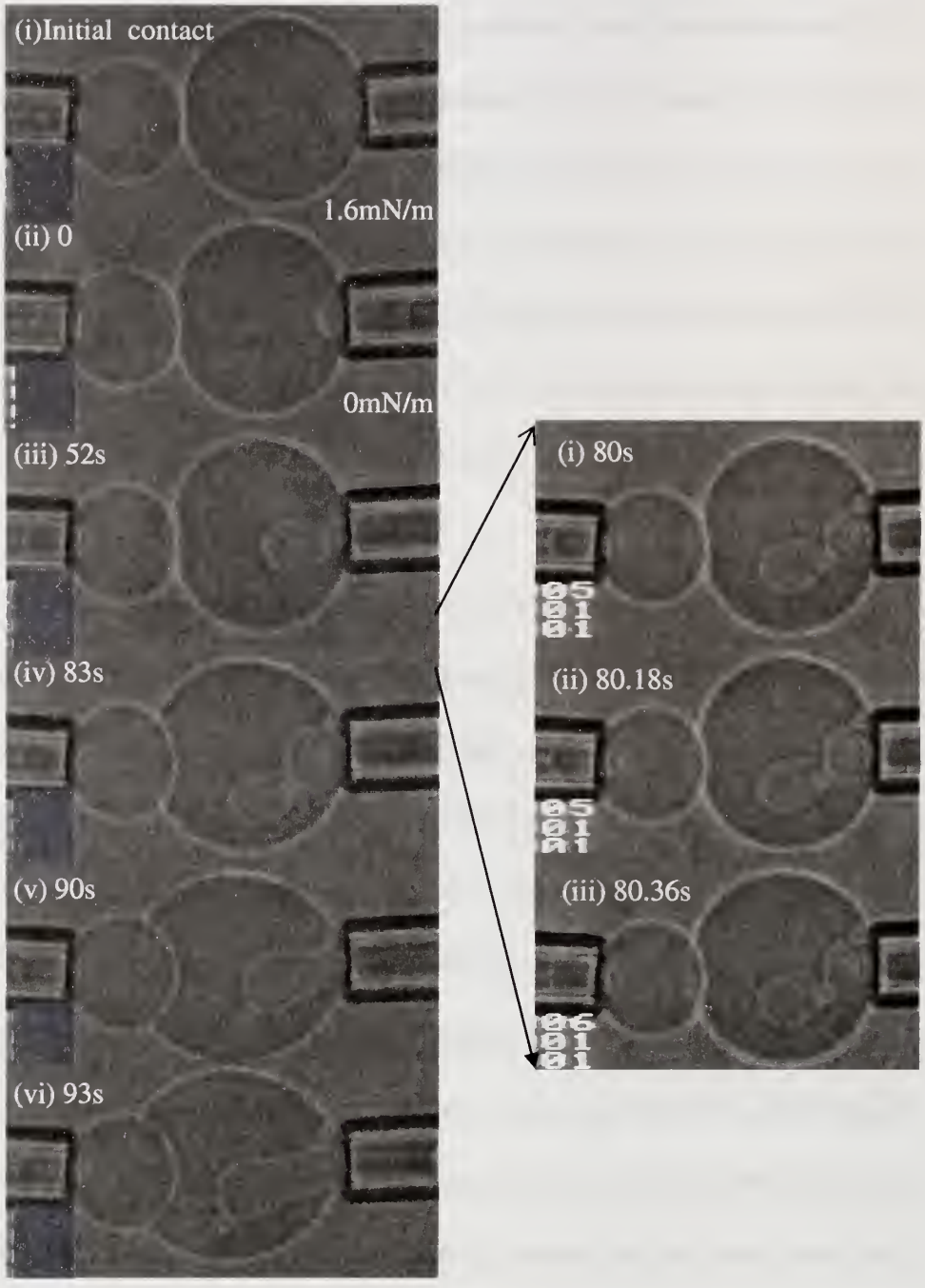

Figure 5.9A Depletion driven adhesion of a stiff PBD-PEO vesicle in 7 wt% PEG near zero membrane tension. The projection invaginates into the main vesicle slowly as a result of slightly positive pressure in the right pipette.

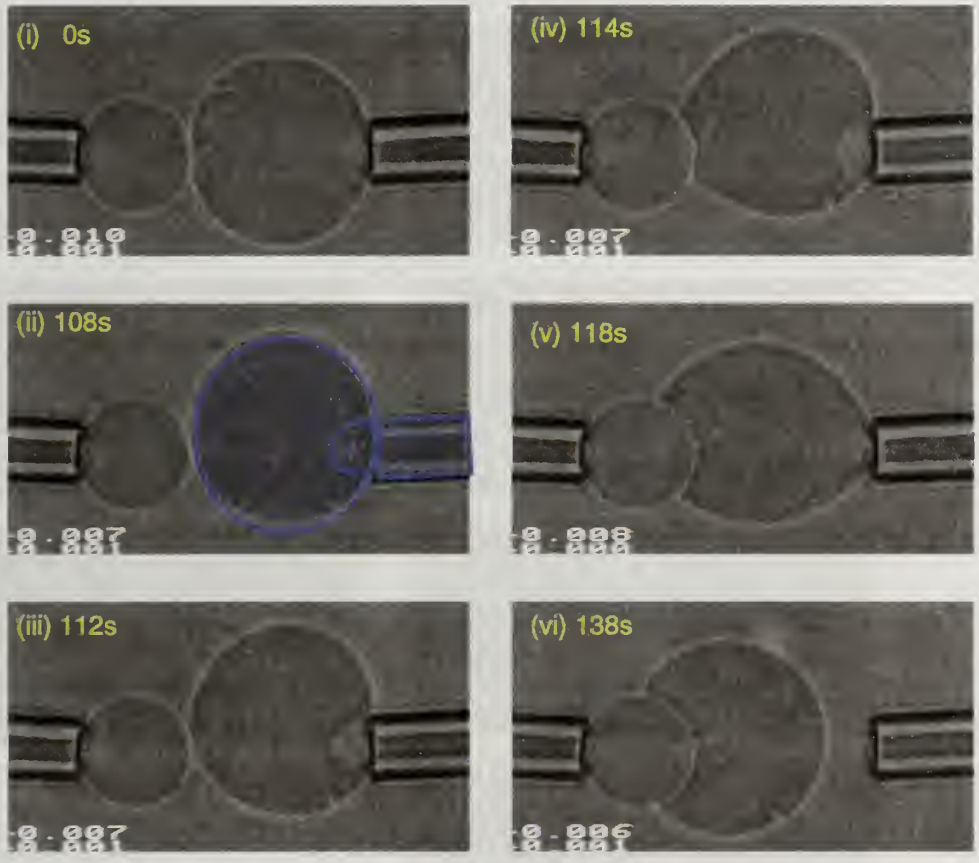

Figure 5.9B Depletion driven adhesion of stiff PBD-PEO vesicles in at 7% PEG solution. Time zero indicates when the suction was reduced to zero and then made slightly positive. The snap into true adhesive contact occurs around 110 seconds as the adhesive kink is then apparent, but not at 108 seconds.

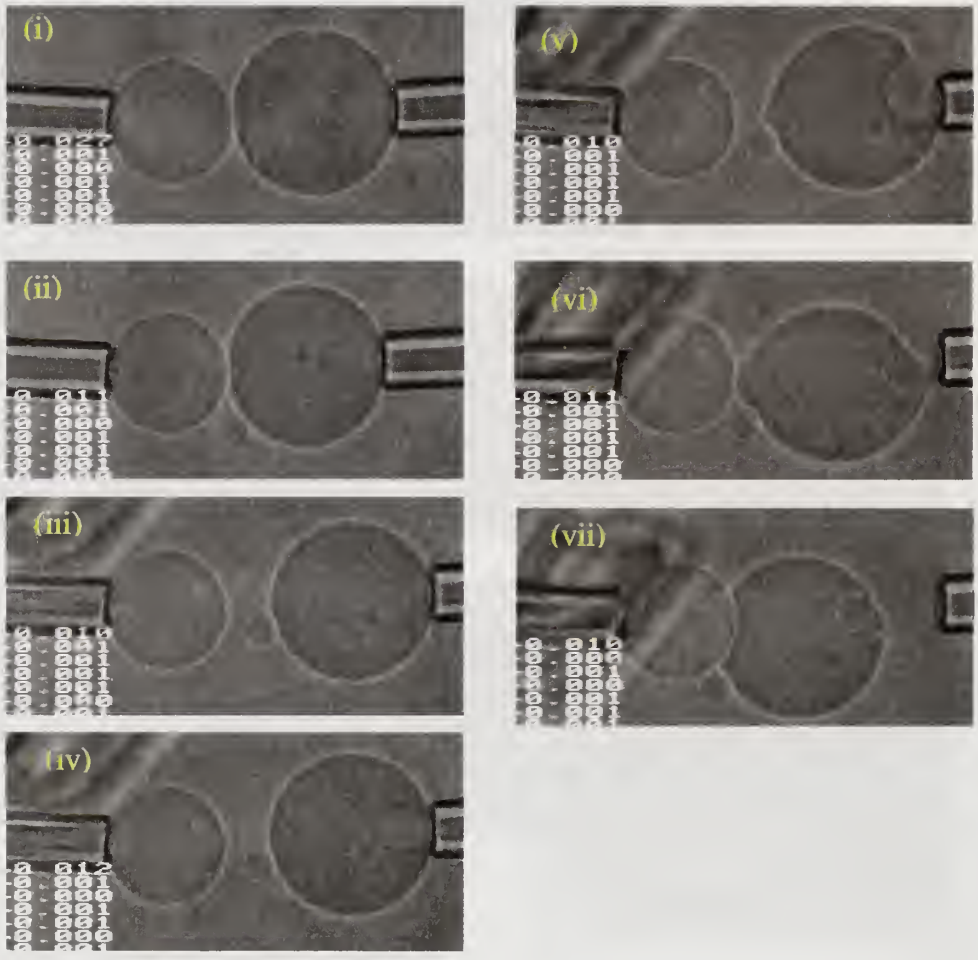

Figure 5.9C Depletion driven adhesion behavior of stiff PBD-PEO vesicles in a 7 wt% solution of PEG. In this particular run, an "invisible" tether was formed (it is most apparent in frame v) and spreading was observed near the tether.

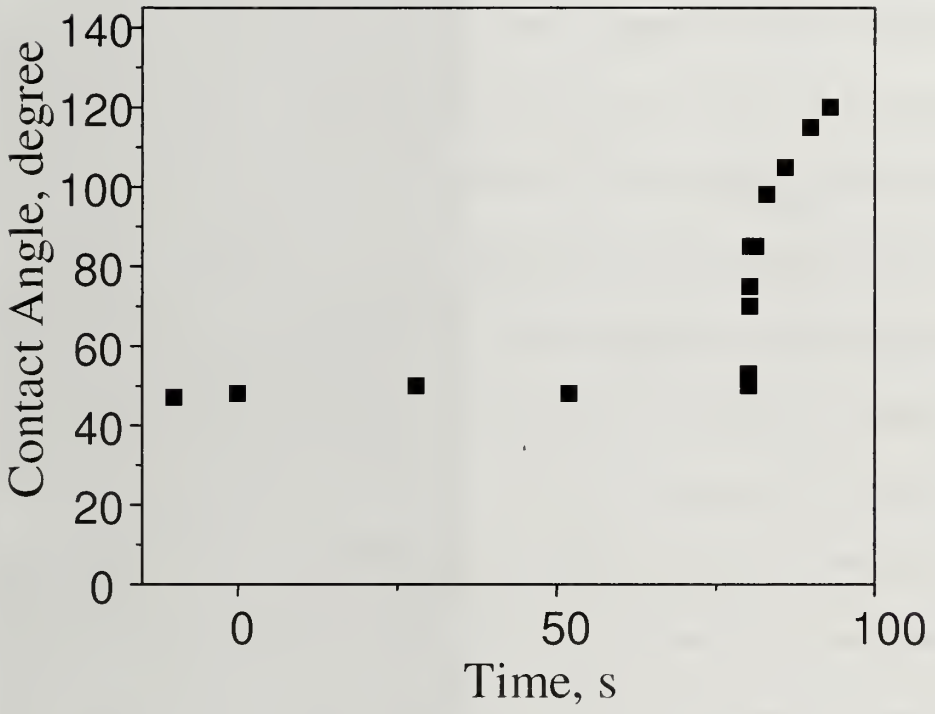

Figure 5.10 Spreading kinetics of stiff PBD-PEO vesicles near zero tension in 7 wt% PEG. Data correspond to the images in Figure 5.9A.

With the stiff vesicles, an interesting follow up experiment was undertaken: Once spreading near zero tension was complete, the membrane tension was increased stepwise, as shown in Figure 5.11. At each step, the membrane stopped moving, so these data represent static contact angles. Here the excess membrane area of the right vesicle, originally consumed via the engulfment of the left substrate vesicle, is again taken into the right pipette to form a projection. Now, however, the kink at the edge of the spreading front remains, as the vesicles are pulled apart in a stepwise fashion. A Young's equation analysis of the peeling contact angle is also shown in Figure 5.11, and apparent adhesion strength of about 1 erg /cm^2 follows from the Young's equation analysis. This value is in excess of the reversible work of adhesion and that measured with the flexible system, 0.33 erg /cm^2. Thus, we see that for the stiffer membrane the assessment of adhesion strength in this case exhibits hysteresis (relative to the spreading experiment, which could only proceed near zero membrane tension), and also includes a viscous loss term that amplifies the thermodynamic work of adhesion. This micropipette experiment therefore gives results typical of many peeling experiments which couple interfacial adhesion with near-interface elasticity: the adhesive energy density exceeds the reversible work of adhesion.

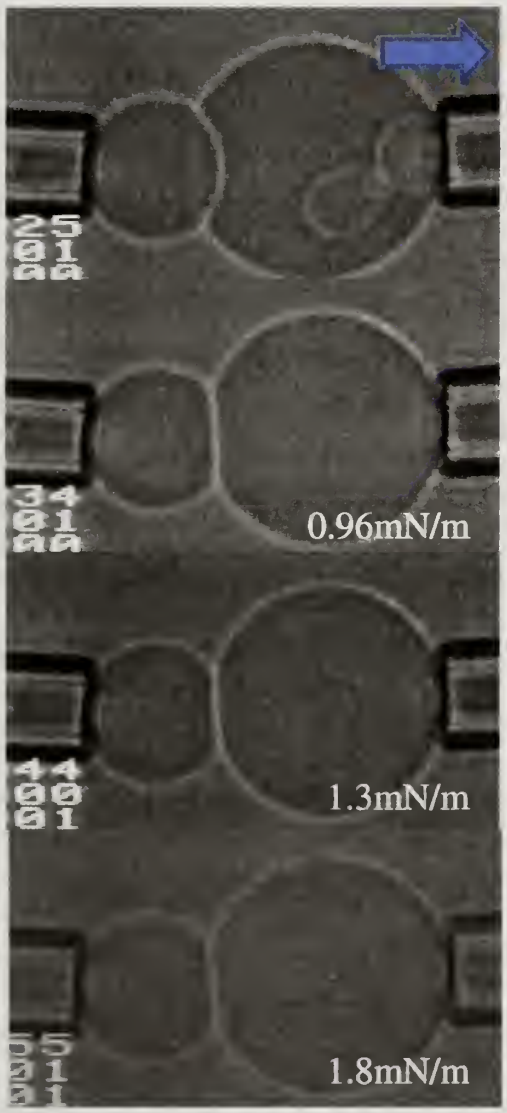

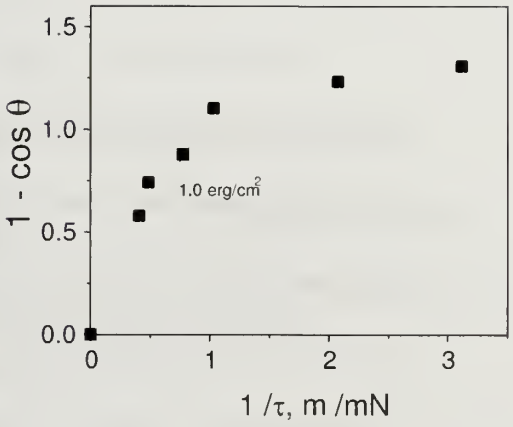

Figure 5.11 Peeling experiment with stiff PBD-PEO vesicles in 7 wt% PEG solution. Images: After spreading proceeds at zero membrane tension, the right vesicle is aspirated back into its pipette. After the projection is again established in the right pipette, the tension is increased stepwise and the static contact angle measured. Data show the Young's analysis for the adhesion energy

5.3.2 Ligand-Receptor Binding

The adhesion and spreading behavior for stiff and flexible vesicle pairs exhibits parallels to that seen for depletion forces, however there are some differences that result from the irreversible nature of the adhesion, which hamper equilibration.

Flexible Vesicles. Figure 5.12 shows the typical progression of adhesion and spreading for a pair of flexible vesicles whose surfaces are fully-functionalized with F-NeutrAvidin and biotin. The right vesicle is held at a low tension of 0.55 mN/m. Once placed in contact at time zero, evidence of adhesion is initially difficult to discern; however, spreading initiates spontaneously at a time near one minute. Then the low tensioned vesicle on the right rapidly engulfs (partially) the high-tension substrate vesicle on the left. As spreading proceeds, the reservoir of area inside the right micropipette is consumed and ultimately the right vesicle escapes its pipette. (Thus, the amount of engulfment is limited by the excess area on the lower tensioned vesicle.) Upon escape, the contact angle decreases slightly, relative to that just before vesicle escape. Termination of the experiment with vesicle escape rather than slowing and stopping of the spreading indicates that the contact angle had not equilibrated while the right vesicle was in the pipette, and that a Young's equation-type analysis is inappropriate.

This signature of adhesion kinetics is similar to that found for stiff membranes subject to strong depletion forces at negligible tensions: There is a latent period on the order of a minute or more followed by abrupt and relatively rapid spreading and

development of the contact angle. With avidin-biotin binding, the contact angle does not equilibrate but rather the vesicle escapes the pipette. Indeed, we find that the duration of latent period exhibits a strong dependence on the density of avidin / biotin functionality on the membrane, in Figure 5.13, diverging at 20%, where the waiting time for spreading became experimentally impractical.

An important point in these studies is the irreversibility of the binding: the vesicles could not be peeled apart at any point beyond the first few seconds of contact, but would instead break. This indicates that irreversible adhesion takes place during the latent period before spreading.

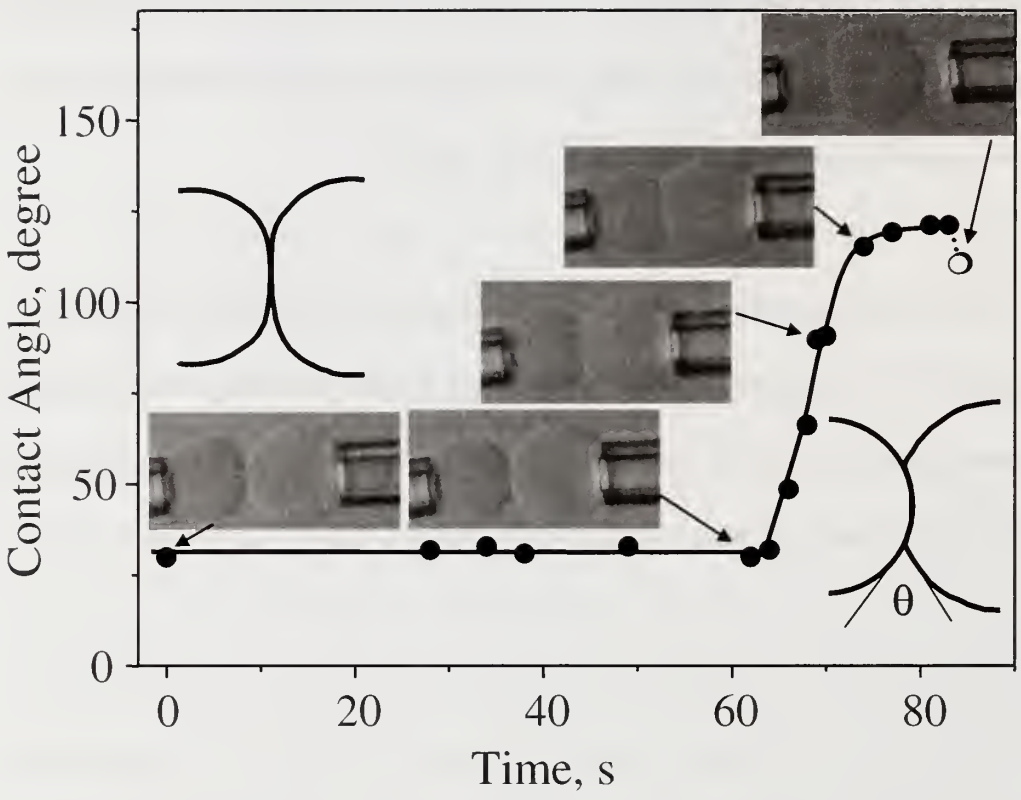

Figure 5.12 Contact angle change as a function of time for 100% biotinylated and F-Neutravidin conjugated flexible DC5329 vesicles.

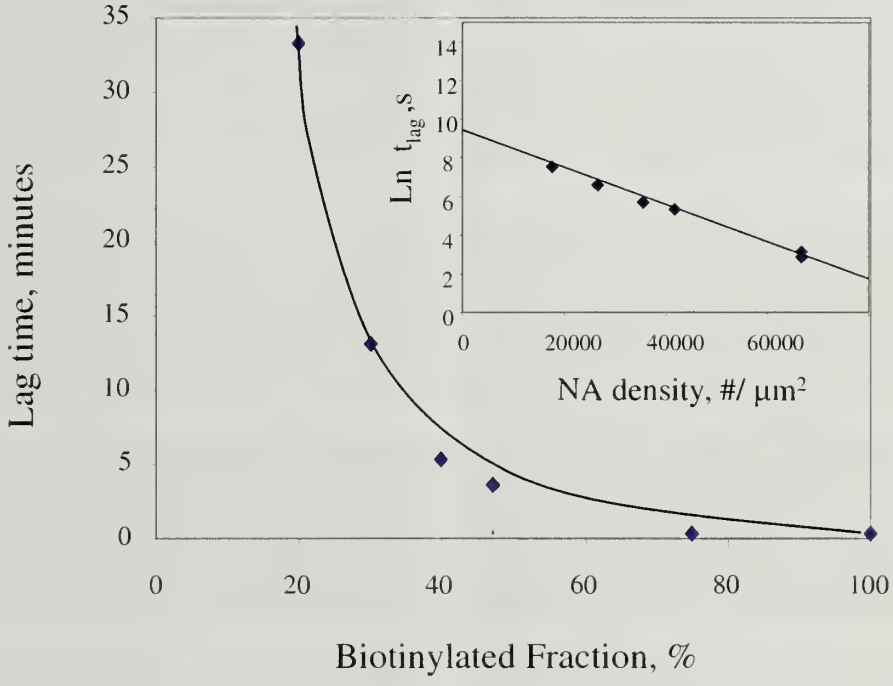

Figure 5.13 For flexible DC5329 vesicles functionalized with biotin and F-NeutrAvidin, lag time as a function of biotinylation fraction. Points are data while curve is fit to activation energy model. Inset shows data on semilog scale.

Adhesion of Stiff Membranes: Even with the strong avidin-biotin driving force for adhesion, fully functionalized stiff vesicles were completely resistant to spreading in Figure 5.14A. In this particular example, the lower tensioned FITC-NeutrAvidin vesicle on the right is held at 0.55 mN /m. In the sequence of micrographs, which include both bright field and fluorescent images, no spreading occurs and there is no recruitment of fluorescent NeutrAvidin to the contact region in the first 6.5 minutes of contact.

Subsequently increasing the membrane tension above 4 mN/m did not separate the vesicles, nor did pulling back on the pipettes. Around 7.5 minutes of contact, the right vesicle escapes the pipette as it is pulled backwards, yet now, even with the membrane tension essentially at zero, there is no increase in the contact area beyond that established initially.

We found it was possible to irreversibly increase the contact area beyond its initial radius by using the right micropipette to "coax" the escaped vesicle up against the substrate vesicle, and to then re-aspirate the right vesicle to prove that the contact area had indeed been forcibly increased. This coaxing procedure could be done in about 10 seconds, by an experienced pipette operator. Likewise, application of too great a suction caused the right vesicle to break, preserving the original contact region, shown in Figure 5.14B for a different vesicle pair.

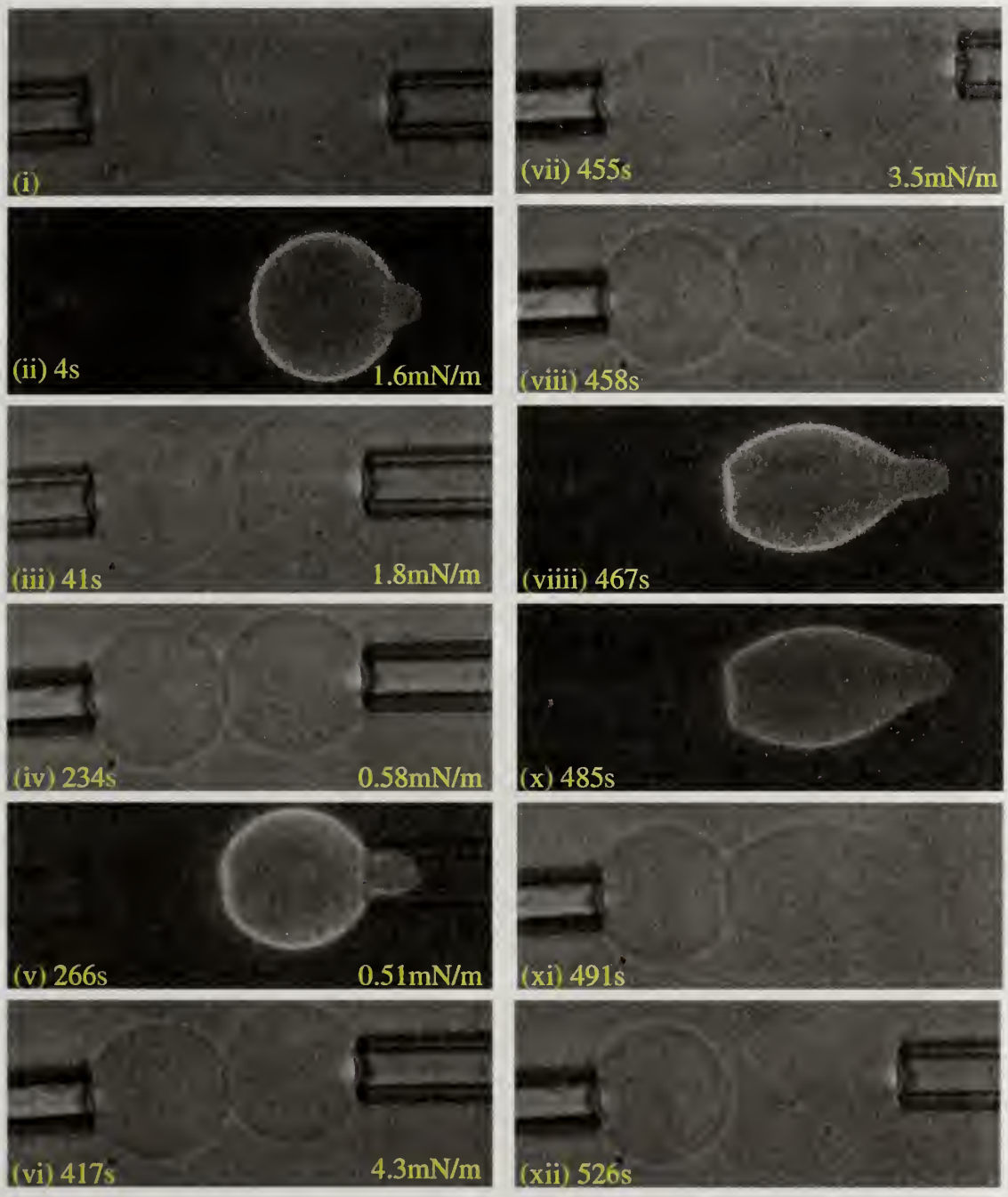

Figure 5.14A Typical video microscope images of of a fully functionalized (f-Neutravidin – biotin) pair of stiff PBD-PEO vesicles. Spreading does not occur after adhesive contact. Vesicles cannot be separated upon pulling, but either break (not shown here) or escape the pipette. This series also shows the slow relaxation in this type of membrane.

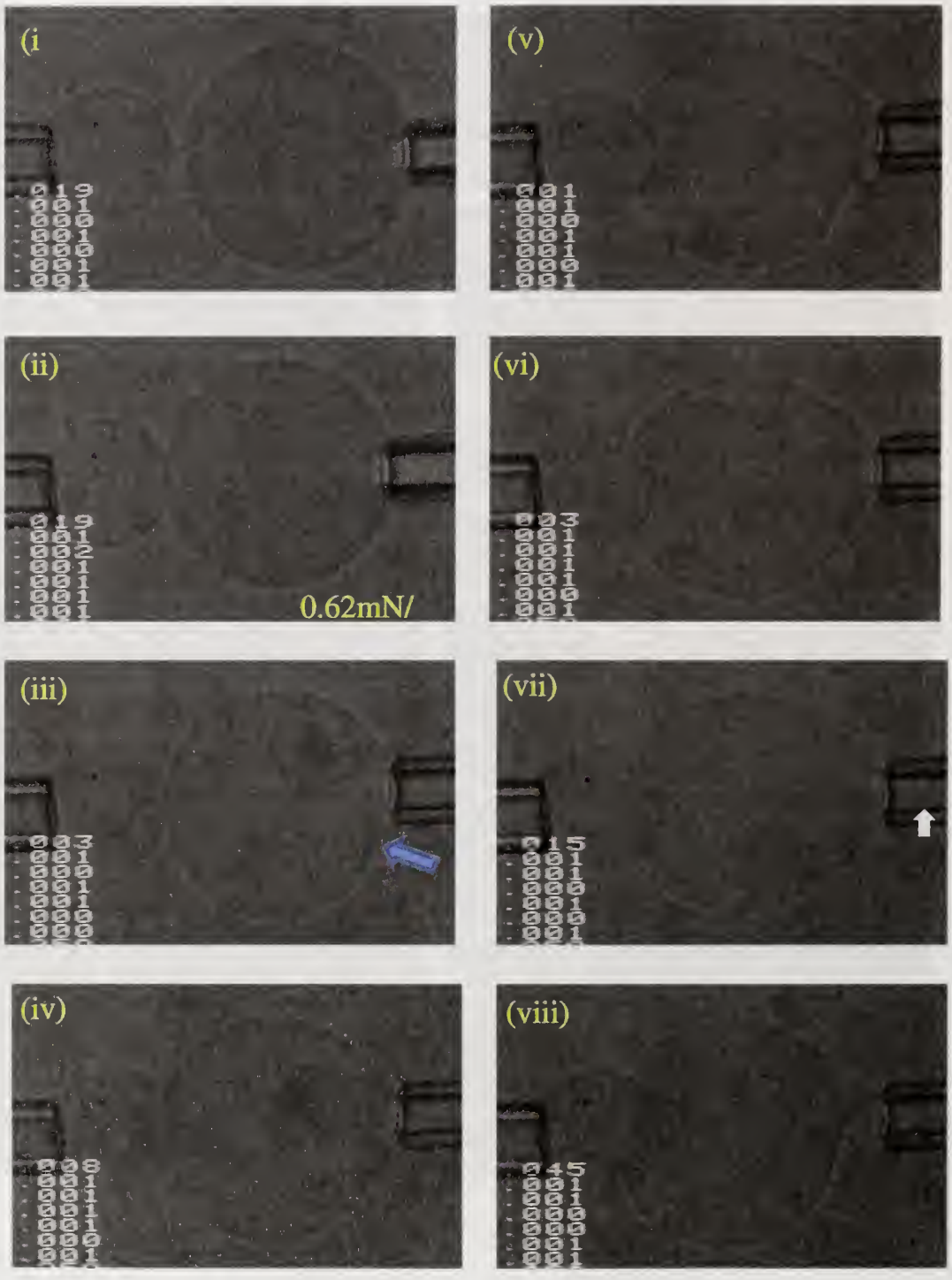

Figure 5.14B Another example of adhesion in a fully functionalized (F-Neutravidin – biotin) pair of stiff PBD-PEO vesicles.Spreading is not spontaneous. However, with positive pressure from the right pipette, the contact area is forced to increase (but the kink is not formed until the tension is increased again from the right, in frame vii.

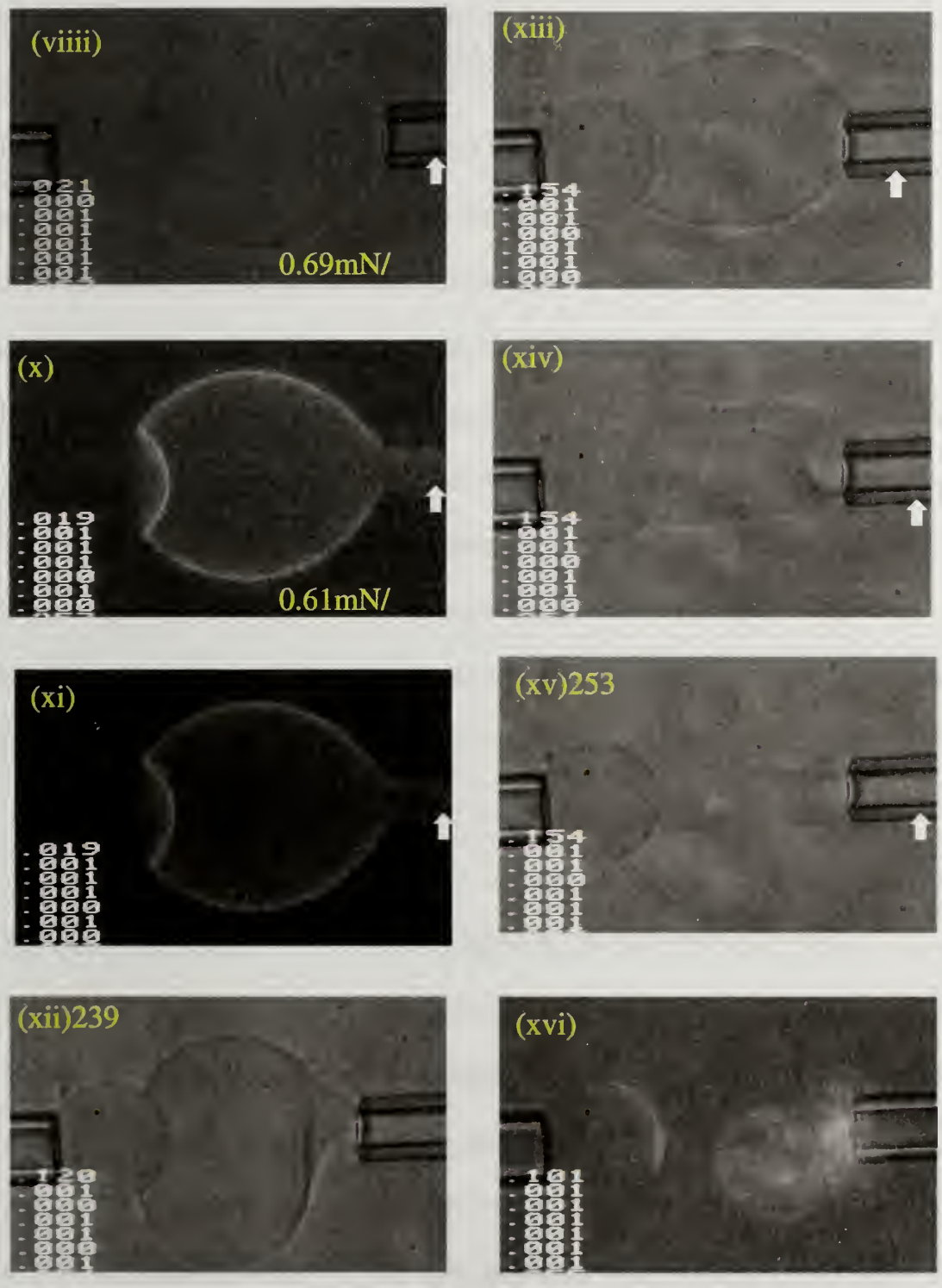

Figure 5.14B, continued. After the tension in crease in frame 7, the tension is reduced again in frame xii and the contact area further increased by pushing on the right vesicle. The tension is increased up to lysis in frame xiii, and the slow membrane rupture process is shown.

5.4 Discussion

In probing the factors affecting adhesive spreading, this study independently varied the membrane bending energy and adhesive strength. The latter was examined for both continuum and point-wise adhesive elements. Though the dense concentration of the receptors was designed to eliminate the impact of membrane diffusivity, there was still time dependence for the development of avidin-biotin bonds as a result of interfacial reaction kinetics. It was generally observed that the flexible membranes were susceptible to both adhesion and spreading while the stiff membranes, though adhesive, did not spread. In cases where spreading occurred spontaneously, there was a visible bend in the lower-tensioned of the two membranes at the perimeter of the contact zone. Spreading did not occur until this bend or kink was formed, and in cases where it never formed, spreading never proceeded.

An estimate of the kink radius follows from literature reports of a capillary length, r_c, over which a macroscopic contact angle was established for dense flaccid (with tensions τ = 1-5μN/m) phospholipids vesicles settling on a rigid substrate of adhesive complimentarity:[41] 100-200 nm. When the membrane is tensed by micropipettes in our study, the kink (or capillary length) will necessarily take on a sharper curvature and a greater bending cost. As there are no other lengthscales in the problem, r_c must scale as $(\kappa_b/\tau)^{1/2}$.[42] Hence for our experiments with micropipette-imposed tensions of 0.1 -1 mN/m, the radius of the kink at the periphery of the contact

zone could be as small as 10 nm. The bending cost to produce this kink acts as a line tension (κ_b/r_c) and is order 1000kT per micron of contact perimeter.

The observation of a lag time for some of the adhesive conditions (and especially its logarithmic dependence on membrane functionality in Figure 5.13) suggest describing spreading as an activated process involving an adhesion nucleus, of radius r_n, that is established when the vesicles are first placed into contact, depending on how forcibly the operator manipulates them. Adhesive forces, with E_{adh} per unit area, act on this contact nucleus uniformly. Depletion forces act almost immediately, on a timescale over which the polymer chains are squeezed from the gap. A lubrication approximation estimates this characteristic drainage time to be $3\ \eta\ \ell\ R_v/\tau\ \theta_e$,[41] which turns out to order of a 0.01 s for our more dilute solutions whose viscosities approach that of water, and longer, in proportion to viscosity, η, for the more concentrated solutions. Here ℓ is a logarithmic factor of order 10. Indeed, the fast development of adhesion and spreading for the flexible membranes demonstrates that depletion is set up rapidly even in the most concentrated, 7 wt% PEG solution. For F-NeutrAvidin-biotin binding, however, the number of cross-bonds across the contact gap increases with time, depending on the interfacial binding rate. This appears to vary substantially, depending on how the avidin is immobilized.[41]

The activation energy, E_a, for spreading, then, sums bending and adhesive contributions:

$$E_a = 2\ \pi\ r_n\ \kappa_b\ /r_c - \pi\ r_n^2\ E_{adh} \qquad (5.3)$$

This form resembles classical nucleation energy. When the initial adhesive contact, r_n, is small, E_a is positive, and bending prohibits spreading. However, above a critical nucleas size, $r_{n\text{-}crit}$, growth of the contact zone is favored and spreading occurs. The size of the critical nucleus follows from allowing first order variations in E_a to vanish:

$$r_{n\text{-}crit} = \kappa_b / (r_c E_{adh}) \qquad (5.4)$$

While we do not exactly know or have control over the size of the initial contact region, equation 5.4 suggests that situations having large critical nuclei would not be expected to spread. Figure 5.15(A) therefore summarizes expected values of $r_{n\text{-}crit}$ for different situations corresponding to the depletion experiments. The level of the depletion force is plotted on the x-axis and the vertical gray bars represent the particular values of the depletion forces corresponding to our different PEG solutions, both measured and calculated from the mean field treatment. Figure 5.15(A) describes the range of possibilities for the flexible membrane system, with $\kappa_b = 9.6$ kT. Since we have only an estimate (10 nm) for sharpness of the bending kink in our system, several possibilities are shown on the different diagonal lines. For example, in the 7 wt% solution which produces depletion forces of 0.33 erg /cm^2, if the bending radius, r_c, were 10 nm, then the critical radius of the contact nucleus would be 12 nm. If the bending radius were 50 nm, then the critical nucleus would be 2 nm. Both these nuclei are small compared to the contact zone one might imagines to result from pushing two vesicles together. Therefore, since the experimental contact nucleus is likely to exceed the critical value, then spreading is favored. Indeed flexible membranes spread immediately upon contact in concentrated PEG solutions. In Figure 5.15(A), however, for the weak

depletion forces associated with 0.1 wt% PEG (mean field calculations suggest 2.6 x 10^{-4} erg cm^2), $r_{n\text{-}crit}$ becomes large, for instance 15 um when r_c = 10 nm. Hence, it is not surprising that even flexible vesicles did not spread and establish meaningful contact angles in these solutions.

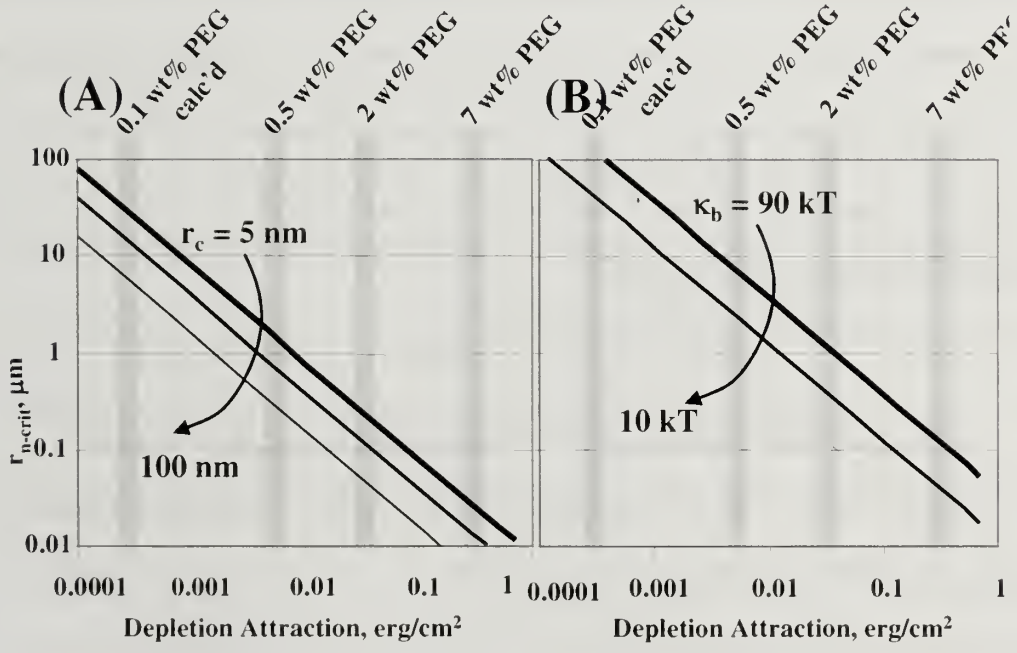

Figure 5.15 Radius of critical adhesion nucleus. (A) For κ_b = 9.6 kT (flexible membrane) and variations in r_c: 5, 10, 25, 50, 100 nm. (B) For r_c = 10 nm and variations in the membrane stiffness, κ_b: 9.6, 30, 90kT. Gray bars show PEG concentrations corresponding to various depletion forces, Measured from contact angle with flexible vesicles, except as indicated, where Calculations were done with mean field approach, per refs [2, 20].

Figure 5.15(B) shows the impact of bending modulus on $r_{n\text{-}crit}$, for a kink radius rc of 10 nm. Here, increasing the bending modulus from 10 to 30 kT, corresponding to our flexible and stiff membranes, makes spreading somewhat more difficult; however, using κ_b=30kT to describe the stiff membranes, the experiments show a greater impact of bending moduli than predicted in Figure 5.15(B). The obvious explanation is that the macroscopically measured bending modulus no longer applies when the kink radius (about 10 nm) approaches the thickness of the membrane, 9.6 nm. To form a kink this sharp would be equivalent to having the sharp curvature of a cylindrical micelle, which is not favored for this polymer. For this reason, predictions for κ_b = 90kT are also included in Figure 5.15(B), as a conservative estimate when the curvature of the kink approaches the membrane thickness.

The lag time observed for zero-tensioned stiff vesicles in 7 wt% PEG demonstrates that the onset of spreading can be controlled by stochastic considerations. From equation 3, one calculates E_a order 1-10 kT for a 100 nm kink (for a flaccid vesicle) and a 100 nm-scale contact nucleus. Notably, the lack of spreading of the flexible vesicles in 0.1 wt% PEG can also be treated as a lag time which happens to be infinite from the practical experimental perspective.

The observation of a lag time for avidin-biotin-driven adhesion of flexible vesicles results from a combination of stochastic and reaction kinetic factors. Once the vesicles are placed in contact, the activation energy to spreading decreases and E_{adh}

increases with time, for instance according to a classic rate law: $E_{adh} = E_{ab}\, k\, \alpha\, C_{biot}\, C_{av}\, t$. Here E_{ab} is about 35 kT,[43] the energy of an F-NeutrAvidin-biotin bond, k is the interfacial rate constant for avidin-biotin binding on our vesicle coronas and α accounts for the fraction of the interfacial molecules which may actually be available (the remainder being buried within the corona or oriented such that binding regions are inaccessible), and C_{biot} and C_{av} are the biotin and F-NeutrAvidin surface concentrations. k, and α are unknown. Thus at each instant in time there is a probability that the vesicles will bend and start to spread, and this probability increases as E_a decreases. The lag time follows as

$$\tau_{lag} = \omega \exp\left[2\pi r_n \kappa_b / r_c - \pi r_n^2 (E_{ab}\, k\, \alpha\, C_{biot}\, C_{av}\, t) \right) \qquad (5.5)$$

where ω is an unknown attempt frequency. Figure 5.13 shows a best fit of the lag time data to equation 5, with $\kappa_b/r_c = 0.10$ kT/nm (a very conservative estimate due to the apparent compromise of the membrane as a result of biotinylation), a contact nucleus of radius 1 μm, and the only fitting parameter, $k\alpha = 1.8\ e^{-7}$ um^2/s. Here ω was chosen to be 1e6 s^{-1} but the predictions from equation 5 turn out to be insensitive to ω for many orders of magnitude from ω = 1 to $1e^{12}$ s^{-1}. The fitted curve does an excellent job of capturing the overall shape of the data and the quantitative measurement.

5.5 Summary

This work has demonstrated, via systematic comparison of two types of vesicle membranes, the influence of different attractive forces on the ability of vesicles to overcome their bending-related energy barriers and begin to spread. With one exception, the stiff membranes did not spread, even though they were able to adhere to substrate vesicles. By contrast, flexible vesicles were able to spread immediately in response to all but the weakest (0.0003 erg /cm^2) depletion forces. In the case of Avidin-Biotin binding, the stiff vesicles adhered but never exhibited membrane kinking or vesicle spreading while flexible vesicles spread following a lag time during which an increasing number of avidin-biotin bonds decreased the spreading energy barrier.

This work did not address the spreading rates that were observed after the initiation of spreading, though in all cases, these were on the order of microns / second. A quantitative analysis of the depletion forces worked well to predict the spreading or lack thereof, for the flexible membrane system. For the stiff vesicles, use of the macroscopic bending modulus in this treatment over-predicted the spreading tendency, but still gave some insight into the vesicles resistance to spread. Use of a more appropriate bending modulus for tight kinks in these thick membranes would reduce the quantitative discrepancy. A semi-quantitative treatment of the avidin-biotin binding was able to anticipate the lag time behavior seen with flexible vesicles, but rigorous quantization was compromised by the unknown binding efficiency of the interfacial

avidins and biotins and by the impact of membrane modification on the bending modulus.

These results call attention to the importance of membrane bending in adhesive processes involving vesicles. While bending and tension has been included in models of colloidal and nanoparticle engulfment which necessarily involve sharp curvature, the role of this sharp curvature has been overlooked in experimental and theoretic treatments of giant vesicles in pipettes. The findings here quantify the diverse possibilities which can be exhibited by stiff and flexible vesicle subject to different types of adhesive forces and suggest how bending should be considered in the design of membrane-based scavengers and drug delivery packages.

REFERENCES

1. Evans, E. A., Analysis of Adhesion of Large Vesicles to Surfaces. *Biophysical Journal* **1980,** 31, (3), 425-431.

2. Evans, E.; Needham, D., Attraction between Lipid Bilayer-Membranes in Concentrated-Solutions of Nonadsorbing Polymers - Comparison of Mean-Field Theory with Measurements of Adhesion Energy. *Macromolecules* **1988,** 21, (6), 1822-1831.

3. Evans, E. A., Force between Surfaces That Confine a Polymer-Solution - Derivation from Self-Consistent Field-Theories. *Macromolecules* **1989,** 22, (5), 2277-2286.

4. Evans, E.; Needham, D., Physical-Properties of Surfactant Bilayer-Membranes - Thermal Transitions, Elasticity, Rigidity, Cohesion, and Colloidal Interactions. *Journal of Physical Chemistry* **1987,** 91, (16), 4219-4228.

5. Discher, B. M.; Won, Y. Y.; Ege, D. S.; Lee, J. C. M.; Bates, F. S.; Discher, D. E.; Hammer, D. A., Polymersomes: Tough vesicles made from diblock copolymers. *Science* **1999,** 284, (5417), 1143-1146.

6. Bermudez, H.; Hammer, D. A.; Discher, D. E., Effect of bilayer thickness on membrane bending rigidity. *Langmuir* **2004,** 20, (3), 540-543.

7. Arifin, D. R.; Palmer, A. F., Physical properties and stability mechanisms of poly(ethylene glycol) conjugated liposome encapsulated hemoglobin dispersions. *Artificial Cells Blood Substitutes and Biotechnology* **2005,** 33, (2), 137-162.

8. Masui, T.; Imai, M.; Nakaya, K.; Taniguchi, T., Effects of grafted polymer chains on lamellar membranes. *Journal of Chemical Physics* **2006,** 124, (7).

9. Bivas, I.; Winterhalter, M.; Meleard, P.; Bothorel, P., Elasticity of bilayers containing PEG lipids. *Europhysics Letters* **1998,** 41, (3), 261-266.

10. Zhang, C.-Z.; Wang, Z.-G., Nucleation of Membrane Adhesion. *Physical Review E* **submitted**.

11. Sackmann, E.; Goennenwein, S., Cell adhesion as dynamic interplay of lock-and-key, generic and elastic forces. *Progress of Theoretical Physics Supplement* **2006**, (165), 78-99.

12. Bruinsma, R. F.; Sackmann, E., In *Physics of Biomolecules and Cells*, Flyvbyerg, H.; Ormos, P.; David, F., Eds. Springer: 2002; Vol. 75 of Les Houches Summer School, pp 287-309.

13. Deserno, M.; Bickel, T., Wrapping of a spherical colloid by a fluid membrane. *Europhysics Letters* **2003,** 62, (5), 767-773.

14. Deserno, M.; Gelbart, W. M., Adhesion and wrapping in colloid-vesicle complexes. *Journal of Physical Chemistry B* **2002,** 106, (21), 5543-5552.

15. Smith, K. A.; Jasnow, D.; Balazs, A. C., Designing synthetic vesicles that engulf nanoscopic particles. *Journal of Chemical Physics* **2007,** 127, (8).

16. Wang, J.; Muthumumar, M., Kinetics of wrapping a colloid by a fluid membrane. *Journal of Chemical Physics* **submitted**.

17. Kloboucek, A.; Behrisch, A.; Faix, J.; Sackmann, E., Adhesion-induced receptor segregation and adhesion plaque formation: A model membrane study. *Biophysical Journal* **1999,** 77, (4), 2311-2328.

18. Guttenberg, Z.; Lorz, B.; Sackmann, E.; Boulbitch, A., First-order transition between adhesion states in a system mimicking cell-tissue interaction. *Europhysics Letters* **2001,** 54, (6), 826-832.

19. Bruinsma, R.; Behrisch, A.; Sackmann, E., Adhesive switching of membranes: Experiment and theory. *Physical Review E* **2000,** 61, (4), 4253-4267.

20. Albersdorfer, A.; Feder, T.; Sackmann, E., Adhesion-induced domain formation by interplay of long-range repulsion and short-range attraction force: A model membrane study. *Biophysical Journal* **1997,** 73, (1), 245-257.

21. Boulbitch, A.; Guttenberg, Z.; Sackmann, E., Kinetics of membrane adhesion mediated by ligand-receptor interaction studied with a biomimetic system. *Biophysical Journal* **2001,** 81, (5), 2743-2751.

22. Nam, J.; Santore, M. A., The adhesion kinetics of sticky vesicles in tension: The distinction between spreading and receptor binding. *Langmuir* **2007,** 23, (21), 10650-10660.

23. de Gennes, P. G.; Puech, P. H.; Brochard-Wyart, F., Adhesion induced by mobile stickers: A list of scenarios. *Langmuir* **2003,** 19, (17), 7112-7119.

24. Brochard-Wyart, F.; de Gennes, P. G., Adhesion induced by mobile binders: Dynamics. *Proceedings of the National Academy of Sciences of the United States of America* **2002,** 99, (12), 7854-7859.

25. Lin, J. J.; Silas, J. A.; Bermudez, H.; Milam, V. T.; Bates, F. S.; Hammer, D. A., The effect of polymer chain length and surface density on the adhesiveness of functionalized polymersomes. *Langmuir* **2004,** 20, (13), 5493-5500.

26. Hategan, A.; Law, R.; Kahn, S.; Discher, D. E., Adhesively-tensed cell membranes: Lysis kinetics and atomic force microscopy probing. *Biophysical Journal* **2003,** 85, (4), 2746-2759.

27. Dimitrov, D. S.; Angelova, M. I., Lipid Swelling and Liposome Formation Mediated by Electric-Fields. *Bioelectrochemistry and Bioenergetics* **1988,** 19, (2), 323-336.

28. Nam, J.; Santore, M. M., Adhesion Plaque Formation Dynamics between Polymer Vesicles in the Limit of Highly Concentated Binding Sites. *Langmuir* **2007,** 23.

29. Hill, R. M.; He, M. T.; Lin, Z.; Davis, H. T.; Scriven, L. E., Lyotropic Liquid-Crystal Phase-Behavior of Polymeric Siloxane Surfactants. *Langmuir* **1993,** 9, (11), 2789-2798.

30. Nilsson, K.; Mosbach, K., Para-Toluenesulfonyl Chloride as an Activating Agent of Agarose for the Preparation of Immobilized Affinity Ligands and Proteins. *European Journal of Biochemistry* **1980,** 112, (2), 397-402.

31. Nilsson, K.; Norrlow, O.; Mosbach, K., Para-Toluenesulfonyl Chloride as an Activating Agent of Agarose for the Preparation of Immobilized Affinity Ligands and Proteins - Optimization of Conditions for Activation and Coupling. *Acta Chemica Scandinavica Series B-Organic Chemistry and Biochemistry* **1981,** 35, (1), 19-27.

32. Hiller, Y.; Gershoni, J. M.; Bayer, E. A.; Wilchek, M., Biotin Binding to Avidin - Oligosaccharide Side-Chain Not Required for Ligand Association. *Biochemical Journal* **1987,** 248, (1), 167-171.

33. Vanroy, N.; Mangelschots, K.; Speleman, F., Improved Immunocytochemical Detection of Biotinylated Probes with Neutralite Avidin. *Trends in Genetics* **1993,** 9, (3), 71-72.

34. NopplSimson, D. A.; Needham, D., Avidin-biotin interactions at vesicle surfaces: Adsorption and binding, cross-bridge formation, and lateral interactions. *Biophysical Journal* **1996,** 70, (3), 1391-1401.

35. Bloustine, J.; Virmani, T.; Thurston, G. M.; Fraden, S., Light scattering and phase behavior of lysozyme-poly(ethylene glycol) mixtures. *Physical Review Letters* **2006,** 96, (8).

36. Kinugasa, S.; Nakahara, H.; Kawahara, J. I.; Koga, Y.; Takaya, H., Static light scattering from poly(ethylene oxide) in methanol. *Journal of Polymer Science Part B-Polymer Physics* **1996,** 34, (3), 583-586.

37. Kuhl, T. L.; Berman, A. D.; Hui, S. W.; Israelachvili, J. N., Part 1. Direct measurement of depletion attraction and thin film viscosity between lipid bilayers in aqueous polyethylene glycol solutions. *Macromolecules* **1998,** 31, (23), 8250-8257.

38. Marsh, D., Scaling and mean-field theories applied to polymer brushes. *Biophysical Journal* **2004,** 86, (4), 2630-2633.

39. Winzor, D. J., Reappraisal of disparities between osmolality estimates by freezing point depression and vapor pressure deficit methods. *Biophysical Chemistry* **2004,** 107, (3), 317-323.

40. Santore, M. M.; Discher, D. E.; Won, Y. Y.; Bates, F. S.; Hammer, D. A., Effect of surfactant on unilamellar polymeric vesicles: Altered membrane properties and stability in the limit of weak surfactant partitioning. *Langmuir* **2002,** 18, (20), 7299-7308.

41. Cuvelier, D.; Nassoy, P., Hidden dynamics of vesicle adhesion induced by specific stickers. *Physical Review Letters* **2004,** 93, (22).

42. Bruinsma, R.; Sackmann, E., Bioadhesion and the dewetting transition. *Comptes Rendus De L Academie Des Sciences Serie Iv Physique Astrophysique* **2001,** 2, (6), 803-815.

43. Helm, C. A.; Knoll, W.; Israelachvili, J. N., Measurement of Ligand Receptor Interactions. *Proceedings of the National Academy of Sciences of the United States of America* **1991,** 88, (18), 8169-8173.

CHAPTER 6

FUTURE WORK

This thesis has demonstrated, for the simplest conceivable set of adhesive driving forces and membrane models, that diverse adhesion and spreading dynamics result from coupling of membrane mechanics with attractions. The simplest continuum and ligand receptor attractions were pursued here. With fluid phospholipids systems that lack complexities due to bending, the depletion-drive and densely functionalized avidin-biotin binding would have been trivial.

With phospholipid-based systems, a number of elaborate and complex mechanisms deriving from physics such as different ranges of attractive elements, and in-membrane phase separation have been the focus of recent study, as discussed in Chapter 1. These works have been very limited and could be further explored with phospholipids and polymers alike. The next obvious step forward from this thesis is to examine the role of membrane bending on these more complicated adhesive dynamic situations.

6.1 Current Observations

Even before adhesion studies in these more complex systems are undertaken, the work in this thesis has raised several important questions yet to be addressed. This thesis successfully explained the presence of a lag time, the ability of some adhesive

vesicles to spontaneously spread, and the inability of others to spread at all; however, complete quantization is forthcoming. One important question raised was the effective bending modulus for thicker membranes which might achieve curvatures on the lengthscales of the membrane thickness. The theoretical literature is lacking in its predictions in this regard. Likewise, this thesis postulated a curvature radius based on scaling arguments, and more refined experiments might still measure the nanometer scale bending shapes at the contact lines to more firmly establish the behaviors proposed here.

This thesis also presented a large body of spreading dynamic behaviors once spreading was nucleated. For the most part, the spreading always occurred quickly, and was generally insensitive to membrane composition and tension over the range of conditions studied. A more quantitative treatment anticipating such spreading dynamics in another open area for modeling.

6.2 Exaggerated Differences between Substrate and Adhering Vesicles

The current work focused on nearly symmetrical situations: In the case of depletion forces, the left and right vesicles were exactly identical except for their sizes and the imposed tensions. In the case of avidin-biotin binding, the underlying biotin densities of the two vesicles were identical and varied together. Especially with this latter situation, we were never able to access the dilute regime where in-plane lateral diffusion affected membrane dynamics. In our studies, lower membrane functionality compromised the adhesive forces needed to overcome the bending barrier to spreading.

In a modified version of our procedure, it might be possible to employ a fully functionalized biotinylated vesicle as the substrate and a vesicle of varying F-NeutrAvidin-conjugated-biotinyl density as the spreading vesicle. Perhaps with many potential binding sites on the substrate, lower F-NeutrAvidin densities could be tolerated and recruitment of fluorescent receptors to the contact region could be recorded and studied if spreading proceeds.

6.3 Effect of two different brush length

The Hammer lab has studied the effect of bimodal brush architecture on membrane binding strength, demonstrating that, for brushes which placed adhesive groups well beyond the main mass of the vesicle corona, the greatest adhesion strengths were observed. The study was not one focusing on dynamics, and indeed the best explanation for these observations is that binding occurred more rapidly in bimodal brushes, so that more bonds needed to be pulled apart at the end of the contact time. Coronas consisting entirely of functionalized short or long brushes were not as an effective in their adhesive behaviors. This study focused only on the apparent maximum membrane binding strength in peeling tests, when the membranes were functionalized with avidin and biotin. The current thesis already finds dramatically different results for functionalized uniform brushes: no peeling could be done. We therefore might expect very different behavior than observed in that previous study, were we to pursue bimodal brush adhesion with our current systems. The bimodal brush could be a particularly enlightening tool concerning the development of adhesive

interactions in a contact zone prior to initiation of spreading. We might imagine that if a bimodal brush increases binding efficiency, that the latent prior to spreading for our systems would be reduced relative to that of the current uniform brushes.

Also for bimodal systems, Sackmann showed that phase separation occurred as a result of exclusion of non-functional longer brushy molecules from adhesive regions whose local compositions were dominated by the adhesive molecules. Interestingly, the Hammer lab did not report any phase separation in their bimodal brushes, an exciting effect which we would hope to find. To our knowledge, adhesion-driven phase separation has not been reported in polymer membrane systems.

6.4 Effect of membrane mixture on to adhesion dynamics

This thesis focused exclusively on situations involving copolymer membranes. As part of the graduate work leading to this thesis, a number of other systems were initially investigated and one particularly promising system was DSPE-PEG(2000)biotin, which we found to be mostly miscible with DC5329 vesicles. Indeed, strong irreversible adhesion was found with small amounts of biotin functionality incorporated in this fashion, suggesting that the biotins were either more accessible or better retained their activity through this approach. Here we would expect diffusion-limited behaviors, and indeed this represented a case where slow spreading dynamics were seen. Pursuit of this system would compliment the faster spreading dynamic seen in this system.

There also exists the possibility of employing phospholipids which phase separate into a gel phase upon cooling. Such phospholipids would be expected to be miscible with polymers in the vesicle membrane at elevated temperatures but phase separate at cool temperatures. Interesting adhesive behavior might be observed for mixed vesicles near the phase separation temperature. Premature phase separation might be triggered by adhesive interactions. We consider this a possibility because of the phase separation reported for mixed vesicles containing non-adhesive brushy molecules.

6.5 Different functionalities such as DNA, ionic binding

There have been several studies of phospholipid adhesion driven by various functionalities such as antibody-antigen, biotin-avidin, electrostatic interactions, and sequence-specific DNA hybridization. By comparison, only avidin-biotin and one antibody-antigen pair have been studied with polymer vesicles, as giant polymeric vesicles have only been recently discovered. The field, therefore, is wide open for studies of functionalized polymer vesicles, which could form the basis for new delivery technologies and, by comparison with phospholipid behavior, inform us on biological behaviors. In particular, since polymer vesicles can survive denser functionalization compared with phospholipids, polymer vesicles present a useful platform for studying the synergistic effects of multiple ligand-receptor pairs, which could trigger cascade effects or direct two-dimensional self-assemblies on the polymeric membrane.

Performing these studies in the spherical vesicle geometry rather than immobilized as flat bilayers better preserves the membrane's fluidity and addresses the significant biological issues of the role of membrane dynamics, membrane shape, and mechanics in the adhesion. This perspective is absent from even the most sophisticated tethered layer platforms.

6.6 Diffusion of functional molecules on the membrane surface

This thesis focused, for ligand-receptor binding, on the regime of densely concentrated adhesive molecules which excluded the possibility of molecular diffusion to the contact zone. In the limit where adhesive molecules are dilute, they can move to contact zone as the interface is growing. This is expected to be the case for both phospholipid and polymer vesicles, though diffusion is slower in the latter. Indeed, for processes governed by the competition between adhesion reaction rates and diffusion rates, polymer vesicles provide a means to access a range of "Damkoler number" space. The diffusivities of tracer molecules in both polymer and phospholipid membranes can be determined using FRAP (Fluorescence Recovery After Photobleaching). This technique has been used primarily to track the tracer molecule movement in flat bilayer membranes (supported or tethered to planar solids).

The combination of the dual micropipette technique and FRAP should produce interesting results, and with some care and reorientation of the pipette geometry relative to the microscope objective, could be used to examine mobility in the contact zone

itself, in addition to the main part of the vesicle. The impact of membrane tension could be readily explored by such a method. This approach would allow one to quantify 1) the species accumulating at the interface, 2) the diffusive mechanism in confinement, in situations where reactions may occur 3) and differences between diffusion in polymer and phospholipid bilayers.

BIBLIOGRAPHY

1. Abe, Y.; Harata, K.; Fujiwara, M.; Ohbu, K., Bilayer structure of glycolipid crystals. Thermal stability of the crystal and state of the alkyl chain. Journal of the Chemical Society-Perkin Transactions 2 1998, (1), 177-186.

2. Akashi, K.; Miyata, H.; Itoh, H.; Kinosita, K., Formation of giant liposomes promoted by divalent cations: Critical role of electrostatic repulsion. Biophysical Journal 1998, 74, (6), 2973-2982.

3. Albelda, S. M.; Smith, C. W.; Ward, P. A., Adhesion molecules and inflammatory injury. Fasеb Journal 1994, 8, (8), 504-512.

4. Albersdorfer, A.; Feder, T.; Sackmann, E., Adhesion-induced domain formation by interplay of long-range repulsion and short-range attraction force: A model membrane study. Biophysical Journal 1997, 73, (1), 245-257.

5. Allen, T. M.; Hansen, C., Pharmacokinetics of stealth versus conventional liposomes - effect of dose. Biochimica Et Biophysica Acta 1991, 1068, (2), 133-141.

6. Anderson, E.; Brown, T.; Picken, D., Novel photocleavable universal support for oligonucleotide synthesis. Nucleosides Nucleotides & Nucleic Acids 2003, 22, (5-8), 1403-1406.

7. Anderson, K. W.; Li, W. I.; Cezeaux, J.; Zimmer, S., Invitro studies of deformation and adhesion properties of transformed-cells. Cell Biophysics 1991, 18, (2), 81-97.

8. Angelova, M. I.; Dimitrov, D. S., Swelling of Charged Lipids and Formation of Liposomes on Electrode Surfaces. Molecular Crystals and Liquid Crystals 1987, 152, 89-104.

9. Arifin, D. R.; Palmer, A. F., Physical properties and stability mechanisms of poly(ethylene glycol) conjugated liposome encapsulated hemoglobin dispersions. Artificial Cells Blood Substitutes and Biotechnology 2005, 33, (2), 137-162.

10. Bailey, S. M.; Chiruvolu, S.; Israelachvili, J. N.; Zasadzinski, J. A. N., Measurements of Forces Involved in Vesicle Adhesion Using Freeze-Fracture Electron-Microscopy. Langmuir 1990, 6, (7), 1326-1329.

11. Bell, G. I., Models for Specific Adhesion of Cells to Cells. Science 1978, 200, (4342), 618-627.

12. Bell, G. I.; Dembo, M.; Bongrand, P., Cell-Adhesion - Competition between Nonspecific Repulsion and Specific Bonding. Biophysical Journal 1984, 45, (6), 1051-1064.

13. Berger, O.; Edholm, O.; Jahnig, F., Molecular dynamics simulations of a fluid bilayer of dipalmitoylphosphatidylcholine at full hydration, constant pressure, and constant temperature. Biophysical Journal 1997, 72, (5), 2002-2013.

14. Bermudez, H.; Brannan, A. K.; Hammer, D. A.; Bates, F. S.; Discher, D. E., Molecular weight dependence of polymersome membrane structure, elasticity, and stability. Macromolecules 2002, 35, (21), 8203-8208.

15. Bermudez, H.; Hammer, D. A.; Discher, D. E., Effect of bilayer thickness on membrane bending rigidity. Langmuir 2004, 20, (3), 540-543.

16. Bernard, A. L.; Guedeau-Boudeville, M. A.; Jullien, L.; di Meglio, J. M., Strong adhesion of giant vesicles on surfaces: Dynamics and permeability. Langmuir 2000, 16, (17), 6809-6820.

17. Bevilacqua, M. P., Endothelial-leukocyte adhesion molecules. Annual Review of Immunology 1993, 11, 767-804.

18. Bivas, I.; Winterhalter, M.; Meleard, P.; Bothorel, P., Elasticity of bilayers containing PEG lipids. Europhysics Letters 1998, 41, (3), 261-266.

19. Bloom, M.; Evans, E.; Mouritsen, O. G., Physical-properties of the fluid lipid-bilayer component of cell-membranes - a perspective. Quarterly Reviews of Biophysics 1991, 24, (3), 293-397.

20. Bloustine, J.; Virmani, T.; Thurston, G. M.; Fraden, S., Light scattering and phase behavior of lysozyme-poly(ethylene glycol) mixtures. Physical Review Letters 2006, 96, (8).

21. Boulbitch, A.; Guttenberg, Z.; Sackmann, E., Kinetics of membrane adhesion mediated by ligand-receptor interaction studied with a biomimetic system. Biophysical Journal 2001, 81, (5), 2743-2751.

22. Boura, C.; Muller, S.; Vautier, D.; Dumas, D.; Schaaf, P.; Voegel, J. C.; Stoltz, J. F.; Menu, P., Endothelial cell - interactions with polyelectrolyte multilayer films. Biomaterials 2005, 26, (22), 4568-4575.

23. Brochard-Wyart, F.; de Gennes, P. G., Adhesion induced by mobile binders: Dynamics. Proceedings of the National Academy of Sciences of the United States of America 2002, 99, (12), 7854-7859.

24. Brochard-Wyart, F.; de Gennes, P. G., Unbinding of adhesive vesicles. Comptes Rendus Physique 2003, 4, (2), 281-287.

25. Bruckner, E.; Sonntag, P.; Rehage, H., Influence of toluene on the bending elastic properties of giant phosphatidylcholine vesicles. Journal of Physical Chemistry B 2000, 104, (10), 2311-2319.

26. Bruinsma, R.; Behrisch, A.; Sackmann, E., Adhesive switching of membranes: Experiment and theory. Physical Review E 2000, 61, (4), 4253-4267.

27. Bruinsma, R.; Sackmann, E., Bioadhesion and the dewetting transition. Comptes Rendus De L Academie Des Sciences Serie Iv Physique Astrophysique 2001, 2, (6), 803-815.

28. Capovilla, R.; Guven, J., Geometry of lipid vesicle adhesion. Physical Review E 2002, 66, (4).

29. Cathcart, M. K.; Culp, L. A., Phospholipid-composition of substrate adhesion sites of normal, virus-transformed, and revertant murine cells. Biochemistry 1979, 18, (7), 1167-1176.

30. Cevc, G.; Marsh, D., Phospholipid Bilayers (Wiley, New York). 1987.

31. Chaudhury, M. K., Rate-dependent fracture at adhesive interface. Journal of Physical Chemistry B 1999, 103, (31), 6562-6566.

32. Choucair, A.; Soo, P. L.; Eisenberg, A., Active loading and tunable release of doxorubicin from block copolymer vesicles. Langmuir 2005, 21, (20), 9308-9313.

33. Chu, Y. S.; Thomas, W. A.; Eder, O.; Pincet, F.; Perez, E.; Thiery, J. P.; Dufour, S., Force measurements in E-cadherin-mediated cell doublets reveal rapid adhesion strengthened by actin cytoskeleton remodeling through Rac and Cdc42. Journal of Cell Biology 2004, 167, (6), 1183-1194.

34. Claessens, M.; van Oort, B. F.; Leermakers, F. A. M.; Hoekstra, F. A.; Stuart, M. A. C., Charged lipid vesicles: Effects of salts on bending rigidity, stability, and size. Biophysical Journal 2004, 87, (6), 3882-3893.

35. Collins, T.; Read, M. A.; Neish, A. S.; Whitley, M. Z.; Thanos, D.; Maniatis, T., Transcriptional regulation of endothelial-cell adhesion molecules - nf-kappa-b and cytokine-inducible enhancers. Faseb Journal 1995, 9, (10), 899-909.

36. Coombs, D.; Dembo, M.; Wofsy, C.; Goldstein, B., Equilibrium thermodynamics of cell-cell adhesion mediated by multiple ligand-receptor pairs. Biophysical Journal 2004, 86, (3), 1408-1423.

37. Cornelissen, J.; Fischer, M.; Sommerdijk, N.; Nolte, R. J. M., Helical superstructures from charged poly(styrene)-poly(isocyanodipeptide) block copolymers. Science 1998, 280, (5368), 1427-1430.

38. Cuvelier, D.; Nassoy, P., Hidden dynamics of vesicle adhesion induced by specific stickers. Physical Review Letters 2004, 93, (22).

39. de Gennes, P. G.; Puech, P. H.; Brochard-Wyart, F., Adhesion induced by mobile stickers: A list of scenarios. Langmuir 2003, 19, (17), 7112-7119.

40. Deserno, M.; Bickel, T., Wrapping of a spherical colloid by a fluid membrane. Europhysics Letters 2003, 62, (5), 767-773.

41. Deserno, M.; Gelbart, W. M., Adhesion and wrapping in colloid-vesicle complexes. Journal of Physical Chemistry B 2002, 106, (21), 5543-5552.

42. Dimitrov, D. S.; Angelova, M. I., Lipid swelling and liposome formation mediated by electric-fields. Bioelectrochemistry and Bioenergetics 1988, 19, (2), 323-336.

43. Discher, B. M.; Won, Y. Y.; Ege, D. S.; Lee, J. C. M.; Bates, F. S.; Discher, D. E.; Hammer, D. A., Polymersomes: Tough vesicles made from diblock copolymers. Science 1999, 284, (5417), 1143-1146.

44. Discher, D. E.; Eisenberg, A., Polymer vesicles. Science 2002, 297, (5583), 967-973.

45. Discher, D. E.; Eisenberg, A., Polymer vesicles. Science 2002, 297, (5583), 967-973.

46. D'Souza-Schorey, C.; Boettner, B.; Van Aelst, L., Rac regulates integrin-mediated spreading and increased adhesion of T lymphocytes. Molecular and Cellular Biology 1998, 18, (7), 3936-3946.

47. Duzgunes, N.; Delima, M. C. P.; Stamatatos, L.; Flasher, D.; Alford, D.; Friend, D. S.; Nir, S., Fusion Activity and Inactivation of Influenza-Virus - Kinetics of Low Ph-induced Fusion with Cultured-Cells. Journal of General Virology 1992, 73, 27-37.

48. Evans, E., Adhesion of Surfactant Membrane Covered Droplets - Special Features and Curvature Elasticity Effects. Colloids and Surfaces 1990, 43, (2-4), 327-347.

49. Evans, E.; Berk, D.; Leung, A., Detachment of agglutinin-bonded red-blood-cells .1. forces to rupture molecular-point attachments. Biophysical Journal 1991, 59, (4), 838-848.

50. Evans, E.; Heinrich, V.; Leung, A.; Kinoshita, K., Nano- to microscale dynamics of P-selectin detachment from leukocyte interfaces. I. Membrane separation from the cytoskeleton. Biophysical Journal 2005, 88, (3), 2288-2298.

51. Evans, E.; Heinrich, V.; Ludwig, F.; Rawicz, W., Dynamic tension spectroscopy and strength of biomembranes. Biophysical Journal 2003, 85, (4), 2342-2350.

52. Evans, E.; Klingenberg, D., Adhesion of polymer-grafted membrane-vesicles in concentrated-solutions of nonadsorbing free polymer. Abstracts of Papers of the American Chemical Society 1995, 210, 50-COLL.

53. Evans, E.; Klingenberg, D. J.; Rawicz, W.; Szoka, F., Interactions between polymer-grafted membranes in concentrated solutions of free polymer. Langmuir 1996, 12, (12), 3031-3037.

54. Evans, E.; Leung, A.; Heinrich, V.; Zhu, C., Mechanical switching and coupling between two dissociation pathways in a P-selectin adhesion bond. Proceedings of the National Academy of Sciences of the United States of America 2004, 101, (31), 11281-11286.

55. Evans, E.; Metcalfe, M., Free-Energy Potential for Aggregation of Giant, Neutral Lipid Bilayer Vesicles by Vanderwaals Attraction. Biophysical Journal 1984, 46, (3), 423-426.

56. Evans, E.; Needham, D., Physical-Properties of Surfactant Bilayer-Membranes - Thermal Transitions, Elasticity, Rigidity, Cohesion, and Colloidal Interactions. Journal of Physical Chemistry 1987, 91, (16), 4219-4228.

57. Evans, E.; Needham, D., Attraction between lipid bilayer-membranes in concentrated-solutions of nonadsorbing polymers - comparison of mean-field theory with measurements of adhesion energy. Macromolecules 1988, 21, (6), 1822-1831.

58. Evans, E.; Rawicz, W., Entropy-Driven Tension and Bending Elasticity in Condensed-Fluid Membranes. Physical Review Letters 1990, 64, (17), 2094-2097.

59. Evans, E. A., Analysis of Adhesion of Large Vesicles to Surfaces. Biophysical Journal 1980, 31, (3), 425-431.

60. Evans, E. A., Minimum energy analysis of membrane deformation applied to pipet aspiration and surface-adhesion of red-blood-cells. Biophysical Journal 1980, 30, (2), 265-284.

61. Evans, E. A., Force between surfaces that confine a polymer-solution - derivation from self-consistent field-theories. Macromolecules 1989, 22, (5), 2277-2286.

62. Evans, E. A.; Calderwood, D. A., Forces and bond dynamics in cell adhesion. Science 2007, 316, (5828), 1148-1153.

63. Fendler, J. H., Polymerized Surfactant Vesicles - Novel Membrane Mimetic Systems. Science 1984, 223, (4639), 888-894.

64. Ghatak, A.; Vorvolakos, K.; She, H. Q.; Malotky, D. L.; Chaudhury, M. K., Interfacial rate processes in adhesion and friction. Journal of Physical Chemistry B 2000, 104, (17), 4018-4030.

65. Ghoroghchian, P. P.; Li, G. Z.; Levine, D. H.; Davis, K. P.; Bates, F. S.; Hammer, D. A.; Therien, M. J., Bioresorbable vesicles formed through spontaneous self-assembly of amphiphilic poly(ethylene oxide)-block-polycaprolactone. Macromolecules 2006, 39, (5), 1673-1675.

66. Gourier, C.; Pincet, F.; Le Bouar, T.; Zhang, Y.; Esnault, J.; Mallet, J. M.; Sinay, P.; Perez, E., Can small complex chains be treated as polymers? Macromolecules 2004, 37, (23), 8778-8784.

67. Gourier, C.; Pincet, F.; Perez, E.; Zhang, Y. M.; Zhu, Z. Y.; Mallet, J. M.; Sinay, P., The natural Lewis(X)-bearing lipids promote membrane adhesion: Influence of ceramide on carbohydrate-carbohydrate recognition. Angewandte Chemie-International Edition 2005, 44, (11), 1683-1687.

68. Green, N. M., Avidin and Streptavidin. Methods in Enzymology 1990, 184, 51-67.

69. Gregoriadis, G.; Florence, A. T., Liposomes in drug delivery - clinical, diagnostic and ophthalmic potential. Drugs 1993, 45, (1), 15-28.

70. Guttenberg, Z.; Lorz, B.; Sackmann, E.; Boulbitch, A., First-order transition between adhesion states in a system mimicking cell-tissue interaction. Europhysics Letters 2001, 54, (6), 826-832.

71. Hales, K.; Pochan, D. J., Using polyelectrolyte block copolymers to tune nanostructure assembly. Current Opinion in Colloid & Interface Science 2006, 11, (6), 330-336.

72. Haluska, C. K.; Riske, K. A.; Marchi-Artzner, V.; Lehn, J. M.; Lipowsky, R.; Dimova, R., Time scales of membrane fusion revealed by direct imaging of vesicle fusion with high temporal resolution. Proceedings of the National Academy of Sciences of the United States of America 2006, 103, (43), 15841-15846.

73. Hammer, D. A.; Tirrell, M., Biological adhesion at interfaces. Annual Review of Materials Science 1996, 26, 651-691.

74. Hategan, A.; Law, R.; Kahn, S.; Discher, D. E., Adhesively-tensed cell membranes: Lysis kinetics and atomic force microscopy probing. Biophysical Journal 2003, 85, (4), 2746-2759.

75. Heinrich, V.; Rawicz, W., Automated, high-resolution micropipet aspiration reveals new insight into the physical properties of fluid membranes. Langmuir 2005, 21, (5), 1962-1971.

76. Helfrich, W., Elastic properties of lipid bilayers - theory and possible experiments. Zeitschrift Fur Naturforschung C-a Journal of Biosciences 1973, C 28, (11-1), 693-703.

77. Helfrich, W., Steric interaction of fluid membranes in multilayer systems. Zeitschrift Fur Naturforschung Section a-a Journal of Physical Sciences 1978, 33, (3), 305-315.

78. Helm, C. A.; Knoll, W.; Israelachvili, J. N., Measurement of Ligand Receptor Interactions. Proceedings of the National Academy of Sciences of the United States of America 1991, 88, (18), 8169-8173.

79. Henriksen, J. R.; Ipsen, J. H., Thermal undulations of quasi-spherical vesicles stabilized by gravity. European Physical Journal E 2002, 9, (4), 365-374.

80. Henriksen, J. R.; Ipsen, J. H., Measurement of membrane elasticity by micro-pipette aspiration. European Physical Journal E 2004, 14, (2), 149-167.

81. Hill, R. M.; He, M. T.; Lin, Z.; Davis, H. T.; Scriven, L. E., Lyotropic Liquid-crystal Phase-Behavior of Polymeric Siloxane Surfactants. Langmuir 1993, 9, (11), 2789-2798.

82. Hiller, Y.; Gershoni, J. M.; Bayer, E. A.; Wilchek, M., Biotin binding to avidin - oligosaccharide side-chain not required for ligand association. Biochemical Journal 1987, 248, (1), 167-171.

83. Hillmyer, M. A.; Bates, F. S., Synthesis and characterization of model polyalkane-poly(ethylene oxide) block copolymers. Macromolecules 1996, 29, (22), 6994-7002.

84. Hori, Y.; Raychaudhuri, S.; Chakraborty, A. K., Analysis of pattern formation and phase separation in the immunological synapse. Journal of Chemical Physics 2002, 117, (20), 9491-9501.

85. Israelachvili, J. N.; Wennerstrom, H., ENTROPIC FORCES BETWEEN AMPHIPHILIC SURFACES IN LIQUIDS. Journal of Physical Chemistry 1992, 96, (2), 520-531.

86. Jahnig, F., Molecular Theory of Lipid-Membrane Order. Journal of Chemical Physics 1979, 70, (7), 3279-3290.

87. Jahnig, F.; Brochard, F., Critical elastic-constants and viscosities above a nematic-smectic-a transition of second-order. Journal De Physique 1974, 35, (3), 301-313.

88. Jang, J.; Ko, S.; Kim, Y., Dual-functionalized polymer nanotubes as substrates for molecular-probe and DNA-carrier applications. Advanced Functional Materials 2006, 16, (6), 754-759.

89. Jeppesen, C.; Wong, J. Y.; Kuhl, T. L.; Israelachvili, J. N.; Mullah, N.; Zalipsky, S.; Marques, C. M., Impact of polymer tether length on multiple ligand-receptor bond formation. Science 2001, 293, (5529), 465-468.

90. Kickelbick, G.; Bauer, J.; Husing, N.; Andersson, M.; Palmqvist, A., Spontaneous vesicle formation of short-chain amphiphilic polysiloxane-b-poly(ethylene oxide) block copolymers. Langmuir 2003, 19, (8), 3198-3201.

91. Kidd, D.; Liu, Y. S.; Cravatt, B. F., Profiling serine hydrolase activities in complex proteomes. Biochemistry 2001, 40, (13), 4005-4015.

92. Kim, D. H.; Klibanov, A. L.; Needham, D., The influence of tiered layers of surface-grafted poly(ethylene glycol) on receptor-ligand-mediated adhesion between phospholipid monolayer-stabilized microbubbles and coated class beads. Langmuir 2000, 16, (6), 2808-2817.

93. Kim, K.; Kim, C.; Byun, Y., Preparation of a PEG-grafted phospholipid Langmuir-Blodgett monolayer for blood-compatible material. Journal of Biomedical Materials Research 2000, 52, (4), 836-840.

94. Kinugasa, S.; Nakahara, H.; Kawahara, J. I.; Koga, Y.; Takaya, H., Static light scattering from poly(ethylene oxide) in methanol. Journal of Polymer Science Part B-Polymer Physics 1996, 34, (3), 583-586.

95. Kita-Tokarczyk, K.; Grumelard, J.; Haefele, T.; Meier, W., Block copolymer vesicles - using concepts from polymer chemistry to mimic biomembranes. Polymer 2005, 46, (11), 3540-3563.

96. Klibanov, A. L.; Maruyama, K.; Beckerleg, A. M.; Torchilin, V. P.; Huang, L., Activity of Amphipathic Poly(Ethylene Glycol)-5000 to Prolong the Circulation Time of Liposomes Depends on the Liposome Size and Is Unfavorable for Immunoliposome Binding to Target. Biochimica Et Biophysica Acta 1991, 1062, (2), 142-148.

97. Kloboucek, A.; Behrisch, A.; Faix, J.; Sackmann, E., Adhesion-induced receptor segregation and adhesion plaque formation: A model membrane study. Biophysical Journal 1999, 77, (4), 2311-2328.

98. Korlach, J.; Schwille, P.; Webb, W. W.; Feigenson, G. W., Characterization of lipid bilayer phases by confocal microscopy and fluorescence correlation spectroscopy. Proceedings of the National Academy of Sciences of the United States of America 1999, 96, (15), 8461-8466.

99. Kozlova, N.; Santore, M. M., Manipulation of micrometer-scale adhesion by tuning nanometer-scale surface features. Langmuir 2006, 22, (3), 1135-1142.

100. Kuhl, T. L.; Berman, A. D.; Hui, S. W.; Israelachvili, J. N., Part 1. Direct measurement of depletion attraction and thin film viscosity between lipid bilayers in aqueous polyethylene glycol solutions. Macromolecules 1998, 31, (23), 8250-8257.

101. Kuhl, T. L.; Berman, A. D.; Hui, S. W.; Israelachvili, J. N., Part 2. Crossover from depletion attraction to adsorption: Polyethylene glycol induced electrostatic repulsion between lipid bilayers. Macromolecules 1998, 31, (23), 8258-8263.

102. Kumar, S.; Hoh, J. H., Direct visualization of vesicle-bilayer complexes by atomic force microscopy. Langmuir 2000, 16, (25), 9936-9940.

103. Lane, P. J. L.; McConnell, F. M.; Clark, E. A.; Mellins, E., Rapid signaling to b-cells by antigen-specific t-cells requires cd18 cd54 interaction. Journal of Immunology 1991, 147, (12), 4103-4108.

104. Lasic, D. D., Novel applications of liposomes. Trends in Biotechnology 1998, 16, (7), 307-321.

105. Lasky, L. A., Selectins - interpreters of cell-specific carbohydrate information during inflammation. Science 1992, 258, (5084), 964-969.

106. Lawrence, M. B.; Springer, T. A., Leukocytes roll on a selectin at physiological flow-rates - distinction from and prerequisite for adhesion through integrins. Cell 1991, 65, (5), 859-873.

107. Leckband, D., Novel recognition mechanisms in biological adhesion. Current Opinion in Colloid & Interface Science 2001, 6, (5-6), 498-505.

108. Lee, J. C. M.; Bermudez, H.; Discher, B. M.; Sheehan, M. A.; Won, Y. Y.; Bates, F. S.; Discher, D. E., Preparation, stability, and in vitro performance of vesicles made with diblock copolymers. Biotechnology and Bioengineering 2001, 73, (2), 135-145.

109. Lee, J. C. M.; Santore, M.; Bates, F. S.; Discher, D. E., From membranes to melts, rouse to reptation: Diffusion in polymersome versus lipid bilayers. Macromolecules 2002, 35, (2), 323-326.

110. Limozin, L.; Barmann, M.; Sackmann, E., On the organization of self-assembled actin networks in giant vesicles. European Physical Journal E 2003, 10, (4), 319-330.

111. Lin, J. J.; Bates, F. S.; Hammer, D. A.; Silas, J. A., Adhesion of polymer vesicles. Physical Review Letters 2005, 95, (2).

112. Lin, J. J.; Ghoroghchian, P.; Zhang, Y.; Hammer, D. A., Adhesion of antibody-functionalized polymersomes. Langmuir 2006, 22, (9), 3975-3979.

113. Lin, J. J.; Ghoroghchian, P.; Zhang, Y.; Hammer, D. A., Adhesion of antibody-functionalized polymersomes. Langmuir 2006, 22, (9), 3975-3979.

114. Lin, J. J.; Silas, J. A.; Bermudez, H.; Milam, V. T.; Bates, F. S.; Hammer, D. A., The effect of polymer chain length and surface density on the adhesiveness of functionalized polymersomes. Langmuir 2004, 20, (13), 5493-5500.

115. Lin, J. J.; Silas, J. A.; Bermudez, H.; Milam, V. T.; Bates, F. S.; Hammer, D. A., The effect of polymer chain length and surface density on the adhesiveness of functionalized polymersomes. Langmuir 2004, 20, (13), 5493-5500.

116. Lin, Z.; Hill, R. M.; Davis, H. T.; Scriven, L. E.; Talmon, Y., Cryo-Transmission Electron-Microscopy Study of Vesicles and Micelles in Siloxane Surfactant Aqueous-Solutions. Langmuir 1994, 10, (4), 1008-1011.

117. Lipowsky, R.; Seifert, U., Adhesion of Vesicles and Membranes. Molecular Crystals and Liquid Crystals 1991, 202, 17-25.

118. Lipowsky, R.; Seifert, U., Adhesion of Membranes - a Theoretical Perspective. Langmuir 1991, 7, (9), 1867-1873.

119. Livnah, O.; Bayer, E. A.; Wilchek, M.; Sussman, J. L., 3-Dimensional Structures of Avidin and the Avidin-Biotin Complex. Proceedings of the National Academy of Sciences of the United States of America 1993, 90, (11), 5076-5080.

120. Longo, M. L.; Waring, A. J.; Hammer, D. A., Interaction of the influenza hemagglutinin fusion peptide with lipid bilayers: Area expansion and permeation. Biophysical Journal 1997, 73, (3), 1430-1439.

121. Maier, C. W.; Behrisch, A.; Kloboucek, A.; Simson, D. A.; Merkel, R., Specific biomembrane adhesion - Indirect lateral interactions between bound receptor molecules. European Physical Journal E 2001, 6, (4), 273-276.

122. Marchi-Artzner, V.; Lorz, B.; Gosse, C.; Jullien, L.; Merkel, R.; Kessler, H.; Sackmann, E., Adhesion of Arg-Gly-Asp (RGD) peptide vesicles onto an integrin surface: Visualization of the segregation of RGD ligands into the adhesion plaques by fluorescence. Langmuir 2003, 19, (3), 835-841.

123. Marsh, D., Scaling and mean-field theories applied to polymer brushes. Biophysical Journal 2004, 86, (4), 2630-2633.

124. Martinez-Rico, C.; Pincet, F.; Perez, E.; Thiery, J. P.; Shimizu, K.; Takai, Y.; Dufour, S., Separation force measurements reveal different types of modulation of E-cadherin-based adhesion by nectin-1 and-3. Journal of Biological Chemistry 2005, 280, (6), 4753-4760.

125. Masui, T.; Imai, M.; Nakaya, K.; Taniguchi, T., Effects of grafted polymer chains on lamellar membranes. Journal of Chemical Physics 2006, 124, (7).

126. McCormick, C. L.; Kirkland, S. E.; York, A. W., Synthetic routes to stimuli-responsive micelles, vesicles, and surfaces via controlled/living radical polymerization. Polymer Reviews 2006, 46, (4), 421-443.

127. McIntosh, T. J.; Advani, S.; Burton, R. E.; Zhelev, D. V.; Needham, D.; Simon, S. A., Experimental Tests for Protrusion and Undulation Pressures in Phospholipid-Bilayers. Biochemistry 1995, 34, (27), 8520-8532.

128. McIntyre, J. C.; Sleight, R. G., Fluorescence assay for phospholipid membrane asymmetry. Biochemistry 1991, 30, (51), 11819-11827.

129. Merkel, R.; Simson, R.; Simson, D. A.; Hohenadl, M.; Boulbitch, A.; Wallraff, E.; Sackmann, E., A micromechanic study of cell polarity and plasma membrane cell body coupling in Dictyostelium. Biophysical Journal 2000, 79, (2), 707-719.

130. Minard-Basquin, C.; Weil, T.; Hohner, A.; Radler, J. O.; Mullen, K., A polyphenylene dendrimer-detergent complex as a highly fluorescent probe for bioassays. Journal of the American Chemical Society 2003, 125, (19), 5832-5838.

131. Moy, V. T.; Florin, E. L.; Gaub, H. E., Intermolecular Forces and Energies between Ligands and Receptors. Science 1994, 266, (5183), 257-259.

132. Mueller, A.; O'Brien, D. F., Supramolecular materials via polymerization of mesophases of hydrated amphiphiles. Chemical Reviews 2002, 102, (3), 727-757.

133. Nam, J.; Santore, M. M., Adhesion plaque formation dynamics between polymer vesicles in the limit of highly concentrated binding sites. Langmuir 2007, 23, (13), 7216-7224.

134. Nam, J.; Santore, M. M., The adhesion kinetics of sticky vesicles in tension: The distinction between spreading and receptor binding. Langmuir 2007, 23, (21), 10650-10660.

135. Nardin, C.; Hirt, T.; Leukel, J.; Meier, W., Polymerized ABA triblock copolymer vesicles. Langmuir 2000, 16, (3), 1035-1041.

136. Nilsson, K.; Mosbach, K., Para-toluenesulfonyl chloride as an activating agent of agarose for the preparation of immobilized affinity ligands and proteins. European Journal of Biochemistry 1980, 112, (2), 397-402.

137. Noppl, D. A.; Needham, D., Avidin-biotin interactions at vesicle surfaces: Adsorption and binding, cross bridge formation, and lateral interactions. Biophysical Journal 1996, 70, (2), SU359-SU359.

138. Pignataro, B.; Steinem, C.; Galla, H. J.; Fuchs, H.; Janshoff, A., Specific adhesion of vesicles monitored by scanning force microscopy and quartz crystal microbalance. Biophysical Journal 2000, 78, (1), 487-498.

139. Pincet, F.; Husson, J., The solution to the streptavidin-biotin paradox: The influence of history on the strength of single molecular bonds. Biophysical Journal 2005, 89, (6), 4374-4381.

140. Pincet, F.; Le Bouar, T.; Zhang, Y. M.; Esnault, J.; Mallet, J. M.; Perez, E.; Sinay, P., Ultraweak sugar-sugar interactions for transient cell adhesion. Biophysical Journal 2001, 80, (3), 1354-1358.

141. Pincet, F.; Perez, E.; Loudet, J. C.; Lebeau, L., From macroscopic adhesion energy to molecular bonds: A test of the theory. Physical Review Letters 2001, 8717, (17).

142. Poteau, S.; Argillier, J. F.; Langevin, D.; Pincet, F.; Perez, E., Influence of pH on stability and dynamic properties of asphaltenes and other amphiphilic molecules at the oil-water interface. Energy & Fuels 2005, 19, (4), 1337-1341.

143. Radler, J.; Sackmann, E., IMAGING OPTICAL THICKNESSES AND SEPARATION DISTANCES OF PHOSPHOLIPID-VESICLES AT SOLID-SURFACES. Journal De Physique Ii 1993, 3, (5), 727-748.

144. Ratanabanangkoon, P.; Gropper, M.; Merkel, R.; Sackmann, E.; Gast, A. P., Mechanics of streptavidin-coated giant lipid bilayer vesicles: A micropipet study. Langmuir 2003, 19, (4), 1054-1062.

145. Raudino, A.; Cambria, A.; Sarpietro, M. G.; Satriano, C., Binding of lipid vesicles to protein-coated solid polymer surfaces: A model for cell adhesion to artificial biocompatible materials. Journal of Colloid and Interface Science 2000, 231, (1), 66-73.

146. Rawicz, W.; Olbrich, K. C.; McIntosh, T.; Needham, D.; Evans, E., Effect of chain length and unsaturation on elasticity of lipid bilayers. Biophysical Journal 2000, 79, (1), 328-339.

147. Richard, A.; Marchi-Artzner, V.; Lalloz, M. N.; Brienne, M. J.; Artzner, F.; Gulik-Krzywicki, T.; Guedeau-Boudeville, M. A.; Lehn, J. M., Fusogenic supramolecular vesicle systems induced by metal ion binding to amphiphilic ligands. Proceedings of the National Academy of Sciences of the United States of America 2004, 101, (43), 15279-15284.

148. Richert, L.; Lavalle, P.; Vautier, D.; Senger, B.; Stoltz, J. F.; Schaaf, P.; Voegel, J. C.; Picart, C., Cell interactions with polyelectrolyte multilayer films. Biomacromolecules 2002, 3, (6), 1170-1178.

149. Ringwald, M.; Schuh, R.; Vestweber, D.; Eistetter, H.; Lottspeich, F.; Engel, J.; Dolz, R.; Jahnig, F.; Epplen, J.; Mayer, S.; Muller, C.; Kemler, R., THE STRUCTURE OF CELL-ADHESION MOLECULE UVOMORULIN - INSIGHTS INTO THE MOLECULAR MECHANISM OF CA-2+-DEPENDENT CELL-ADHESION. Embo Journal 1987, 6, (12), 3647-3653.

150. Rodriguez, N.; Pincet, F.; Cribier, S., Giant vesicles formed by gentle hydration and electroformation: A comparison by fluorescence microscopy. Colloids and Surfaces B-Biointerfaces 2005, 42, (2), 125-130.

151. Sackmann, E., Membrane bending energy concept of vesicle-shape and cell-shape and shape-transitions. Febs Letters 1994, 346, (1), 3-16.

152. Sackmann, E., Thermo-elasticity and adhesion as regulators of cell membrane architecture and function. Journal of Physics-Condensed Matter 2006, 18, (45), R785-R825.

153. Sackmann, E.; Duwe, H. P.; Engelhardt, H., Membrane Bending Elasticity and Its Role for Shape Fluctuations and Shape Transformations of Cells and Vesicles. Faraday Discussions 1986, (81), 281.

154. Sackmann, E.; Feder, T., Budding, fission and domain formation in mixed lipid vesicles induced by lateral phase-separation and macromolecular condensation. Molecular Membrane Biology 1995, 12, (1), 21-28.

155. Sackmann, E.; Goennenwein, S., Cell adhesion as dynamic interplay of lock-and-key, generic and elastic forces. Progress of Theoretical Physics Supplement 2006, (165), 78-99.

156. Sackmann, E.; Kas, J.; Radler, J., On shape transformations and shape fluctuations of cellular compartments and vesicles. Physica Scripta 1993, T49A, 111-118.

157. Santore, M. M., Dynamics in adsorbed homopolymer layers: Understanding complexity from simple starting points. Current Opinion in Colloid & Interface Science 2005, 10, (3-4), 176-183.

158. Santore, M. M.; Discher, D. E.; Won, Y. Y.; Bates, F. S.; Hammer, D. A., Effect of surfactant on unilamellar polymeric vesicles: Altered membrane properties and stability in the limit of weak surfactant partitioning. Langmuir 2002, 18, (20), 7299-7308.

159. Sarda, S.; Pointu, D.; Pincet, F.; Henry, N., Specific recognition of macroscopic objects by the cell surface: Evidence for a receptor density threshold revealed by micrometric particle binding characteristics. Biophysical Journal 2004, 86, (5), 3291-3303.

160. Satomaeda, M.; Uchida, M.; Graner, F.; Tashiro, H., Quantitative-evaluation of tissue-specific cell-adhesion at the level of a single-cell pair. Developmental Biology 1994, 162, (1), 77-84.

161. Silas, J. A.; Lin, J.; Bates, F. S.; Hammer, D. A., Mechanics of adhesion at the surface of polymer vesicles. Abstracts of Papers of the American Chemical Society 2006, 231.

162. Simon, J.; Kuhner, M.; Ringsdorf, H.; Sackmann, E., Polymer-induced shape changes and capping in giant liposomes. Chemistry and Physics of Lipids 1995, 76, (2), 241-258.

163. Smith, A. S.; Lorz, B. G.; Seifert, U.; Sackmann, E., Antagonist-induced deadhesion of specically adhered vesicles. Biophysical Journal 2006, 90, (3), 1064-1080.

164. Smith, A. S.; Seifert, U., Effective adhesion strength of specifically bound vesicles. Physical Review E 2005, 71, (6).

165. Smith, K. A.; Jasnow, D.; Balazs, A. C., Designing synthetic vesicles that engulf nanoscopic particles. Journal of Chemical Physics 2007, 127, (8).

166. Snow, S. A.; Hill, R. M.; He, M. T.; Lin, Z. C.; Davis, H. T.; Scriven, L. E., Liquid-Crystal Phase-Behavior of Siloxane Surfactants. Abstracts of Papers of the American Chemical Society 1993, 205, 244-COLL.

167. Stanton, K. J.; Frewin, M. B.; Gudewicz, P. W., Heterologous desensitization of IL-8-mediated chemotaxis in human neutrophils by a cell-binding fragment of fibronectin. Journal of Leukocyte Biology 1999, 65, (4), 515-522.

168. Stayton, P. S., Biophysics - May the force be with you. Nature 1999, 397, (6714), 20-21.

169. Strigl, M.; Simson, D. A.; Kacher, C. M.; Merkel, R., Force-induced dissociation of single protein A-IgG bonds. Langmuir 1999, 15, (21), 7316-7324.

170. Tareste, D.; Pincet, F. R.; Brellier, M.; Mioskowski, C.; Perez, E., The binding energy of two nitrilotriacetate groups sharing a nickel ion. Journal of the American Chemical Society 2005, 127, (11), 3879-3884.

171. Tordeux, C.; Fournier, J. B.; Galatola, P., Analytical characterization of adhering vesicles. Physical Review E 2002, 65, (4).

172. Toscano, A.; Santore, M. M., Fibrinogen adsorption on three silica-based surfaces: Conformation and kinetics. Langmuir 2006, 22, (6), 2588-2597.

173. Trauble, H.; Sackmann, E., Studies of crystalline-liquid crystalline phase-transition of lipid model membranes .3. structure of a steroid-lecithin system below and above lipid-phase transition. Journal of the American Chemical Society 1972, 94, (13), 4499-&.

174. Vanroy, N.; Mangelschots, K.; Speleman, F., Improved immunocytochemical detection of biotinylated probes with neutralite avidin. Trends in Genetics 1993, 9, (3), 71-72.

175. Vittet, D.; Prandini, M. H.; Berthier, R.; Schweitzer, A.; MartinSisteron, H.; Uzan, G.; Dejana, E., Embryonic stem cells differentiate in vitro to endothelial cells through successive maturation steps. Blood 1996, 88, (9), 3424-3431.

176. Webster, O. W., Living polymerization methods. Science 1991, 251, (4996), 887-893.

177. Winzor, D. J., Reappraisal of disparities between osmolality estimates by freezing point depression and vapor pressure deficit methods. Biophysical Chemistry 2004, 107, (3), 317-323.

178. Won, Y. Y.; Paso, K.; Davis, H. T.; Bates, F. S., Comparison of original and cross-linked wormlike micelles of poly(ethylene oxide-b-butadiene) in water: Rheological properties and effects of poly(ethylene oxide) addition. Journal of Physical Chemistry B 2001, 105, (35), 8302-8311.

179. Wong, J. Y.; Kuhl, T. L.; Israelachvili, J. N.; Mullah, N.; Zalipsky, S., Direct measurement of a tethered ligand-receptor interaction potential. Science 1997, 275, (5301), 820-822.

180. Woodle, M. C., Surface-modified liposomes - assessment and characterization for increased stability and prolonged blood-circulation. Chemistry and Physics of Lipids 1993, 64, (1-3), 249-262.

181. Woolley, D. W.; Longsworth, L. G., Isolation of an antibiotin factor from egg white. J. Biol. Chem. 1942, 142, 285-90.

182. You, J.; Mastro, A. M.; Dong, C., Application of the dual-micropipet technique to the measurement of tumor cell locomotion. Experimental Cell Research 1999, 248, (1), 160-171.

183. Zamir, E.; Geiger, B., Molecular complexity and dynamics of cell-matrix adhesions. Journal of Cell Science 2001, 114, (20), 3583-3590.

184. Zhang, Y.; Hammer, D. A.; Graves, D. J., Competitive hybridization kinetics reveals unexpected behavior patterns. Biophysical Journal 2005, 89, (5), 2950-2959.

185. Zuckerman, D. M.; Bruinsma, R. F., Vesicle-vesicle adhesion by mobile lock-and-key molecules: Debye-Huckel theory and Monte Carlo simulation. Physical Review E 1998, 57, (1), 964-977.

4416-17